IMPERIAL COLLEGE OF SCIENCE, TECHNOLOGY AND MEDICINE

University of London

STRUCTURAL DYNAMIC MODIFICATION USING EXPERIMENTAL DATA

by

Graham William SKINGLE

B.Sc.(Eng.), London

A thesis submitted to the University of London for
the degree of Doctor of Philosophy and for the
Diploma of Imperial College.

Dynamics Section
Department of Mechanical Engineering
Imperial College of Science, Technology and Medicine
London SW7

July, 1989

In memory of Jeffrey David Wilkins.

A very good friend and an example to us all,
he lived every moment of his life to the full.

ABSTRACT

This thesis describes an investigation into the practical and efficient implementation of structural modification methods using experimentally-derived models. Structural modification techniques and the associated methods for collection, assessment and analysis of experimental data are reviewed in a literature survey, from which the topics for detailed study in this thesis are identified_

The standard theory for impedance coupling and modal coupling structural modification methods is presented with discussion of the specific advantages and disadvantages of each when used with experimental data. Developments of the impedance coupling method are shown which improve both the computational efficiency (very substantially) and the potential accuracy. From impedance coupling theory and a rational fraction form of description for a Frequency Response Function (FRF), a new technique has been developed to enable calculation of the sensitivity of modes to specific simple modifications. The input data are the resonance and anti-resonance frequencies obtained directly from point FRFs, measured in a preliminary survey of a structure, without the need for extensive modal analysis procedures. A detailed measurement survey can then be confined to the sensitive locations on the structure where particular care must be taken to avoid influencing the response with the measurement equipment. Ranking the coordinates in their order of importance for influencing each mode by simple modification provides a valuable insight into the subsequent design and selection of practical modifications.

Problems of inconsistency and spatial and modal insufficiency in the measured data are considered in detail. It is shown that rotational degree-of-freedom properties can be vital if certain joint conditions are to be modelled correctly. Difficulties with the derivation of these properties from measured translational FRFs are discussed, together with the implications for the type of joints used in the attachment of modifications.

Throughout the thesis, simple examples are used for illustration of many specific points. A comprehensive case study of a helicopter structure is presented which draws together many of the topics of the study in a demonstration and critical evaluation of the current ability to select the most appropriate site for a modification and then to predict the effects of that modification using experimental data.

Acknowledgements

I would like to thank my supervisor at Imperial College, Professor D. J. Ewins, for the constant valuable help and guidance that he has given throughout the period of this work. My thanks are also due to Mr D. A. Robb and all other members of the Dynamics Section, for their helpful advice and discussions on a wide range of vibration test and analysis topics.

The author gratefully acknowledges the financial support of the Ministry of Defence during the course of this study and for the provision of excellent facilities in the Materials and Structures Department of the Royal Aerospace Establishment.

I am especially grateful to Mr R. J. Davies, Dr M. Nash and Mr C. Hatch for their valuable contributions and assistance throughout this work. I would also like to thank Mr E. Hopgood for his cheerful and willing help in the production of numerous items required during the helicopter case study.

Finally, my most sincere thanks are reserved for my mother and father, their continuous support and encouragement has enabled me to pursue my studies without hindrance.

Nomenclature

The list of symbols described below represents the standard notation used throughout this thesis.

$_rA_{jk}$	–	r^{th} mode shape coefficient for coordinates j and k.
C_{jk}		Static flexibility for coordinates j and k.
f		Force.
I_{jk}	–	Inertance between coordinates j and k.
j		$\sqrt{-1}$
k	–	Stiffness.
k_e	–	Effective stiffness (ref. Salter skeleton).
$_rK_{jk}$	–	High-frequency residual term.
m	–	Mass.
me	–	Effective mass (ref. Salter skeleton).
$_rM_{jk}$		Low-frequency residual term.
t	–	Time.
x	–	Displacement.
$\dot{x}$ orv	–	Velocity.
$\ddot{x}$	–	Acceleration.
[1		Matrix.
{ }	–	Vector.
[F]	–	Force matrix.
[H]	–	Inertance matrix.
[I]	–	Identity matrix.
[K]	–	Stiffness matrix.
Ml		Mass matrix.
[T]		Transformation matrix.

ω		Frequency in radians/second.
${}^{jk}\omega_i$	–	i^{th} anti-resonance frequency for coordinates j and k.
Ω_r	–	r^{th} resonance frequency.
ξ_{jk}	–	Static accelerance for coordinates j and k
λ_r	–	r^{th} eigenvalue.
α_{jk}	–	Inertance for coordinates j and k.
${}_r\theta_j$ ${}_r\phi_j$	–	j^{th} components of r^{th} eigenvectors.
ζ_r	–	Viscous damping coefficient for r^{th} mode.
η_r	–	Hysteretic damping factor for r^{th} mode.
A	–	Difference (as used in AFRF).
$[\theta]$ $[\phi]$	–	Eigenvector matrices.
$[\lambda]$	–	Eigenvalue matrix.
$[\alpha]$ $[\beta]$	–	Inertance matrices.

Table of Contents.

Chapter 1

Introduction

Chapter 2

Structural Modification – Theoretical Basis

Chapter 3

Sensitivity Analysis

Chapter 4

Practical Considerations

Chapter 5

Incompleteness and Inaccuracy of Dynamic Models

Chapter 6

Case Study

Chapter 7

Conclusions

References

APPENDICES

Chapter 1

Introduction

1.1 Preliminaries

Modem techniques for the design and manufacture of structures in which materials are used far more efficiently than previously possible have led to structures that are now more susceptible to vibration problems. Structures are designed to be just as strong as necessary using the minimum amount of material, but the component parts, plates and beams, etc. no longer have the individual stiffnesses of their previously overdesigned counterparts. Additionally, modem trends to all welded construction, and components milled from solid material (e.g. fighter aircraft wing skins which incorporate web sections), generate components that have little inherent damping. As a result, modem structures are more likely to be excited into resonance, and when they are, to have very high response levels due to the virtual absence of damping. Such conditions can lead quickly to fatigue failure of the components.

For any aerospace structure the consequences of vibration are generally more severe than for similar ground-based structures. Methods for alleviating these vibration problems are restricted by structural and aerodynamic constraints and by performance requirements: any mass addition reduces the available payload by the same amount. A modem helicopter is a good example of a structure that is particularly prone to structural vibration problems and it is important that vibration of these structures is controlled in the most efficient and economical way. Therefore, helicopter-like structures provide the main focus for the work contained in this thesis.

Fortunately, there are still many joints in aerospace structures that are riveted or bolted, and a large number of these joints also incorporate some form of adhesive or sealing compound. These joint features provide damping but can also make the structure non-linear in its vibrational behaviour, and thence more difficult to model theoretically.

1 .1.1 Cause, Consequence and Control of Helicopter Vibration

The level of vibration found in a helicopter is generally higher than that experienced in fixed-wing aircraft, especially when the helicopter is operating at high thrust or forward speed. The primary causes of vibration in a helicopter are the high excitation forces generated by the rotor blades and the downwash from each passing blade impinging on the fuselage and tail surfaces. In forward flight, the main rotor system provides lift and thrust simultaneously and the blades experience cyclic aerodynamic loading as the apparent airspeed over each blade changes with the angle of the blade to the direction of flight. At high forward speed the airflow at the tip of the advancing blade reaches a transonic condition where there is a dramatic increase in blade drag. Simultaneously, smooth airflow over the tip of the retreating blade cannot be sustained and a stall results, causing large oscillatory loads in the blade and control system. Each blade experiences a complete loading cycle in one revolution of the rotor and, therefore, the fundamental excitation frequency transmitted to the airframe is given by (the number of blades, N) x (the rotation speed, R), e.g. 'NR' which is approximately 22 Hz for a 4-bladed Westland 30 helicopter. These oscillatory loads provide a source of excitation that can lead to structural vibration problems.

High vibration levels in a helicopter have several important consequences; the environment can be uncomfortable and noisy so that pilots, crew and passengers cannot tolerate the vibration for long periods of time. Fixed-wing aircraft have much lower levels of vibration and, to some extent, expectations of passengers are set by the fixed-wing standards. Military use of helicopters requires the crew to perform complex tasks at times throughout the mission (e.g. weapons delivery, search and reconnaissance) and prolonged vibration takes its toll by reduction in the efficiency with which the tasks are executed. The reduction in performance of the pilot and crew occurs much more rapidly if the predominant vibration frequencies coincide with certain resonances of the human body, such as eyeball jitter. Furthermore, as military weapons and associated electronic systems become more sophisticated their performance and reliability can be impaired by vibration of the helicopter. Excessive vibration is also damaging to the components,

critical flight systems and the structure of the helicopter itself and hence frequent, costly, inspection and maintenance may be necessary.

There are three methods that have been used for the control of vibration in the airframe of a helicopter

(i) Reduce the vibration excitation at the source – the main rotor blades

One of the most effective ways to minimise helicopter vibration is to use as many blades as possible, thereby increasing the fundamental 'NR' excitation frequency – hence the evolution of five-bladed helicopters from the more conventional four-bladed designs. Considerations of hub complexity and blade manufacture and maintenance costs set a practical limit on the number of blades used.

Passive, torsional vibration absorbers can be fitted to the rotor head but they suffer from the disadvantage that they only operate in the plane of the rotor disc. Forces induced by lift changes on the blades due to stall, etc., are perpendicular to the plane of the rotor disc and, therefore, unaffected by the vibration absorber mounted to the rotor head.

Advances in materials technology have allowed production of aeroelastically adaptive rotor blades with new aerofoil sections and blade tip planforms that delay the onset of blade stall and improve the transonic performance of the blade tips. Rotor blades of this type, with precisely matched dynamic and aeroelastic characteristics, have shown promising reductions in excitation at the rotor head. This is another passive vibration reduction technique.

An active vibration reduction technique – Higher Harmonic Control (HHC) – has been used to allow precise control of the pitch of each blade. Hydraulic actuators replace direct pitch linkages, thereby facilitating much greater control of the aerodynamic loading. With this technique it is essential that the frequency responses of each actuator ate identical and that an accurate and reliable control algorithm can be devised. Some reservations have been expressed with regard to reliability and maintenance aspects of these systems and the potential influence of any malfunctions on rotor performance and airworthiness. The hydraulic power required for this type of active system is typically about 30 h.p. for the Westland 30 helicopter.

(ii) Reduce the coupling between the rotor/gearbox/engine raft and the airframe

A combination of active and passive vibration isolation systems is used in the Active Control of Structural Response (ACSR) system developed by Westland Helicopters. Hydraulic actuators are connected in parallel with elastomeric mountings between the raft and the airframe. The actuators are computer controlled to minimise a summation of key response functions at the blade passing frequency. Only a single response frequency is considered otherwise the computations become impractical. Because the actuators are in parallel with the elastomeric support and do not carry any steady load, there are no airworthiness problems and an added bonus is that the hydraulic power is considerably less than for HHC – about 4 h.p. for the complete installation in a Westland 30.

(iii) Tailor the dynamic characteristics of the airframe to ensure minimal response at anticipated excitation frequencies

The initial design and production of a helicopter airframe that has satisfactory dynamic characteristics is notoriously difficult, even with the availability of sophisticated Finite Element (F.E.) analysis tools (some engineers even recommend that the designer should try to place everything in resonance as a way of ensuring that it will be off resonance when it is built!). The benefits of adaptive rotor blades, HHC and ACSR can be lost completely if the airframe has a lightly damped resonance corresponding with an excitation frequency.

The dynamic characteristics of an existing airframe may be altered by active or passive modifications but, whichever method is chosen, it is desirable to make the modifications at or between the most sensitive points, thereby minimising any weight penalty.

1.1.2 Design and Selection of Structural Modifications

Many basic vibration problems can be investigated and minimized by the use of vibration prediction and analysis techniques during the design phase of a project. Since there is no hardware available for testing at the early stages, the techniques are invariably based on finite element models produced from component drawings. However, there are so many features and properties of real components, mechanisms and materials that are difficult to represent adequately in a finite element model that the use of such a model, in isolation, is considered to be insufficient. Once a prototype component has been produced, vibration testing and analysis is almost always required in order to validate the finite element model

and the results therefrom More often than not, the finite element model is then adjusted to reflect the vibration characteristics actually measured.

If the measured characteristics of a structure are such as to indicate the possibility of a vibration problem arising in service, then some structural modifications may be required. In the past, suitable modifications have been devised on an informed trial-and-error basis, by people with a wealth of experience in the field Each time a modification was made, the structure had to be re-tested to ensure that the vibration characteristics were acceptable. If not, the whole sequence of events was repeated in an iterative fashion, until a successful conclusion was reached. This was a very costly and time-consuming operation which eventually resulted in a structure with acceptable dynamic characteristics, but not one in which the changes had been made in the most efficient manner, nor in which an optimum solution had necessarily been obtained.

The advent of relatively cheap computing and advanced analysis techniques allows a mathematical model of a structure to be created directly from measured data. Modification techniques can be used with these measured data to enable a large number of different modifications to be evaluated much more quickly and effectively than was previously possible. Once a suitable modification is found using an experimentally-derived mathematical model of the structure, the actual modification can be incorporated in the real structure which will then undergo one further complete vibration test to confirm the predictions. The whole process may involve only two complete vibration tests, although many different modifications will have been 'tried'. This can mean a great saving in costs because, usually, it is the acquisition of the data which represents the largest single cost in any vibration test.

The main disadvantage of using an experimentally-based approach is that it is only available once a prototype structure has been built. At this stage, the project is well advanced and the basic design, configuration and construction of the structure has been finalised, thus severely restricting the type and extent of any physical changes which can be made.

The initial process by which a modification is designed and selected can be improved if the sensitivities of points on the structure to simple types of modification (such as added masses or stiffnesses) are known. The intention is to select the most effective site and type of modification at the earliest possible stage, preferably at a preliminary measurement stage. A new method for calculating resonance frequency sensitivities for single degree-of-freedom mass or stiffness modifications is developed in this thesis. The method is

readily implemented, and is based on the use of resonance and anti-resonance frequencies of the original unmodified structure. The sensitivity characteristics resulting from the analysis enable each degree-of-freedom to be ranked in its order of importance for modification, for each mode of vibration.

Once an order of importance has been established for the coordinates at which modifications may be incorporated, then decisions can be taken as to which degrees-of-freedom should be measured for use in the full coupling analysis. Furthermore, if the sensitive coordinates are identified as a result of a preliminary measurement survey, special care can be devoted to the acquisition of accurate and reliable data from those coordinates during the full survey. The overall data acquisition task is made more efficient by concentrating the effort on the important, sensitive, degrees-of-freedom and reducing the amount of superfluous data measured.

In the design of a vibration test program, sensitivity data can be very useful but it is important to remember that there are 6 degrees-of-freedom for each point on the structure. If the rotational motion of points is ignored, 75% of the full FRF matrix is lost. For basic troubleshooting applications, the limited data set (without rotations) is not usually too restrictive. However, for use in prediction of the characteristics of a modified structure, the omission of rotational data may be very serious -- especially when the modification attachment involves anything other than simple pin-joints. The measurement of a complete set of rotational FRF properties is known to be difficult and some detailed discussions and examples are presented in this work to illustrate the consequences of neglecting rotational degree-of-freedom in coupling analyses. One interesting finding is that the measurement of a rotational **response** is not too difficult but, the practical application of a pure torque to provide a rotational **excitation** to a vibrating structure is significantly more difficult.

1.1.3 A Note on Terminology and Glossary of Terms

Frequency Response Function (FRF)

A frequency response function (FRF) is a frequency-dependent quantity derived from knowledge of both magnitude and phase of a harmonic response and the excitation causing that response. There are a number of different quantities that are classed as frequency response functions, and these can be divided into two distinct groups;

(a) those denoting (response/force) characteristics; and,

(b) those denoting (force/response) characteristics.

Each group can be subdivided further and categorized according to the actual response parameter measured; displacement, velocity or acceleration. All the different quantities have specific names which are summarized below.

Response type	(a) response/force	(b) force/response
Displacement	$\frac{x}{f}$ = Receptance	$\frac{f}{x}$ = Dynamic Stiffness
Velocity	$\frac{\dot{x}}{f}$ = Mobility	$\frac{f}{\dot{x}}$ = Mechanical Impedance
Acceleration	$\frac{\ddot{x}}{f}$ = Inertance or Accelerance	$\frac{f}{\ddot{x}}$ = Apparent Mass

Table 1.1

For harmonic motion the quantities in each column of Table 1.1 are related very simply by the ratio $j\omega$; $j = \sqrt{-1}$ and ω is the 'circular' frequency in radians/second.

$$\ddot{x} = j\omega\dot{x} = -\omega^2 x$$

Because of this simple relationship, generic terms are often used to describe any of the quantities in one column of the Table. Throughout this work, and in common with many other publications, the following generic terms have been adopted,

Inertance for response/force quantities in general

and,

Impedance for force/response quantities in general.

Measurement Practicalities

In the above general definitions of inertance and impedance properties, important practical conditions have been omitted. They are,

(i) for inertance quantities – all points on the structure must be completely **unrestrained** except for the single force excitation point. In mathematical terms,

$$\text{receptance} = \left(\frac{x_j}{f_j}\right) \quad \text{with } f_k = 0 \text{ for all } k \neq j$$

and;

(ii) for impedance quantities – all points on the structure must be completely **restrained** except for the single motion input point,

$$\text{dynamic stiffness} = \left(\frac{f_i}{x_j} \right) \quad \text{with} \quad x_k = 0 \text{ for all } k \neq j$$

Direct measurement of impedance quantities is virtually impossible since the requirement to ground all coordinates on the structure, other than the motion input point, is very difficult to achieve practically. In contrast, measurement of inertance quantities can be simple; for a grounded structure, no special precautions are necessary and for a free structure, the only requirement is for a suspension system which imposes minimum restraint on the structure under test, e.g. air bags, rubber bungee cords or soft springs. Consequently, the majority of vibration measurements made are inertance type measurements for the simple reason that they arc considerably easier to obtain.

Forced Response

Measurement of a forced response alone yields what is known as an operating response. This response may arise from many different, simultaneous, excitations distributed throughout the structure. A forced response can be considered as a linear summation of the appropriate FRFs, assuming that the structure is linear and that the force distribution is known or can be estimated. The forced response is a useful indicator of the operating characteristics of the structure but it is not very useful for diagnosis of the cause of a particular problem, nor for detailed investigations of structural modification or optimisation.

Natural Frequency

A natural frequency of a system is defined as a frequency at which free vibration can take place. Natural frequencies are **modal properties.**

Resonance

In simple terms, the resonances of a structure are defined as the set of excitation frequencies for which minimum force input produces a maximum – and possibly damaging – response. The resonance frequencies are characteristics of the frequency response function and generally coincide with the natural frequencies.

The magnitude of the response at resonance is controlled by the amount of damping present in the structure. For light damping levels, a resonance occurs when the forcing frequency is approximately equal to a natural frequency.

Anti-resonance

An anti-resonance is defined as a frequency at which the ratio of the response at a point to the force input tends to zero; a frequency at which the structure most strongly resists being made to move at all at a point of excitation. This can happen when there is zero motion at either the response measurement location, or at the excitation point. Anti-resonances are specific to the force and response locations – they are local properties.

Degree-of-Freedom

The term 'degree-of-freedom' can be used with reference to physical space or to modal space. It is important to note the differences in meaning of the two uses of the term. First, when degree-of-freedom is used in relation to physical space, it refers to a physical coordinate point and direction. Terms such as coordinate, location and point are synonymous for the physical space usage of degree-of-freedom. Second, degree-of-freedom can be used in relation to modal space, in which case, the degree-of-freedom refers to a complete mode of vibration. In this work there are many references to 'single degree-of-freedom modification'. These single degree-of-freedom modifications are in physical space, i.e. a modification is considered which is only active at one point and in one coordinate direction. Although the modification is only active in one physical coordinate, the effects of the modification may extend to all of the modes of vibration. The modification is **not** single degree-of-freedom with reference to modal space.

Interface and Passenger Degrees-of-Freedom (coordinates)

The terms **interface** and **passenger degrees-of-freedom** refer to physical space and are used in connection with the theoretical structural modification procedures. Interface degrees-of-freedom are the coordinates on each component that are joined together directly and are thus actively involved in the structural modification. The term 'passenger coordinate' covers all the coordinates that are not directly involved in the coupling.

1.2 Literature Survey

The technique of structural modification using experimental data encompasses many aspects of experimental modal analysis and requires the collection of more extensive and

more accurate data than are necessary for less demanding applications. For the present review of the literature, four broad areas for survey have been identified:-

(i) collection, assessment and analysis of experimental data;

(ii) derivation or measurement of rotational degrees of freedom;

(iii) structural modification methods; and

(iv) sensitivity aspects for optimum structural modification.

1.2.1 Collection, Assessment and Analysis of Experimental Data

Of all the different stages in the experimental modal analysis of a real structure, the collection and assessment of experimental data is the least well defined. There are many things that are left to personal preference, engineering judgement and experience rather than being covered by strict rules and procedures, as used with the later, more mathematical, stages. This situation probably reflects the wide diversity of structures that are now subjected to vibration test and analysis. The variability of FRF measurements as made by different organizations, but for the same structure, has been highlighted clearly by Ewins in a recent survey [1], where he advocates the need for much greater care in the collection and assessment of experimental data.

It is known that there is a strong correlation between the thoroughness with which a modal test is planned and a successful outcome. Ewins [2] points out the prime importance of planning the complete vibration analysis procedure, from test right through to final usage of the processed data, in order that just sufficient quantity of the right quality data are measured The ultimate usage of the data influences the way in which it is measured and how carefully it is analysed. Stroud [3][4] proposes a complete pre-test analysis of the structure using the best available F.E. model, but as such an analytical model is not always available, this approach may not be applicable. Ewins and Sainsbury [5] discuss the quantity and type of data required to enable predictions of the coupled properties of a simple beam with a block mass; another similar exercise was conducted by Damms [6] for coupling two beam structures.

Recently, Elliott [7] has shown that the spatial positioning of transducers on the base structure must be adequate to describe the motion of the modified structure as well as the base condition. If the modified state could not be measured adequately with the transducers as they are positioned, then prediction of the effects of the modification will

be unsuccessful. The problem is termed "modal insufficiency". Once again, this reinforces the need for a comprehensive preliminary survey in which possible modifications are proposed. Estimations of the modified structural behaviour then allow transducers to be placed in the correct positions on the base structure for the full tests.

As an example of the engineering judgement involved in vibration testing, the selection of a suitable pushrod for the measurements described in the paper by Damms, [6], was largely a matter of trial and error. More detailed studies of the influence of the pushrod on vibration measurements are discussed in works by Silva [8][9] and methods for designing pushrods for particular applications have now been developed by Mitchell [10] and Heiber [11], although the quantity and type of input data required makes these impracticable in most circumstances.

Work by Gleeson [12][13] has shown the care needed in mounting and aligning accelerometers on a structure so that errors are not induced by the method of attachment, or by excessive transverse motion. Ewins [14] has also shown how inaccurate positioning transducers on locally flexible parts of a structure can lead to wide variations in the measured results. Furthermore, the adverse effects that the measuring equipment can have on the structure under test are illustrated by this author [15] and by Hopton [16].

Early vibration measurements were made using a Transfer Function Analyser (TFA) and sinusoidal excitation at discrete frequencies, but with the advent of computer aided testing systems and cheap Fast Fourier Transform (FFT) processors the emphasis shifted towards broadband testing techniques. An excellent summary of the many types of broadband excitation functions has been produced by Olsen [17], which notes the advantages and disadvantages of each. The apparent demise of sine testing was lamented by Lang [18] in 1985 and it is interesting to note that more sophisticated sine testing techniques are now appearing once more [19].

Apart from the standard checks for reciprocity and repeatability, there has been little work presented on means for assessing the quality of experimental data at the time of collection, although the subject has been broached by this author [20][21]. Stroud [3] mentions the use of 'test-support analysis' where powerful, on-line, computers are used for rapid evaluation and assessment of the test results. The assessment consists of identification of modal parameters and orthogonality checks of the measured modes with the analytic modes produced in a 'pre-test analysis' – a type of modal assurance criterion. Once again, though, such methods are not applicable if an analytic model is unavailable. Several papers, including [22] & [23], have reported ways by which the quality of a modal

database can be estimated from the ability to predict accurately the effects of simple modifications. However, this is not thought to be a very reliable method due to the influence of other factors and, furthermore, it is too remote from the testing phase to be of any practical use.

With regard to the analysis of experimental data, since the introduction and development of cheap and powerful computational facilities, a vast quantity of work has been published. The basis for many of the analysis methods in common use today is presented in works by Brown, Allemang, Zimmerman and Mergeay [24], Ewins [25], Stroud [26] and Fiillerkrug [27], which cover single reference single degree-of-freedom (SDoF) and multi-degree-of-freedom (MDoF) methods and multiple reference MDoF time domain methods. A unique interpretation of FRF curves in terms of their "skeletal properties" is to be found in an interesting book by Salter [28].

The extensive modal surveys presented by Stroud [4] show how the implementation of different excitation and analysis techniques on the same structure can be used to build confidence in the final modal models. The desirability of an indication of the degree of accuracy for any given model, is noted by Goyder [29], so that judgements can be made as to the suitability of the model for further analysis purposes. Quite how this degree of accuracy should be determined is not explained.

Works by Hopton [16], Wei [30], and Skingle [15] show the typical types of errors that can occur through incorrect or incomplete modal analysis. Unfortunately, there are relatively few of these most informative examples – professional pride dictates that only successful results shall be presented!

1.2.2 Derivation or Measurement of Rotational Degrees-of-Freedom

The possible need for the measurement of rotational degrees-of-freedom FRFs was considered by Ewins and Sainsbury [5] and, later, Henderson [31] and Crowley [32] have demonstrated the actual influence of rotational coordinates in a coupling analysis. As indicated by Crowley, the need for rotational degrees-of-freedom is not universal; it is highly dependent on the type of modification and the nature of the motion at the coupling points. Similarly, papers by Smiley [33] and O'Callahan [34] develop, with examples, reasons why rotational degrees-of-freedom can be vital. A theoretical necessity to include rotational degrees-of-freedom in a coupling prediction can often be eclipsed by the practical difficulties of measuring such quantities. There arc two different approaches used

in the measurement and calculation of rotational FRF properties: (a) direct from measured FRF data, and (b) from complex mathematical operations on identified mode shapes.

Ewins and Gleeson [35] propose an experimental method for multi-directional measurements on beams and further work has been done by Silva [9] using a 'T-Block' transducer method. A more sophisticated technique, than that described by Silva [9], for the measurement of the full FRF matrix at a point, which includes the cross-axis effects of the accelerometers, has been developed by Mead and Heron [36]. Nevertheless, despite meticulous attention to detail, the calculated mobility terms which involved at least one rotational degree-of-freedom deviated somewhat from the theoretical predictions. Several possible reasons for the discrepancies are cited, but of particular interest is the influence of the contact stiffness between the 'transducer' and the structure, the sire of the 'transducer' and the dynamic range of the FRF measurements used in the calculations. These key factors were identified as being responsible for poor rotational degree-of-freedom estimations in the case study of a modern helicopter presented in chapter 6. The limitations of accelerometers used in the measurement of rotational properties are discussed by Gleeson [13] and Licht [37].

O'Callahan [38] and Haisty and Springer [39] propose methods for determining the rotational degree-of-freedom information by fitting spline functions to the mode shape data and then differentiating to find the slopes. These methods have been shown to work satisfactorily with data produced from F.E. analysis, but no results are presented for experimental input data. Avitable [40] presents a method which uses transformation matrices, derived from a F.E. model of a structure, to expand the measured data set to include the required rotational degree-of-freedom properties. Once again though, such methods are only applicable if a F.E. model is available, and then the accuracy of the results is linked with the accuracy of the F.E. model.

In recent years optical techniques, such as laser doppler velocimeters and vibration pattern imagers, have been developed. The large quantities of response data that can be obtained by use of these techniques will provide much more accurate information about the deflection shapes of a vibrating structure than is presently available. From the accurate deflection shapes it is possible to derive the rotational responses. However, although it is possible to measure all the translational and rotational responses by these techniques, there is still no method for excitation of the structure with a pure torque.

1.2.3 Structural Modification Methods

Structural modification methods can be divided into two groups: (a) FRF Impedance Coupling methods, and (b) Modal Synthesis methods. The analytical basis for the impedance coupling method is described in the standard reference work by Bishop & Johnson [41], and implementation of the method for practical structures is discussed by many authors, such as Ewins [42], Goyder [29], and Lamonita [43]. The basic theory for the modal synthesis method can be found in works by Snyder [44] and Lang [45], and an adaptation of the method has been developed by Luk and Mitchell [46][47].

In theory, both the impedance coupling and modal synthesis coupling methods should give the same results. In practice, however, each method has limitations which should be clearly understood if assessment of the results is to be valid. Reviews of both categories of modification methods have been conducted by Craig [48] and Jones [49] which show the strengths and weaknesses of each type. FRF impedance coupling methods have the advantages that out-of-range modes can be incorporated easily through the use of residual terms and the final results of the modification prediction are in the most convenient form for assessing the overall performance of the coupled structure – FRFs. Residual terms cannot easily be incorporated directly into the model if a modal synthesis method is used [88], and the immediate results of this type of analysis are in terms of eigenvalues and eigenvectors – one stage removed from the FRFs of the modified structure. However, the modal synthesis method does have one major advantage over the impedance method, computationally it is very much simpler. Recently though, development of the impedance coupling method by Jetmundsen, Bielawa and Flannelly [50] has made this method more efficient, especially for large structural models with few coupling points, narrowing the gap with modal synthesis methods quite considerably.

1.2.4 Sensitivity Aspects

As the design of structures has grown more and more scientific, the structures have become highly efficient in terms of their utilization of materials. Although this is particularly relevant to aerospace structures, where unnecessary structural mass detracts from the available payload, the trend is filtering down to more everyday objects, driven by the ever-increasing cost of raw materials. If modification of a structure is necessitated by some unwanted operational characteristics, then the efforts to produce an efficient, economical structure in the first place can be negated by a clumsy approach to the design and siting of a modification. Studies of the sensitivity of a structure to various changes have led to the concept of sensitivity analysis, whereby more efficient modifications can

be designed and selected. In an early allusion to sensitivity, Jones [51] considers the effect of small changes in mass and stiffness on the natural frequencies of a vibrating system, and concludes that the change in any mode frequency, for a given modification, is partly dependent upon the value of that frequency in relation to those of the other modes of the system. Other work [52], [53] and [54] has shown that it is the relationship of the resonances to the anti-resonances that is of greater importance than the spacing of the resonances alone.

Many of the sensitivity analysis techniques have their roots in F.E. analysis, with early references to rates of change of eigenvalues and eigenvectors by Fox and Kapoor [55]. More recently, sensitivities of eigenvalues and eigenvectors have been studied extensively by Vanhonacker [56][57], where the emphasis is placed on methods requiring the input of modal analysis data only. However, the methods involve lengthy calculation procedures and rely quite heavily on the identified eigenvector matrices, even for the eigenvalue derivatives. Rather than using the sensitivity analysis results solely as a method for identifying types and locations for modifications, Vanhonacker has used the techniques for the prediction of the effects of small or large changes. In some instances, this has necessitated the use of 2^{nd} order sensitivities of eigenvalues and eigenvectors. Equations for the 2^{nd} order sensitivities are even more complicated than those for the 1^{st} order sensitivities. In a similar analysis procedure, Chou [58] notes that the calculation of higher order sensitivities becomes too complicated to be practical and To [89] suggests that use of higher order sensitivities in prediction of modified resonance frequencies may not be beneficial in all cases. Furthermore, the accuracy with which the actual behaviour of the structure is represented by these higher order sensitivities must be questioned, especially if the input data for the calculations are derived from measurements.

A different approach to sensitivity analysis was initiated by the discovery, in 1972 by Vincent [59], that the locus of a point response to a single excitation at a fixed frequency when a single structural (M, K, or C) parameter was varied, was circular when plotted in the Argand plane. The plots are similar to Nyquist plots, where frequency is varied while the structural parameters remain constant. Developments of what has become known as the Vincent Circle theorem, have been made by Done, Hughes and Webby [60][61], in which simultaneous modifications of two structural parameters are considered, and feasible regions of the response points in the Argand plane are identified. Several other developments have also been reported; Gaukroger [62] considers the application of the method to undamped structures, for which the characteristic circles degenerate into straight lines, and it is argued that this application of the analysis gives greater insight into the effect of structural modifications than it does when applied to damped systems. In

extending the ideas yet further to include many points of interest and many simultaneous structural parameter changes, Sobey [63][64] exceeds the capabilities of the circle presentation and reverts to consideration of a mean square weighted response function. A strain energy method is presented by Hanson [65] in which structural elements with the highest strain energy are targeted for modification. The results are compared closely with those of Vincent's Circle analyses, and although the same elements were identified for modification it was concluded that the strain energy method was more suitable when many elements are to be considered for changes simultaneously.

A different technique for sensitivity analysis has been developed by this author [66] which is based on the use of experimental FRF data directly, and produces the differential eigenvalue sensitivities to point mass or stiffness changes. The input data are resonance and anti-resonance frequencies and can be obtained directly from measured FRFs – no modal analysis is necessary – which can be a considerable advantage in preliminary investigations.

1.3 Review of the Present State-of-the-Art of Modal Testing and Analysis

As indicated in the literature survey, there are numerous different methods for data collection. In recent years, increasingly sophisticated techniques have been developed to meet the requirements for extensive quantities of high quality data. These developments have resulted in very expensive and complex packages of computer controlled measuring equipment and analysis software. In order to obtain the best results from these systems, the user must have a detailed knowledge of how the data are processed. As the test and analysis systems become more complicated, the number of people who really know how they work and how to run them to their best advantage becomes smaller. A great deal of insight into many vibration problems can be gained by proper use of the simplest equipment coupled with a thorough knowledge and understanding of basic vibration measurement and analysis theory. Extension of the basic theory with straightforward, easy to implement, techniques for data assessment seems to have been eclipsed by these more glamorous methods.

One area in which a great deal more work is required is that of assessing the quality and accuracy of measured data. Preferably, this assessment should be available as soon as possible after the data are measured so that repeat measurements can be made, if necessary, without delay. Some assessment methods presently available are too remote from the data collection phase to be of any real use – in all but research applications.

Throughout the course of this work, the vector difference FRF (AFRF) has been used very successfully for the clear assessment of various types of data, e.g. repeatability, reciprocity, raw data vs synthesised data, etc. All the data assessment methods, including the AFRF, are used to provide an indication of the quality of the data only. The absolute accuracy of measured vibration data (i.e. X ± Y%) is very difficult to quantify because an 'exact answer' is only available for comparison in purely theoretical studies. With experimentally measured data there are so many unknowns and possible sources of error (structure loading by the measuring equipment, transducer calibration errors, digitization errors, etc.) that normal error analysis methods yield unrealistic error bands. Generally, there is no substitute for painstaking attention to detail for the collection of good, high quality data. However, as the emphasis tends towards collection of greater quantities of data, the quality will undoubtedly suffer as a result of the associated tedium felt by operators. The problem is that large measurement surveys are often approached with a 'sledge hammer' method – measure everything in sight, just in case it turns out to be important at a later stage. If it is known from preliminary analysis that certain coordinates are particularly sensitive to modification, and therefore important, there is more incentive to make these measurements accurately. While no quantitative assessment can be made, a sensitivity analysis can provide a ranking of the degrees-of-freedom in their order of importance for altering the frequency of a particular mode. When testing time and resources are limited, this information can be of great value in helping to decide which data should be measured and which measurements can be eliminated. The concept of sensitivity studies is not new (see section 1.2.4) but, once again, it is important that the techniques can be readily implemented at an early enough stage in any vibration measurement program for subsequent use of the results in the design of modifications and formulation of the full measurement test schedule. A criticism of sensitivity analysis methods presently available is that they do not produce results at a sufficiently early stage to be useful. The sensitivity analysis method developed during the course of this work provide; results that are available soon after measurement of the data, and without the need for modal analysis.

Mathematical methods for prediction of the effects of a structural modification on the dynamic characteristics of a structure are well developed in theory (impedance and modal coupling methods). However, there is still scope for development of the practical implementation of these coupling techniques. Experimentally-derived vibration data are neither accurate nor complete and both these deficiencies can have a significant influence on the quality of coupling prediction results. Furthermore, use of numerical computational algorithms in the coupling prediction calculations (especially for matrix inversion in the impedance coupling method) can also give rise to errors. Computers have a finite accuracy

and the number of repetitive operations required in the numerical inversion of a large matrix can cause errors to build up quickly. Such problems will be exacerbated at frequencies close to the natural frequencies of the structure and modification components when the matrices become nearly singular and the computations take much longer to converge to a solution, if at all. As the size of the dynamic models increases, the computational time for modification predictions escalates rapidly. A large proportion of the time is taken up with calculations involving passenger coordinates. Passenger coordinate information is not required for calculation of global properties of the modified structure but for calculation of the local properties only. The computational effort is not used in the most efficient manner. Several new formulations of the impedance coupling method are presented in this work that improve the way in which the calculations are performed. The number of matrix inversions is reduced by a factor of three and the size of the matrix for inversion is cut down to the number of interface coordinates. When the ratio of interface coordinates to passenger coordinates is small, very substantial improvements in computational speed are achieved.

There is a definite requirement for some research into the ‘accuracy’ of results that can be achieved from coupling predictions based on experimentally-derived data. If, for instance, only a portion of the required input data are available, what will be the effect on the final results and will it be worthwhile continuing the study if it is not feasible to measure all of the data?

1.4 Outline and Scope of this Work

The work presented in this thesis can be divided into four sections,

(i) a review of impedance and modal coupling theories with some recent developments of the impedance coupling method that can improve the calculation speed and efficiency very significantly;

(ii) the development of a simple sensitivity analysis technique which indicates the most efficient sites for the modification, working from data collected during a preliminary survey of a structure;

(iii) an investigation of the practical aspects of vibration testing that influence the type, quantity and quality of data that can be collected. Additionally, the consequences of some of the practical measurement limitations on the results from a coupling analysis have been studied; and,

(iv) the techniques, analysis methods and assessment tools developed in the theoretical stages of this study have been applied to the measurement of a modem helicopter and subsequent study of some simple modifications. In this demonstration of the present ability to predict the effects of modifications using experimentally-derived data, theoretical predictions of the effects of modifications are compared critically with the measured results when the actual modifications are made.

One aim of this work is a demonstration of the present ability to predict the effects of a simple practical modification on a real structure (chapter 6). It was intended that rotational information should be included in these predictions but rotational measurements proved to be beyond the capabilities of the apparatus and techniques and, therefore, the modifications were limited to those in which rotational degrees-of-freedom could be ignored. Although the resulting predictions for the dynamic characteristics of the modified structure showed the correct trends, there were still some discrepancies between the exact detail of the predicted and measured FRFs for the modified structure. These differences have been traced to alterations in the base structure's properties not considered in the modification. Even with knowledge of the possible cause of the problem, its solution would have necessitated very many more FRF measurements for a range of contrived loading conditions. Such measurements may have enabled correct prediction of the actual measured result, but these measurements were not the type that would be made as part of a normal measurement survey.

Although this study is primarily aimed at devising methods for aerospace structures, the techniques will be equally applicable to other structures which have a less demanding or restrictive vibration environment.

Chapter 2

Structural Modification – Theoretical Basis

2.1 Introduction

Mathematical techniques for the prediction of the effects that a modification will have on a structure's vibration characteristics are commonly known as structural modification or coupling methods. The great advantage of such techniques is that they do not involve extensive trial and error procedures on the structure itself – any modification refinement procedures are carried out on the the mathematical model of the structure. Whichever method of structural modification prediction is used, the accuracy of the final results will depend heavily upon the quality and extent of the mathematical models of the base component(s). Therefore, it is absolutely vital that the mathematical model of the structure is a true and accurate representation of the characteristics of the real structure. Discussion of whether or not the model is an accurate representation will be left until chapters 4 and 5.

In this chapter, the main methods of structural modification prediction are presented and reviewed, with emphasis placed on experimentally-based techniques.

2.1.1 Structural Modification Methods

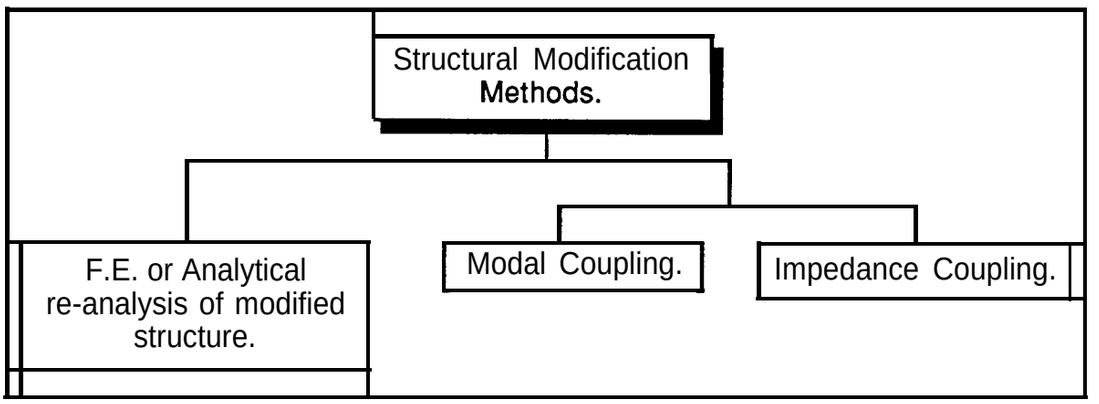

Techniques for prediction of the Effects of Structural Modifications.

Figure 2.1

Methods for the prediction of the behaviour of modified structures can be divided into three categories, as shown in Figure 2.1. The least flexible of the three methods is complete F.E. or theoretical **re-analysis** of the modified structure – in effect, the equations of motion for the complete modified structure are derived and solved. Such methods are of greatest use in the design stages of a project when there is no physical example of the structure available for test.

It is possible to address a vibration problem using measured modal properties and this is the basis of the modal coupling method as presented here. Alternatively, instead of modal properties, the impedance coupling method uses **FRFs** directly. The impedance coupling method has some advantages when the structure has a high modal density and an infinite number of modes (where consideration of residuals becomes important with the modal coupling method: chapter 5) but, generally, the impedance method has the disadvantage that a large quantity of data is involved.

Modal coupling and impedance coupling methods are predominantly experimentally-based methods, but they can also be used with the appropriate data derived from F.E. or analytic models. This can be especially useful when investigating the effects of a theoretical modification to an actual structure, where the properties of the modification may be derived from an analytical or F.E. model and the structure is represented by measured parameters. Whichever coupling method is adopted, an important assumption which is made is that the structure is **linear.** At the present time, there are no experimentally based procedures for including the effects of non-lineatities and any non-linear analytic or F.E. based methods are highly computational and require complete definition of the non-linear elements. Providing that any non-linearities are not too great, acceptable predictions of the

2.1.1 Structural Modification Methods

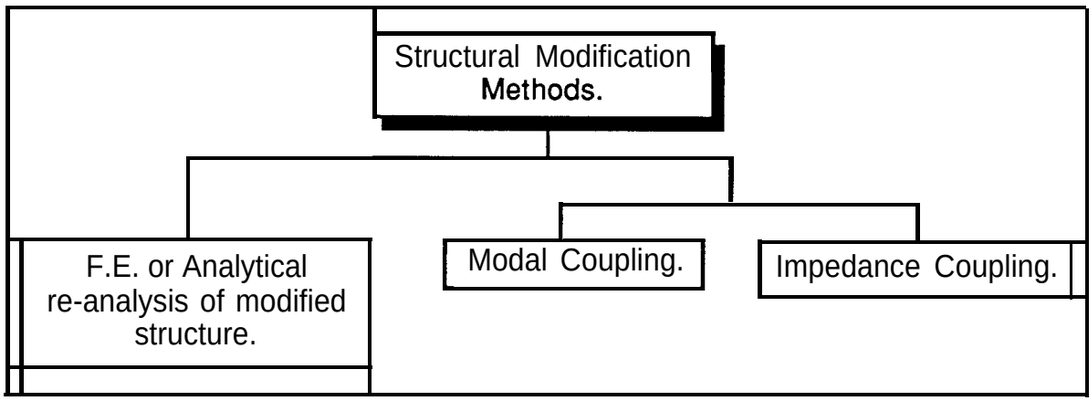

Techniques for prediction of the Effects of Structural Modifications.

Figure 2.1

Methods for the prediction of the behaviour of modified structures can be divided into three categories, as shown in Figure 2.1. The least flexible of the three methods is complete F.E. or theoretical **re-analysis** of the modified structure – in effect, the equations of motion for the complete modified structure are derived and solved. Such methods are of greatest use in the design stages of a project when there is no physical example of the structure available for test.

It is possible to address a vibration problem using measured modal properties and this is the basis of the modal coupling method as presented here. Alternatively, instead of modal properties, the impedance coupling method uses **FRFs** directly. The impedance coupling method has some advantages when the structure has a high modal density and an infinite number of modes (where consideration of residuals becomes important with the modal coupling method: chapter 5) but, generally, the impedance method has the disadvantage that a large quantity of data is involved.

Modal coupling and impedance coupling methods are predominantly experimentally-based methods, but they can also be used with the appropriate data derived from F.E. or analytic models. This can be especially useful when investigating the effects of a theoretical modification to an actual structure, where the properties of the modification may be derived from an analytical or F.E. model and the structure is represented by measured parameters. Whichever coupling method is adopted, an important assumption which is made is that the structure is **linear.** At the present time, there are no experimentally based procedures for including the effects of non-lineatities and any non-linear analytic or F.E. based methods are highly computational and require complete definition of the non-linear

effects of modifications may be obtained using a linearised model (or several piecewise linearised models). However, it is well known that the task of showing that a system contains a non-linearity is considerably easier than locating and identifying the type and magnitude of the non-linearity -- which is by no means straightforward.

The theory underlying the impedance coupling and modal coupling methods is presented in the following sections, together with brief comments on how and when each method should be used.

2.2 The Impedance Coupling Method

2.2.1 Theory

Prediction of the dynamic behaviour of a modified structure by means of the impedance coupling method requires the knowledge of a specific set of FRFs. As mentioned earlier, these FRFs may be derived from a number of different sources, but care must be taken to include the maximum amount of relevant data, i.e. number of points considered on the structures and the type and extent of the data; data for rotational degrees-of-freedom must be included along with that for translational degrees-of-freedom where necessary. In the illustrative example used below (Figures 2.2 and 2.3), degrees-of-freedom numbers 4 and 5 represent the interface coordinates (those actively involved in the coupling) while the remainder constitute passenger degrees-of-freedom which may be included to provide data for specific key points on the structure other than the modification points (e.g. the pilot's seat in an aircraft), or for purposes of identifying the modified mode shapes. The only data available here are a 5x5 FRF matrix for component A and a 4x4 FRF matrix for component B.

Consider the two components A and B, which are to be joined together in two degrees-of-freedom (4 and 5) to form component C.

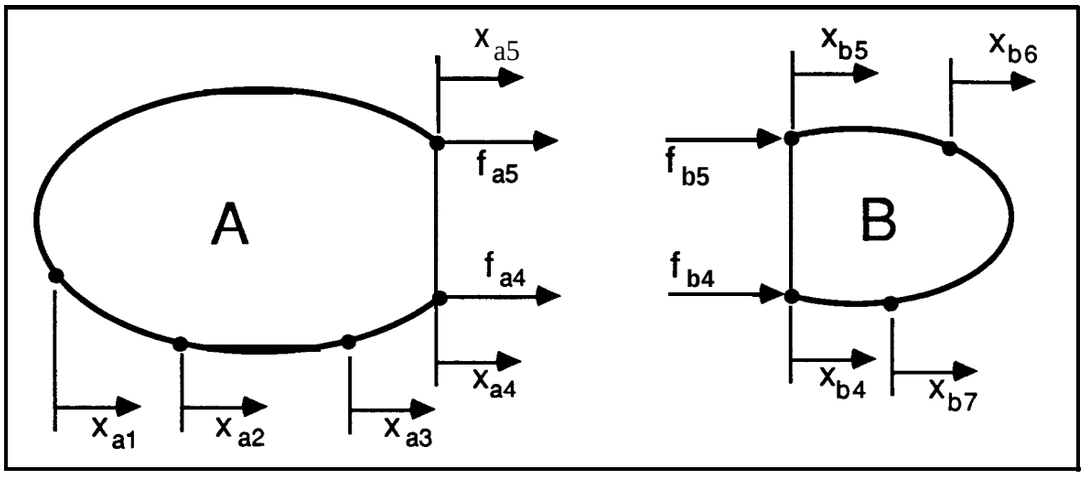

Definition of Coordinates for the Base Components.

Figure 2.2

In this statement of the impedance coupling method displacement and receptance quantities have been used for convenience. The final 'impedance coupling' equations derived (equations 2.10 and 2.11) are equally applicable for mobility or inertance data.

For compatibility of the displacements at the connection points,

$$x_{a5} = x_{b5} = x_{c5} \quad \text{and} \quad x_{a4} = x_{b4} = x_{c4} \qquad \ldots\ldots\ldots\ldots\ldots\ldots\ldots\ldots (2.1)$$

For equilibrium of the forces at the connection points,

$$f_{a5} + f_{b5} = f_{c5} \quad \text{and} \quad f_{a4} + f_{b4} = f_{c4} \qquad \ldots\ldots\ldots\ldots\ldots\ldots\ldots\ldots (2.2)$$

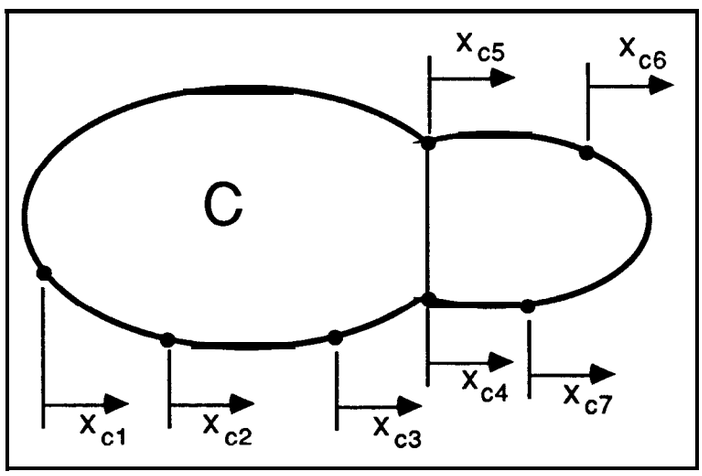

Coordinate Definition for the Modified Structure.

Figure 2.3

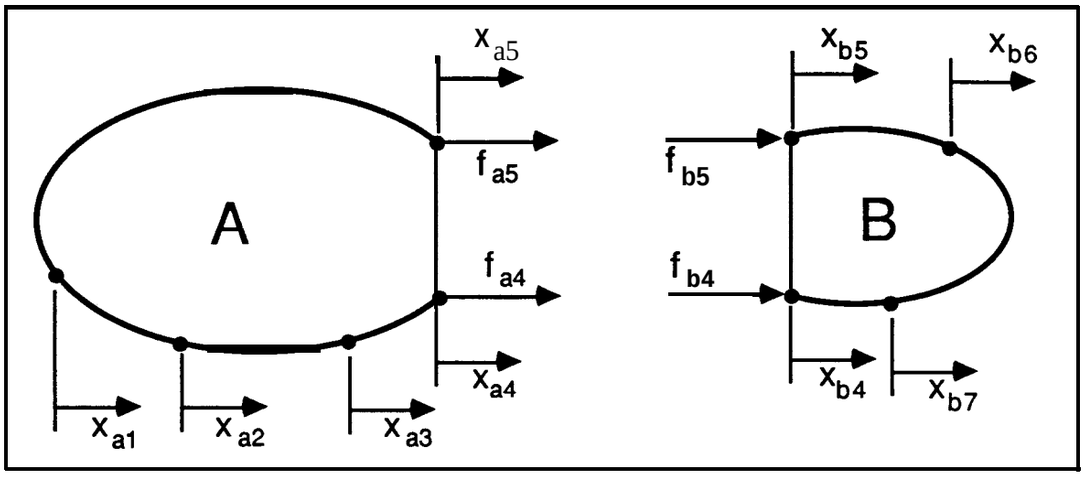

Definition of Coordinates for the Base Components.

Figure 2.2

In this statement of the impedance coupling method displacement and receptance quantities have been used for convenience. The final 'impedance coupling' equations derived (equations 2.10 and 2.11) are equally applicable for mobility or inertance data.

For compatibility of the displacements at the connection points,

$$x_{a5} = x_{b5} = x_{c5} \quad \text{and} \quad x_{a4} = x_{b4} = x_{c4} \qquad \ldots\ldots\ldots\ldots\ldots\ldots\ldots\ldots (2.1)$$

For equilibrium of the forces at the connection points,

$$f_{a5} + f_{b5} = f_{c5} \quad \text{and} \quad f_{a4} + f_{b4} = f_{c4} \qquad \ldots\ldots\ldots\ldots\ldots\ldots\ldots\ldots (2.2)$$

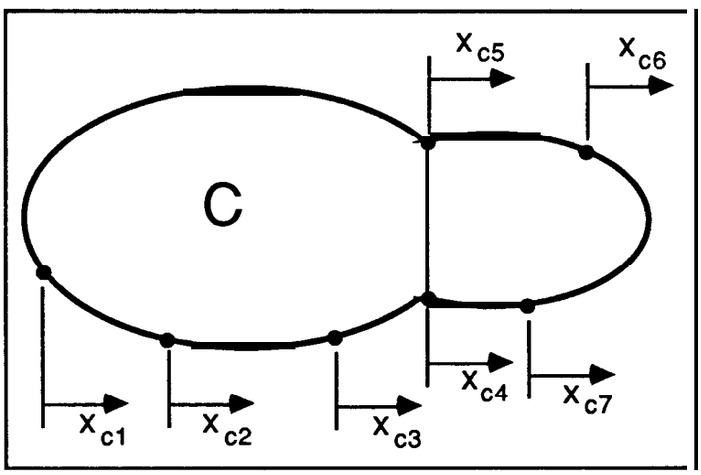

Coordinate Definition for the Modified Structure.

Figure 2.3

Now, receptance is defined as the ratio of the displacement to the applied force -

$$\text{Receptance } \alpha_{(\omega)} \equiv \frac{x.e^{i\omega t}}{f.e^{i\omega t}} \quad \ldots\ldots\ldots\ldots\ldots\ldots\ldots\ldots\ldots\ldots (2.3)$$

where, x = amplitude of harmonic displacement response,
f = amplitude of harmonic forcing,
$i = \sqrt{-1}$,
ω = frequency in radians/second, and
t = time.

Therefore, for component A, the receptance matrix is defined in the following way:

$$\begin{Bmatrix} x_{a1} \\ x_{a2} \\ x_{a3} \\ x_{a4} \\ x_{a5} \end{Bmatrix} = \begin{bmatrix} \alpha_{a(\omega)} \end{bmatrix} \cdot \begin{Bmatrix} f_{a1} \\ f_{a2} \\ f_{a3} \\ f_{a4} \\ f_{a5} \end{Bmatrix} \quad \ldots\ldots\ldots\ldots\ldots\ldots\ldots\ldots\ldots\ldots\ldots\ldots\ldots\ldots (2.4)$$

similarly, for component B and the resulting component C:

$$\begin{Bmatrix} x_{b4} \\ x_{b5} \\ x_{b6} \\ x_{b7} \end{Bmatrix} = \begin{bmatrix} \alpha_{b(\omega)} \end{bmatrix} \cdot \begin{Bmatrix} f_{b4} \\ f_{b5} \\ f_{b6} \\ f_{b7} \end{Bmatrix} \quad \ldots\ldots\ldots\ldots\ldots\ldots\ldots\ldots\ldots\ldots\ldots\ldots\ldots\ldots (2.5)$$

$$\begin{Bmatrix} x_{c1} \\ x_{c2} \\ x_{c3} \\ x_{c4} \\ x_{c5} \\ x_{c6} \\ x_{c7} \end{Bmatrix} = \begin{bmatrix} \alpha_{c(\omega)} \end{bmatrix} \cdot \begin{Bmatrix} f_{c1} \\ f_{c2} \\ f_{c3} \\ f_{c4} \\ f_{c5} \\ f_{c6} \\ f_{c7} \end{Bmatrix} \quad \ldots\ldots\ldots\ldots\ldots\ldots\ldots\ldots\ldots\ldots\ldots\ldots\ldots\ldots (2.6)$$

Assuming that each of the receptance matrices is non-singular, equations (2.4), (2.5) and (2.6) can be rearranged to give -

$$\{f_a\} = [\alpha_a]^{-1} . \{x_a\} \quad ; \{f_b\} = [\alpha_b]^{-1} . \{x_b\} \text{ and } \{f_c\} = [\alpha_c]^{-1} . \{x_c\} \quad \ldots.(2.7)$$

Now, invoking the equilibrium condition expressed in equation (2.2)

$$\{f_c\} = \{f_a\} \oplus \{f_b\} = \left([\alpha_a]^{-1} . \{x_a\}\right) \oplus \left([\alpha_b]^{-1} . \{x_b\}\right) \quad \ldots\ldots\ldots\ldots\ldots\ldots (2.8)$$

(where the $\oplus$ sign represents an addition with due regard for the physical nature of the coupling), and including the compatibility condition of equation (2.1), gives:

$$\{f_c\} = \left([\alpha_a]^{-1} \oplus [\alpha_b]^{-1}\right)\{x_c\} \quad \ldots\ldots\ldots\ldots\ldots\ldots\ldots\ldots\ldots\ldots (2.9)$$

and by comparison of equation (2.9) with equation (2.7): $\{f_c\} = [\alpha_c]^{-1} . \{x_c\}$

It can be seen that, $[\alpha_c]^{-1} = (w\text{-}1 \oplus [\alpha_b]^{-1})$ $\ldots\ldots\ldots\ldots\ldots\ldots\ldots\ldots\ldots\ldots\ldots\ldots (2.10)$

The receptance matrix for the coupled structure is formed by "adding" the receptance matrices of the constituent components. The form of this matrix "addition" is shown diagrammatically in Figure 2.4.

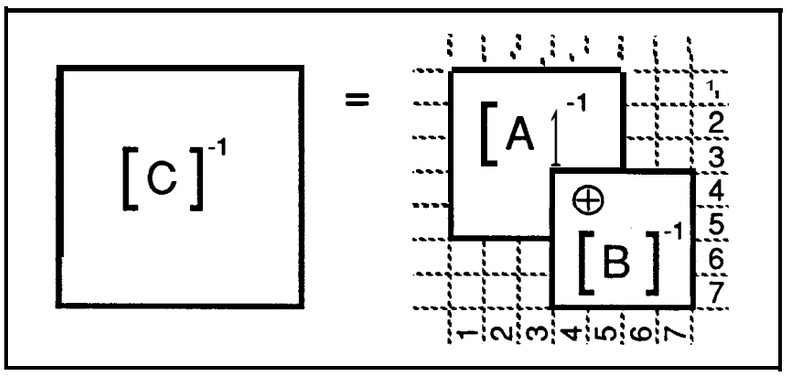

Diagrammatic Representation of Matrix "Addition".

Figure 2.4

For the special case of coupling in one degree of freedom and where interest is confined to the coupling degree-of-freedom, the matrices revert to single terms, and equation (2.10) becomes -

$$\frac{1}{\alpha_c} = \frac{1}{\alpha_a} + \frac{1}{\alpha_b} \quad \ldots\ldots\ldots\ldots\ldots\ldots\ldots\ldots\ldots\ldots (2.11)$$

2.2.2 Discussion of the Impedance Coupling Method

In concept, the impedance coupling method is very simple and can be used with FRF data derived from various different sources; F.E. model, analytic model or, more commonly, from test measurements. The results produced by the impedance coupling method are in the form of **FRFs** for the modified structure. These **FRFs** can be used directly in predictions of the forced response of a modified structure. Since the ultimate aim of a structural modification investigation is an improvement in the operating characteristics of the structure, having the results presented in FRF format is considered a desirable feature.

The FRF data produced using F.E. or analytic models is self-consistent – all the FRFs have exactly the same resonance frequencies – but they may be inaccurate owing to various simplifying assumptions which are inevitable with such models. Raw measured data, however, may be less extensive and may show the resonance frequencies for all the FRFs at slightly different frequencies – due to experimental or systematic errors in the measurements. However, measured data does include the effects of all the modes and any non-linear elements. The inconsistencies with measured data can give rise to numerical ill-conditioning problems in the inversion of the impedance matrices which can be overcome if the raw measured data are first subjected to modal analysis and then the FRFs are synthesised from the modal database. By definition, all the synthesised FRFs are consistent and the system has been linearised, but unless sufficient modes have been analysed, or residual terms are included in the synthesis, valuable information will be lost in the process.

The size of the matrices involved in the coupling procedure depends very much on the number of interface coordinates – those degrees-of-freedom actively involved in the coupling – and the number of additional points for which the modified behaviour is required – the 'passenger' coordinates. The minimum size of the matrices in any given coupling analysis is the number of interface coordinates, in which case characteristics of the modified system are only available for the interface coordinates. The global modal properties of the modified system – modified natural frequencies and dampings – can be obtained by modal analysis of the FRFs produced by the coupling analysis. As more and more passenger coordinates are included, for full characterisation of the modified mode shapes, the matrices quickly become large and, it should be remembered that three full matrix inversions are required for each frequency point considered. The large additional computational effort necessary at present prohibits the inclusion of numerous passenger coordinates. However, recent developments of the impedance coupling method – notably by Jetmundsen, Bielawa and Flannelly [SO] – have reduced the number of inversions at each frequency point from three to one, and the size of the matrix for inversion is only that of the number of interface coordinates, regardless of the number of passenger coordinates incorporated. In reference [50], the final result is quoted but in the following sections a derivation of the result and further adaptations are presented.

2.2.3 Reformulation of the Impedance Coupling Method

The basic coupling equation (2.10) can be expressed as:

$$[C]^{-1} = [A]\text{-}' \oplus [B]^{-1} \quad \text{.....} \quad (2.12)$$

where the ⊕ 'addition' reflects the physical coupling of the components.

Equation (2.12) can be written more formally as:

$$[C]^{-1} = \begin{bmatrix} [A^{-1}] & 0 \\ 0 & 0 \end{bmatrix} + \begin{bmatrix} 0 & 0 \\ 0 & [B^{-1}] \end{bmatrix} \quad \text{.....(2.13)}$$

The impedance matrices are augmented with zeros (zero matrices or vectors) to facilitate **direct** addition; the zeros in each matrix correspond with the degrees-of-freedom which are entirely related to the other component. The interface degrees-of-freedom are contained in the overlapping parts of the [A] and [B] matrices.

Unfortunately the augmented matrices of equation (2.13) are singular and cannot be inverted. However, the equation can be rewritten, without loss of generality, as:

$$[C]^{-1} = \begin{bmatrix} [A] & 0 \\ 0 & [I] \end{bmatrix}^{-1} + \begin{bmatrix} [I] & 0 \\ 0 & [B^{-1}] \end{bmatrix} - \begin{bmatrix} [I] & 0 \\ 0 & [I] \end{bmatrix}^{-1} \quad \text{.....(2.14)}$$

Small identity matrices are included in the augmented matrices and then subtracted again. By this means, the augmented matrices referring to components A and B become diagonal partitioned impedance matrices which **can be** formed by inversion of similar inertance **type** matrices.

$$[C]^{-1} = \begin{bmatrix} [A] & 0 \\ 0 & [I] \end{bmatrix}^{-1} + \begin{bmatrix} [I] & 0 \\ 0 & [B] \end{bmatrix}^{-1} - \begin{bmatrix} [I] & 0 \\ 0 & [I] \end{bmatrix}^{-1} \quad \text{.....(2.15a)}$$

Now, if we adopt the following notation:

$$[A_A] = \begin{bmatrix} [A] & 0 \\ 0 & [I] \end{bmatrix} \qquad [B_A] = \begin{bmatrix} [I] & 0 \\ 0 & [B] \end{bmatrix} \qquad [I_A] = \begin{bmatrix} [I] & 0 \\ 0 & [I] \end{bmatrix}$$

Equation (2.15a) becomes:

$$[C]^{-1} = [A_A]^{-1} + [B_A]^{-1} - [I_A] \quad \text{.....(2.15b)}$$

By appropriate pre- and post-multiplications, the following equation for the impedance of the coupled structure is obtained:

$$[C]^{-1} = [A_A]^{-1} ([B_A] + [A_A] - [A_A].[I_A].[B_A]) [B_A]^{-1} \quad \text{....(2.16)}$$

Inversion of both sides of this equation leads to an expression for the inertance of the coupled structure:

$$[C] = [B_A] ([B_A] + [A_A] - [A_A].[I_A].[B_A])^{-1} [A_A] \quad \text{.....(2.17)}$$

Now, we let

$$[A_A] = \begin{bmatrix} A_{11} & A_{12} & 0 \\ A_{21} & A_{22} & 0 \\ 0 & 0 & I \end{bmatrix} \quad \text{and} \quad [B_A] = \begin{bmatrix} I & 0 & 0 \\ 0 & B_{22} & B_{23} \\ 0 & B_{32} & B_{33} \end{bmatrix} \quad \text{.....(2.18)}$$

where the constituent elements A_{11}, A_{12},...etc. can be single numbers, sub-matrices or vectors. After some algebraic manipulation (given in Appendix A) we obtain the following expression,

$$[C] = \begin{bmatrix} A_{11} & A_{12} & 0 \\ A_{21} & A_{22} & 0 \\ 0 & 0 & B_{33} \end{bmatrix} - \begin{bmatrix} A_{12}.[A_{22}+B_{22}]^{-1}.A_{21} & A_{12}.[A_{22}+B_{22}]^{-1}.A_{22} & -A_{12}.[A_{22}+B_{22}]^{-1}.B_{23} \\ A_{22}.[A_{22}+B_{22}]^{-1}.A_{21} & A_{22}\,[A_{22}+B_{22}]^{-1}.A_{22} & -A_{22}.[A_{22}+B_{22}]^{-1}.B_{23} \\ -B_{32}.[A_{22}+B_{22}]^{-1}.A_{21} & -B_{32}.[A_{22}+B_{22}]^{-1}.A_{22} & B_{32}.[A_{22}+B_{22}]^{-1}.B_{23} \end{bmatrix}$$

or, more concisely as:

$$[C] = \begin{bmatrix} A_{11} & A_{12} & 0 \\ A_{21} & A_{22} & 0 \\ 0 & 0 & B_{33} \end{bmatrix} - \begin{Bmatrix} A_{12} \\ A_{22} \\ -B_{32} \end{Bmatrix} . [A_{22}+B_{22}]^{-1} . \{ A_{21} \; A_{22} \; -B_{23} \} \quad \text{.....(2.29)}$$

First, it will be noted that the number of matrix inversions has been reduced from three in the original method to one in the new approach. Second, the size of the matrix for inversion in the new method is only that of the number of interface coordinates. In most modification studies, the total size of the model is much greater than the number of interface coordinates and, therefore, reducing both the number of matrix inversions **and the** size of the matrix inversions represents a very large saving in computational time. Hence, the formulation of equation (2.29) is much more advantageous than that of the original coupling procedure, equation (2.10).

The first matrix of equation (2.28) is a representation of the unmodified characteristics of the base components, with A as the "reference" component. The second matrix of equation (2.28) is a difference matrix between the representations of the constituent components and the modified structure. Further consideration is given to these difference functions in later chapters.

The form of the result shown in equation (2.29) can be checked by a much simpler analysis, where interest is restricted to the interface degrees-of-freedom only.

$$[C]^{-1} = [A]^{-1} + [B]^{-1} \quad \ldots\ldots\ldots\ldots\ldots\ldots\ldots\ldots\ldots\ldots \quad (2.30)$$

$$[C]^{-1} = [A]^{-1}([B]+[A])[B]^{-1} \quad \ldots\ldots\ldots\ldots\ldots\ldots\ldots\ldots \quad (2.31)$$

$$[C] = [B]([B]+[A])^{-1}[A] \quad \ldots\ldots\ldots\ldots\ldots\ldots\ldots\ldots\ldots\ldots \quad (2.32)$$

or,
$$[C] = ([A]+[B]-[A])([B]+[A])^{-1}[A] \quad \ldots\ldots\ldots\ldots\ldots \quad (2.33)$$

and therefore,
$$[C] = [A] - [A]([B]+[A])^{-1}[A] \quad \ldots\ldots\ldots\ldots\ldots\ldots\ldots \quad (2.34)$$

In common with equation (2.29), the final result of this analysis, equation (2.34), only requires one matrix inversion and the inertance properties of the modified structure are given as those of the base component [A], together with a difference matrix-

$$[A]([B]+[A])^{-1}[A].$$

The new method has been tested for a system with component A having 6 degrees-of-freedom (3 passenger degrees-of-freedom and 3 interface degrees-of-freedom) and component B having 3 degrees-of-freedom, all of which relate to the interface. The results for the modified structure were found to be identical to those obtained using the standard method, and approximate timing of the computations showed the new method to be 2.5 times faster than the original. For larger models with proportionally fewer interface degrees-of-freedom compared with the total number of degrees-of-freedom of interest, the savings will be substantially greater.

2.2.4 Refinement of Method for Spring Modification Components

One disadvantage of the new method, as presented above, is that it does not permit the use of idealised spring element modifications on their own. All the dynamic property matrices

required in the new method are of the inertance **'form'** of (response/force), i.e. inertance, mobility, or receptance – but such matrices do not exist for simple spring elements. However, a further refinement can be made for such cases:

Assume that the modifying component consists only of spring elements, and that the points of interest are confined to the main structure A, i.e. the modification component is described solely by $[B_{22}]^{-1}$, the impedance matrix for the interface degrees-of-freedom of component B. For convenience, we shall make the following substitution:

$$[B_{22}]^{-1} = [\beta_{22}]$$

Therefore, equation (2.13) becomes -

$$[C]^{-1} = \begin{bmatrix} A_{11} & A_{12} \\ A_{21} & A_{22} \end{bmatrix}^{-1} + \begin{bmatrix} 0 & 0 \\ 0 & \beta_{22} \end{bmatrix} \qquad \text{(2.35)}$$

re-arrangement gives:

$$[C]^{-1} = \begin{bmatrix} A_{11} & A_{12} \\ A_{21} & A_{22} \end{bmatrix}^{-1} \cdot \left[\begin{bmatrix} I & 0 \\ 0 & I \end{bmatrix} + \begin{bmatrix} A_{11} & A_{12} \\ A_{21} & A_{22} \end{bmatrix} \begin{bmatrix} 0 & 0 \\ 0 & \beta_{22} \end{bmatrix} \right] \qquad \text{(2.36)}$$

and inversion of the whole equation produces:

$$[C] = \left[\begin{bmatrix} I & 0 \\ 0 & I \end{bmatrix} + \begin{bmatrix} A_{11} & A_{12} \\ A_{21} & A_{22} \end{bmatrix} \begin{bmatrix} 0 & 0 \\ 0 & \beta_{22} \end{bmatrix} \right]^{-1} \begin{bmatrix} A_{11} & A_{12} \\ A_{21} & A_{22} \end{bmatrix} \qquad \text{(2.37)}$$

or,
$$[C] = \left[\begin{bmatrix} I & 0 \\ 0 & I \end{bmatrix} + \begin{bmatrix} 0 & A_{12}\beta_{22} \\ 0 & A_{22}\beta_{22} \end{bmatrix} \right]^{-1} \begin{bmatrix} A_{11} & A_{12} \\ A_{21} & A_{22} \end{bmatrix} \qquad \text{(2.38)}$$

From which it can be shown that:

$$[C] = \begin{bmatrix} A_{11} & A_{12} \\ A_{21} & A_{22} \end{bmatrix} - \begin{Bmatrix} A_{12} \\ A_{22} \end{Bmatrix} [\beta_{22}] [I + A_{22}\beta_{22}]^{-1} \{ A_{21} \; A_{22} \} \qquad \text{(2.39)}$$

Where the A_{ii} elements are inertance sub-matrices, and $[\beta_{22}]$ is an impedance matrix.

This formulation retains the advantage that there is only one matrix inversion and the size of this matrix is limited to the number of interface degrees-of-freedom.

2.3 The Modal Coupling Method

2.3.1 Theory

The classical matrix equation of motion for forced vibration of a non-proportionally damped multi-degree of freedom system can be written as-

$$[M]\{\ddot{x}\} + [C]\{\dot{x}\} + [K]\{x\} = \{F\} \quad \ldots\ldots\ldots\ldots\ldots\ldots (2.40)$$

[M] = mass matrix.
[C] = viscous damping matrix.
[K] = stiffness matrix.

all these matrices are square (N by N) and it is assumed that they are all symmetric.

If N is the order of the system (number of modes), the matrix equation consists of N second order differential equations in $\{x\}$. Using the method developed by Frazer, Duncan and Collar [67], these N second order differential equations can be transformed into 2N first order differential equations by changing the variables -- transformation into 2N space.

Introduce the variable $(v) = \{\dot{x}\}$, and rewrite equation (2.40) as -

$$[M]\{\dot{v}\} + [C]\{\dot{x}\} + [K]\{x\} = \{F\} \quad \ldots\ldots\ldots\ldots\ldots\ldots (2.41)$$

With the identity $[M]\{\dot{x}\} - [M]\{v\} = \{0\}$ ..... (2.42)

Now, combine these equations to form the single matrix equation -

$$\begin{bmatrix} 0 & M \\ M & C \end{bmatrix}\begin{Bmatrix} \dot{v} \\ \dot{x} \end{Bmatrix} + \begin{bmatrix} -M & 0 \\ 0 & K \end{bmatrix}\begin{Bmatrix} v \\ x \end{Bmatrix} = \begin{Bmatrix} 0 \\ F \end{Bmatrix} \quad \ldots\ldots\ldots\ldots\ldots\ldots (2.43)$$

The matrices and vectors are all now of order 2N. For free vibration, the problem reduces to:

$$\begin{bmatrix} 0 & M \\ M & C \end{bmatrix}\begin{Bmatrix} \dot{v} \\ \dot{x} \end{Bmatrix} + \begin{bmatrix} -M & 0 \\ 0 & K \end{bmatrix}\begin{Bmatrix} v \\ x \end{Bmatrix} = \{0\} \quad \ldots\ldots\ldots\ldots\ldots\ldots (2.44)$$

and assume the following form of solution:

$$\{x\} = \{\phi\} e^{\lambda t} \quad \text{..... (2.45)}$$

where λ is a complex variable.

Therefore, $\{v\} = \{\dot{x}\} = \lambda \{\phi\} e^{\lambda t}$ ..... (2.46)

and, $\{\dot{v}\} = \{\ddot{x}\} = \lambda^2 \{\phi\} e^{\lambda t}$ ..... (2.42)

Substituting equations (2.45), (2.46) and (2.47) into equation (2.44), and simplifying;

$$\left[\begin{bmatrix} 0 & M \\ M & C \end{bmatrix} \lambda_r \begin{Bmatrix} \lambda_r \phi_r \\ \phi_r \end{Bmatrix} + \begin{bmatrix} -M & 0 \\ 0 & K \end{bmatrix} \begin{Bmatrix} \lambda_r \phi_r \\ \phi_r \end{Bmatrix} \right] e^{\lambda_r t} = \{0\} \quad \text{.....(2.48)}$$

and therefore,

$$\left[\lambda_r \begin{bmatrix} 0 & M \\ M & C \end{bmatrix} + \begin{bmatrix} -M & 0 \\ 0 & K \end{bmatrix} \right] \begin{Bmatrix} \lambda_r \phi_r \\ \phi_r \end{Bmatrix} = \{0\} \quad \text{.....(2.49)}$$

where λ_r is an eigenvalue of the unmodified system
and, $\{\phi_r\}$ is an eigenvector of the unmodified system.

The orthogonality relations are stated as:

$$[\phi]^T \begin{bmatrix} 0 & M \\ M & C \end{bmatrix} [\phi] = [I] \quad \text{.....(2.50)}$$

$$[\phi]^T \begin{bmatrix} -M & 0 \\ 0 & K \end{bmatrix} [\phi] = -[\lambda 1 \quad \text{..... (2.5 1)}$$

where: $[\phi] = \left[\begin{Bmatrix} \lambda_r \phi_r \\ \dots \\ \phi_r \end{Bmatrix} : \begin{Bmatrix} \lambda_r^* \phi_r^* \\ \dots \\ \phi_r^* \end{Bmatrix} \right]$, a matrix of all the eigenvectors for the unmodified system in 2N space, and $[\lambda] = \begin{bmatrix} \lambda_r & & \\ \dots & \dots & \dots \\ 0 & & \lambda_r^* \end{bmatrix}$, a diagonal matrix of the associated eigenvalues. (N.B. here, the * superscript denotes complex conjugate.)

For a Stiffness Modification

Following the derivation in [45], assume that a stiffness modification, [AK], is made between two points, such that the modification may be described by the following equation,

$$[AK] = k.(t)\{t\}^T \quad \text{.....(2.52)}$$

where: k is the spring stiffness and (t) is a tie vector which describes the physical connections. For example, the tie vector for a single spring connected between two degrees-of-freedom would be $\{t\} = \begin{Bmatrix} 0 \\ \vdots \\ 1 \\ \vdots \\ -1 \\ \vdots \\ 0 \end{Bmatrix}$, with 1 and -1 at the connection degrees-of-freedom only.

Taking similar steps to those for the derivation of equation (2.44), the following eigenvalue problem can be derived for the modified system:

$$\begin{bmatrix} 0 & M \\ M & C \end{bmatrix} \begin{Bmatrix} \dot{v} \\ \dot{x} \end{Bmatrix} + \begin{bmatrix} -M & 0 \\ 0 & K+\Delta K \end{bmatrix} \begin{Bmatrix} v \\ x \end{Bmatrix} = \{0\} \quad \text{..... (2.53)}$$

This system of equations could be solved by a standard eigensolution, but this requires knowledge of the original [M], [K], and [C] matrices. When the problem is approached from the experimental side, these matrices will not be known and the following form of solution is adopted:

assume a new form of solution

$$\{x) = \{\Phi\} e^{\Lambda t} \quad \text{.....(2.54)}$$

where Λ is a complex eigenvalue of the modified system
and $(\Phi\}$ is an eigenvector of the modified system.

Therefore, $(v\} = \{\dot{x}\} = A\{\Phi\} e^{\Lambda t}$ ..... (2.55)

and $\{\dot{v}\} = \{\ddot{x}\} = \Lambda^2\{\Phi\} e^{\Lambda t}$ ..... (2.56)

leading to the following equation for the free vibration of the modified system:

$$\left[\Lambda_r \begin{bmatrix} 0 & M \\ M & C \end{bmatrix} + \begin{bmatrix} -M & 0 \\ 0 & K \end{bmatrix} + \begin{bmatrix} 0 & 0 \\ 0 & \Delta K \end{bmatrix} \right] \begin{Bmatrix} \Lambda_r \Phi_r \\ \Phi_r \end{Bmatrix} = \{0\} \quad \text{.....(2.57)}$$

Now, the original eigenvector matrix $[\phi]$ is made up from a set of orthogonal eigenvectors and hence the new eigenvector can be formed from a weighted summation of the original eigenvectors. Therefore, assume:

$$\begin{Bmatrix} \Lambda_r \Phi_r \\ \Phi_r \end{Bmatrix} = [\phi] \{W_r\} \quad \text{..... (2.58)}$$

where $\{W_r\}$ is the weighting vector, and substitute this equation into equation (2.57) to give:

$$\left[\Lambda_r \begin{bmatrix} 0 & M \\ M & C \end{bmatrix} + \begin{bmatrix} -M & 0 \\ 0 & K \end{bmatrix} + \begin{bmatrix} 0 & 0 \\ 0 & \Delta K \end{bmatrix} \right] [\phi] \{W_r\} = \{0\} \quad \text{..... (2.59)}$$

Now, expand and pre-multiply through by $[\phi]^T$:

$$\left[\Lambda_r [\phi]^T \begin{bmatrix} 0 & M \\ M & C \end{bmatrix} [\phi] + [\phi]^T \begin{bmatrix} -M & 0 \\ 0 & K \end{bmatrix} [\phi] + [\phi]^T \begin{bmatrix} 0 & 0 \\ 0 & \Delta K \end{bmatrix} [\phi] \right] \{W_r\} = \{0\} \quad \text{..(2.60)}$$

and employ the orthogonality relations stated in equations (2.50) & (2.5 1) to give:

$$\left[\Lambda_r [\ I\ ] - [\ \lambda\ ] + [\ \phi]^T \begin{bmatrix} 0 & 0 \\ 0 & \Delta K \end{bmatrix} [\phi] \right] \{W_r\} = \{0\} \quad \text{.....(2.61)}$$

From equation (2.52), [AK] = k.(t) $\{t\}^T$ and by extending the tie vectors to 2N space, with zeros,

$$\begin{bmatrix} 0 & 0 \\ 0 & \Delta K \end{bmatrix} = k. \begin{Bmatrix} 0 \\ t \end{Bmatrix} \begin{Bmatrix} 0 \\ t \end{Bmatrix}^T \quad \text{..... (2.62)}$$

then, $$\left[\Lambda_r [\ I\ ] - [\ \lambda\ ] + k [\phi]^T \begin{Bmatrix} 0 \\ t \end{Bmatrix} \begin{Bmatrix} 0 \\ t \end{Bmatrix}^T [\phi] \right] \{W_r\} = \{0\} \quad \text{.....(2.63)}$$

If we now define a new vector, $$\{U\} = [\phi]^T \begin{Bmatrix} 0 \\ t \end{Bmatrix} \quad \text{.....(2.64)}$$

then, $$\left[\Lambda_r[\,I\,] - [\,\lambda\,] + k\{U\}\{U\}^T\right]\{W_r\} = \{0\} \qquad (2.65)$$

or, $$\left[\Lambda_r[\,I\,] - [\,\lambda\,]\right]\{W_r\} + k\{U\}\{U\}^T\{W_r\} = \{0\} \qquad (2.66)$$

The vector product $\{U\}^T\{W_r\}$ is a scalar quantity, which we shall define as μ_r (unknown).

Thus, $$\left[\Lambda_r[\,I\,] - [\,\lambda\,]\right]\{W_r\} + \mu_r k\{U\} = \{0\} \qquad (2.67)$$

and hence, $$\{W_r\} = -\mu_r k\left[\Lambda_r[\,I\,] - [\,\lambda\,]\right]^{-1}\{U\} \qquad (2.68)$$

Therefore,

$$\begin{Bmatrix}\Lambda_r\Phi_r\\ \Phi_r\end{Bmatrix} = [\phi]\{W_r\} = -\mu_r k[\phi]\left[\Lambda_r[\,I\,] - [\,\lambda\,]\right]^{-1}\{U\} \qquad (2.69)$$

Substitute equation (2.68) into equation (2.65) to yield -

$$-\mu_r k\left[\Lambda_r[\,I\,] - [\,\lambda\,] + k\{U\}\{U\}^T\right]\left[\Lambda_r[\,I\,] - [\,\lambda\,]\right]^{-1}\{U\} = \{0\} \qquad (2.70)$$

or, $$-\mu_r k\left[[\,I\,] + k\{U\}\{U\}^T\left[\Lambda_r[\,I\,] - [\,\lambda\,]\right]^{-1}\right]\{U\} = \{0\} \qquad (2.71)$$

Now, pre-multiply through by $\{U\}^T$

$$-\mu_r k\{U\}^T\{U\} - \mu_r k^2\{U\}^T\{U\}\{U\}^T\left[\Lambda_r[\,I\,] - [\,\lambda\,]\right]^{-1}\{U\} = 0 \qquad (2.72)$$

Note that $-k\{U\}^T\{U\}$ is a scalar constant, and can be divided out, so that:

$$\mu_r\left[1 + k\{U\}^T\left[\Lambda_r[\,I\,] - [\,\lambda\,]\right]^{-1}\{U\} = 0\right. \qquad (2.73)$$

I

and, for $\mu_r \neq 0$:

$$1 + k\{U\}^T \left[\Lambda_r[I] - [\lambda]\right]^{-1} \{U\} = 0 \quad \text{.....(2.74)}$$

$$\frac{1}{k} + \{U\}^T \left[\Lambda_r[I] - [\lambda]\right]^{-1} \{U\} = 0 \quad \text{.....(2.75)}$$

Now, $\left[\Lambda_r[I] - [\lambda]\right]^{-1}$ is a diagonal matrix, so its inverse consists simply of the reciprocal of the individual diagonal elements, and hence equation (2.75) can be rewritten without the use of matrix notation as -

$$\frac{1}{k} + \sum_{n=1}^{2N} \left(\frac{U_n^2}{\Lambda_r - \lambda_n}\right) = 0 \quad \text{.....(2.76)}$$

This is a polynomial in Λ_r which can be solved to give the new natural frequencies for the modified system. Substitution of these values into equation (2.69) enables the corresponding eigenvectors to be calculated. Subsequently, modal synthesis may then be used to generate the FRFs for the modified system.

Mass or Damping Modifications

From equation (2.52) onwards, the analysis has been for a stiffness modification. Other simple types of idealised modification are also possible, such as damping modifications and mass modifications. By similar analysis to that described above for a stiffness modification, it is found that equation (2.76) is replaced by -

$$\frac{1}{C\Lambda_r} + \sum_{n=1}^{2N} \left(\frac{U_n^2}{\Lambda_r - \lambda_n}\right) = 0 \quad \text{.....(2.77)}$$

for a damping modification.

The analysis for a mass modification is made easier if, instead of the identity of equation (2.42), we use

$$[K]\{\dot{x}\} - [K]\{v\} = \{0\} \quad \text{.....(2.78)}$$

and then stack the equations (2.41) and (2.78) as follows -

$$\begin{bmatrix} M & C \\ 0 & K \end{bmatrix} \begin{Bmatrix} \dot{v} \\ \dot{x} \end{Bmatrix} + \begin{bmatrix} 0 & K \\ -K & 0 \end{bmatrix} \begin{Bmatrix} v \\ x \end{Bmatrix} = \begin{Bmatrix} F \\ 0 \end{Bmatrix} \quad \ldots\ldots\ldots\ldots\ldots\ldots\ldots\ldots (2.79)$$

The analysis is, once again, similar to that described above for the stiffness modification and it is found that equation (2.76) is replaced by -

$$\frac{1}{m\Lambda_r} + \sum_{n=1}^{2N} \left(\frac{V_n^2}{\Lambda_r - \lambda_n} \right) = 0 \quad \ldots\ldots\ldots\ldots\ldots\ldots\ldots\ldots (2.80)$$

for a mass modification. The important difference between this equation and equations (2.76) and (2.77) is in the definition of the numerator of the summation. For equations (2.76) and (2.77), the numerators are formed from components of the vector (U), given by equation (2.64),

$$\{U\} = [\phi]^T \begin{Bmatrix} 0 \\ t \end{Bmatrix}$$

For equation (2.80) the numerators in the summation are formed from components of the vector $\{V\}$.

where, $\{V\} = [\theta]^T \begin{Bmatrix} t \\ 0 \end{Bmatrix}$ ..... (2.8 1)

and, $[\theta]$ is the eigenvector matrix for equation (2.79)

The modal coupling method requires knowledge of the eigenvalues and eigenvectors of the unmodified system only and the mass, stiffness and damping descriptions of the modification.

2.4 Discussion of Coupling Methods

2.4.1. Practicalities for Implementation of the Coupling Methods

It can be seen that the modal coupling method requires much less input data than the impedance coupling method – simply because the modal description of the vibration characteristics of a structure is more compact than a corresponding description using FRFs. In both of these coupling methods, the vibration properties of the modified

structure are produced in the same format as the input data, i.e. for the modal coupling method, input and output data are in the form of modal and/or spatial parameters. Modal parameter description of the vibration characteristics is not the most useful since, frequently, the object of the modification exercise is to improve the operational performance, characterised by forced response functions, and these must be derived from appropriate weighted summations of the frequency response functions. These are available directly from the impedance coupling method, but in the case of the modal coupling method, must be generated in a further stage of analysis.

When applying the modal coupling method, it is important to recall some of the assumptions made in the modal analysis stages of the process. The basis of modal analysis is that the behaviour of a structure can be described by a sum of all the (N) modal contributions. This can be expressed for a single FRF as:

$$\alpha_{jk}(\omega) = \sum_{r=1}^{N} \left(\frac{{}_r\phi_j \, {}_r\phi_k}{\Omega_r\zeta_r + i\,(\omega - \Omega_r\sqrt{1-\zeta_r^2})} + \frac{{}_r\phi_j^* \, {}_r\phi_k^*}{\Omega_r\zeta_r + i\,(\omega + \Omega_r\sqrt{1-\zeta_r^2})} \right)$$

..... (2.82)

In practical applications, this series is truncated to the number of modes measured, with the implicit assumption that the contribution to the response of the modes which have not been measured is negligible; i.e. the response can be described completely by a linear summation of the **measured** modes. When a modification is made, the structure will exhibit new response characteristics. Now, using the modal coupling method for predicting the modified response, it can be seen that the new eigenvectors (mode shapes) are simply formed from weighted summations of the original eigenvectors – equation (2.69). Therefore, ultimately, the response of the modified structure is still described by summation of the **original measured** modes. This assumes that the actual modified response can still be described adequately by the original measured modes. If the modification brings into play a higher mode of vibration, not incorporated in the original measured set, then the modified response can no longer be described by the original set of measured modes and the result predicted from the analysis will be erroneous. Elliott [7] terms this effect 'modal insufficiency'. Bolted beam stiffener type modifications tend to cause these effects because the stiffeners restrain rotary motion which is a more important feature than translational motion in the higher order modes -just those modes that are left out of the base model.

2.4.2 Equivalence of Coupling Methods

By comparison of the terms in equation (2.76) for a point SDoF modification, with equation (2.82), it can be seen that:

$$\sum_{n=1}^{2N}\left(\frac{U_n^2}{\Lambda_r-\lambda_n}\right)\equiv\sum_{r=1}^{N}\left(\frac{{}_r\phi_k\,{}_r\phi_k}{\Omega_r\zeta_r+i\,(\omega-\Omega_r\sqrt{1-\zeta_r^2})}+\frac{{}_r\phi_k^*\,{}_r\phi_k^*}{\Omega_r\zeta_r+i\,(\omega+\Omega_r\sqrt{1-\zeta_r^2})}\right)$$

$$=\alpha_{kk} \qquad \text{..... (2.83)}$$

and hence that equation (2.76) can be m-written as:

$$\frac{1}{k}+\alpha_{kk}(\Omega_r)=0 \qquad \text{..... (2.84)}$$

with Ω_r as the new natural frequencies of the modified system.

Now, it has been shown that using the impedance coupling method for a SDoF modification, equation (2.1 1), leads to the following equation for the natural frequencies for a system modified by the addition of an idealised single degree-of-freedom spring component:

$$0=\frac{1}{\alpha_a}+k$$

and therefore,

$$\frac{1}{k}+\alpha_a=o \qquad \text{..... (2.85)}$$

Equations (2.84) and (2.85) are identical.

Provided **complete** representations of the systems are used, the impedance coupling and modal coupling methods are equivalent.

2.5 Review of Chapter 2

In this chapter two methods for predicting the effects of a structural modification have been presented – the impedance coupling method and the modal coupling method. Both of these techniques can be used with data derived from experimental measurements of the base structure and the modification component. The modal coupling method uses a more concise form of description for the dynamic characteristics (a modal model) than the

impedance coupling method (a response model; FRFs). However, the data required for assessment of the performance of a modification are usually FRFs or a forced response solution and thus the impedance coupling results are directly applicable.

The results obtained by use of either method will be identical providing that the dynamic description of the base components is accurate and complete. When the dynamic models are derived from measured data, the results of the coupling predictions can differ quite substantially unless steps are taken to account for the effects of out-of-range modes.

Developments of the impedance coupling method have been made which improve the computational speed and efficiency very significantly. These improvements reduce both the number of matrix inversions and the size of the matrices for inversion and the effects will be particularly apparent when there are relatively few interface coordinates compared with the number of passenger coordinates. This situation is encountered frequently in the assessment of modifications to aerospace structures where the physical modifications tend to be localised but their effects must be investigated for the whole of the structure. Actually, the ideal modification would be a small localised modification that had a major beneficial effect on the dynamic behaviour of the whole of the structure. In this way the modification would not reduce the available pay-load or accessibility by very much.

The new formulation of the impedance coupling method is not applicable for stiffness type modifications because the method requires impedance descriptions of the components which are not available for an idealised spring element. To overcome this restriction a further refinement of the method was undertaken to yield a suitable form of the equation that could accept the impedance description of simple spring elements directly.

By use of these new impedance coupling methods with data derived from experimental structural measurement surveys there is no apparent deterioration in the accuracy of the results but a very marked improvement in the speed of calculation.

Chapter 3

Sensitivity Analysis

3.1 Introduction

In the past, the initial selection and design of structural modifications to solve a vibration problem have been dependent largely upon the expertise of people who have worked for many years on the particular types of structures and their associated vibration problems. Selection of a suitable modification is more a matter of “this worked before for a similar problem” rather than design of a new modification for the particular case. The intention should be to select the most efficient type of modification, at the earliest possible stage and, for this, it is advantageous to know the sensitivities of the resonance frequencies to particular types of simple modification.

3.2 Background

3.2.1 The Behaviour of Resonance Frequencies on Grounding a Single Degree-of-Freedom

When a single degree-of-freedom (coordinate) of a structure is grounded, the resonance frequencies all shift downwards to what were the point anti-resonance frequencies for the degree-of-freedom which has been grounded. Consider the impedance coupling equation for a general spring type modification, equation (2.34)

$$[C] = \begin{bmatrix} A_{11} & A_{12} \\ A_{21} & A_{22} \end{bmatrix} - \begin{Bmatrix} A_{12} \\ A_{22} \end{Bmatrix} [\beta_{22}] [I + A_{22}\beta_{22}]^{-1} \{ A_{21} \; A_{22} \}$$

A **refers** to inertances of the unmodified structure; and,

β refers to impedances of the spring modification.

For a single degree-of-freedom modification equation (2.34) can be simplified to,

$$[C] = \begin{bmatrix} A_{11} & A_{12} \\ A_{21} & A_{22} \end{bmatrix} - \left(\frac{\beta_{22}}{1 + A_{22}\beta_{22}} \right) \begin{Bmatrix} A_{12} \\ A_{22} \end{Bmatrix} \{ A_{21} \; A_{22} \} \quad \ldots\ldots\ldots\ldots\ldots\ldots\ldots (3.1)$$

Now, since

$$\frac{\beta_{22}}{1 + A_{22}\beta_{22}} = \frac{1}{\frac{1}{\beta_{22}} + A_{22}}$$

and as the impedance of the spring, β_{22}, tends to infinity (the structure becomes grounded at the modification point), $\frac{1}{\beta_{22}}$ tends to zero, so that equation (3.1) becomes -

$$[C] = \begin{bmatrix} A_{11} & A_{12} \\ A_{21} & A_{22} \end{bmatrix} - \frac{1}{A_{22}} \begin{bmatrix} A_{12}A_{21} & A_{12}A_{22} \\ A_{22}A_{21} & A_{22}A_{22} \end{bmatrix} \quad \ldots\ldots\ldots\ldots\ldots (3.2)$$

Thus,

$$[C] = \begin{bmatrix} \left[A_{11} - \frac{A_{12}A_{21}}{A_{22}} \right] & \{0\} \\ \{0\} & 0 \end{bmatrix} \quad \ldots\ldots\ldots\ldots\ldots\ldots\ldots\ldots\ldots (3.3a)$$

In summary, by grounding a single degree-of-freedom, the order of the system is reduced by one, and the remaining FRFs for the modified system may be calculated from the matrix equation;

$$[C_{11}] = \left[A_{11} - \frac{A_{12}A_{21}}{A_{22}} \right] \quad \ldots\ldots\ldots\ldots\ldots\ldots\ldots\ldots\ldots\ldots\ldots\ldots (3.3b)$$

The new resonance frequencies are given by the solution of $A_{22} = 0$ .It should be noted that $A_{22} = 0$ is the equation for the anti-resonance frequencies of the point FRF for the unmodified structure at location 2; i.e. the new resonance frequencies are identical to the old anti-resonance frequencies of the point FRF at the location of the single degree-of-freedom modification.

3.2.2 The Behaviour of Anti-Resonance Frequencies on Grounding a Single Degree-of-Freedom

The anti-resonance frequencies of certain FRFs do not alter when a structure is modified in a single degree-of-freedom. In particular, the anti-resonance frequencies of FRFs having at least one degree-of-freedom in common with the single degree-of-freedom modification remain unchanged. All the other anti-resonances are affected by the modification.

Example

The behaviour of the resonance frequencies and the point anti-resonance frequencies for a structure with a single degree-of-freedom modification are illustrated by this following example. A mass is attached at the tip of a free-free beam in one transverse translational degree-of-freedom only. The point FRF for the modification degree-of-freedom is plotted in Figure 3.1 for several values of added mass. It can be seen that there are no changes in the anti-resonance frequencies but that the resonance frequencies all shift, progressively, down towards the preceding anti-resonances. The maximum possible frequency shifts for this modification are given by the separation of the anti-resonances and the resonances, i.e. R_n-AR_n. If a grounded spring was attached in place of the mass, the resonances would shift up towards the succeeding anti-resonances and the maximum possible frequency shifts for this modification would be given by the separation of the resonance and anti-resonance frequencies, i.e. AR_{n+1}-R_n.

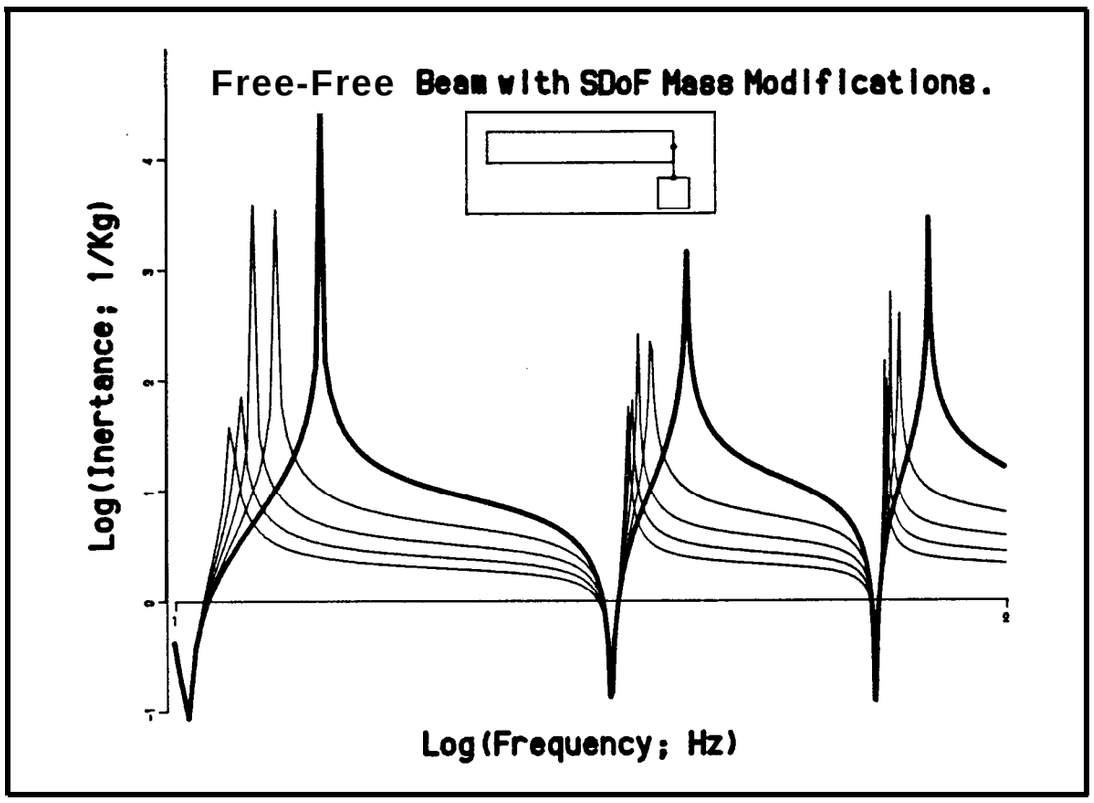

Example – SDoF Mass Modification to the Tip of a Free-Free Beam.

Figure 3.1

It is interesting to consider what happens at the limits, where the mass or stiffness of a single degree-of-freedom modification is infinite. From a practical viewpoint there is no difference between attaching an infinite mass at a point or connecting that point to ground through a spring of infinite stiffness. In the above example however, the resonance frequencies move in opposite directions for mass and stiffness modifications (as would be expected), leading to apparently different states at the limits. Fortunately, it can be shown, mathematically, that the results as the mass or stiffness modifications reach infinity are identical. As an illustration of this point, consider the following simple 2DoF system:

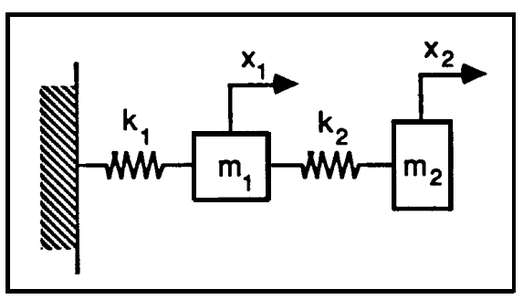

2 DoF Mass-Spring System.

For which the natural frequencies are given by;

$$\omega^2 = \frac{(k_1m_2+k_2m_2+k_2m_1) \pm \sqrt{(k_1m_2+k_2m_2+k_2m_1)^2 - 4m_1m_2k_1k_2}}{2m_1m_2} \quad \ldots\ldots\ldots (3.4)$$

(i) 'Ground' the structure by letting m_1 tend to infinity, to obtain,

$$\omega^2 = \frac{(k_2 \pm k_2)}{2\ m_2} \quad \ldots\ldots\ldots (3.5)$$

Therefore, $\omega^2 = \frac{k_2}{m_2}$ or, $\omega^2 = 0$ ……(3.6)

(ii) Now 'ground' the structure by letting k_1 tend to infinity, to obtain,

$$\omega^2 = \frac{(m_2 \pm m_2)}{0} \quad \ldots\ldots\ldots (3.7)$$

Therefore, $\omega^2 = \infty$ or, $\omega^2 = \frac{0}{0}$, which is indeterminate.

In this case, L'Hospital's Rule must be used to find the limit , giving $\omega^2 = \frac{k_2}{m_2}$, the same as for (i) above.

It should be noted, however, that the modes indicated as having natural frequencies of 0 Hz and ∞ Hz are degenerate modes because the modal constants for these modes are identically zero. The order of the system is reduced from two to one; grounding a degree-of-freedom reduces the system order by one.

3.2.3 Physical Interpretation of the fact that Anti-resonances of certain FRFs do not move when Single Degree-of-Freedom Modifications are made

In order to provide a physical explanation of this phenomenon it is first necessary to understand the nature of an anti-resonance. An anti-resonance is defined as a frequency at which the ratio of the response at a point to a force input tends to zero. This can happen when there is zero response at location i, or when infinite force is required at location j. Both these conditions can be related to nodal points (points of zero motion) in the deflection shape of the structure at that particular excitation frequency. If the response location is at a nodal point (Figure 3.2), then it is obvious that there will be an anti-resonance at this frequency in the FRF. Alternatively, if the excitation location is at a nodal point this will also give rise to an anti-resonance because an infinite force will be necessary to achieve any response.

In summary, the anti-resonances are the set of frequencies for which there are nodal points in the deflection shape of the structure at either the response location i or the excitation location j.

Now, consider the effects of a single degree-of-freedom mass modification at location k, at a single frequency, for an arbitrary structure with the operating deflection shape at this frequency shown in Figure 3.2. At this particular frequency the unmodified structure has a nodal point in the deflection shape at location k.

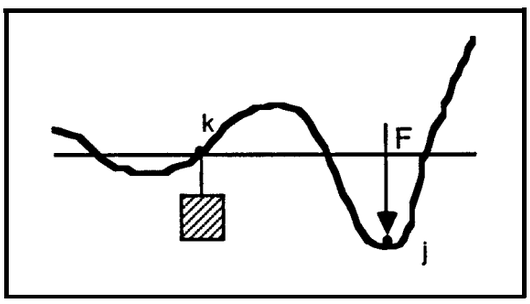

Figure 3.2

There is no translational motion at location k and so a modification in this single translational degree-of-freedom will have no effect on the structure and, hence, no effect on any of the anti-resonances for FRFs with the force or response location at k, i.e. the anti-resonance frequencies will remain unchanged for all the FRFs in the k^{th} row and k^{th} column of the FRF matrix, Figure 3.3.

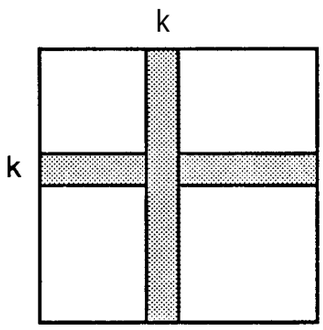

Figure 3.3

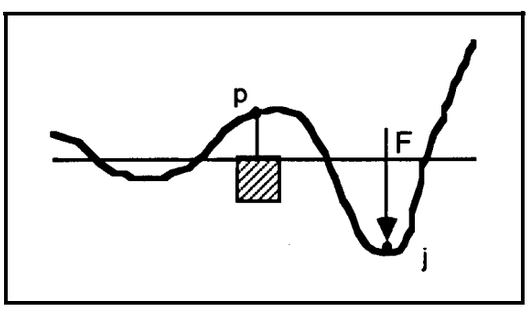

Figure 3.4

If the modification is made at a point (p) which is not at a nodal point, Figure 3.4, the modification will affect the structural behaviour. There will no longer be nodal points at the original locations on the structure and, hence, all the anti-resonances are shifted.

In this illustration, the single degree-of-freedom modification is considered to be the translational motion of a mass. Consequently, all subsequent discussion relates to the

translational motion of the structure and the mass. If the rotational motion of the mass had been chosen as the modification degree-of-freedom, the relevant nodal points on the structure would have been positioned very differently. The nodal points, referred to above, are nodal points in the translational sense; they are not nodal points in the rotational sense. The rotational nodal points are at positions of zero slope, at the peaks and troughs of the operating deflection shape shown, whereas the translational nodal points are at the positions of zero deflection.

As a useful indication of whether or not any given modification can be considered a single degree-of-freedom modification, the converse of this criterion is used – if all the anti-resonance frequencies for the FRFs involving the single modification degree-of-freedom remain the same as for the unmodified state, then the modification is indeed single degree-of-freedom. Otherwise, it can be stated that the modification is effective in more than one degree-of-freedom. This test can be implemented very easily at the time of measurement and can save a large amount of wasted effort by identifying, at an early stage, that the modification is not in a single degree-of-freedom.

How is this of practical use? Various authors [23], [77] have proposed methods for verification of a modal database by comparison of the predicted and measured results for a simple modification – the assumption being that if the predicted and measured results exhibit a high level of agreement, then the modal database is sufficiently extensive and accurate. The simple modification often chosen is that of a single degree-of-freedom mass addition. Now, if the actual modification made is not in a single degree-of-freedom the two sets of results (predicted and measured) do not represent the same modified structure and direct comparisons are meaningless. A simple check of the anti-resonance frequencies for the measured FRF data will show whether the modification made is effective in a single degree-of-freedom only and whether any further comparison of the measured and predicted results is worthwhile. Careful inspection of the anti-resonances for the point FRF data presented in [77] shows that there are noticeable shifts and, hence, that the modifications assumed to be in a single degree-of-freedom are, in fact, active in more than one degree-of-freedom and so the supposed validation of the modal database is fallacious.

As mathematical proof of this observation, consider equation (2.29) applied for a single degree-of-freedom modification in degree-of-freedom number 2, where the elements A_{22} and B_{22} are single numbers.

$$[C] = \begin{bmatrix} A_{11} & A_{12} \\ A_{21} & A_{22} \end{bmatrix} - \begin{Bmatrix} A_{12} \\ A_{22} \end{Bmatrix} . [A_{22}+B_{22}]^{-1} . \{ A_{21} \; A_{22} \} \qquad \ldots.(3.8)$$

$$\text{hence, } [C] = \begin{bmatrix} A_{11} & A_{12} \\ A_{21} & A_{22} \end{bmatrix} - \frac{1}{A_{22}+B_{22}} \begin{bmatrix} A_{12}A_{21} & A_{12}A_{22} \\ A_{22}A_{21} & A_{22}A_{22} \end{bmatrix} \quad \ldots\ldots\ldots\ldots\ldots\ldots\ldots\ldots (3.9)$$

Now the anti-resonance frequencies can be found for the modified system by solving the equations individually for $C_{ij} = 0$:

For C_{11} : the coordinates of component A that are not actively involved in the modification at the coupling interface (the passenger coordinates for component A).

$$C_{11} = A_{11} - \frac{A_{12}A_{21}}{A_{22}+B_{22}} = 0 \quad \ldots\ldots\ldots\ldots\ldots\ldots\ldots\ldots\ldots\ldots (3.10)$$

Since $\frac{A_{12}A_{21}}{A_{22}+B_{22}} \neq 0$ for all ω, there will be new anti-resonance frequencies for the modified FRFs associated with these passenger coordinates of component A.

For **C_{12} and C_{21}.**

$$C_{12} = A_{12} - \frac{A_{12}A_{22}}{A_{22}+B_{22}} = A_{12}\left(1 - \frac{A_{22}}{A_{22}+B_{22}}\right) = o \quad \ldots\ldots\ldots\ldots\ldots\ldots\ldots (3.11)$$

Since $B_{22} \neq 0$, A_{12} must be equal to zero for the identity to be true, and hence the anti-resonance frequencies for C_{12} & A_{12} are the same. By' symmetry, this also applies for C_{21}.

For **C_{22}.**

$$C_{22} = A_{22} - \frac{A_{22}A_{22}}{A_{22}+B_{22}} = A_{22}\left(1 - \frac{A22}{A_{22}+B_{22}}\right) = o \quad \ldots\ldots\ldots\ldots\ldots\ldots\ldots (3.12)$$

Again, $B_{22} \neq 0$ and therefore $A_{22} = 0$, hence the anti-resonance frequencies for C_{22} & A_{22} are the same also; i.e. the anti-resonance frequencies for the $\{C_{12}\}$, $\{C_{21}\}$, and $\{C_{22}\}$ elements of the modified structure are identical to those of the $\{A_{12}\}$, $\{A_{21}\}$, and $\{A_{22}\}$ elements of the component structure respectively. The anti-resonance frequencies remain unchanged for all the FRFs that have at least one force or response coordinate in common with the single degree-of-freedom modification (at location 2 in this case).

As an example, consider the following simple 2 degree-of-freedom mass and spring system shown in Figure 3.5.

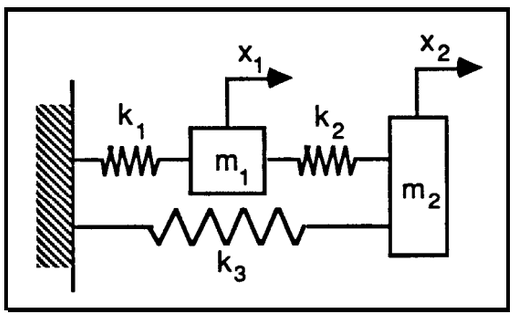

Example 2 DoF Mass & Stiffness System.

Figure 3.5

The matrix equation of motion is -

$$\begin{bmatrix} m_1 & 0 \\ 0 & m_2 \end{bmatrix}\begin{Bmatrix} \ddot{x}_1 \\ \ddot{x}_2 \end{Bmatrix} + \begin{bmatrix} (k_1+k_2) & -k_2 \\ -k_2 & (k_2+k_3) \end{bmatrix}\begin{Bmatrix} x_1 \\ x_2 \end{Bmatrix} = \begin{Bmatrix} f_1 \\ f_2 \end{Bmatrix} \quad \ldots\ldots\ldots\ldots\ldots\ldots (3.13)$$

from which, $[\alpha_{(\omega)}] = [[K] - \omega^2[M]]^{-1}$

$$= \frac{1}{\det}\begin{bmatrix} (k_2+k_3)-\omega^2 m_2 & k_2 \\ k_2 & (k_1+k_2)-\omega^2 m_1 \end{bmatrix} \quad \ldots\ldots\ldots\ldots (3.14)$$

with, $\det = \omega^4(m_1m_2) - \omega^2(k_1m_2+k_2m_1+k_2m_2+k_3m_1) + k_1k_2 + k_1k_3 + k_2k_3$ ..... (3.15)

The natural frequencies are given by setting the determinant to zero; i.e. det = 0. The anti-resonance frequencies are given by setting the terms in $[\alpha_{(\omega)}]$ to zero, individually. Hence, there are no anti-resonances for the off-diagonal terms in this example, since $k_2 \neq 0$, equation (3.14).

α_{11} has an anti-resonance at a frequency of $\sqrt{\frac{k_2+k_3}{m_2}}$ rads/sec. ..... (3.16)

and,

α_{22} has an anti-resonance at a frequency of $\sqrt{\frac{k_1+k_2}{m_1}}$ rads/sec. ..... (3.17)

It will be noticed that equation (3.16) for the anti-resonance frequency for α_{11} does not contain either k_1 or m_1 ; the parameters that would be altered in single degree-of-freedom modifications at point 1. Therefore, this anti-resonance frequency is unaffected by such modifications at point 1. Similarly,equation (3.17) for the anti-resonance frequency of α_{22} does not contain either k_3 or m_2 , the parameters involved in single degree-of-freedom modification at point 2.

3.2.4 Insufficiency of Anti-resonance to Resonance Frequency Separation Alone, as an Indication of Sensitivity

Although it has been concluded that the separation of the resonance and anti-resonance frequencies is important in deducing the sensitivity of a mode to a single degree-of-freedom modification at a certain point, [51] and [52], the separations of the resonance and anti-resonance frequencies in the point FRFs are not sufficient alone. The 'effective mass' of the mode in that FRF (as defined by the Salter Skeleton [28]) also plays an important role. If the separation between the resonance frequency of a mode and the preceding anti-resonance frequency is the same for two point FRFs, then the point with the smaller 'effective mass' for that mode will be the more sensitive. Consider the following example for a 2DoF system, Figure 3.6.

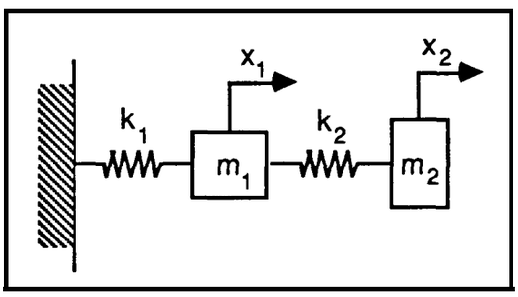

let $m_1=2$ Kg ; $m_2=1$ Kg
$k_1=k_2=1000$N/m.

Example 2DoF System.

Figure 3.6

For free vibration,

$$\begin{bmatrix} m_1 & 0 \\ 0 & m_2 \end{bmatrix}\begin{Bmatrix} \ddot{x}_1 \\ \ddot{x}_2 \end{Bmatrix}+\begin{bmatrix} (k_1+k_2) & -k_2 \\ -k_2 & k_2 \end{bmatrix}\begin{Bmatrix} x_1 \\ x_2 \end{Bmatrix} = \begin{Bmatrix} 0 \\ 0 \end{Bmatrix} \quad \text{.....(3.18)}$$

and the resonance frequencies (equivalent to the natural frequencies in this case) are obtained by solution of the equation formed by setting the determinant of $[[K] - \omega^2[M]]$ to zero – a quadratic equation in ω^2.

$$\omega^4(m_1m_2) - \omega^2(k_1m_2+k_2m_1+k_2m_2) + k_1k_2 = 0 \quad \text{.....(3.19)}$$

This results in resonance frequencies of 2.7238 Hz and 6.5758 Hz. The anti-resonance frequencies for the point FRFs for locations 1 and 2 are given by $\sqrt{\frac{k_2}{m_2}}$ and $\sqrt{\frac{k_1+k_2}{m_1}}$ respectively. For the system with the properties shown above, the anti-resonance frequencies are identical, and equal to 5.0329 Hz. A plot of the point FRFs for locations 1 and 2 is shown in Figure 3.7.

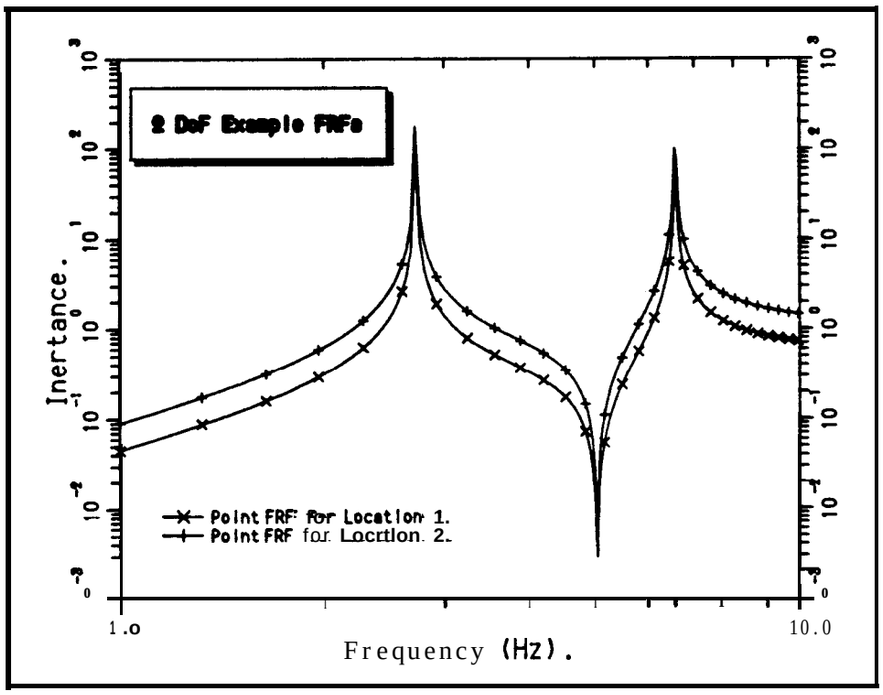

Point FRFs for the Example 2DoF System.

Figure 3.7

Although the FRFs display the same resonance and anti-resonance frequencies, the 'effective mass' and 'effective stiffness' characteristics are different. For the 1st mode, the effective masses (m_e) are given by -

$$m_e = \frac{k_e}{\omega^2} \qquad \text{.....(3.20)}$$

where, k_e = effective stiffness; the low frequency asymptotic stiffness value.

At point 1, $k_e = k_1$ and at point 2, $k_e = \frac{k_1 k_2}{k_1 + k_2}$, giving the effective mass for mode number 1 at point 1 as 3.41 Kg and the effective mass for mode number 2 at point 1 as 1.7 1 Kg. Therefore it is concluded that since the anti-resonance frequencies are equal, because point 2 has the smaller effective mass for mode number 1 it will be more sensitive to single degree-of-freedom modification than point 1. This reasoning is borne out by the variation of the resonance frequency for mode number 1 to single degree-of-freedom modifications at points 1 and 2 respectively, which is shown in the graph of Figure 3.8. The modifications were achieved by connecting a further spring (k_3) between the point in question and ground.

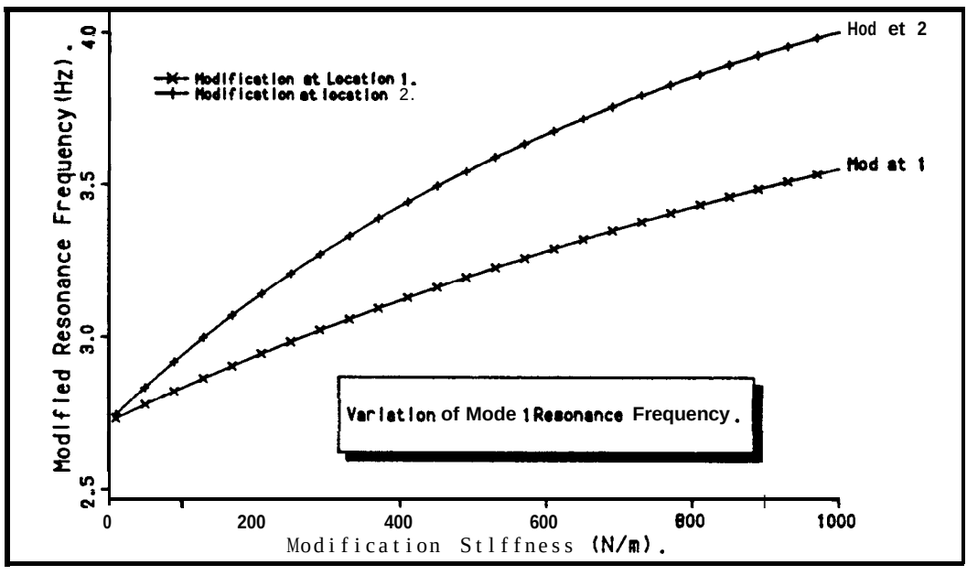

Variation of Mode 1 Resonance Frequency for Different SDoF Stiffness Modifications.

Figure 3.8

If we focus attention on mode number 2, the effective masses are; for point 1, 2 Kg, and, for point 2,1 Kg (the reciprocals of the high frequency asymptotic values of the inertance in each case). Once again, point 2 has the smaller effective mass and therefore will be the more sensitive location for the purposes of modification. The variation of mode number 2 resonance frequencies with different single degree-of-freedom stiffness modifications is shown in Figure 3.9.

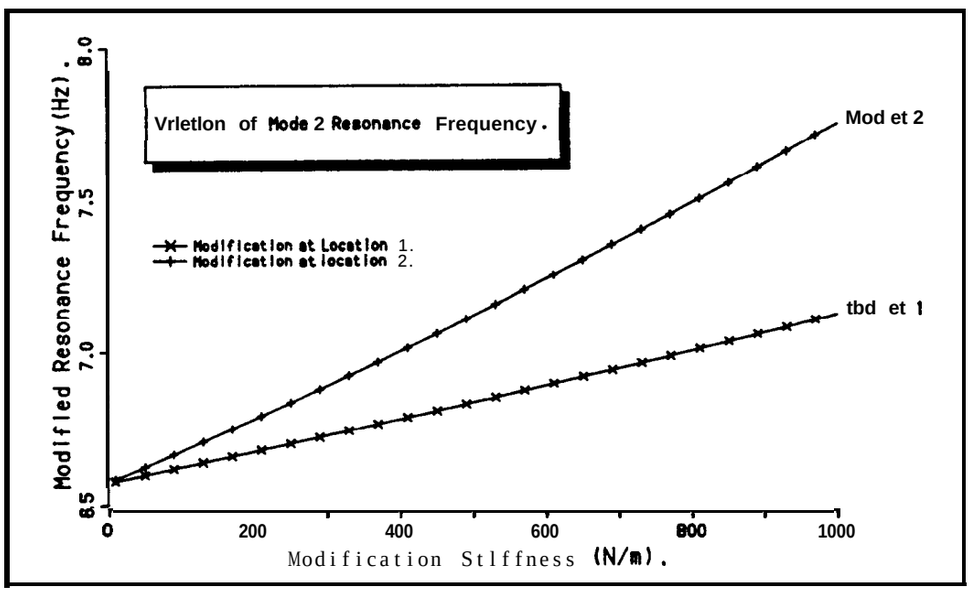

Variation of Mode 2 Resonance Frequency for Different SDoF Stiffness Modifications.

Figure 3.9

Once all the sensitivities have been derived in this way, the degrees-of-freedom can be ranked in order of 'importance' for single degree-of-freedom mass or stiffness point modifications. To relieve a particular vibration problem, subsequent real modifications can be designed which exploit fully the sensitive degrees-of-freedom identified in the 'ranking table', thus providing an efficient solution.

3.3 Theoretical Development of Sensitivity Analysis

3.3.1 Rational Fraction Description of FRFs for Undamped Systems

(i) A Grounded Structure

It has been shown in several papers, e.g. references [73] and [74], that any FRF of a grounded undamped structure can be described completely in terms of resonance frequencies, anti-resonance frequencies (although in some cases the anti-resonance frequencies may be imaginary – see later) and a constant:

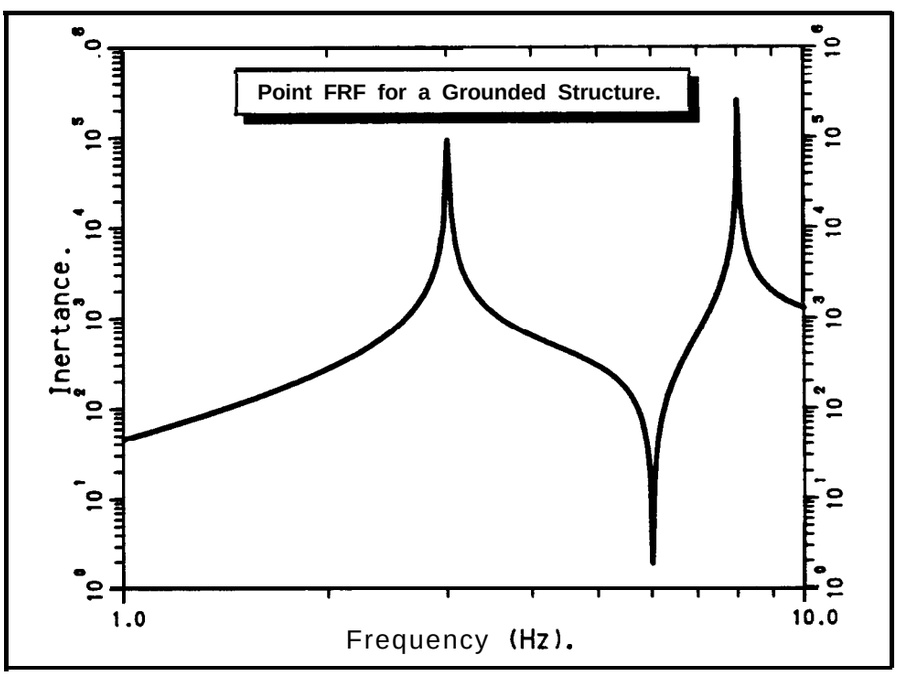

Point FRF for a 'Grounded* Structure.

Figure 3.10a

$$I_{jk}(\omega) = \frac{-\omega^2 C_{jk} \prod_{i=1}^{N-1} \left(1 - \frac{\omega^2}{{}^{jk}\omega_i^2}\right)}{\prod_{r=1}^{N} \left(1 - \frac{\omega^2}{\Omega_r^2}\right)} \qquad \text{.....(3.21)}$$

where: $I_{jk}(\omega)$ = Inertance between points j and k.

C_{jk} = Static Flexibility

ω = Frequency

Ω_r = r^{th} resonance frequency.

${}^{jk}\omega_i$ = i^{th} anti-resonance frequency for I_{jk}

N.B. The 1st anti-resonance is defined as that one **following the 1st** resonance.

The equation was first derived by Duncan [74] and, thus, will be referred to as Duncan's Equation.

If it is assumed that a system is undamped, then a measured driving point FRF (j=k), e.g. Figure 3.10a, can be characterised by this equation. Knowledge of only N resonance frequencies, (N-l) real anti-resonance frequencies, and a single point on the FRF curve (used to calculate C_{jj}) is required. Although most systems have an infinite number of resonance frequencies, quite accurate results for the inertance can be obtained using a finite number of modes (N), providing that the ratio of $\left(\frac{\omega^2}{\Omega_N^2}\right)$ is small: a situation which is easily obtained in practical applications.

The static flexibility (C_{jk}) can be determined from the low-frequency asymptote of the FRF or by use of equation (3.21), in a rearranged form, with the resonance and anti-resonance frequencies and an inertance value (I_{jk}) at a frequency ω. The point chosen on the FRF curve will be identified as a 'reference point'. Comparison of the static flexibilities derived using several different reference points with that determined from the low-frequency asymptote provides a means for assessing the accuracy of the assumed model.

(ii) A Free Structure

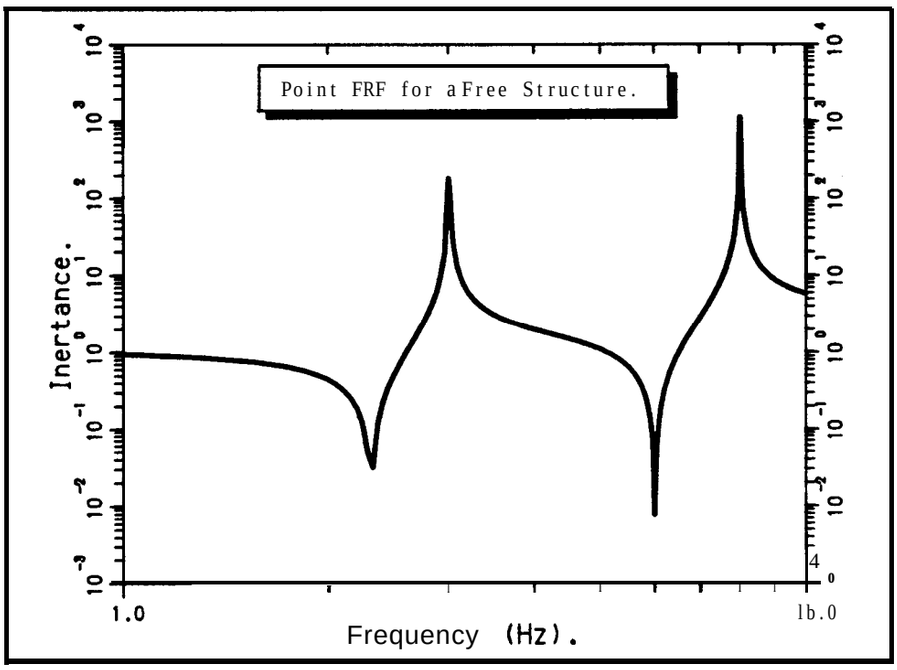

Point FRF for a 'Free' Structure.

Figure 3.11a

For a free undamped structure, the inertance can be expressed as :

$$I_{jk}(\omega) = \frac{\xi_{jk} \prod_{i=1}^{N} \left(1 - \frac{\omega^2}{jk\omega_i^2}\right)}{\prod_{r=1}^{N} \left(1 - \frac{\omega^2}{\Omega_r^2}\right)} \quad \ldots\ldots\ldots\ldots\ldots\ldots\ldots\ldots \quad (3.22)$$

where: ξ_{jk} = Static Accelerance

N.B. In this case, the 1st anti-resonance is defined as that **preceding the 1st** non-zero resonance.

The main differences between a point FRF for a grounded structure and a point FRF for a free structure occur below the first resonance frequency and can be seen by comparison of Figures 3.10a & 3.1 la. The point FRF for a grounded structure is asymptotic to a stiffness line at very low frequencies, whereas the point FRF for a free structure exhibits an anti-resonance below the **first** resonance and becomes asymptotic to a mass line for frequencies below the anti-resonance.

Imaginary Anti-resonance Frequencies

It has been stated above that any FRF of an undamped structure can be described completely by equation (3.21) or equation (3.22), for grounded or free structures respectively. For point FRFs, resonance and real anti-resonance characteristics alternate; there is always a real anti-resonance between each successive pair of resonance peaks. For the situation where the force and response points are not the same – a transfer FRF – a real anti-resonance need not occur between two successive resonances and there may be a 'minimum' instead of a 'zero'. Practical difficulties arise in this situation, although there are, mathematically, still N-l anti-resonance frequencies for a transfer FRF, some of them are imaginary, and only the real anti-resonances can be extracted by visual inspection of a measured FRF.

An FRF with an imaginary anti-resonance frequency has been synthesised using equation (3.21). The FRF is shown in Figure 3.10b and has the appearance of a transfer FRF, i.e. no 'anti-resonance' feature between the resonances just a minimum. The input data used in the generation of this FRF are identical to those used for the FRF of Figure 3.10a, except that the original real anti-resonance frequency of 6 Hz has been made purely imaginary, e.g. (0 + i6) Hz. This imaginary anti-resonance frequency could not be determined from visual inspection of the transfer FRF.

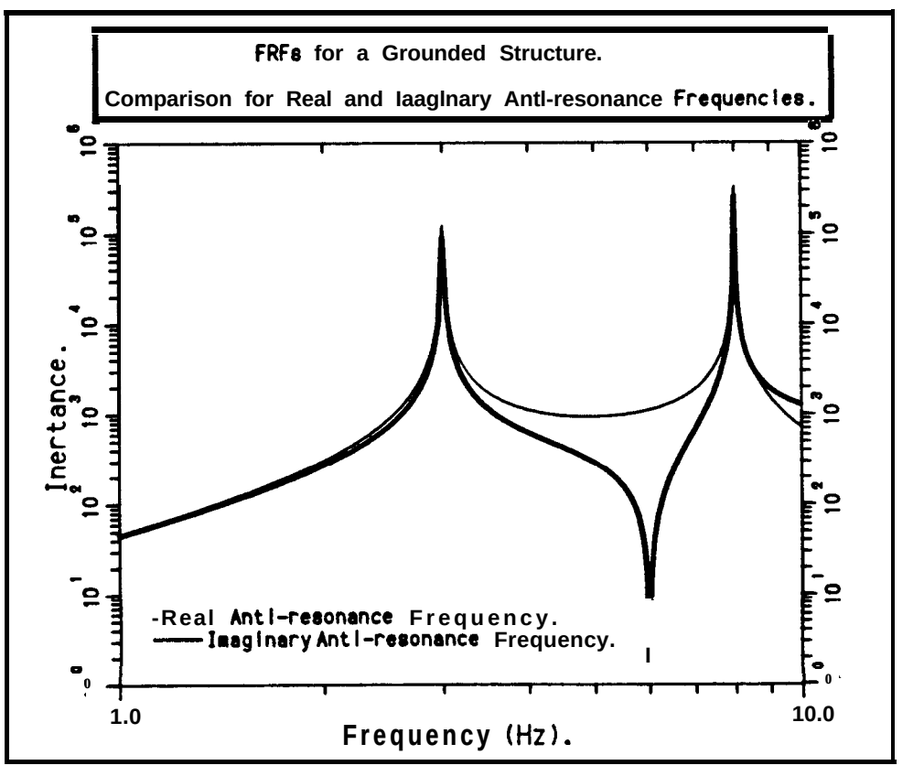

Comparison of FRFs for Real & Imaginary Anti-Resonance Frequencies.

Figure 3.10b

Figure **3.10c** shows the transition of the point FRF (Figure **3.10a)** to the transfer FRF (Figure **3.10b)** as the anti-resonance frequency is changed from a real to an imaginary value. The phase relationship is also plotted and the smoothing out of the **180°** phase change associated with the real anti-resonance can be seen. The **180°** phase changes at the resonances remain unaltered.

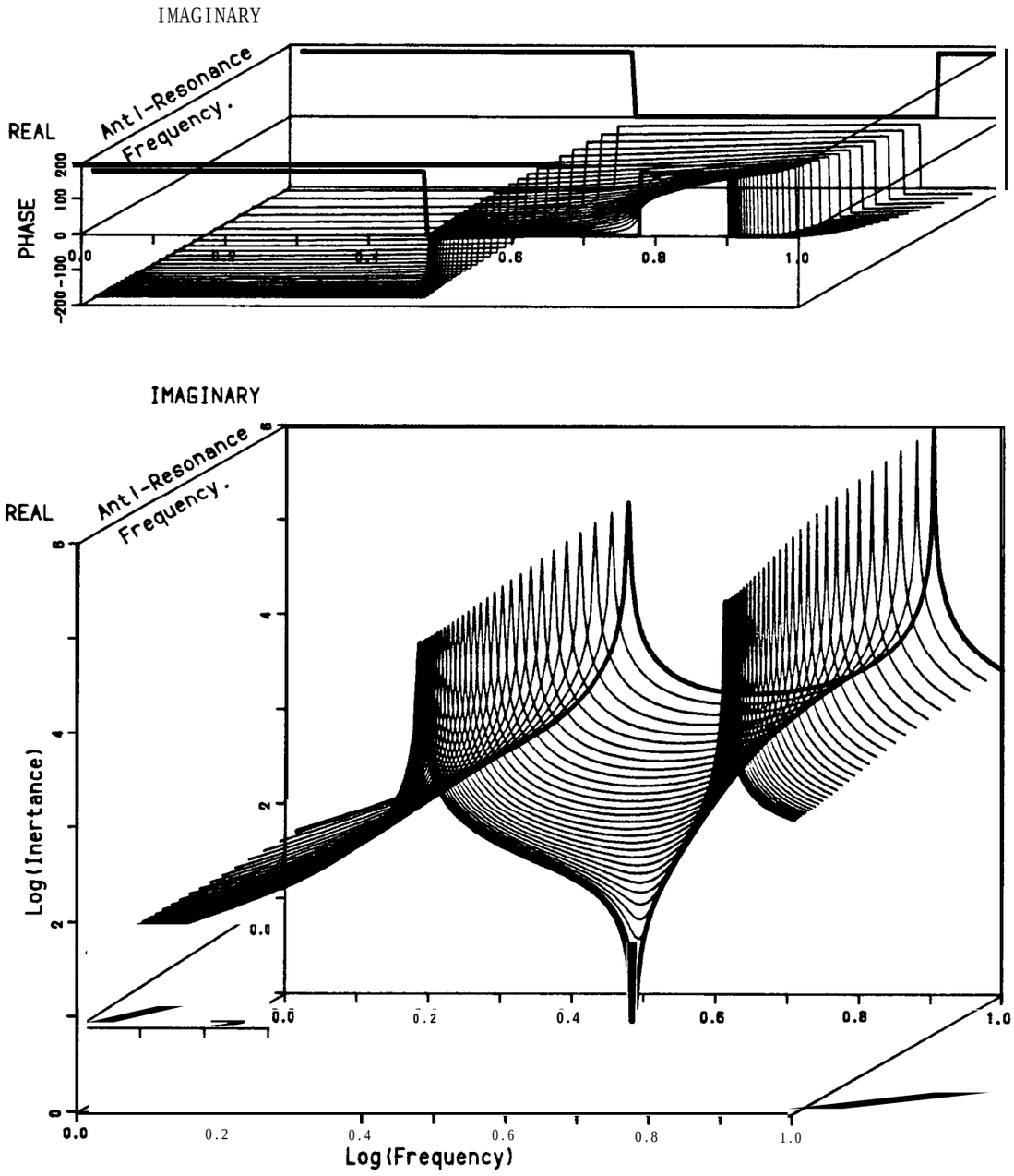

3-D Plot Showing the Transition Between the FRF of a Grounded Structure with a Real Anti-Resonance Frequency and that with an Imaginary Anti-resonance Frequency.

Figure **3.10c**

3.3.2 Resonance Sensitivity for a Point Single Degree-of-Freedom Mass Modification to a Grounded Structure

The resonance sensitivities of a **grounded structure** for a point single degree-of-freedom mass modification are derived using simple impedance coupling theory together with Duncan's equation (3.21). The derivation is set out below.

The impedance coupling equations for one coupling coordinate only reduce to,

$$\frac{1}{\alpha}+\frac{1}{\beta}=\frac{1}{\gamma} \qquad \text{.......(3.23)}$$

Where a and β are the component point inertances (at the attachment location j) and γ is the point inertance of the coupled structure for coordinate j. The resonance frequencies of the modified structure (Ω_R) are given by $\frac{1}{\gamma}=0$

and hence $\qquad \alpha+\beta=0 \qquad$ ....(3.24)

Now, working with inertances, a is given by equation (3.21) for the point j, and $\beta=\frac{1}{m}$ for a mass modification, so that;

$$\frac{-\,\Omega_R{}^2.C_{jj}\,.\prod_{i=1}^{N-1}\left(1-\frac{\Omega_R{}^2}{{}_{jj}\omega_i{}^2}\right)}{\prod_{r=1}^{N}\left(1-\frac{\Omega_R{}^2}{\Omega_r{}^2}\right)}+\frac{1}{m}=0 \qquad \text{.......(3.25)}$$

where Ω_R are the modified resonance frequencies, and re-arrangement gives,

$$m\,\Omega_R{}^2\,C_{jj}\prod_{i=1}^{N-1}\left(1-\frac{\Omega_R{}^2}{{}_{jj}\omega_i{}^2}\right)-\prod_{r=1}^{N}\left(1-\frac{\Omega_R{}^2}{\Omega_r{}^2}\right)=0 \qquad \text{.......(3.26)}$$

Solution of this polynomial equation in Ω_R will yield the resonance frequencies for the modified structure.

Definition of the Resonance Frequency Sensitivity Parameter

We shall define the **sensitivity** of the resonance frequencies to a mass addition in a single coordinate, as the differential $\frac{d\Omega_R}{dm}$.

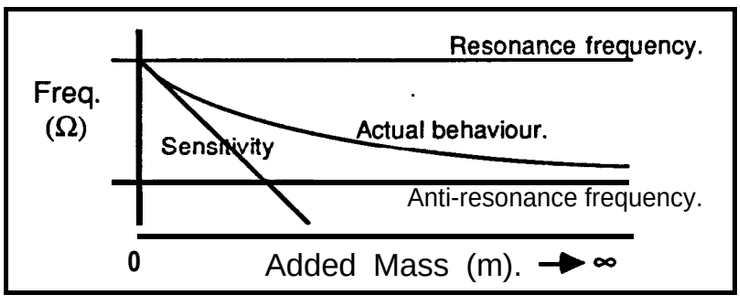

Definition of Sensitivity.

Figure 3.12

The sensitivity to be calculated is a mathematical sensitivity in that it is the slope of the frequency vs added mass graph (Figure 3.12), for zero added mass. Actual, finite, mass additions may have a different effect on the resonance frequencies to that predicted through use of the sensitivity values.

Differentiating equation (3.26) with respect to mass, using the following formula for the differentiation of a product,

$$\frac{d}{dm}\left\{\prod_{r=1}^{N}\left(1-\frac{x}{y}\right)\right\}=\frac{dx}{dm}\cdot\left[\prod_{r=1}^{N}\left(1-\frac{x}{y}\right)\right]\cdot\sum_{r=1}^{N}\left(\frac{1}{x-y}\right) \qquad \text{.....(3.27)}$$

leads to,

$$\frac{d\Omega_R}{dm}=\frac{\Omega_R\ C_{jj}\prod_{r=1}^{N-1}(\Omega_r^2)\prod_{i=1}^{N-1}\left(1-\frac{\Omega_R^2}{j\omega_i^2}\right)}{2\left[\frac{\Omega_N^2-\Omega_R^2}{\Omega_N^2}\cdot\sum_{i=1}^{N-1}\left(\frac{\Omega_i^2-j\omega_i^2}{j\omega_i^2-\Omega_R^2}\prod_{r\neq i}^{N-1}(\Omega_r^2-\Omega_R^2)\right)-\frac{1}{\Omega_R^2}\prod_{r=1}^{N-1}(\Omega_r^2-\Omega_R^2)\right]_I}$$

..... (3.28)

for the sensitivity of resonance frequencies to single degree-of-freedom modifications (for the full derivation of equation (3.28), see Appendix B). Evaluation of equation (3.28) requires the resonance frequencies of the modified system and, hence, prior solution of equation (3.26), or measurement of the modified system. However, for the purposes of ranking the coordinates, solution of equation (3.26) is avoided because the ranking is based on the **initial** sensitivities, i.e. for m tending to zero. Consider this limiting case for one mode at a time, so that Ω_R (the modified resonance frequency) tends to Ω_P the corresponding resonance frequency of the unmodified structure. After some algebraic manipulation we find that,

$$\left.\frac{d\Omega_P}{dm}\right|_{m=0} = \frac{-C_{jj}.\Omega_p.\prod_{r=1}^{N}(\Omega_r^2).\prod_{i=1}^{N-1}(_{jj}\omega_i^2 - \Omega_p^2)}{2.\prod_{i=1}^{N-1}(_{jj}\omega_i^2).\prod_{r\neq p}^{N}(\Omega_r^2 - \Omega_p^2)} \quad \text{.....(3.29)}$$

This equation allows the sensitivities of each resonance frequency to be calculated for a single degree-of-freedom mass modification at any position on a structure (j) for which a point FRF is available. Arrangement of the sensitivities in decreasing order gives the 'Order of Importance' ranking of the coordinates for single degree-of-freedom mass modifications.

This sensitivity parameter is expressed in terms of frequency shift/Kg of added mass. For comparison of the sensitivities of several modes it has been found that a 'percentage sensitivity' is of more direct use. The percentage sensitivity is simply the sensitivity expressed in equation (3.29) divided by the resonance frequency of the mode under consideration, and multiplied by 100, giving an expression in terms of percentage (%) frequency shift/Kg of added mass. The relative importance of modification at one point for various modes can be assessed more easily with this parameter.

3.3.3 Resonance Sensitivity for a Point Single Degree-of-Freedom Stiffness Modification to a Grounded Structure

An analysis, similar to that of section 3.3.2 for a mass modification, has also been made for a single degree-of-freedom stiffness modification. The stiffness modification is modelled as a spring, one end of which is connected to the point in question and the other end is grounded. The polynomial equation giving the new resonance frequencies (Ω_R) for the modified system is:

$$k\,C_{jj}\prod_{i=1}^{N-1}\left(1 - \frac{\Omega_R^2}{_{jj}\omega_i^2}\right) + \prod_{r=1}^{N}\left(1 - \frac{\Omega_R^2}{\Omega_r^2}\right) = 0 \quad \text{.....} \quad (3.30)$$

or

$$\frac{1}{k} + \alpha_{jj}(\Omega_R) = 0 \quad \text{.....} \quad (3.31)$$

and the corresponding expression for the stiffness sensitivity is:

$$\left.\frac{d\Omega_P}{dk}\right|_{k=0} = \frac{C_{jj}.\prod_{r=1}^{N}(\Omega_r^2).\prod_{i=1}^{N-1}(\ddot{u}\omega_i^2 - \Omega_p^2)}{2.\Omega_P.\prod_{i=1}^{N-1}(\ddot{u}\omega_i^2).\prod_{r\neq p}^{N}(\Omega_r^2 - \Omega_p^2)} \quad \ldots\ldots\ldots\ldots\ldots\ldots\ldots\ldots (3.33)$$

3.3.4 Relationship Between Mass and Stiffness Sensitivities

It will be noted that there is a close similarity between the mass and stiffness sensitivities of equations (3.29) and (3.32) – in fact they are related very simply:

$$\left.\frac{d\Omega_P}{dk}\right|_{k=0} = \frac{-1}{\Omega_p^2}\cdot\left.\frac{d\Omega_P}{dm}\right|_{m=0} \quad \ldots\ldots\ldots\ldots\ldots\ldots\ldots\ldots\ldots (3.33)$$

This relationship shows that the ranking of degrees-of-freedom from these sensitivity calculations will be **identical** whether a mass or stiffness modification is to be made. A simple explanation of this relationship is given below.

Consider the Salter skeleton mass and stiffness lines [28] for a single mode -

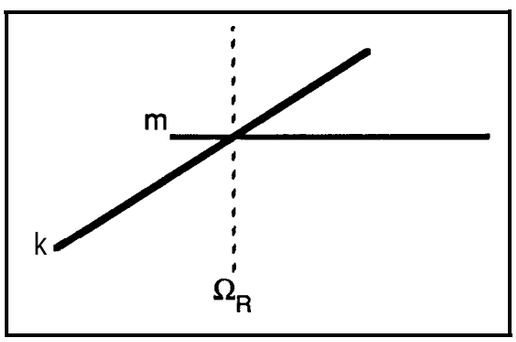

Salter Skeleton for a Single Mode.

Figure 3.13

By definition, $\frac{k}{m} = \Omega_R^2$

Now, if we require a shift in the resonance frequency from Ω_R to $\Omega_R\left(1+\frac{\Delta\Omega_R}{\Omega_R}\right)$. There **are two** possible ways this could be achieved.

(a) Increase k while m is kept constant;

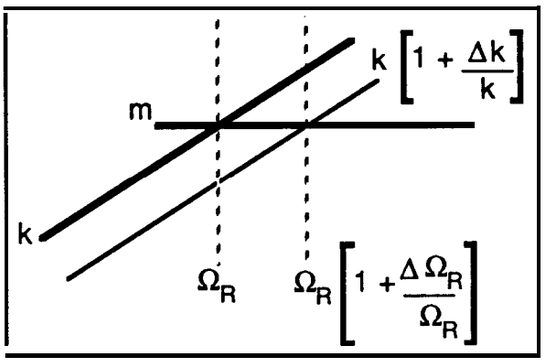

Skeleton for Increased Stiffness (k).

Figure 3.14

$$\frac{k\left(1+\frac{\Delta k}{k}\right)}{m}=\left(\Omega_R\left(1+\frac{\Delta\Omega_R}{\Omega_R}\right)\right)^2 \qquad \text{.....} \quad (3.34)$$

or, (b) Decrease m while k is kept constant;

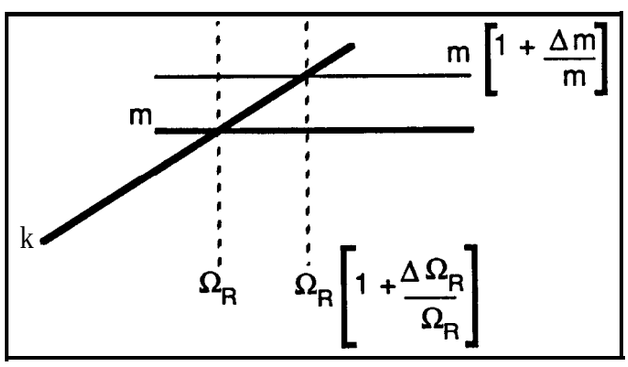

Skeleton for Increased Mass (m).

Figure 3.15

$$\left(\frac{k}{m\left(1+\frac{\Delta m}{m}\right)}\right)=\left(\Omega_R\left(1+\frac{\Delta\Omega_R}{\Omega_R}\right)\right)^2 \qquad \text{.....} \quad (3.35)$$

Now, equating equations 3.34 and 3.35;

$$\left(\frac{k}{m\left(1+\frac{\Delta m}{m}\right)}\right)=\left(\frac{k\left(1+\frac{\Delta k}{k}\right)}{m}\right) \qquad \text{.....} \quad (3.36)$$

gives, $$1+\frac{\Delta m}{m}+\frac{A\,k}{k}+\frac{\Delta m\,\Delta k}{mk} \quad 1 \qquad \ldots\ldots (3.37)$$

Neglecting 2nd order quantities and using the definition of Ω_R,

$$\frac{\Delta m}{m}=\frac{-\Delta k}{k} \quad \text{and therefore,} \quad \frac{k}{m}=\frac{-\Delta k}{\Delta m}=\Omega_R^2$$

Hence, $$\frac{Ak}{Am}=-\Omega_R^2 \qquad \ldots\ldots (3.38)$$

Now, when equation (3.38) is compared with equation (3.33) -

$$\left.\frac{d\Omega_R}{dk}\right|_{k=0}=-\frac{1}{\Omega_R^2}\left.\frac{d\Omega_R}{dm}\right|_{m=0} \quad \text{for which, rearrangement gives,} \quad \frac{d\Omega_R}{dm}\cdot\frac{dk}{d\Omega_R}=-\Omega_R^2$$

the similarity becomes clear.

3.3.5 Sensitivity Analysis for Free Structures

The sensitivity analysis so far has concentrated on single degree-of-freedom mass and stiffness modifications to grounded structures. As shown in equations (3.21) and (3.22), the rational fraction representation of grounded and free structures is quite similar and thus the theory for the sensitivity analysis of free structures follows the same lines as those for grounded structures presented in sections 3.3.2 and 3.3.3 above.

If a single degree-of-freedom mass modification (m) is made to a free structure at location j, then by suitable manipulation of equation (3.22), it will be seen that the resonance frequencies for the modified structure can be obtained from solution of the equation:

$$m\,.\,\xi_{jj}\,.\prod_{i=1}^{N}\left(1-\frac{\Omega_R^2}{jj\omega_i^2}\right)+\prod_{i=1}^{N}\left(1-\frac{\Omega_R^2}{\Omega_i^2}\right)=0 \qquad \ldots\ldots (3.39)$$

The sensitivity of the resonance frequencies to this single degree-of-freedom mass modification is derived by differentiating equation (3.39) with respect to m,

$$\frac{d\Omega_R}{dm}=\frac{-\xi_{jj}\prod_{r=1}^{N}(\Omega_r^2)\;\prod_{i=1}^{N}\left(1-\frac{\Omega_R^2}{jj\omega_i^2}\right)}{2.\Omega_R.\sum_{i=1}^{N}\left(\frac{\Omega_i^2-jj\omega_i^2}{jj\omega_i^2-\Omega_R^2}\prod_{r\neq i}^{N}(\Omega_r^2-\Omega_R^2)\right)} \qquad \ldots\ldots (3.40)$$

and taking the limit as the added mass tends to zero, giving:

$$\left.\frac{d\Omega_p}{dm}\right|_{m=0} = \frac{\prod_{i=1}^{N}\left(1 - \frac{\Omega_p^2}{j\omega_i^2}\right)}{2\Omega_p \prod_{r\neq p}^{N}(\Omega_r^2 - \Omega_p^2)} \qquad (3.41)$$

As in Section 3.3.4, the resonance frequency sensitivities for a single degree-of-freedom stiffness modification are directly related to those for a single degree-of-freedom mass modification by:

$$\left.\frac{d\Omega_p}{dk}\right|_{k=0} = -\frac{1}{\Omega_p^2} \cdot \left.\frac{d\Omega_p}{dm}\right|_{m=0} \qquad (3.42)$$

3.3.6 Internal Modification Between Two Points, and the Use of Difference FRFs (ΔFRFs)

In sections 3.3.2, 3.3.3 and 3.3.5 above, the theory is presented which allows calculation of the resonance frequency sensitivities for single coordinate mass or stiffness modifications to free or constrained structures. It is important to remember that they are the sensitivities to single degree-of-freedom modifications. A single degree-of-freedom mass modification can be achieved by connecting a mass to the structure through a suitable joint, i.e. a pushrod. A single degree-of-freedom stiffness modification can be made by connecting one end of a spring to the structure and grounding the other end. However, if a spring is connected between two points on the structure, which is a typical forrn of structural modification, there are 2 degrees-of-freedom involved – independent motion of each end of the spring – and the sensitivity analysis results derived from normal FRFs will not apply. Consider the simple structure shown in Figure 3.16:

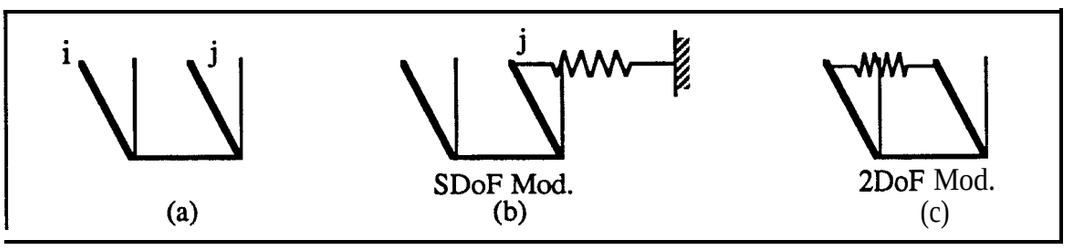

First Mode of Vibration.

Figure 3.16

A single degree-of-freedom stiffness modification, as shown in Figure 3.16(b), will affect the structure because there is relative motion between the ends of the spring. Sensitivity analysis with data from the normal FRF will correctly predict the sensitivity of

mode number 1 to modification at location j. If the 2DoF modification shown in (c) is made, there will be no effect on the structure because there is no relative motion between the ends of the spring. The simple sensitivity analysis results for locations i and j are not applicable in this case. Consider next the effects of the same modifications on the 2nd mode, Figure 3.17:

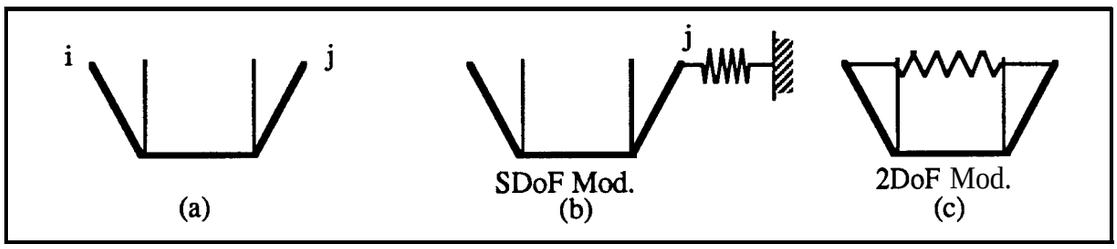

Second Mode of Vibration.

Figure 3.17

The single degree-of-freedom modification, Figure 3.17(b), will have a similar effect on the structure to that on the 1st mode but, the 2 degree-of-freedom modification will now have a very significant influence on this mode – even greater than the single degree-of-freedom modification – because there is a large relative motion of the ends of the spring. This 2nd mode will be more sensitive to the 2 degree-of-freedom modification than to the single degree-of-freedom modification for which the normal sensitivity analysis applies.

Difference FRFs

The sensitivity analysis for a particular coordinate is performed using the point FRF for that coordinate (sections 3.3.2 to 3.3.5). By default, the reference for both the force and response measurements is ground: the force is measured between the point and ground and the response is measured relative to ground. If this reference were to be altered from ground, such that the force measured was that between locations i and j, and the response was that of i relative to j, then the resulting “point FRF” (point difference FRF, AFRF) would be different to those for locations i or j alone. A sensitivity analysis using this point difference FRF would predict correctly the sensitivities of modes 1 and 2 to the modification shown in Figure 3.17(c).

As a specific example we shall use the simple undamped 2 degree-of-freedom system of section 3.2.4.

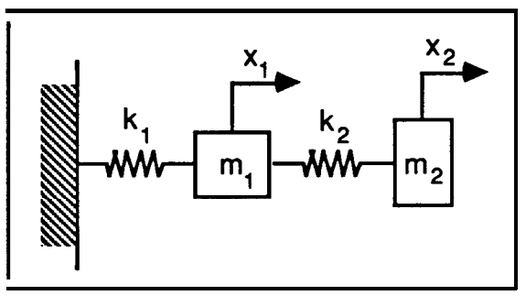

Figure 3.18

The matrix equation of motion for the 2 degree-of-freedom system, with the coordinate system as shown, is given by equation (3.18):

$$\begin{bmatrix} m_1 & 0 \\ 0 & m_2 \end{bmatrix}\begin{Bmatrix} \ddot{x}_1 \\ \ddot{x}_2 \end{Bmatrix}+\begin{bmatrix} (k_1+k_2) & -k_2 \\ -k_2 & k_2 \end{bmatrix}\begin{Bmatrix} x_1 \\ x_2 \end{Bmatrix}=\begin{Bmatrix} 0 \\ 0 \end{Bmatrix}$$

The choice of the x_1, x_2 coordinate system is purely arbitrary and the following definition of coordinate system (x_1 and y) is equally valid. Instead of using x_2 we adopt a new coordinate, y, defined as the difference between x_2 and xl; $y=(x_2 - x_1)$. The matrix equation of motion for this choice of coordinates is then,

$$\begin{bmatrix} m_2 & m_2 \\ m_2 & (m_1+m_2) \end{bmatrix}\begin{Bmatrix} \ddot{y} \\ \ddot{x}_1 \end{Bmatrix}+\begin{bmatrix} k_2 & 0 \\ 0 & k_1 \end{bmatrix}\begin{Bmatrix} y \\ x_1 \end{Bmatrix}=\begin{Bmatrix} 0 \\ 0 \end{Bmatrix} \quad \text{..... (3.43)}$$

The natural frequencies, which are global properties, are identical whichever coordinate definition is used – and for an undamped system the resonance frequencies are equal to the natural frequencies. The anti-resonance frequencies, however, will be different for each particular FRF and for each choice of coordinates. For a system with the following mass and stiffness properties:

$m_1 = 3$ Kg $\quad m_2 = 1$ Kg

and, $k_1 = k_2 = 1000$N/m.

the resonance frequencies are; 2.4263 Hz and, 6.0275 Hz

and the point anti-resonance frequencies are,

for the (x_1,x_1) coordinate system ..... 5.0329 Hz

for the (x_2,x_2) coordinate system ..... 4.1094 Hz

and for the 'difference' coordinate system (y,y) ..... 2.5165 Hz

The three point FRFs for the system are shown in Figure 3.19;

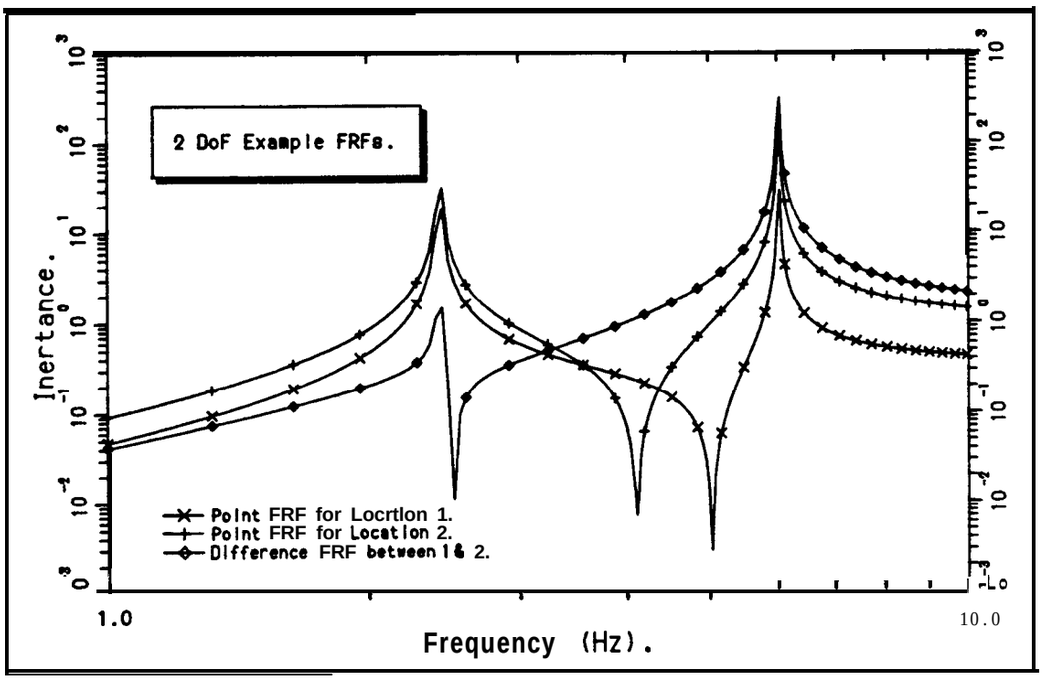

Point FRFs & Point Difference FRF for the Example 2DoF System.

Figure 3.19

By use of equation (3.32) the stiffness sensitivities of modes 1 and 2 have been calculated for separate single degree-of-freedom modifications in coordinates x_1, x_2 and y.

Mode	Sensitivity $\frac{\%}{N/m}$	Point FRF DoF. x_1	x_2	Y
1	$\left.\frac{d\Omega_1}{dk}\right\|_{k-0}$	45.8e-3	77.7e-3	4.2e-3
2	$\left.\frac{d\Omega_2}{dk}\right\|_{k=0}$	4.2e-3	22.3e-3	45.8e-3

It will be seen that, as expected, modification in coordinate y has very little effect for mode number 1, but a very significant effect for mode number 2. The variations of the resonance frequencies for a range of the modifications are shown in Figures 3.20 and 3.21.

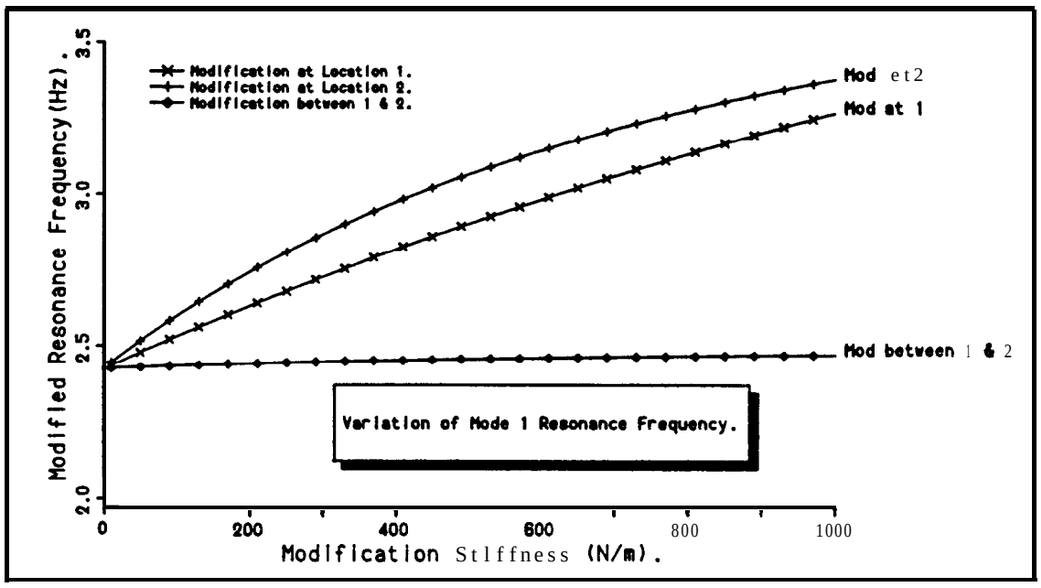

Variation of Mode 1 Resonance Frequency with Stiffness K_3.

Figure 3.20

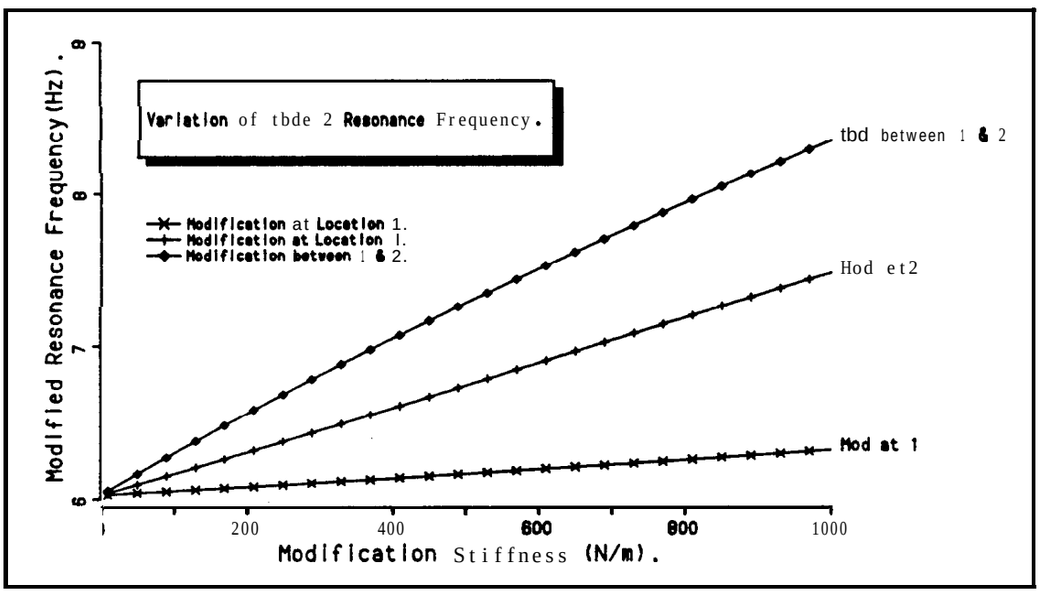

Variation of Mode 2 Resonance Frequency with Stiffness K_3.

Figure 3.21

Consequently, when considering modifications involving the use of stiffness elements internally in a structure, the sensitivity analysis results based on the measurement coordinate system should be treated with caution. It is possible, however, to derive the "point difference FRFs" from the normal FRFs alone by a triple product transformation as shown below.

Consider the coordinate systems used in equations (3.18) and (3.43). Inertance matrices [a] and [β] can be formed from the modal properties as follows;

$$[\alpha] = [\theta].[\lambda_r^2 - \omega^2]^{-1}.[\theta]^T$$

and,

$$[\beta] = [\phi].[\lambda_r^2 - \omega^2]^{-1}.[\phi]^T$$

The eigenvalues (natural frequencies) will always be the same regardless of the system of coordinates used. However, the mass normalised eigenvector matrices are different; $[\theta]$ for the X_1, X_2 coordinate system and $[\phi]$ for the Y, X_1 coordinate system.

Now, if we assume that these eigenvector matrices can be related by the transformation matrix [T], such that;

$$[\phi] = [T].[\theta]$$

Then,

$$[T].[\alpha] = [T].[\theta].[\lambda_r^2 - \omega^2]^{-1}.[\theta]^T$$

and,

$$[T].[\alpha].[T]^T = [T].[\theta].[\lambda_r^2 - \omega^2]^{-1}.[\theta]^T.[T]^T$$

Now,

$$[\phi]^T = [\theta]^T.[T]^T$$

and therefore,

$$[T].[\alpha].[T]^T = [\phi].[\lambda_r^2 - \omega^2]^{-1}.[\phi]^T$$

or,

$$[T].[\alpha].[T]^T = [\beta]$$

The transformation matrix between the eigenvectors, [T], is the same as the transformation matrix between the two coordinate systems, in this case;

$$\begin{bmatrix} Y \\ X_1 \end{bmatrix} = \begin{bmatrix} -1 & 1 \\ 1 & 0 \end{bmatrix} \cdot \begin{bmatrix} X_1 \\ X_2 \end{bmatrix}$$

In summary, the difference FRFs may be calculated from;

$$[H_D] = [T].[H].[T]^T \quad \ldots\ldots\ldots\ldots\ldots\ldots\ldots\ldots \quad (3.44)$$

where: $[H_D]$ = n by n matrix of 'difference FRFs'
$[H]$ = p by p matrix of measured FRFs
$[T]$ = n by p transformation matrix.

As an alternative to this method of calculation, if at an early stage it is thought that this additional difference sensitivity analysis might be necessary, it may be better to measure and store the force and response spectra separately for each location. Any desired AFRF can then be formed by appropriate combination of the force and response spectra directly.

3.3.7 Second Order Sensitivities

In the work presented by Vanhonacker [56] & [57] and VanBelle [76], sensitivity values are used in series expansions to provide estimates of the modified structure's new resonance frequencies. It has also been shown that, to estimate the resonance frequencies for finite modifications, the first order sensitivity parameters alone may not be sufficient, i.e. using only the first two terms in the Maclaurin's series expansion of equation (3.28).

Maclaurin's Series: $f(x) = f(0) + xf'(0) + \frac{x^2}{2!}f''(0) + \ldots\ldots = \sum_{r=0}^{\infty} \frac{x^r}{r!} f^{(r)}(0)$ .... (3.45)

Greater accuracy in the estimation of resonance frequencies for modified structures can be achieved by including more terms in this series, but this necessitates the higher order differential functions. Equations (3.28) and (3.40) have been differentiated once more (Appendix B) to yield the following expressions for the 2^{nd} order mass sensitivities for grounded and free structures -

For a Grounded Structure -

$$\frac{d^2\Omega}{dm^2} = \left(\frac{d\Omega_R}{dm}\right)^2\left[\frac{-4}{C_{jj}.\Omega_R}.\frac{d\Omega_R}{dm}.(*).\prod_{i=1}^{N-1}\left(\frac{jj\omega_i^2}{\Omega_i^2(jj\omega_i^2 - \Omega_R^2)}\right) + 2\Omega_R\sum_{i=1}^{N-1}\left(\frac{1}{\Omega_R^2 - jj\omega_i^2}\right) + \frac{1}{\Omega_R}\right]$$

with,

$$(*) = \left\{\frac{1}{\Omega_R}\left(\frac{1}{\Omega_R^2}\prod_{r\neq 1}^{N-1}(\Omega_r^2 - \Omega_R^2) + \sum_{r=1}^{N-1}\prod_{s\neq r}^{N-1}(\Omega_s^2 - \Omega_R^2)\right)\right.$$

$$+ \Omega_R\left(1 - \frac{\Omega_R^2}{\Omega_N^2}\right)\sum_{i=1}^{N-1}\left(\left(\frac{\Omega_i^2 - jj\omega_i^2}{jj\omega_i^2 - \Omega_R^2}\right)\left[\frac{1}{jj\omega_i^2 - \Omega_R^2}\prod_{r\neq i}^{N-1}(\Omega_r^2 - \Omega_R^2) - \sum_{r=i}^{N-1}\prod_{\substack{s\neq r\\ s\neq i}}^{N-1}(\Omega_s^2 - \Omega_R^2)\right]\right)$$

$$\left. - \frac{\Omega_R}{\Omega_N^2}\sum_{i=1}^{N-1}\left(\frac{\Omega_i^2 - jj\omega_i^2}{jj\omega_i^2 - \Omega_R^2}\right)\prod_{r\neq i}^{N-1}(\Omega_r^2 - \Omega_R^2)\right\}$$

..... (3.46a)

and, for a Free Structure -

$$\frac{d^2\Omega}{dm^2} = \Omega_R\left(\frac{d\Omega_R}{dm}\right)^2\left[\frac{4\Omega_R}{\xi_{jj}}.\frac{d\Omega_R}{dm}.(*).\prod_{i=1}^{N}\left(\frac{jj\omega_i^2}{\Omega_i^2(jj\omega_i^2 - \Omega_R^2)}\right) + 2.\sum_{i=1}^{N}\left(\frac{1}{\Omega_R^2 - jj\omega_i^2}\right) - \frac{1}{\Omega_R^2}\right]$$

with,

$$(*) = \sum_{i=1}^{N}\left(\frac{\Omega_i^2 - jj\omega_i^2}{jj\omega_i^2 - \Omega_R^2}\right)\left[\frac{1}{jj\omega_i^2 - \Omega_R^2}\prod_{r\neq i}^{N}(\Omega_r^2 - \Omega_R^2) - \sum_{r=i}^{N}\prod_{\substack{s\neq r\\ s\neq i}}^{N}(\Omega_s^2 - \Omega_R^2)\right]$$

..... (3.46b)

It is clear that further differentiation to derive higher order differentials would be far too complicated.

Similar long and complicated 2nd order sensitivity terms have been used successfully by Vanhonacker, and Van Belle to give improved accuracy, but it is noted by Chou [58] that calculation of further order sensitivities becomes yet more complicated and of dubious practical use.

3.3.8 Example – 1st and 2nd Order Sensitivities for a Beam

A free beam with a single degree-of-freedom mass modification at the tip has been used in a numerical study to illustrate the variation of resonance frequency and its first and second differentials with changes in the added mass. The unmodified beam is taken as the base condition and a range of positive and negative mass additions to the tip of the beam have been considered (negative modification masses represent mass removals). For each modification the new resonance frequencies were found and used with the anti-resonance frequencies (which remain unaltered) in equations (3.40) and (3.46b) for calculation of the first and second differentials of the first mode frequency with respect to the added mass. All the resonance and anti-resonance frequencies up to 5 kHz were used in these calculations (7 modes) and the mass addition ranged from -0.5 Kg through to +0.5 Kg. Since the mass of the unmodified beam is only 1.04 Kg the maximum positive and negative mass additions represent significant structural modifications.

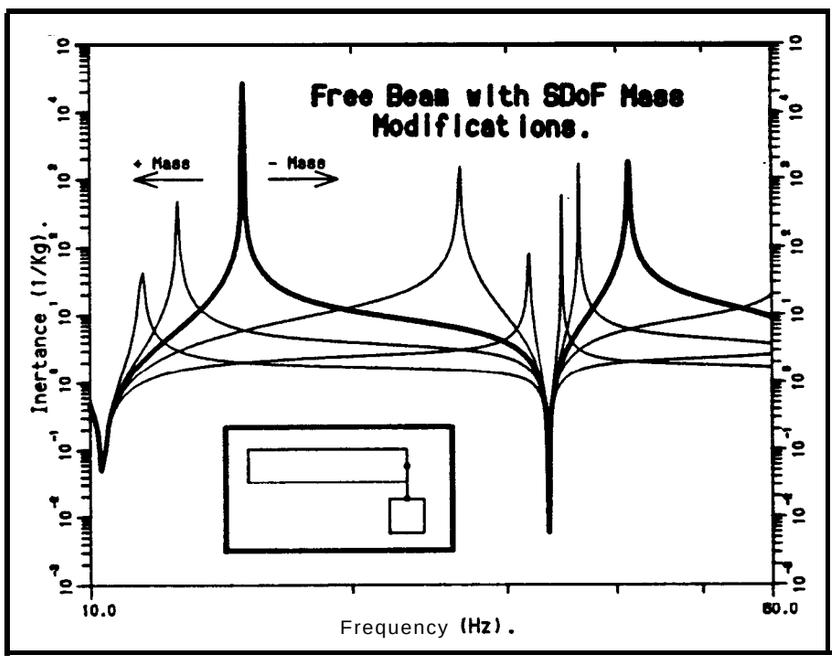

Free-Free Beam with SDoF Mass Modifications at the Tip.

Figure 3.22

A selection of FRFs for the total range of mass modifications is shown in Figure 3.22. As mass is added, the resonance frequencies all drop relative to the unmodified state and when mass is 'removed', the frequencies increase. In each case it can be seen that the frequency shifts are bounded by the adjacent anti-resonance frequencies for the modification coordinate point FRF. In Figure 3.23a the variation in resonance frequency for the first mode is shown for the full range of added masses. For negative mass

additions the curve is asymptotic to the succeeding anti-resonance frequency and for positive mass additions the **curve** is asymptotic to the preceding anti-resonance frequency. The slope of this curve is the fiit differential with respect to mass, as calculated by equation **(4.40),** and is shown in Figure **3.23b.**

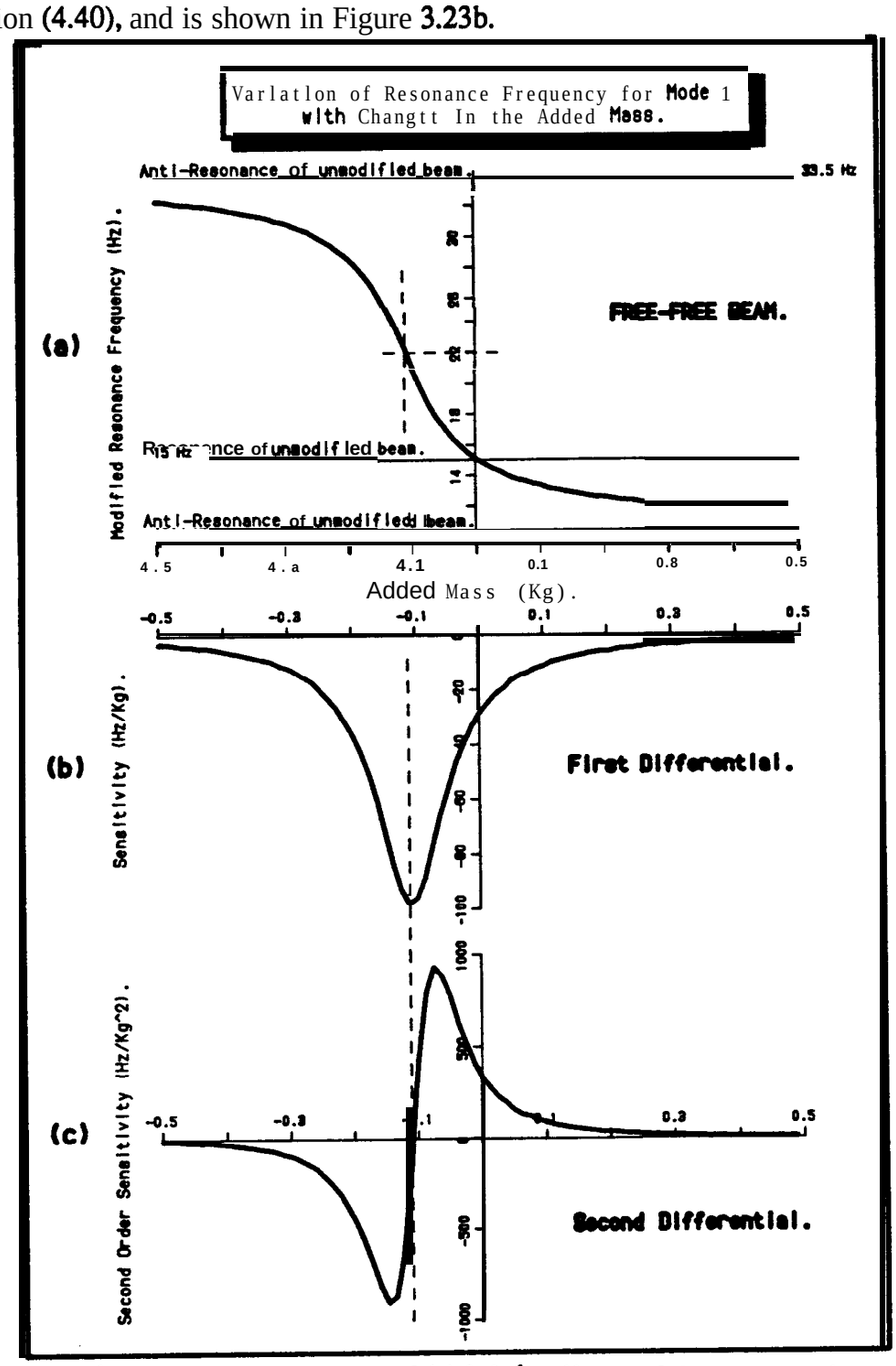

Variation of Resonance Frequency and 1st & 2nd Differential Sensitivities for Mode 1 with Changes in the SDoF Mass Modification.

Figure 3.23

In section 3.3.2 the sensitivity has been defined as $\frac{d\Omega_P}{dm}\Big|_{m=0}$, which is the point where the first differential curve crosses the Y-axis. As the mass modifications become larger and larger (+ve or -ve) the incremental changes in the resonance frequencies become progressively smaller and the first differential becomes asymptotic to zero. It would appear that, in this example, the slope has the largest value when the actual resonance frequency of the modified beam is mid-way between the adjacent anti-resonances, i.e. at approximately 22 Hz. The second differential of the resonance frequency with respect to the added mass is the slope of the first differential curve and this is shown in Figure 3.23c. All the curves are finite and continuous.

By consideration of Figure 3.24a it can be seen that if the resonance of interest for the unmodified structure is close to the succeeding anti-resonance then predictions of the shifts in the resonance frequency for positive mass additions will be under-estimates. Conversely, if the resonance for the mode of interest for the unmodified structure is close to the preceding anti-resonance (Figure 3.24b) the predicted shifts in the resonance frequency for positive mass additions will be over-estimates. The transition between over- and under-estimation of the frequency shifts occurs when the second differential curve passes through zero.

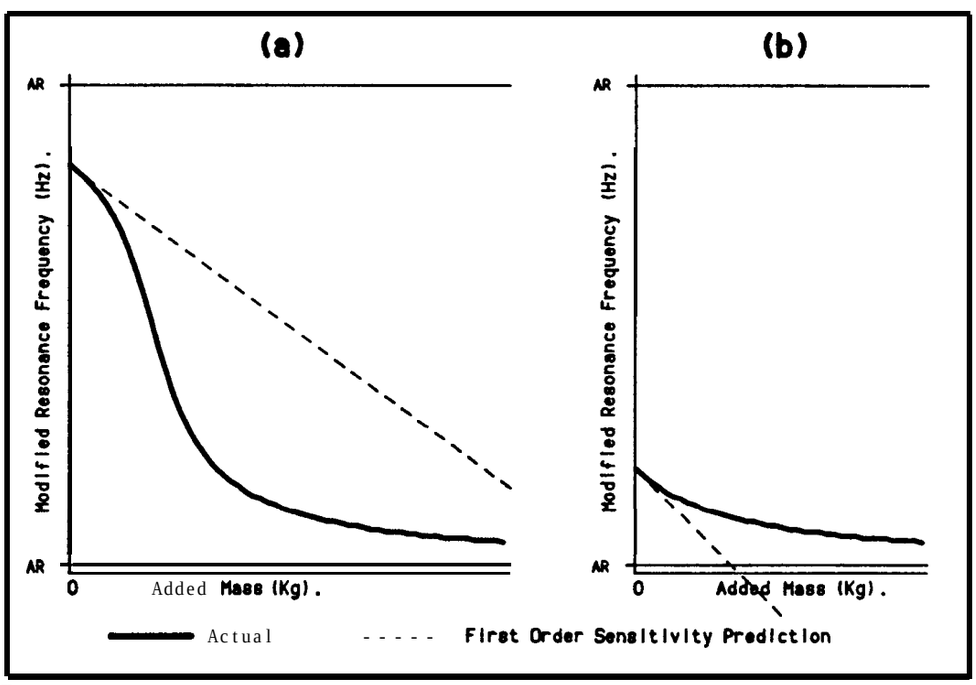

FIG3_24.EZ

Consequences of 1st Order Sensitivity Predictions for Stiffness-like and Mass-like structures.

Figure 3.24

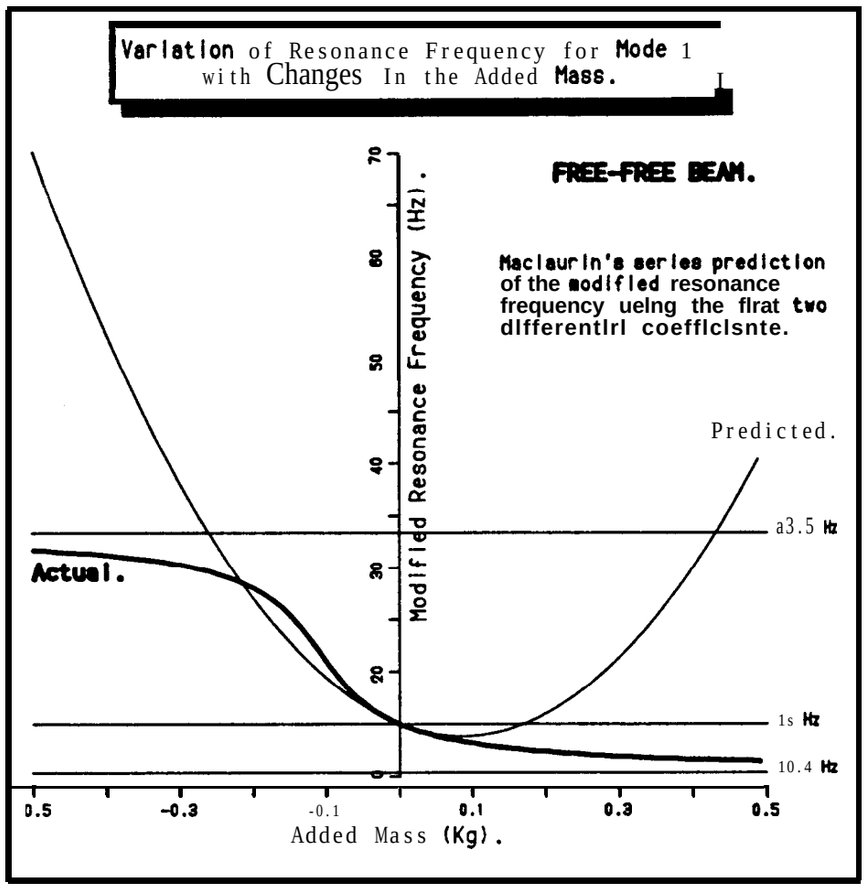

Maclaurin's Series Prediction of the Modified Resonance Frequency using the First Two Differential Coefficients.

Figure 3.25

For the unmodified beam (added mass = 0) the first resonance frequency is 15 Hz, the sensitivity is -28.14 Hz/Kg and the second order sensitivity is 329.04 **Hz/Kg^2.These** values have been used in the Maclaurin's series expansion (equation 3.45) for estimation of the new resonance frequencies of the beam for a range of mass modifications. The predicted variation of the modified resonance frequency is plotted together with the actual variation in Figure 3.25. It can be seen that the parabolic form of the prediction only agrees with the actual behaviour for modifications over the range -0.1 to +O. 1 Kg. Outside of this range there are very serious discrepancies between the prediction and the actual behaviour. Therefore, it can be concluded that for macro modifications, the use of terms up to and including second order differentials in a Maclaurin's series expansion for the modified resonance frequencies is still not very accurate.

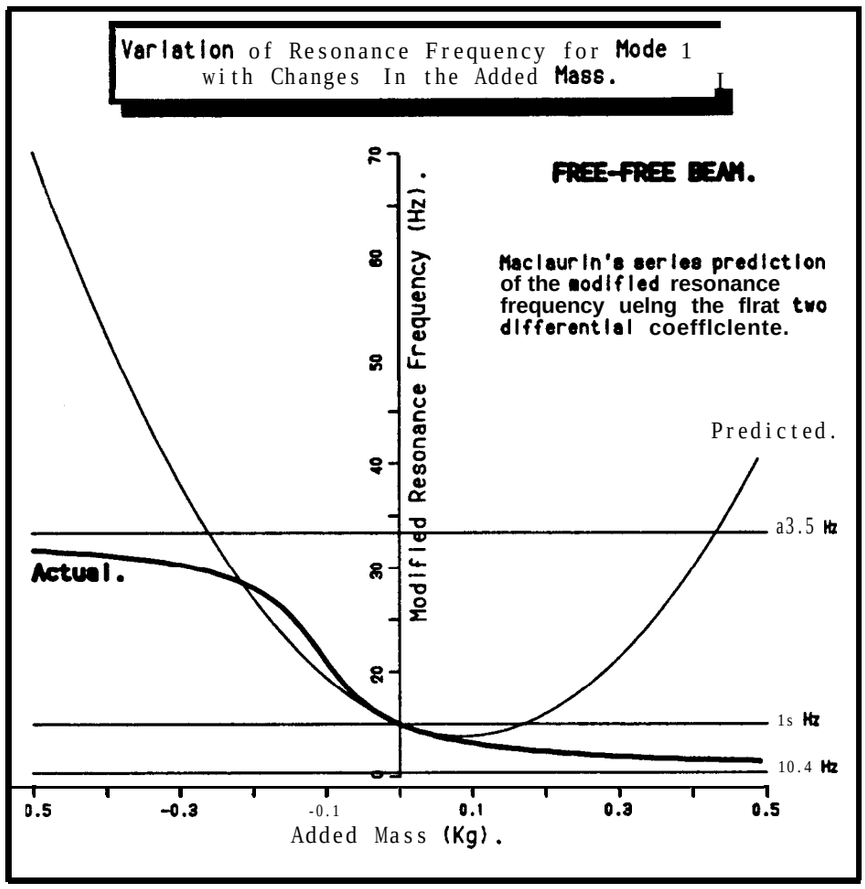

Maclaurin's Series Prediction of the Modified Resonance Frequency using the First Two Differential Coefficients.

Figure 3.25

For the unmodified beam (added mass = 0) the first resonance frequency is 15 Hz, the sensitivity is -28.14 Hz/Kg and the second order sensitivity is 329.04 **Hz/Kg^2.These** values have been used in the Maclaurin's series expansion (equation 3.45) for estimation of the new resonance frequencies of the beam for a range of mass modifications. The predicted variation of the modified resonance frequency is plotted together with the actual variation in Figure 3.25. It can be seen that the parabolic form of the prediction only agrees with the actual behaviour for modifications over the range -0.1 to +O. 1 Kg. Outside of this range there are very serious discrepancies between the prediction and the actual behaviour. Therefore, it can be concluded that for macro modifications, the use of terms up to and including second order differentials in a Maclaurin's series expansion for the modified resonance frequencies is still not very accurate.

3.4 Anti-resonance Sensitivity for a Single Degree-of-Freedom Mass Modification at a Remote Point

The resonance frequency sensitivities to single degree-of-freedom point mass or stiffness modifications are global sensitivities for modification at particular points – because resonance frequencies are global properties. It has already been shown, in sections 3.2.2 and 3.2.3, that the anti-resonance frequencies of FRFs having at least one degree-of-freedom in common with the modification point do not change, but anti-resonances in all other FRFs will shift. In just the same way as resonances can be moved away from a troublesome excitation frequency, it may be desirable to move a particular anti-resonance characteristic to the troublesome excitation frequency. However, it should always be remembered that anti-resonance characteristics are local properties of FRFs – dependent upon the choice of force and response coordinates. Positioning of an anti-resonance of one FRF at a particular frequency does not mean that there will be an anti-resonance at that frequency in all the other FRFs – unlike the behaviour of resonances. For successive sequential single degree-of-freedom modifications, it may be necessary to know the extent to which the anti-resonances have shifted as a result of the preceding modifications. For these reasons, a further analysis has been performed to derive the sensitivities of anti-resonance frequencies to a single degree-of-freedom modification in a remote degree-of-freedom. The analysis begins with the matrix form of impedance coupling theory and the general form of Duncan's equation, then follows similar steps to those taken for the resonance frequency sensitivities.

Using the matrix form of the impedance coupling technique:

$$[\alpha]^{-1} \oplus [\beta]^{-1} = [\gamma]^{-1} \quad \ldots\ldots\ldots\ldots\ldots\ldots\ldots\ldots\ldots\ldots \quad (3.47)$$

For a 2 degree-of-freedom system, with a point mass modification made in degree-of-freedom number 1,

$$\frac{1}{\alpha_{11}\alpha_{22} - \alpha_{12}^2} \cdot \begin{bmatrix} \alpha_{22} & -\alpha_{12} \\ -\alpha_{12} & \alpha_{11} \end{bmatrix} + \begin{bmatrix} -\omega^2 m & 0 \\ 0 & 0 \end{bmatrix} = [\gamma]^{-1} \quad \ldots\ldots\ldots\ldots\ldots\ldots (3.48)$$

hence,

$$\gamma_{22} = \alpha_{22} + \frac{\alpha_{12}^2 \omega^2 m}{1 - \alpha_{11}\omega^2 m} \quad \ldots\ldots\ldots\ldots\ldots\ldots\ldots\ldots\ldots\ldots \quad (3.50)$$

Now, using the following forms of Duncan's equation,

$$\alpha_{11}(\omega) = \frac{-\frac{\omega^2}{{}_{11}\omega_i^2}\prod_{i=1}^{N-1}\left(1 - \frac{\omega^2}{{}_{11}\omega_i^2}\right)}{\prod_{r=1}^{N}\left(1 - \frac{\omega^2}{\Omega_r^2}\right)} \qquad \alpha_{12}(\omega) = \frac{C_{12}\cdot\prod_{i=1}^{N-1}\left(1 - \frac{\omega^2}{{}_{12}\omega_i^2}\right)}{\prod_{r=1}^{N}\left(1 - \frac{\omega^2}{\Omega_r^2}\right)}$$

$$\alpha_{22}(\omega) = \frac{C_{22}\cdot\prod_{i=1}^{N-1}\left(1 - \frac{\omega^2}{{}_{22}\omega_i^2}\right)}{\prod_{r=1}^{N}\left(1 - \frac{\omega^2}{\Omega_r^2}\right)}$$

..... (3.51)

eventually yields:

$$\gamma_{22} = \frac{C_{22}\left(\prod_{i=1}^{N-1}\left(1 - \frac{\omega^2}{{}_{22}\omega_i^2}\right)\right)\left[\prod_{r=1}^{N}\left(1 - \frac{\omega^2}{\Omega_r^2}\right) - \omega^2 m C_{11}\prod_{i=1}^{N-1}\left(1 - \frac{\omega^2}{{}_{11}\omega_i^2}\right)\right] + \omega^2 m\left[C_{12}\prod_{i=1}^{N-1}\left(1 - \frac{\omega^2}{{}_{12}\omega_i^2}\right)\right]}{\prod_{r=1}^{N}\left(1 - \frac{\omega^2}{\Omega_r^2}\right)\left[\prod_{r=1}^{N}\left(1 - \frac{\omega^2}{\Omega_r^2}\right) - \omega^2 m C_{11}\prod_{i=1}^{N-1}\left(1 - \frac{\omega^2}{{}_{11}\omega_i^2}\right)\right]}$$

....(3.52)

as the point FRF at location number 2 – the remote point – for the modified system.

Now, represent γ_{22} as:

$$\gamma_{22} = \frac{C^*_{22}\cdot\prod_{i=1}^{N-1}\left(1 - \frac{\omega^2}{{}_{22}\omega^*_i{}^2}\right)}{\prod_{r=1}^{N}\left(1 - \frac{\omega^2}{\Omega^*_r{}^2}\right)} \qquad \text{..... (3.53)}$$

where, the * superscript here denotes values for the modified system

Now, choose to evaluate the equations (3.52) and (3.53) at the new anti-resonance frequencies of the point FRF at location number 2, $\omega = \omega_A = {}_{22}\omega_i^*$, where γ_{22} tends to zero, leaving:

$$C_{22}\prod_{i=1}^{N-1}\left(1 - \frac{\omega_A{}^2}{{}_{22}\omega_i^2}\right)\left[\prod_{r=1}^{N}\left(1 - \frac{\omega_A{}^2}{\Omega_r^2}\right) - \omega_A{}^2 m C_{11}\prod_{i=1}^{N-1}\left(1 - \frac{\omega_A{}^2}{{}_{11}\omega_i^2}\right)\right] + \omega_A{}^2 m\left[C_{12}\prod_{i=1}^{N-1}\left(1 - \frac{\omega_A{}^2}{{}_{12}\omega_i^2}\right)\right]^2 = 0$$

..... (3.54)

Solution of this polynomial equation in ω_A will yield the point anti-resonance frequencies at the remote location for the modified structure.

In the same way as for the resonance frequency sensitivity analysis, we shall define the sensitivity of the anti-resonance frequencies to mass addition, as; $\left.\frac{d\{^{22}\omega_A\}}{dm_1}\right|_{m1=0}$

Differentiating equation (3.54) with respect to m_1, using equation (3.27) and taking the limiting case as m tends to zero (ω_A tends to ω_a; the anti-resonance of the unmodified structure) leads to:

$$\left.\frac{d\omega_a}{dm}\right|_{m1=0} = \frac{\omega_a \, C_{12}^2 . \prod_{i=1}^{N-1}\left(1 - \frac{\omega_a^2}{^{12}\omega_i^2}\right)\prod_{i=1}^{N-1}\left(^{22}\omega_i^2\right)}{2C_{22}\prod_{r=1}^{N}\left(1 - \frac{\omega_a^2}{\Omega_r^2}\right)\prod_{i\neq a}^{N-1}\left(\omega_a^2 - {}^{22}\omega_i^2\right)} \qquad \text{.....(3.55)}$$

Some of the transfer FRF anti-resonance frequencies may not be real (section 3.3.1), and so determination of these from a measured FRF is difficult. Therefore, we make a substitution using equation (3.5 1) to obtain:

$$\left.\frac{d\omega_a}{dm}\right|_{m1=0} = \frac{I_{12}^{\,2}(^{22}\omega_a)\prod_{r=1}^{N}\left(\Omega_r^2 - {}^{22}\omega_a^2\right)\prod_{i=1}^{N-1}\left(^{22}\omega_i^2\right)}{2C_{22}\,{}^{22}\omega_a{}^3\prod_{r=1}^{N}\left(\Omega_r^2\right)\prod_{i\neq a}^{N-1}\left(^{22}\omega_a^2 - {}^{22}\omega_i^2\right)} \qquad \text{.....(3.56)}$$

where: $I_{12}(^{22}\omega_a)$ is the 1,2 transfer inertance evaluated at a frequency corresponding to one of the 2,2 anti-resonance frequencies.

Once again, the sensitivity is given by a simple expression but, this time, it requires the resonance and anti-resonance frequencies for the coordinates under consideration, and specific values of the transfer inertance between those coordinates. Transfer measurements of a structure are necessary so that these anti-resonance sensitivities may be calculated.

3.5 Application of Sensitivity Equations to a Cantilever Beam

A theoretical model of a cantilever beam was developed, enabling FRFs to be derived for the beam at positions 25%, 33%, 50%, 66% and 75% of the beam length from the clamped end. The resonance and anti-resonance frequencies used were taken from these calculated FRFs. In addition to the resonance and anti-resonance frequencies, the static flexibilities for all the FRFs (C_{ij}) are required in equation (3.29) for the calculation of the sensitivities. The static flexibility values for each point FRF were calculated using equation (3.21), and the resonance and anti-resonance frequencies and the value of the inertance (I,) at a frequency of 1 Hz. The static flexibilities calculated in this way agree well with the low-frequency asymptotes of the inertance functions – which could also be used for calculation of the static flexibilities if it was so desired.

Resonance sensitivities have been calculated for the first four modes at each of the stations along the beam, for translation/translation point functions. The results are shown in Table 3.1.

The sensitivities from Table 3.1 have been ranked with the most sensitive first, and this is shown in Table 3.2. This ranking for a single degree-of-freedom point mass modification compares favourably with the ranking of Table 3.3 which was produced by ordering the frequency shift values observed for 1 Kg single degree-of-freedom mass additions (N.B. the cantilever beam mass is 1.04 Kg). The ranking is not identical, but this is due to the fact that the ranking for Table 3.3 is based on

$$\frac{\Omega_p(m=0) - \Omega_p(m=1Kg)}{m},$$

while the ranking for Table 3.1 is based on the resonance sensitivity, defined as $\left.\frac{d\Omega_P}{dm}\right|_{m=0}$. The differences in these slopes accounts for the differences in ranking observed.

To confirm this explanation, frequency shift values were calculated and ordered for mass additions progressively less than 1 Kg. As the mass addition became very small, the ranking based on the calculated frequency shifts showed better and better agreement with the ranking based on the sensitivity.

The cantilever beam model incorporates 1% hysteretic damping, but it will be recalled that the theory upon which the sensitivity equations are based is for an undamped system.

3.5 Application of Sensitivity Equations to a Cantilever Beam

A theoretical model of a cantilever beam was developed, enabling FRFs to be derived for the beam at positions 25%, 33%, 50%, 66% and 75% of the beam length from the clamped end. The resonance and anti-resonance frequencies used were taken from these calculated FRFs. In addition to the resonance and anti-resonance frequencies, the static flexibilities for all the FRFs (C_{jj}) are required in equation (3.29) for the calculation of the sensitivities. The static flexibility values for each point FRF were calculated using equation (3.21), and the resonance and anti-resonance frequencies and the value of the inertance (I,) at a frequency of 1 Hz. The static flexibilities calculated in this way agree well with the low-frequency asymptotes of the inertance functions – which could also be used for calculation of the static flexibilities if it was so desired.

Resonance sensitivities have been calculated for the first four modes at each of the stations along the beam, for translation/translation point functions. The results are shown in Table 3.1.

The sensitivities from Table 3.1 have been ranked with the most sensitive first, and this is shown in Table 3.2. This ranking for a single degree-of-freedom point mass modification compares favourably with the ranking of Table 3.3 which was produced by ordering the frequency shift values observed for 1 Kg single degree-of-freedom mass additions (N.B. the cantilever beam mass is 1.04 Kg). The ranking is not identical, but this is due to the fact that the ranking for Table 3.3 is based on

$$\frac{\Omega_P(m=0) - \Omega_P(m=1Kg)}{m},$$

while the ranking for Table 3.1 is based on the resonance sensitivity, defined as $\left.\frac{d\Omega_P}{dm}\right|_{m=0}$. The differences in these slopes accounts for the differences in ranking observed.

To confirm this explanation, frequency shift values were calculated and ordered for mass additions progressively less than 1 Kg. As the mass addition became very small, the ranking based on the calculated frequency shifts showed better and better agreement with the ranking based on the sensitivity.

The cantilever beam model incorporates 1% hysteretic damping, but it will be recalled that the theory upon which the sensitivity equations are based is for an undamped system.

Damping of the level normally found in structural components (1% – 2%) does not seem to influence the resonance frequency sensitivities to any significant extent.

		Resonance Sensitivity (Hz/Kg) for the Cantilever Beam				
Mode	Frequency	@25%	@33%	@50%	@66%	@75%
1	2.36	-0.043	-0.120	-0.534	-1.32	-1.96
2	14.80	-4.94	-9.79	-14.8	-5.67	-0.619
3	41.23	-41.6	-44.1	0.00	-33.5	-27.4
4	80.87	-76.8	-10.2	-87.8	-3.10	-65.5

Resonance Frequency Sensitivities for the Cantilever Beam.

Table 3.1

, Mode	Position (%)
4	50
3	25
4	25
4	75
3	33
3	66
3	75
2	50
2	33
2	25
2	66
4	33
1	75
1	66
1	50
2	75
1	33
1	25
4	66
3	50

Order of Importance Ranking, Based on Resonance Frequency Shifts for a 1Kg Mass Addition. (Most Sensitive First)

Table 3.2

Mode	Position (%)
4	50
4	25
4	75
3	33
3	25
3	66
3	75
2	50
4	33
2	33
2	66
2	25
4	66
1	75
1	66
2	75
1	50
1	33
1	25
3	50

Order of Importance Ranking, Based on Resonance Frequency Sensitivities. (Most Sensitive First)

Table 3.3

3.6 Discussion of Theoretical Sensitivity Expressions

The sensitivity equations [(3.29), (3.32), (3.41) and (3.56)] are all expressions containing products of resonance and anti-resonance frequencies. All the calculations can be implemented easily on a computer. Once the FRF measurements have been made, the input data required are readily available without the need for modal analysis procedures. Peak- and valley-picking routines can be used directly on raw FRF data plots to yield the required resonance and anti-resonance frequencies.

Closely spaced modes of a structure will give rise to problems with this sensitivity technique, as they do for other analysis techniques. The resonance frequency sensitivity analysis relies on the use of resonance and anti-resonance frequencies from point FRFs. Sufficiently high frequency resolution must be used for the measurement of such data in order to define all the resonance and anti-resonance frequencies adequately.

Absorber structures are commonly used as a means of correcting vibration problems in structures. The simplest absorber structure is a single degree-of-freedom mass/spring system, and an attempt was made to derive a sensitivity expression for just such a simple modification, in the same way as had been done for individual mass and stiffness elements previously. However, it was found that this type of analysis is not applicable because the absorber introduces an extra mode into the system, and the concept of relating frequency shifts directly is no longer valid.

As a generalisation, the sensitivity analysis techniques developed in this chapter cannot be used for anything other than simple mass or spring elements alone, because all other modifications introduce extra modes. Nevertheless, if a particular modification can be described adequately by mass or spring elements, albeit in a piecewise fashion over various frequency bands, then these analyses will be valid for each particular frequency band.

If this type of sensitivity analysis is undertaken using data from a preliminary survey of a structure, then assessments can be made as to the suitability of certain locations for the purpose of excitation for the full measurement survey. Ideally, the excitation should be applied through a relatively insensitive degree-of-freedom. Identification of the sensitive coordinates should ensure that sufficient care is taken during the full measurement survey, so that the data are contaminated as little as possible by any of the measuring apparatus. Conditions relating to the collection of experimental data are discussed further in chapters 4 and 5.

3.6.1 The Influence of Damping

The sensitivity analysis study has been based on the use of rational fraction equations for the FRF properties of undamped structures. In practice, though, all structures have some damping. One effect of damping is to limit the level of the response at resonance and at anti-resonance. At resonance, the 'Q-factor' is reduced from infinity, for an undamped system, to $\frac{1}{2\zeta}$. At an anti-resonance, the magnitude of the response is a small, but finite, value rather than zero. Furthermore, viscous damping alters the actual natural frequencies and the anti-resonance frequencies. For an undamped system, the resonance frequencies are equal to the natural frequencies of the system but, for example, for a proportionally damped system the natural frequencies are the 'damped natural frequencies', given by,

$$\Omega_r \sqrt{1 - \zeta_r^2} .$$

The anti-resonance frequencies are affected in a similar way by the damping because they arise from cancellation of all the individual modal contributions. When the damping is small and evenly distributed throughout the structure, the resonance and anti-resonance frequencies can be assumed to be approximately equal to the resonance and anti-resonance frequencies of the undamped structure.

The rational fraction equations are interesting in that the effects of damping are not included in the sense of limiting the responses at resonance and anti-resonance frequencies, but they may be included, implicitly, in the definition of the resonance and anti-resonance frequencies used in the equations. When resonance and anti-resonance frequencies are derived directly from FRF curves, they are the properties of the damped system. An FRF curve synthesised using the rational fraction equation with damped structural data will have undamped resonance and anti-resonance features at the damped frequencies. In the sensitivity analysis procedure it is only the resonance and anti-resonance frequencies that are of any importance, hence, whether or not resonance and anti-resonance features are damped or undamped is irrelevant, provided that all the frequencies are correct. Furthermore, since it is intended that the sensitivity analysis should be used only as a method for ranking modification sites in their order of importance for influencing particular modes, discrepancies will be unimportant providing that the ranking is not altered.

3.6.2 General Comments on the use of Experimental Data

In many cases, even real anti-resonances are not defined clearly in measured FRFs, and it is difficult to ascribe accurate anti-resonance frequencies. It is possible to use synthesised FRFs in which the anti-resonances are defined just as clearly as the resonances. However, at an early stage of the procedure, the creation and validation of a modal database is wasteful. It is much more advantageous to have the anti-resonances defined more clearly in the measured data. To try and obtain better quality data around the anti-resonances, it has been suggested that greater care could be taken throughout the measurements. In some circumstances improvements can be made by changing the type of testing method – such as changing broadband testing to sine testing using a Frequency Response Analyser and concentrating data points in the anti-resonance regions as well as in the resonance regions. While this is possible for translational type measurements which are to be used directly, it is impractical for 'derived' FRFs (such as difference FRFs) for which the specific anti-resonance frequencies only emerge after processing. Only if some prior measurements and calculations have been undertaken to deduce the approximate location of all the anti-resonances will it be possible to concentrate the frequency data points in the correct ranges.

3.6.3 An Alternative Definition of Sensitivity

The sensitivity parameter presented in the foregoing sections is the sensitivity of **resonance frequencies** to changes at or between locations j and k on the structure, e.g. $\left.\frac{d\Omega_p}{dK_s}\right|_{K_s=0}$.

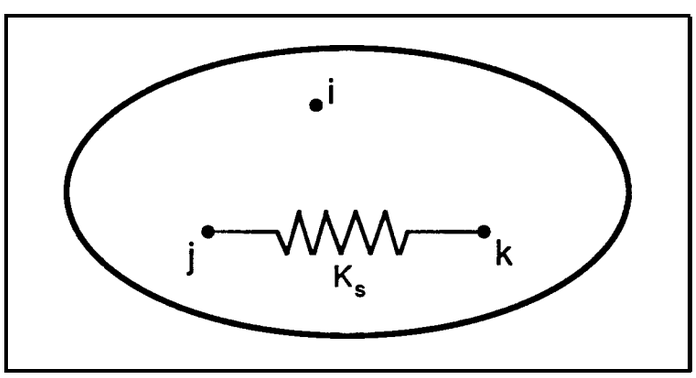

Figure 3.26

The sensitivity to stiffness changes between two points will probably be the most useful in practice because the most likely modifications will be internal stiffness changes to the structure.

An alternative view of sensitivity is the sensitivity of the response at a remote location, say i, to a change between locations j and k. It might be possible to calculate and plot a response sensitivity such as,

$$\left.\frac{d\ddot{x}_i}{dK_s}\right|_{K_s=0}$$

as a function of frequency. The function would be dependent upon -

- the single response location chosen (i);
- the pair of locations between which the modification is made (j and k); and
- the particular forcing function used (the response is dependent upon the input).

Therefore, it can be seen that the sensitivity analysis would require interpretation of a large number of frequency dependent sensitivity functions simultaneously. As an example, consider a structure which has n points of interest -

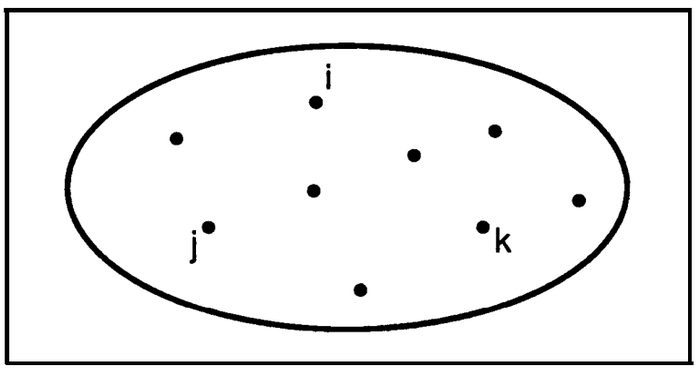

Figure 3.27

The number of different 2-point spring modifications that can be made is given by selecting any 2 from n, with the order unimportant; the combination

$$\left({}^{n}C_{r}\right) = \frac{n!}{r!(n-r)!}, \text{ where } r = 2.$$

For each of these different spring modifications there are n possible response locations that could be considered. In total therefore, there are $\frac{n.n!}{r!(n-r)!}$ frequency-dependent

sensitivity functions that could be calculated for each forcing function chosen. A simple system consisting of only 9 points of interest would produce 324 sensitivity functions for each forcing function – a vast quantity of information. The amount of data can be reduced substantially if interest is restricted to a very small frequency range, or to a single frequency, but nevertheless, interpretation of $\frac{n.n!}{r!\ (n - r)!}$ single sensitivity values would be no simple task.

In the resonance frequency sensitivity method developed in this chapter, the sensitivities are single numbers (instead of frequency-dependent functions) and relate to global shifts of the resonance frequencies. It is necessary to calculate the sensitivities for the particular modes of interest only, for all the different 2-point spring modifications that can be made. If the number of modes of interest is m, the number of sensitivity values to be assessed will be $\frac{m.n!}{r!\ (n - r)!}$, potentially still a large number of sensitivities to be assessed. It should be remembered, though, that the sensitivity function developed in this chapter is independent of any forcing function and that the number of modes of interest (m) will usually be considerably less than the number of points of interest (n).

3.7 Review of Chapter 3

Techniques for predicting the effects which given modifications will have on the dynamic characteristics of a structure are well proven. Two of the prediction methods are reviewed in chapter 2. The selection and design of modifications to overcome a particular vibration problem are much less well documented. Usually, the modifications are designed from previous experience with similar types of problems. Although the modifications chosen may bring about an acceptable vibration performance, they might not provide the optimum solution. For the majority of ground-based machinery, such as machine tools, washing machines etc., the only real penalty of an inefficient modification is the cost of any unnecessary material used in the modification. With an aerospace structure however, there is the additional penalty that any unnecessary mass in the modification detracts from the available payload.

The selection of the most efficient sites for modifications – termed “sensitivity analysis” – at an early stage, has two main benefits -

(i) modifications can be designed to exploit the sensitive properties of the structure; and

(ii) the full measurement survey can be tailored to include sufficient quantity and quality of data at the possible modification sites to enable accurate and detailed prediction of the effects of the modification.

In this chapter a new approach to sensitivity analysis has been developed. The new approach evolved from observations of FRF characteristics for a structure before and after single degree-of-freedom modifications. It was found that -

- when a single degree-of-freedom modification is made, the anti-resonance frequencies do not change for FRFs which have at least one coordinate in common with the modification degree-of-freedom; and
- as the size of the single degree-of-freedom modification is increased the resonance frequencies of the modified structure shift towards the (fixed) anti-resonance frequencies of the point FRF for the modification degree-of-freedom.

The emphasis is placed on the use of data measured during a preliminary measurement survey so that the analysis can be performed at the earliest possible stage. It would be possible to use data from an analytical or F.E. model of the structure at the design stage, but the uncertainties associated with un-validated models may be too great for any confidence to be placed in the results. Furthermore, at the design stage there is wide freedom and scope for changes in the basic structure to solve potential vibration problems and this would be far better than any of the add-on type modifications for which this sensitivity analysis is intended.

The new approach to sensitivity analysis requires measurement of point FRFs for all the degrees-of-freedom of interest, from which resonance and anti-resonance frequencies are extracted. These frequencies are substituted into simple equations for the sensitivity of the resonance frequencies to single degree-of-freedom mass or stiffness modifications at given points. From the sensitivity values derived, the modification degrees-of-freedom can be ranked in their “order-of-importance” for influencing any particular mode. These rankings can be used in the subsequent design and selection of a suitable modification to move a given resonance away from an excitation frequency. An important fact to remember is that the rankings are identical whether single degree-of-freedom mass or single degree-of-freedom stiffness modifications are being considered.

The use of the sensitivity equations has been extended to allow consideration of spring modifications between two internal points on a structure. In this case, the ‘point difference FRFs’ are required for the calculations and, unless these AFRFs are measured directly, it

is necessary to transform the standard FRF data or to record measured force and response data separately, rather than combined into a single FRF as is normal practice. By this means it is possible to calculate any AFRF at a subsequent stage. This extension to the sensitivity analysis method is particularly advantageous because the majority of practical modifications involve stiffness changes between internal points on structures.

Although the range of modifications for which the analysis is directly applicable is still restricted, the identification of the sensitive degrees-of-freedom for modification **is** valid in a general sense and can be used to guide the design of practical modifications. As noted by Sobey, **[63],** it is assumed that the most effective individual single degree-of-freedom modifications will be just as effective when applied together as a practical modification.

The main practical difficulties with this sensitivity analysis technique lie in the determination of the anti-resonance frequencies **–** particularly when broadband testing methods are used and the definition of anti-resonance features can be rather poor. In such circumstances it may be necessary to adopt a stepped-sine testing method whereby the anti-resonances can be defined much more accurately.

Chapter 4

Practical Considerations

4.1 Introduction

4.2 Overview of Testing Methods

There are several different approaches for measurement of the dynamic characteristics of a structure. Historically, the approaches have been divided into Phase-Resonance methods (Normal Mode testing or Sine Dwell testing) and Phase-Separation methods (Stepped Sine Sweep and Broadband testing).

Phase-resonance methods rely on the ability to excite a single mode of vibration by use of multiple shakers with independently variable force levels. The shakers each produce sinusoidal excitation at the same frequency and are either in-phase or out-of-phase with a reference source. The "normal-mode" excitation set-up effectively cancels the damping in the structure – the exciting forces are distributed such that each energy sink is cancelled by a corresponding energy source – and a single real mode can be excited. In this condition of normal-mode vibration, the excitation frequency is the undamped natural frequency of the mode, the response at all the points on the structure is in quadrature with the forces and the structural responses relate directly to the mode shape vector. This method can be very powerful and is popular for the ground vibration testing of aircraft structures because of the ability to measure real normal modes (for direct comparison with F.E. studies) and the ability to characterise non-linearities by study of the structural responses for a wide range of force input levels. The main difficulties with normal-mode testing are the selection of excitation locations, the tuning of the force pattern and the choice of excitation

frequency. The complete process has to be repeated for each different mode and consequently the testing time can be lengthy.

Phase-separation methods rely on the fact that the forced response of a linear structure is a weighted linear summation of all the uncoupled modes of the structure. The forced response to a known excitation is measured and then the modal parameters are extracted by means of mathematical curve fitting techniques. Phase-separation methods generally produce less accurate results than the phase-resonance methods and this is due, primarily, to the mathematical assumption that the actual responses are formed from a linear combination of the modes. In fact, the measured data may be inconsistent and contain the effects of non-linearities. Nevertheless, with more and more sophisticated analysis techniques and coupled with the fact that the phase-separation methods are much cheaper, easier and quicker to implement than the phase-resonance techniques, the phase-separation methods are now the predominant form of vibration testing.

Stepped sine testing and broadband testing are two types of phase-separation methods of vibration testing that will be discussed further in this brief overview. The requirements for extending the simple single point testing methods to multi-point methods are also presented together with discussion of some of the multi-point testing techniques.

Although each method has specific advantages and disadvantages, the selection of a testing technique is frequently based on the type of equipment available rather than its suitability for a particular job.

4.2.1 Sine Testing

In the sine testing technique, a shaker is used to excite the structure sinusoidally at a single, precisely controlled, frequency. The structure is allowed to settle under this excitation and then steady-state measurements are made of the magnitude and phase relationship between the input force and the response at the precise excitation frequency for any desired response location. Division of the response by the force input gives the value of the FRF at that particular frequency. The excitation frequency is then changed by a small increment and the measurement process is repeated once the structure has settled at the new frequency. By this means, the FRF can be constructed for any frequency range. There are no restrictions on the frequency spacing imposed by the testing method, although there may be restrictions due to the analysis methods to be used.

At each excitation frequency the structure's response is allowed to settle to remove any transient effects associated with the step change in excitation frequency from the previous measurement. This settling period is particularly important for excitation frequencies close to resonances of the structure where transient changes cause the structure to 'ring-on'. The transient effects will be included in the measurement if insufficient time is allowed for them to die away. A clear indication of whether the settling period is long enough can be obtained by performing the measurement twice around a resonance peak, once with an increasing frequency sweep, and once with a decreasing frequency sweep. An example is presented in Figure 4.1 where the resonance peaks occur at different frequencies for the two measurements (the decreasing frequency sweep producing a lower resonance frequency than the increasing frequency sweep), the transient effects have not had sufficient time to decay and the settling time should be increased.

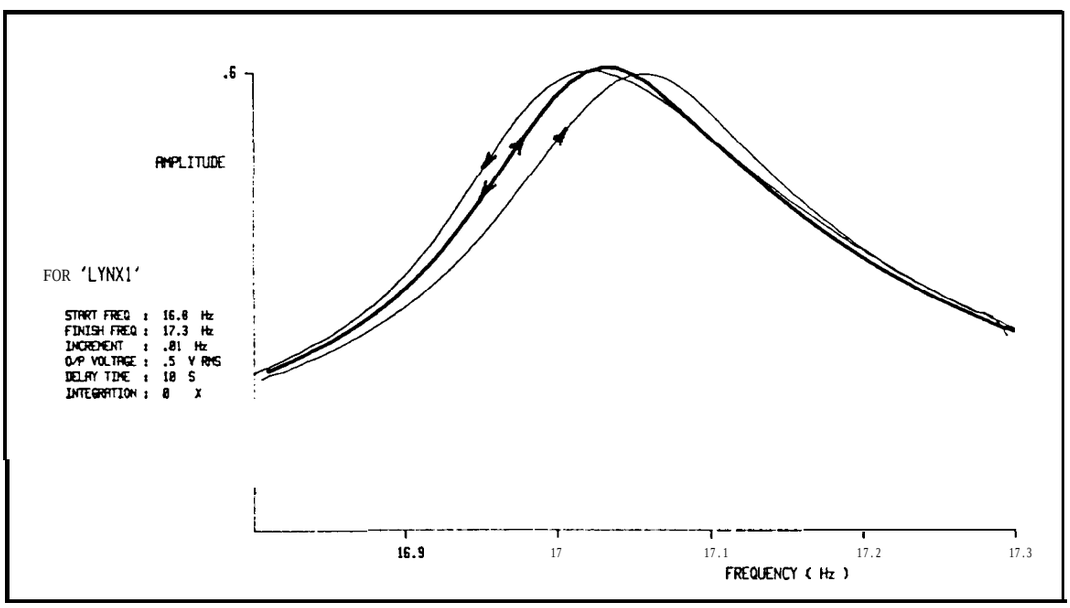

Example of Sine Sweep Rate Influences on Measured FRFs.

Figure 4.1

In a perfect environment, once the structure has had time to settle, a single measurement of force and response should be sufficient to define the point on the FRF accurately. However, in practice, noise is invariably superimposed on the signals to be measured and it is prudent to make several measurements of the data and to calculate an average value. Fortunately, one of the properties of random noise is that, considered over a long enough period of time, the averaging process will reduce the random errors on the data to zero. Averaging will only reduce the effects of random errors, it will not reduce the effects of systematic errors introduced by the test set-up.

A prime advantage of the sine testing technique is the large signal to noise ratio for all the force and response measurements. This is a consequence of the single excitation frequency for each measurement – there are no other significant sources of excitation to contaminate the results. Furthermore, the input ranges for the force and response signals can be adjusted automatically for each excitation frequency point, which allows the best possible use of the measuring equipment.

The ability to concentrate data points in regions of greatest rates of change on FRFs is particularly advantageous for efficient and accurate definition of resonance peaks and anti-resonance troughs.

4.2.2 Broadband Testing

For broadband testing, the structure is excited with a signal containing energy over a wide range of frequencies simultaneously. The time-domain force and response signals are filtered, digitized and then passed through a Fourier analysis process to transform the time-domain information to frequency-domain spectra. By appropriate combination of the force and response spectra, the required FRFs for the structure can be derived, Because of constraints imposed by the Fourier analysis process, the frequency point spacing is constant across the whole measurement frequency range. This represents an inefficient use of the limited number of frequency points available because they cannot be concentrated in the regions of greatest change on the FRFs – around the resonances and anti-resonances.

There are very many different types of excitation that can be used for broadband testing. Probably the simplest form of excitation method is hammer testing. A specially-instrumented hammer is used to impact the structure at the desired excitation point, A very short sharp excitation pulse is produced – approximating a Dirac delta function – which has a flat spectrum over a wide frequency range, although the amount of energy contained in the impact pulse is necessarily small. By using hammer tips with different resiliences, different pulse widths can be obtained. The main advantage of hammer testing is that the excitation equipment (the hammer) is small, light and cheap. It is used mainly for diagnostic purposes rather than for precise measurement of FRF properties. Disadvantages of the hammer testing method are related to the inconsistency of the excitation – the impact pulse is difficult to control accurately in size, in shape, in direction and the duration of the pulse is very small compared with the measurement time frame. Furthermore, pulse excitation is a major disadvantage when the structure contains non-linearities.

The most popular form of excitation is by use of an electromagnetic shaker driven with a signal from the data acquisition system. The mechanical set-up is identical to that used for sine testing. Two common types of broadband excitation signals – random and pseudo random – will be discussed here.

Random

A true random excitation signal has a continuous spectrum which is flat across an infinite frequency range. In practice, 25 kHz is considered as an infinite frequency range in some data acquisition systems. The random time-domain excitation signal is a reasonable approximation to the type of excitation found in many typical installations. The probability distribution of the random excitation is approximately Gaussian (Normal), with a peak to RMS ratio of about 3:1. Additionally, for a linear system, the probability distribution of the response to this excitation is also approximately Gaussian. Due to the random nature of the excitation the structural response does not tend to "peak-up" at resonance frequencies to the same extent as it does with some other forms of excitation (e.g. swept sine) and hence, this type of excitation does not cause undue problems when applied to non-linear structures. However, because the force and response signals are random, a weighting function (e.g. Hanning window) must be applied to these signals before the Discrete Fourier Transform (DFT) is performed, otherwise the mathematical assumptions of periodicity in the measurement time frame are invalid.

The force and response signals from the transducers contain energy at all frequencies (the true spectra are continuous), but because the measurement time frame is of a finite length, the Fourier Analysis produces spectra that are discrete, rather than continuous, functions. Therefore, there is a 'spreading' of energy from the actual continuous spectra into adjacent spectral lines – this phenomenon is known as leakage.

Pseudo Random

Pseudo random excitation is a special form of periodic excitation that has several benefits for signal processing. Although called random, it is not random in the true sense of the word. Within a time period equal to the analysis time frame, the signal is random, but the same signal is then repeated continuously. Usually, the signals are generated inside the data acquisition equipment in the frequency-domain. Once the measurement frequency range and number of frequency lines have been selected, a flat excitation frequency spectrum is generated by setting the magnitude of all spectral lines to the same value. The phases of the spectral components are then randomised. By use of the Inverse Fourier

Transform (IFT) this frequency-domain spectrum is transformed into the time-domain to produce a random-like excitation signal in the analysis time frame. As a consequence of generating the signal in this way, it is exactly periodic in the analysis time frame and hence both the force and the response signals will be periodic in the analysis time frame also. Therefore, there is no requirement for application of any window function to this type of data. In fact, it has been shown [15] that it is detrimental to the quality of the results to apply **any** form of window function to this type of data, other than a uniform window. Because the signals are exactly periodic in the analysis time frame, they only contain energy at the precise spectral component frequencies of the analysis and, therefore, there are no leakage problems when pseudo random excitation signals are used.

Since the pseudo random excitation signal only contains energy in the frequency range of interest, the signal-to-noise ratios for the measured force and response signals are much better than they would be with pure random excitation.

Every different randomised arrangement of the spectral component phases will give a different time-domain signal. If a large number of these signals are inspected, it is found that the peak to RMS ratio is more often worse than3:1, than better (the peak-to-RMS ratio for a pure random signal). However, it is possible to arrange the phase relationships of the spectral components such that the time-domain signal has the special form of a swept sine -

$$f(t) = \sin (at)^* \qquad \ldots\ldots(4.1)$$

which has the instantaneous frequency given by $\left[\frac{d}{dt}\left\{ (at)^2 \right\} = 2a^2t \right]$. For this signal the spectral components have the following relationship-

$$F(\Omega_r) = \frac{1+i}{a}\left(\frac{\pi}{2}\right)^{\frac{1}{2}}.\ \exp\left(\frac{-i\Omega_r^{\,2}}{4a^2}\right) \qquad \ldots\ldots (4.2)$$

Providing that the sweep rate is not too rapid – each cycle is approximately a sine wave of constant frequency – the peak-to-R&IS ratio of the signal will be very similar to that of a pure sine wave, i.e. 1.41: 1. For measurement of the input signal, this low peak-to-RMS ratio is advantageous. Unfortunately, by the nature of the excitation signal, the structural response builds up very significantly in the resonance regions, leading to high peak-to-RMS ratios in the measured responses. Furthermore, an excessive response range, such as this, can cause problems when the structure contains non-linearities because these non-linearities will be exercised to a greater extent than with a less well ordered excitation.

Detailed derivations of the equations relating to the sine sweep excitation functions may be found in the paper by White and Pinnington [71].

4.2.3 Single-Point Testing

The most common form of vibration testing used today is 'single-point' testing. A single excitation input is used for each set of tests, although many response points can be measured simultaneously if sufficient data acquisition channels are available. The standard FRFs can be calculated simply, because the response at each point is due solely to the single excitation force – which is the definition of an inertance type of FRF (see section 1.1.3). With a series of tests using a single excitation point it is possible to measure data for one column of the FRF matrix. Data for the other columns can be measured subsequently by repeating the measurements for a different excitation position. Inconsistencies may occur in the measured data as the set of force and response transducers are moved to all the required locations on the structure.

A deficiency with single point testing is that, by its nature, the energy input is very localised. In large heavily-damped structures the excitation energy is quickly dissipated before it has propagated far within the structure. In an effort to excite remote regions, the single point forcing level is sometimes increased to excessive levels, thereby exercising local non-linearities to a much greater extent than would otherwise be the case if the excitation energy were distributed more evenly throughout the structure.

4.2.4 Multi-Point Testing

When testing large complicated structures with numerous joints, the undoubted presence of non-linearities and the fact that the vibration energy is quickly dissipated within the structure can indicate that the use of multi-point testing is preferable to a series of single-point tests. By using multi-point excitation, a larger amount of energy can be fed into the structure more uniformly than with single-point excitation and the vibration amplitudes at various locations can be kept much closer to those found in operation. Energy is supplied to the structure by several shakers, and so smaller and cheaper shakers can be used than would be necessary for single-point testing. Furthermore, the effects of non-linearities, which may occur with excessive single-point forcing, can be substantially reduced. Connection of all the shakers to the structure before the start of the test also means that systematic errors, which are a result of repositioning the shaker for a series of single-point tests, do not occur. The influence of the shakers on the structure is not removed, it just remains constant throughout the whole of the test programme – a static base-condition

error. Additionally, simultaneous measurement of multiple columns of the FRF matrix means that the overall test time is shortened and there is less opportunity for structural changes (with time, temperature or humidity) to affect the measured results.

The most commonly used multiple shaker technique is known as Multi-Point Random (MPR). For all multi-point excitation techniques, more sophisticated computer programs are necessary to extract the standard FRFs from the measured data. To comply with the mathematical assumptions made in the analysis, it is important that the excitation inputs to the structure are pure random and uncorrelated. Although it is possible to ensure that the excitation signals driving the shakers are uncorrelated, it does not necessarily follow that the excitation force signals are uncorrelated At the resonance frequencies, in particular, it is found that the motion of the structure tends to correlate the actual multiple forcing inputs, leading to degradation in the quality of the derived FRFs at these frequencies.

As a consequence of using broadband random excitation a window function (e.g. the Hanning window) must be applied to the measured force and response signals before Fourier transformation. Leakage is a potential problem and because of the large quantity of superfluous high-frequency excitation energy, the signal-to-noise ratio is less than it would be with a pseudo random type of excitation. Unfortunately, multiple pseudo random excitation sources, as defined above, would be 100% correlated.

A new multi-point testing technique that is gaining in popularity is the Multi-phased Stepped Sine technique (MPSS) developed by SDRC [19]. In essence, the technique is a combination of the phase-resonance and phase separation methods of vibration testing. By using multiple inputs with specific mono-phased force patterns (forces in-phase or out-of-phase with each other), sweeps are made over the complete frequency range of interest. The data are analysed and by use of the Multi-variate Mode Indicator Function (MMIF), it is possible to identify the specific force patterns required to excite each normal mode. Narrow frequency sweeps are performed around each resonance, using the appropriate force patterns and the results obtained can be analysed easily by circle fitting methods. At the undamped natural frequency the displacements of the system correspond to the undamped normal mode shape – the basis of the phase-resonance technique of vibration testing.

The benefits of the MPSS technique are the high signal-to noise ratio and the variable frequency point spacing, all combined with a multi-point test configuration that allows full identification of modes with a multiplicity greater than one. The FRF data obtained by this method are generally smoother and easier to analyse than data from MPR type tests.

Interleaved Spectral Excitation Technique (INSET)

Many of the disadvantages with present multi-point testing techniques (MPR and MPSS) can be avoided with a new testing method known as INSET **(INterleaved** Spectral Excitation Technique) **[79].** The generation and use of the excitation signals is the main difference between this technique and those presently available. The signal generation is similar to that used for pseudo random signals described above. A single discrete excitation spectrum is formed with spectral components of equal magnitude set at the analysis frequencies. The frequency spectrum is then divided up into parts – one part for each of the excitation sources, e.g. if there are to be 2 excitation sources the frequency spectrum is split into 2 parts. There is no theoretical restriction on how the frequency spectrum is split between the shakers, but for the best spatial distribution of excitation frequency energy the individual spectra are formed by "combing" the complete spectrum, e.g. for 2 excitation sources the **1st** spectrum would consist of line numbers **(2n),** n=O to $\frac{N}{2}$ from the complete spectrum, and the **2nd** spectrum would be formed from lines (2n + **1),** as shown in Figure 4.2.

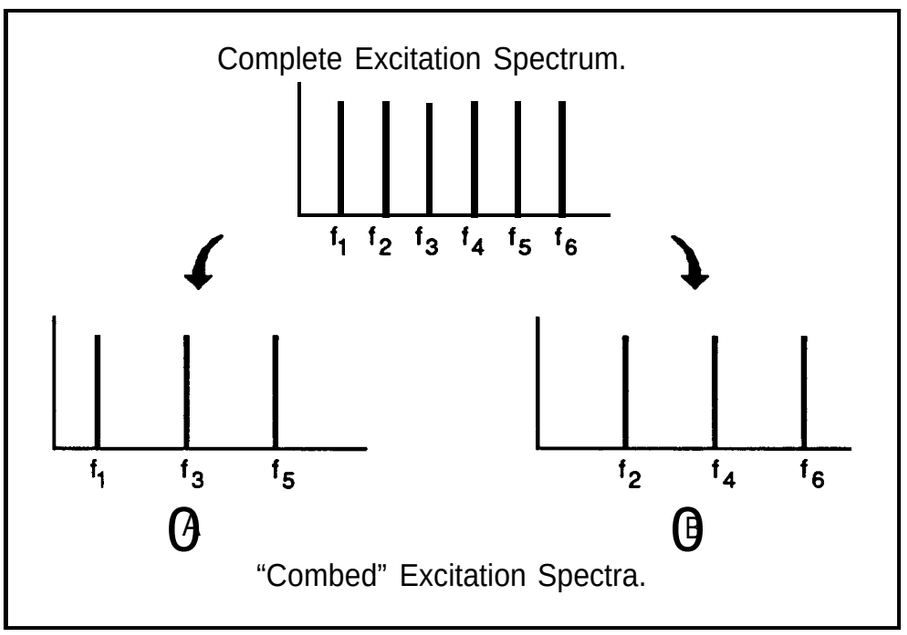

Derivation of Excitation Spectra.

Figure 4.2

Once the spectral content of each excitation source has been decided, the phase relationships have to be fixed. An Inverse Fourier Transform **(IFT)** of each spectrum produces the time-domain signals required. By careful arrangement of the phases of the components in each spectrum it is possible to generate time-domain excitation signals

having a minimum peak-to-RMS ratio. This is advantageous in reducing the degree to which non-linear elements are exercised.

So that each forcing location experiences the full excitation spectrum, the different signals are fed to each shaker in turn. To avoid any transients associated with switching the excitation signals it is necessary to have a settling period after each change before any further data are collected, This is analogous to the settling period mentioned in reference to sine sweep testing.

Derivation of the standard FRF properties is a simple process, best illustrated by a simple example.

Consider a system with two points of interest and a two-point INSET test set-up, Figure 4.3. The complete excitation spectrum is assumed to consist of 6 components from which the two individual excitation spectra (A & B) are “combed”, as shown in Figure 4.2.

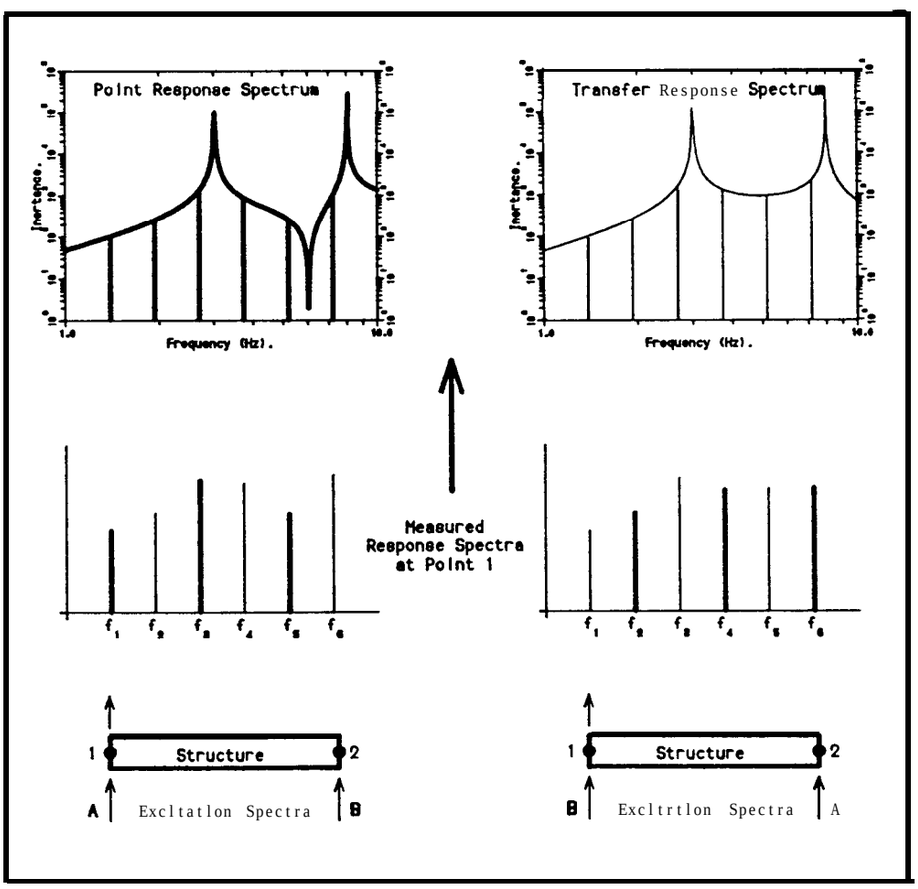

Derivation of Frequency Response Functions from INSET Data.

Figure 4.3

Initially, the excitation signal from the IFT of A is applied at location 1 and the signal from B is applied at location 2. We shall consider the response at location 1 to this excitation. Since the overall excitation contains energy at all the spectral frequencies the responses will also contain energy at all the spectral frequencies. However, the response at frequency f_1 must be due to excitation A because this is the only excitation containing energy at f_1. Excitation A is applied at location 1 and therefore it can be concluded that the response spectral component at f_1 represents a point measurement; similarly for f_3 and f_5. Response at frequency f_2 is the result of excitation B, applied at location 2, and hence it represents a transfer measurement – as for f_4 and f_6. When the excitations are reversed, so that signal A is applied at location 2 etc, the point and transfer response spectra can be completed.

Mathematically;

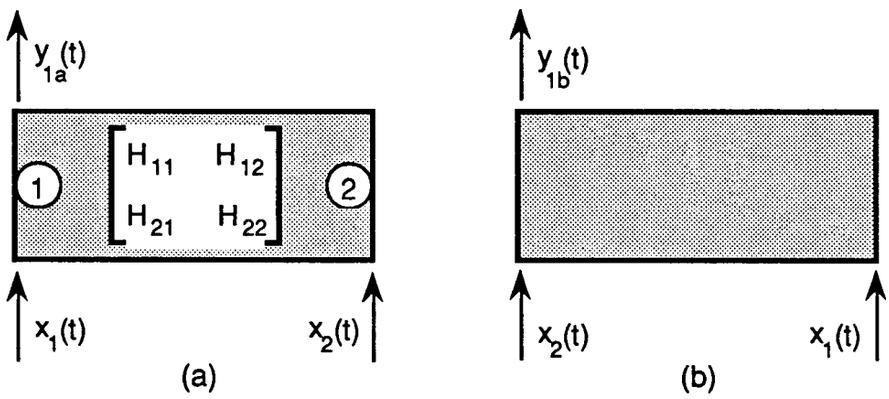

Figure 4.4

The Fourier Transformed response $Y_{1a}(f)$ of the system shown in Figure 4.4 is given by

$$Y_{1a}(f) = H_{11}(f).X_1(f) + H_{12}(f).X_2(f) \quad \text{.....(4.3)}$$

and for Y n,(f)

$$Y_{1b}(f) = H_{11}(f).X_2(f) + H_{12}(f).X_1(f) \quad \text{..... (4.4)}$$

Now, $X_1(f)$ is non-zero for, say, odd lines of the spectrum, i.e. $f_1, f_3, \ldots$ etc, and $X_2(f)$ is non-zero for even lines of the spectrum, i.e. $f_2, f_4, \ldots$ etc. Therefore, from equation (4.3),

$$Y_{1a(f1.3.\ \ldots)} = H_{11}.X_1(f_{1,3}\ldots) \quad \text{..... (4.5)}$$

$$Y_{1a}(f_{2,4,\ \ldots}) = H_{12}.X_2(f_{2,4,\ \ldots}) \quad \text{..... (4.6)}$$

and from equation (4.4) -

$$Y_{1b}(f_{1,3\ldots}) = H_{12}.X_1(f_{1,3,\ldots}) \quad \ldots\ldots(4.7)$$

$$Y_{1b}(f_{2,4\ldots}) = H_{11}.X_2(f_{2,4,\ldots}) \quad \ldots\ldots(4.8)$$

Combining equations (4.5) and (4.8)

$$Y_{1a}(f_{1,3\ldots}) + Y_{1b}(f_{2,4,\ldots}) = H_{11}.X_1(f_{1,3\ldots}) + H_{11}.X_2(f_{2,4\ldots}) \quad \ldots\ldots(4.9)$$

$$= H_{11}(X_1(f_{1,3\ldots}) + X_2(f_{2,4\ldots})) \quad \ldots\ldots(4.10)$$

Now, $(X_1(f_{1,3\ldots}) + X_2(f_{2,4\ldots}))$ is equal to the original excitation spectrum (say, X_0) before "combing".

Therefore, $Y_{1a}(f_{1,3\ldots}) + Y_{1b}(f_{2,4,\ldots}) = H_{11}.X_0$ .....(4.11)

and the point FRF $H_{11} = \dfrac{Y_{1a}(f_{1,3,\ldots}) + Y_{1b}(f_{2,4,\ldots})}{X_0}$ .....(4.12)

Similarly, combining equations (4.6) and (4.7) gives the transfer FRF as -

$$H_{12} = \frac{Y_{1a}(f_{2,4,\ldots}) + Y_{1b}(f_{1,3,\ldots})}{X_0} \quad \ldots\ldots(4.13)$$

Averaging of the excitation and response spectra can be done in exactly the same way as with standard single-point excitation techniques. Because the excitation signals are generated by IFT of finite discrete frequency spectra with components at the analysis frequencies, the time-domain signals are exactly periodic in the analysis time frame and there is no requirement for any windowing of the excitation or response signals (see section on pseudo random signals).

Only two excitation points have been used in this example, but it is a simple matter to extend the technique for as many excitation locations as required (providing suitable equipment is available).

A disadvantage of the interleaved spectral excitation technique is that it cannot be implemented with many of the vibration measurement systems currently available as it requires multiple channels of Digital to Analogue Conversion (DAC) that can be controlled, switched and synchronised with the analysis time frame. Most readily-available vibration measurement systems only have a single channel of DAC and, even then, there is insufficient facility for user control of the DAC itself or of the signals fed to the DAC.

Despite the obvious advantages of the interleaved spectral excitation technique, equipment and time limitations inhibited its use for practical vibration measurements during the course of this work.

4.3 Shaker – Structure Interactions

It is known that, on a log-log plot, the sharpness of the resonance and anti-resonance features should be the same [25]. For broadband random testing, the frequency resolution across the whole frequency range of interest is constant and, so, it is easy to assess whether this criterion is met. Very often it is not, see Figure 4.5.

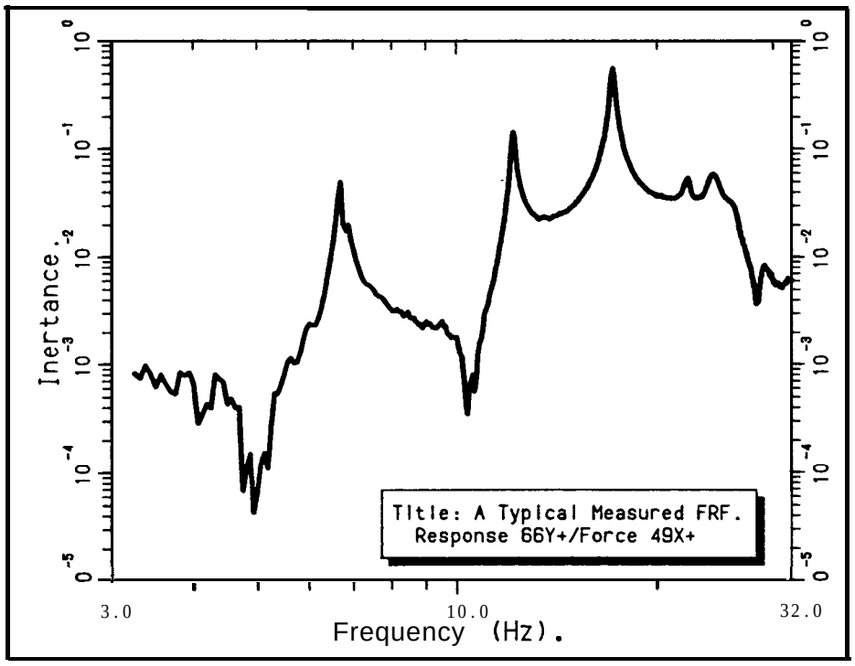

A Typical Measured FRF.

Figure 4.5

The anti-resonances are much less well defined than the resonances. In normal circumstances this is not seen to be too much of a problem because interest is focussed on resonances rather than anti-resonances. This is unfortunate because the anti-resonances provide a highly visual and accurate check on the performance of any modal analysis and the subsequent synthesis of FRFs.

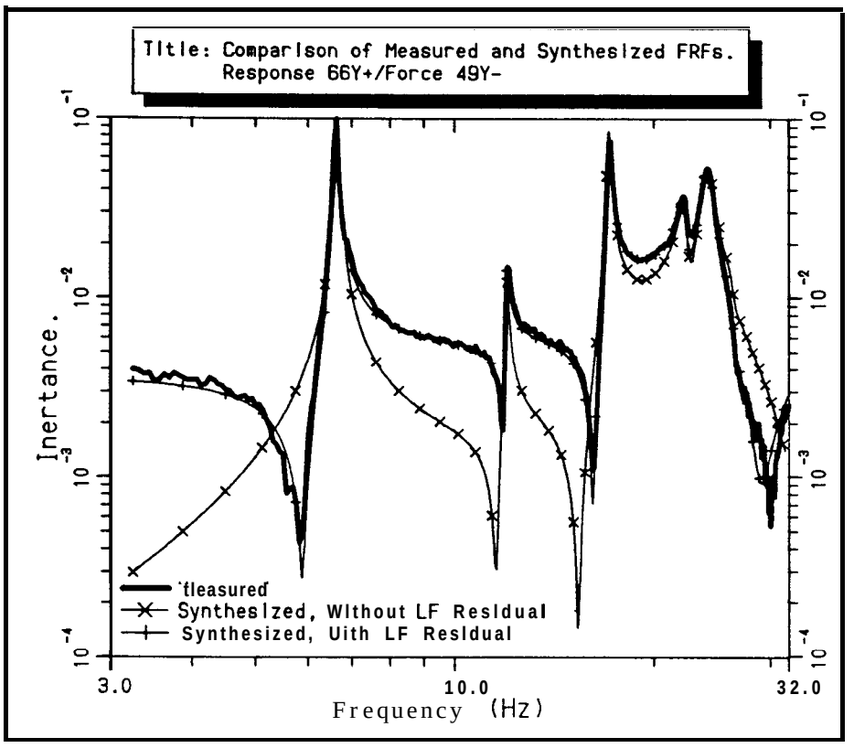

Comparison of Measured & Synthesised FRFs.

Figure 4.6

When measured and synthesised FRFs are compared directly, Figure 4.6, the anti-resonances from the two sets of data will only match if all the modes have been analysed correctly and any residual effects have been taken into account. This is because an anti-resonance is a result of the contributions of all modes summing together to give zero. In the vicinity of a resonance the structural behaviour is dominated by a single mode and the contribution of all the other modes becomes relatively insignificant. In fact, this is the assumption upon which the single degree-of-freedom analysis methods are based. When the sensitivity analysis method, developed in chapter 3, is to be used it is important that the measured anti-resonances are defined as clearly as the resonances, to facilitate direct extraction of all resonance and anti-resonance frequencies by visual inspection or use of a cursor feature available on the analyser. For this reason, it is necessary to understand why the anti-resonance characteristics are not usually as well defined as the resonance characteristics when broadband random testing methods are employed so that some effort can be directed towards improving the situation. The explanation is based in the relationship of the force and response signals through resonance and anti-resonance regions and the maximum dynamic range of the measuring equipment.

It is possible to produce an excitation signal from the analyser that has a flat spectrum. The signal is amplified and used to drive an electromagnetic shaker but the actual force

excitation applied to the structure (measured with a force gauge) does not have a flat spectrum, due to the mechanical interaction between the shaker, its suspension, and the structure. This is illustrated by the following arbitrary example, Figure 4.7:

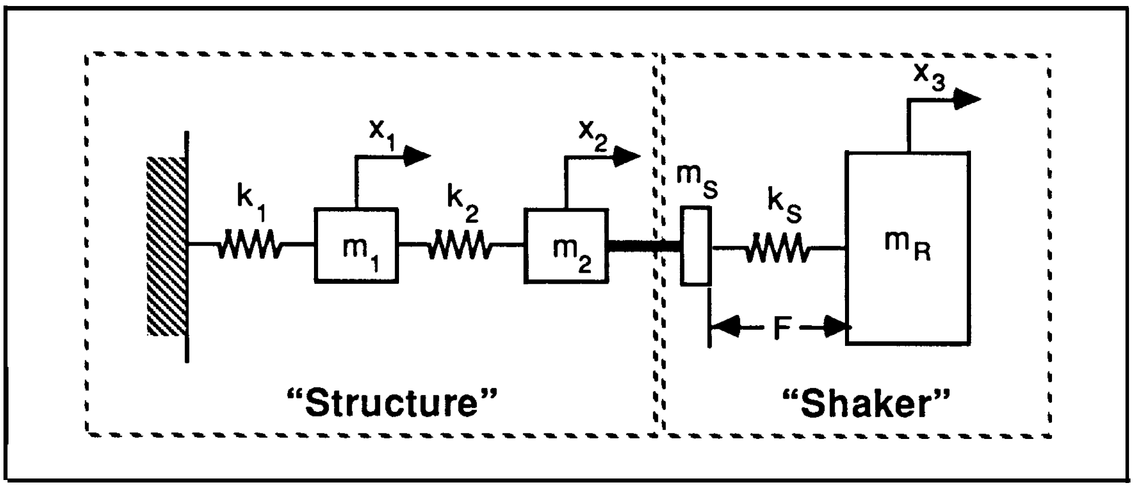

Example System used for Representation of Shaker-Structure Interaction.

Figure 4.7

The 'structure' is modelled as a grounded 2 degree-of-freedom mass and spring system. The shaker model consists of 3 elements; a mass (m,) representing the moving components such as the coil, the table and the pushrod etc., a spring (k_s) representing the stiffness of the coil suspension arrangement and a large mass (m_R) equivalent to the total reaction mass of the shaker. The force (F) generated inside the shaker has a uniform spectrum and is considered to act between the moving mass and the reaction mass of the shaker, i.e. in parallel with the suspension spring. The moving parts of the shaker are connected to the force gauge on the structure by a pushrod.

We assume that for the 'structure';

$k_1 = 1000$ N/m $\qquad k_2 = 1000$ N/m

$m_1 = 3$ Kg $\qquad m_2 = 1$ Kg

and for the shaker ;

$m_s = 0.0025$ Kg $\qquad k_s = 125$ N/m

$m_R = 10$ Kg $\qquad F = 6.68$ N

The response vector {x) is given by solution of -

$$\{x\} = \left[[K] - \omega^2[M]\right]^{-1}.\{F\} \qquad (4.14)$$

where, [M] and [K] are the system mass and stiffness matrices and {F) is the forcing vector.

The force transmitted from the shaker to the structure (F_T) is given by -

$$F_T = F - \left(\omega^2 m_s - k_s\right)x_2 - k_s x_3 \qquad (4.15)$$

The receptances that would be measured in an experimental investigation can then be calculated by dividing the appropriate response parameter by F_T. For this example, the point receptance for location 2 has been chosen for illustration. The Force, Response and FRF characteristics are shown together on a log-log plot in Figure 4.8. The resonance and anti-resonance frequencies calculated for the structure are 2.4263 Hz, 6.0275 Hz and 4.1094 Hz respectively (see the example of section 3.3.6) and they are shown correctly by the derived FRF in this plot.

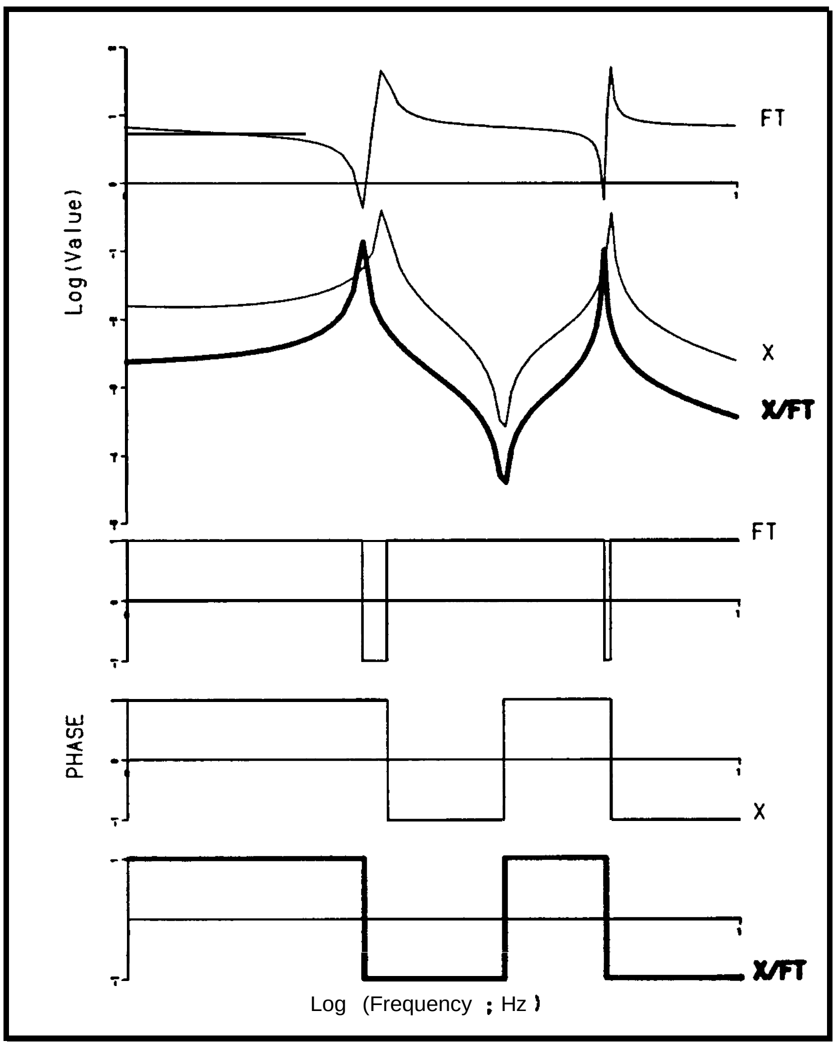

Force, Response and Receptance Functions for a Typical Test.
Figure 4.8

A careful study of these characteristics is instructive for understanding the interactions between the structure and the shaker. At very low frequencies the transmitted force, F_T, and the displacement at the interface, x_2, are in phase with each other. F_T passes through zero as the frequency is increased to the first resonance frequency. The maximum response occurs at a frequency slightly higher than the resonance frequency. Between the resonance frequency and the frequency of maximum response, the force F_T and the response x_2 are out of phase. The force is working in opposition to the motion of m_2. As the response reaches a peak and passes from $+\infty$ to $-\infty$ the magnitude of the force also reaches a peak, but passes from $-\infty$ to $+\infty$. Since both the force and the response each reach an infinite value simultaneously, the ratio of the response and force (the FRF) has a finite value. The force, F_T, and the response, x_2, remain out of phase until the anti-resonance frequency, where the response passes through zero. The phases of F_T and x_2 are now the same as they were at frequencies below the fiist resonance and the sequence of phase changes is repeated for the second mode.

The key factors to note are that resonance occurs at zero force input and that an anti-resonance occurs at zero response. At resonance, almost all the force generated within the shaker is used to accelerate the moving parts of the shaker and almost nothing is transmitted through to the structure. In the limit, the dynamic range of the force can be reduced to zero (Figure 4.9) by setting m_s and k_s to zero (the size of the reaction mass is then irrelevant). In this situation, the dynamic range of the response is identical to that of the receptance function.

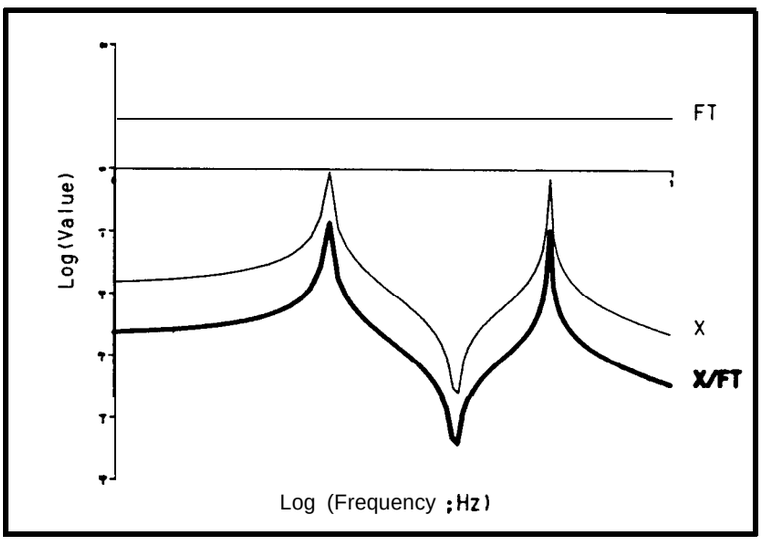

Force, Response and Receptance Functions for m_s and k_s set to Zero.

Figure 4.9

For most practical situations, where the dynamic range of the force function is greater than zero, the dynamic range of the response function will be greater than the dynamic range of the receptance function.

In cases where the moving mass of the shaker is large, there is little movement of the shaker or the structure, and the dynamic range of the response can be reduced below that of the receptance function, Figure 4.10.

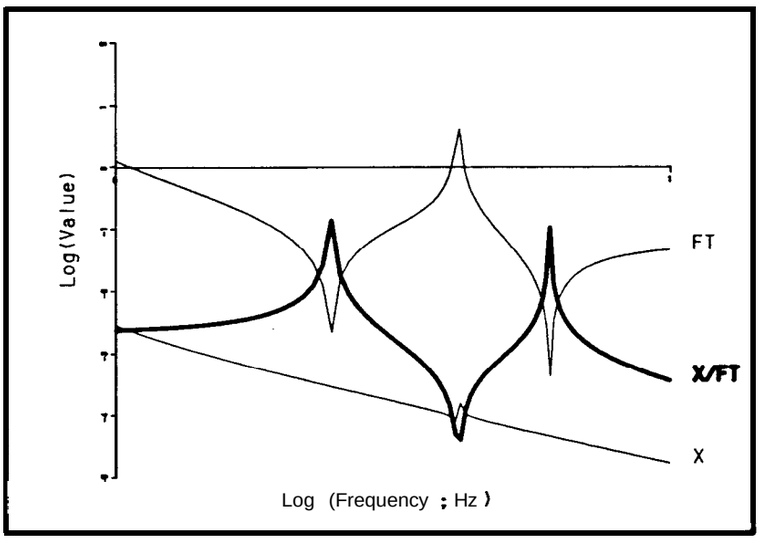

Force, Response and Receptance Functions for a Large Shaker Moving Mass.

Figure 4.10

It can be seen that, provided that the shaker and reaction mass are selected correctly for a given structure, the dynamic range of the force signal can be reduced to manageable levels, whereas the dynamic range of the response signal remains comparatively unchanged. Correct matching of the shaker to the structure means selecting a shaker that has minimum moving mass and minimum coil support stiffness for the necessary force levels. The reaction mass should be as large as possible, although, special care should be taken when augmenting the reaction mass of a shaker by bolting on additional masses, as the centre of gravity of the shaker must remain in-line with the forcing axis. If the centre of gravity is displaced from the forcing axis, the reaction mass is less effective and undesirable rotational motion of the shaker system will result from the excitation forces.

4.4 Preliminary Data Collection and Assessment

4.4.1 Preliminary Survey

There are so many factors which affect the final outcome of a coupling analysis that it is believed strongly that an assessment of the expected results will only be possible from a thorough, and possibly extensive, preliminary survey. The aim of such a survey is to give some guidance as to the relative importance of different degrees-of-freedom at the coupling points, for selected types of modifications, and the care with which they must be measured.

Measurement Frequency Range

Usually, in structural modification exercises, the region of interest is focussed on a relatively small frequency range, situated about a problem frequency at the operating condition of the machine. This small frequency range should be considered in careful detail both before and after the modification prediction, so that the precise effect of the modification in that region can be properly assessed.

Although the main interest is concentrated in a narrow frequency range, it is still vital to have a much wider picture of the situation. It may be that as a consequence of improving the dynamic characteristics in one particular frequency range, detrimental effects occur elsewhere. This should be known, so that the overall suitability of a modification can be assessed.

It has already been mentioned that the final results will be judged over a small frequency range around a particular frequency of interest. However, it is important to remember that the input data may have to be collected accurately for a very much wider frequency range, particularly if a process of modal analysis and subsequent synthesis of the FRFs is to be employed. In principle, if the raw measured FRF data were to be used directly in a coupling analysis, then it would be necessary to measure data only over the small frequency range of interest because this data includes the effects of **all** the modes of vibration. Nevertheless, it has been found that slight inconsistencies in the raw data (brought about by taking several measurements sequentially rather than all simultaneously) leads to predictions for the FRFs of the modified structure that are contaminated by ‘breakthroughs’ from the original data [31]. This problem can be avoided if all the data are measured simultaneously, or the if FRFs are synthesised from a modal database. Practically, it is not possible to collect all the data for the complete FRF matrix

in one simultaneous multi-point excitation measurement – such a measurement would necessitate an excitation source and a response transducer at every degree-of-freedom of interest, including rotational degrees-of-freedom.

If the FRFs used in a coupling analysis are to be synthesised from a modal database, then either: (i) sufficient modes must be included in the measured frequency range to account for the effect of out-of-range modes in the narrow frequency band of interest, or (ii) residual terms must be accurately defined and incorporated for each FRF to be used in the modification procedure. The question of what is a 'sufficient number of modes'? depends upon factors such as the local modal density and modal dampings, and whether there are any dominant modes nearby. It will be highly specific to the particular structure, and the modification sites chosen. Once a sufficient number of modes have been measured and analysed for one row or column of the FRF matrix, then all the terms in the matrix may be synthesised accurately from the modal database. However, while the agreement of measured and synthesised FRFs serves as a check on the results for the unmodified structure, there is still no guarantee that the model will be adequate for accurate prediction of the effects of any given modification.

If an impedance coupling method is used, the effects of out-of-range modes can be included by the addition of residuals to the synthesised FRFs. The residual terms approximate the effects of the out-of-range modes in the frequency range of interest. However, if a modal coupling method is used, it is not easy to add in such correction factors.

Frequency Resolution

Adequate definition of the resonance features of a FRF is most important since these data points are highly influential in the modal analysis process. Circle-fitting of single modes in the Nyquist plane presentation of an FRF provides a clear example of the need for sufficient data points in the upper half of the Nyquist circle, i.e. between the half-power points. From preliminary measurements and the following analysis, it is a relatively simple task to calculate the frequency resolution necessary to define the circle adequately for the purposes of modal analysis; consider the Nyquist circle in Figure 4.11:

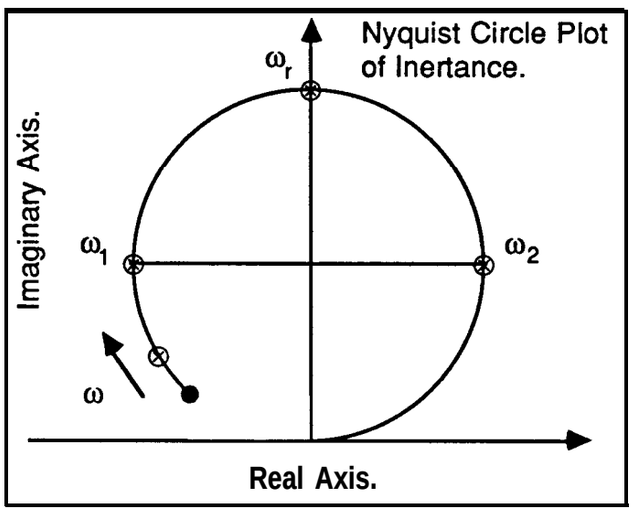

Derivation of a Criterion for Frequency Point Spacing.
Figure 4.11

If we require a **minimum** of three points between the half-power points, ω_1, ω_r and ω_2, to define the circle for analysis purposes, then the frequency spacing ($\delta\omega$) is given by -

$$\delta\omega = \frac{(\omega_2 - \omega_1)}{2} \quad \text{.....(4.16)}$$

It can be shown that for small levels of viscous damping,

$$\zeta_r \approx \frac{(\omega_2 - \omega_1)}{2\omega_r} \quad \text{.....(4.17)}$$

where ζ_r = viscous damping coefficient for r^{th} mode.
ω_r is the resonance frequency,
ω_1 and ω_2 are the half-power points.

Therefore, by substituting equation (4.16) into equation (4.17), the point frequency spacing ($\delta\omega$) is found to be,

$$\delta\omega = \zeta_r\omega_r \quad \text{.....(4.18)}$$

For hysteretic damping and close to a resonance, $\eta_r = 2\zeta_r$ and the expression for the point frequency spacing becomes,

$$\delta\omega = \frac{\eta_r}{2}\,\omega_r \quad \text{.....(4.19)}$$

For broadband random testing, the frequency resolution is generally dictated by the properties of the lowest frequency mode of interest. Elsewhere in the frequency range, the resolution is usually more than adequate – data points are used inefficiently. The maximum number of data points for a test is limited by the data block size available in the analyser. Thus, in combination, the necessary resolution (for the low frequency modes) and the restricted number of data points limit the frequency range that can be measured in any one test. If the frequency range of interest is larger than this, there are two options available;

(i) measure the additional frequency range using zoom measurements; or,

(ii) reduce the frequency resolution and re-measure over a larger baseband frequency range.

The choice is dependent largely upon the features of the analyser and the number of channels measured simultaneously. Implementation of the zoom method requires significantly more computational power and it is usual for either, (a) the number of frequency points or, (b) the number of channels to be reduced by a factor of 2. Zoom measurement has the advantage over extended baseband testing in that the data points are used more efficiently – each mode is measured only once – however, zoom measurements take longer than standard baseband measurements and there are some computational difficulties (frequently zoom FRFs have a 'spike' at the centre-frequency). When using extended baseband testing methods, the low frequency modes are measured several times over, each with gradually increasing frequency spacing as the frequency range is extended. In the subsequent modal analysis phase, only the highest frequency resolution data for each mode is used – the lower resolution data is superfluous.

Any noise on the force signal is likely to influence the resonances whereas noise on the response signal will affect the anti-resonances. To minimise these effects of noise, different estimators of the FRF can be used; for the best estimate of resonances, where there is noise on the response signal, H_1 should be used, and H_2 should be used where there is noise on the force signal. The reverse applies for the anti-resonances. Derivation of these results can be found in reference [80].

Quantity of Data – Number of Degrees-of-Freedom to Measure

The quantity of data to measure depends largely upon the purposes for which the data are required. If the data are only required to identify the resonance frequencies of the structure a small number of FRFs is all that is necessary. To be able to characterise the mode shapes uniquely requires significantly more data. If the purpose of measuring the structure

is to obtain data for use in a coupling analysis of the behaviour of the structure when modified in some way, the measurements must include, as a minimum, FRF data for all the degrees-of-freedom actively involved in the coupling. The minimum quantity of data will enable the new resonance frequencies for the modified structure to be identified but it is probably insufficient to define the new mode shapes adequately. Further discussions on the type and quantity of data necessary for the accurate prediction of the effects of a modification is left until chapter 5.

In chapter 3 the concept of a point difference FRF between two points on a structure was introduced for the calculation of the resonance frequency sensitivities to stiffness modifications between selected pairs of points. At the outset of a measurement survey it should be decided whether investigation of internal spring modifications is appropriate and, hence, whether these point difference FRFs will be required. If so, the data recorded in the measurement survey should include the excitation and response spectra separately, in addition to the normal FRFs. Calculation of the point difference FRF between any pair of degrees-of-freedom is then a matter of appropriate combination of the separate excitation and response spectra for the two degrees-of-freedom involved.

Presently it is envisaged that part of a preliminary survey may consist of making quick – but not necessarily highly accurate – 6 degree-of-freedom point measurements for each of the possible modification sites. This data would then be used together with similar data for the modification component, to establish the relative importance of all the degrees-of-freedom, hence giving some idea of the type and quantity of data to be measured for the interface degrees-of-freedom.

Quality of Measured and Synthesised Data

During the preliminary survey, and indeed throughout the full modal test, some checks should be done to assess the quality of the measured data. If the starting point for any structural modification procedure – the synthesised FRFs – does not represent the structure accurately, then erroneous results for the eventual predictions must be expected.

There are several techniques already in general use which can provide an indication of the quality of the data, e.g. repeatability, reciprocity and coherence. However, application of some of these techniques in a much more systematic, rigorous and critical manner will give a better performance than is presently achieved. Almost always, repeatability and reciprocity checks are done by ‘eyeballing’ sets of FRF curves to see if there are any major differences. The comparisons are made significantly easier if difference function

(AFRF) curves are plotted for the sets of data – in just the same way, the difference functions can be used in the assessment of the performance of different modifications.

4.4.2 Difference Functions

The AFRF is defined as the following vector difference:

$\Delta FRF(\omega)$ = $FRF(\omega)$ for comparison - Reference $FRF(\omega)$.

or AH(o) = H'(o) - H(o)

It has the same units as the original FRF, and the same 'form', i.e., Receptance, Mobility, Inertance, etc., and indeed, exhibits the properties and characteristics of a multi-degree-of-freedom linear system. A single AFRF curve is easier to read and interpret than small differences between two FRF curves, once the various features of the difference curves have been characterised and are familiar.

The AFRF is the **vector** difference of the two FRFs at each frequency ω. This is shown clearly in the Argand plane (Figure 4.12) where the functions are assumed to have slightly different resonance frequencies. The vector joining the two response function vectors is the difference, and the magnitude of this difference vector can often exceed the magnitude of one of the constituent FRF vectors.

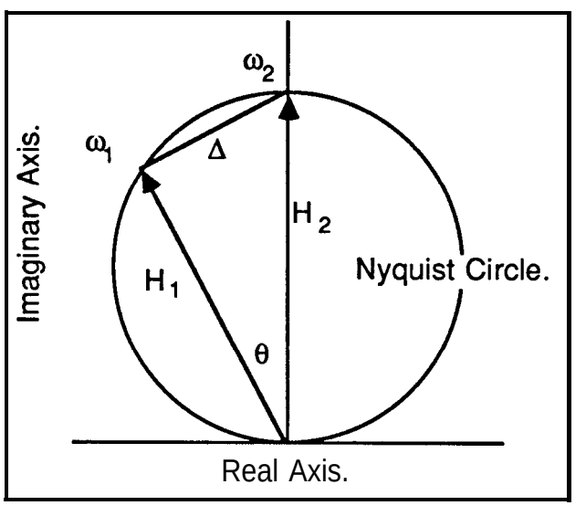

Derivation of the Vector Difference Function.

Figure 4.12

The difference is given by the vector difference: $\Delta = (H_2 - H_1)$

Now, if we assume that $|\Delta| = |H_1|$, then $\theta = \frac{\pi}{4}$ rads (45°) and, $H_2 = \sqrt{2}\, H_1$

On a log plot, the difference in the magnitudes of H_1 and H_2 would be 3 db in a total range of the function of possibly 60 db and, therefore, not easily seen.

The difference between a half-power point frequency and the resonance frequency is given by $\xi\omega_r$ (from equation 4.16). For a system with a viscous damping of 1% critical there would only need to be a 1% shift in the measured resonance frequency for the magnitude of the AFRF to be the same as one of the constituent FRFs, i.e. the difference function is a very sensitive function. Without very careful inspection of the FRF Bode plots, even differences as large as this can be difficult to see.

Use of the AFRF in Repeatability and Reciprocity Checks

Repeatability checks are a means of assessing the stability of the structural characteristics over a period of time. It is always assumed that the structure does not change with time or as a result of the excitation itself but there are a number of practical effects that can alter the characteristics of a structure;

e.g. Bolts slackening,
Release of pre-loads,
Fretting,
Environmental factors, such as temperature and humidity.

For a linear conservative system, Maxwell's Rule of Reciprocity applies: the measured FRF for a force at location j and a response at location i should correspond directly with the measured FRF for a force at location i and response at location j. The FRF matrix is symmetric and this property can be used as a check on the quality of the measured data. Additionally, the reciprocity check can give an indication of shaker and accelerometer loading effects on the structure. When making reciprocity check measurements the positions of the shaker and accelerometer are reversed. If the shaker and accelerometer have negligible effect on the structure, then there should be good reciprocity (all else being equal). But if the shaker and accelerometer do have a significant loading effect on the structure, then the effects in the two configurations will be different and the reciprocity check will reveal differences between the FRFs.

Repeatability and reciprocity checks are usually carried out over a frequency range incorporating several modes, with the emphasis placed on the magnitudes of the functions. In keeping with this practice, the magnitude of the AFRF is plotted alongside

the two FRFs of the repeatability or reciprocity check for comparison. It is important that the AFRF is interpreted with reference to the FRFs, from which it was derived, to understand the possible causes of any large discrepancies indicated. If a large peak on the AFRF corresponds with a resonance region of the constituent FRFs, then it is likely that the difference is due to a slight shift in the natural frequency. When a peak occurs away from resonance, it is usually caused by differences in the magnitudes of the FRFs.

AFRF Examples

The following examples show the benefits to be gained from the use of the AFRF in the presentation of repeatability and reciprocity data. The measurements are all taken from a survey of an aerospace structure, with the repeatability measurements made over a period of one week The same level of input excitation was used for all the measurements and, in the case of the reciprocity measurements; no attempt was made to keep the response at a particular point the same for each excitation. Therefore, there could be the influences of non-linearities included in these results.

The AFRF in Repeatability Checks

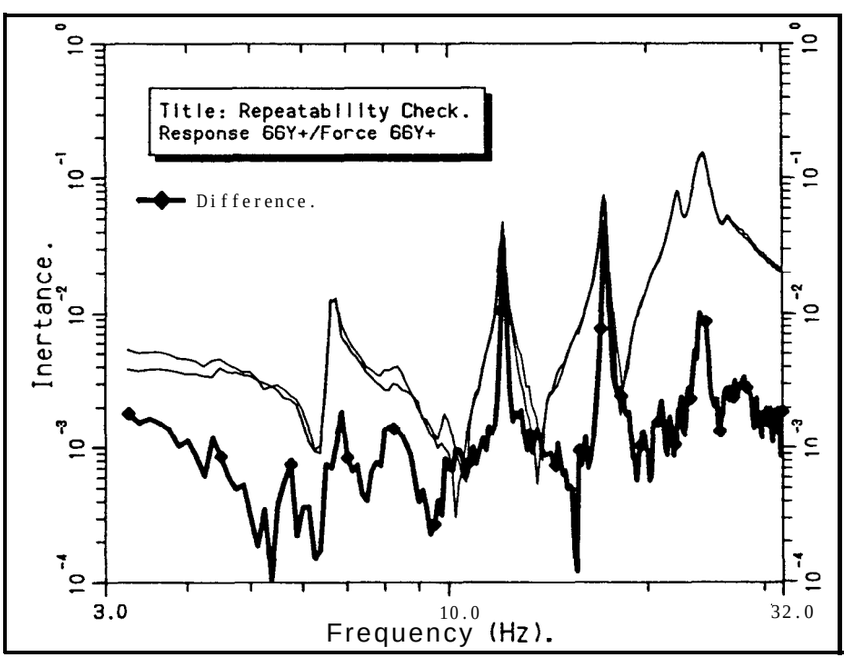

Repeatability Check using the AFRF.

Figure 4.13

The two point FRF measurements, shown in Figure 4.13, were made at different times as a check of the measurement repeatability. The vector difference between these two

functions has been calculated and forms the AFRF which shows clearly the large differences between the FRF measurements around the resonance regions. Without the AFRF it would be all too easy to dismiss the small differences in the magnitude plots of the FRFs.

The AFRF is of little value on its own, only when it is **plotted** alongside the FRFs from which it was derived can meaningful interpretations be made.

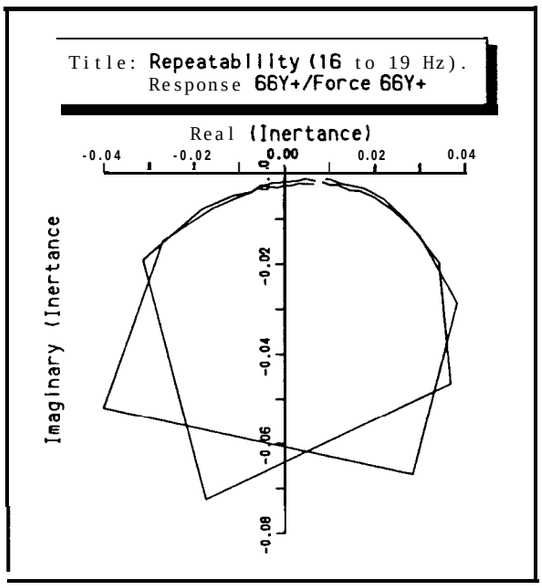

Nyquist Plot of Repeatability Measurements (16–19 Hz).

Figure 4.14

In Figure 4.14, small portions of the same two FRF curves shown in Figure 4.13, are plotted in the Argand plane around the 4th resonance (from 16 to 19 Hz). Although the data points from the two FRFs are now widely separated, in the vicinity of resonance it would be a reasonable assumption to say that they all lie on the same modal circle. The differences are due to a slight shift in the resonance frequency and, because frequency information is not usually displayed on an Argand plot, the resonance frequency shift is not easy to deduce without further analysis.

The AFRF and Reciprocity Checks

The use of the AFRF in assessing the reciprocity of measured FRFs is shown in Figure 4.15; two measured reciprocal FRFs are plotted together with the AFRF. It will be noticed that the largest differences occur in the resonance regions. Once again, this is due primarily to slight shifts in the resonance frequencies rather than to changes in the magnitudes of the FRFs; the 3rd mode at around 11 Hz and the 4th mode at about 17 Hz illustrate this clearly. An enlarged portion (16 to 19 Hz) of the plot is shown in

Figure 4.16 where the shift in the resonance frequency can be seen clearly. Frequency shifts such as this, caused through different loading of the structure by the measuring apparatus for the two measurements, are not always quite so obvious but, nevertheless, they can still give rise to problems at the modal analysis stage.

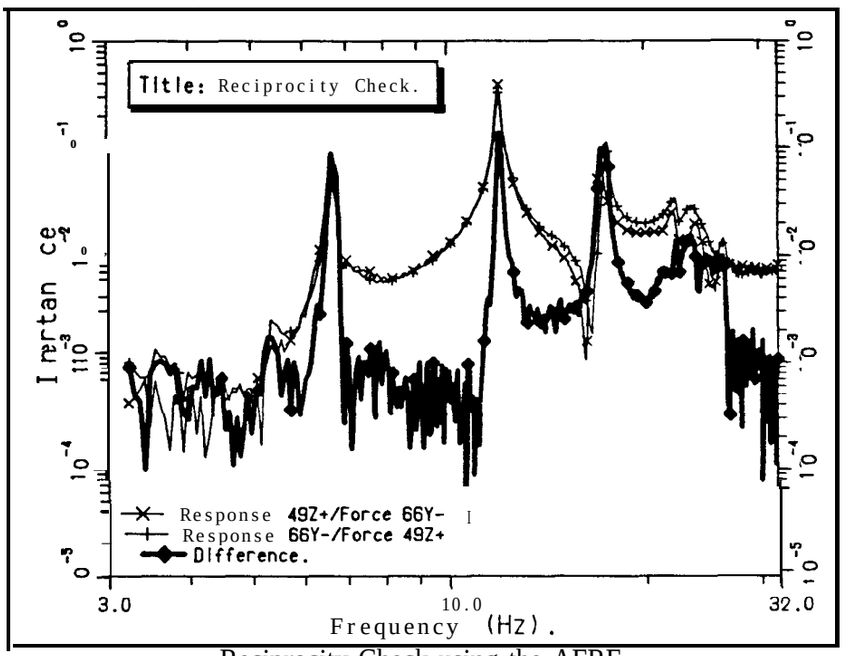

Reciprocity Check using the AFRF.

Figure 4.15

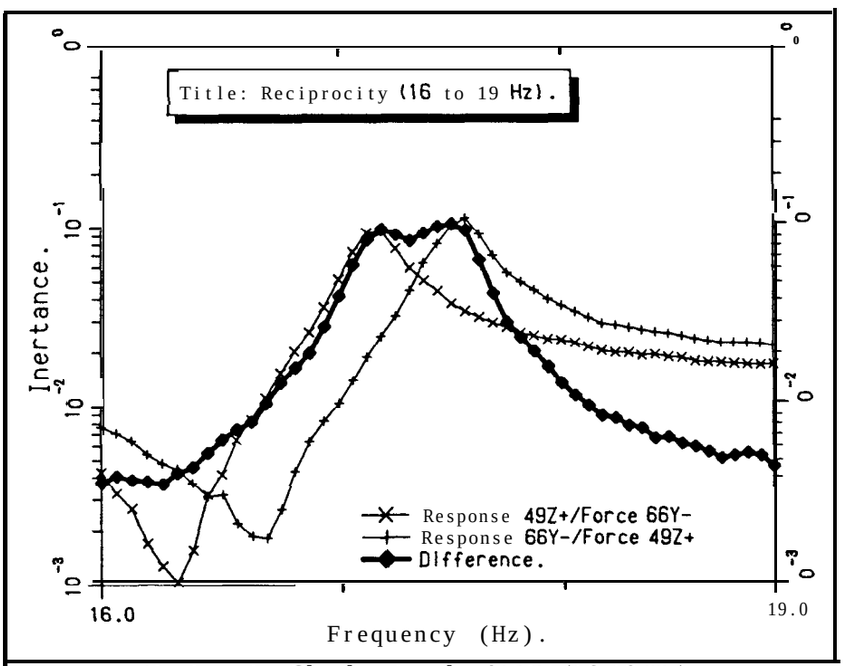

Reciprocity Check using the AFRF (16-19 Hz).

Figure 4.16

It is interesting to plot these FRFs and the AFRF for the 16 to 19 Hz frequency range in the Argand Plane, Figure 4.17. The circles described by the two FRF measurements are similar and without further analysis or inclusion of frequency information the frequency shift is not obvious. However, the AFRF describes a cardioid shape, rotated 90° from the modal circles. This is a feature of the AFRF which is characteristic of a shift in the resonance frequency between the two constituent FRFs [21].

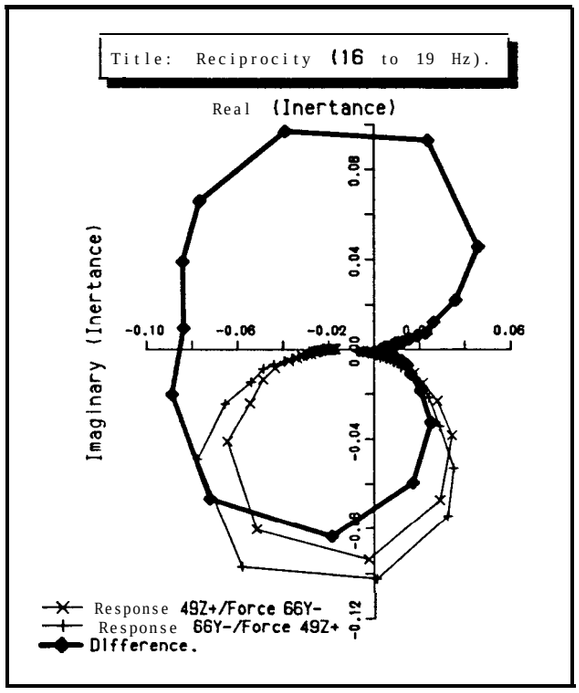

Nyquist Plot of Reciprocity Check using the AFRF (16-19 Hz).

Figure 4.17

Quality of Modal Analysis Data

A further use for the AFRF is in the assessment of the quality of modal analysis data. In Figure 4.18, a measured FRF is compared with the same function synthesised, from a modal database created from analysis of measured data. The first point to notice is that the synthesised function is smooth, whereas the measured function is rather “noisy”, particularly in the anti-resonance regions. This smoothing represents a large proportion of the low-level AFRF. Again, in the resonance regions, the AFRF shows marked increases indicating that the measured resonance and the resonance synthesised from the modal database do not quite coincide. Nevertheless, in this case, the AFRF for the measured and synthesised FRFs has a similar general appearance to the AFRF for the repeatability

measurements of the same function, Figure 4.13. It can be concluded therefore, that the synthesised FRF is a good representation of the actual FRF in this particular case.

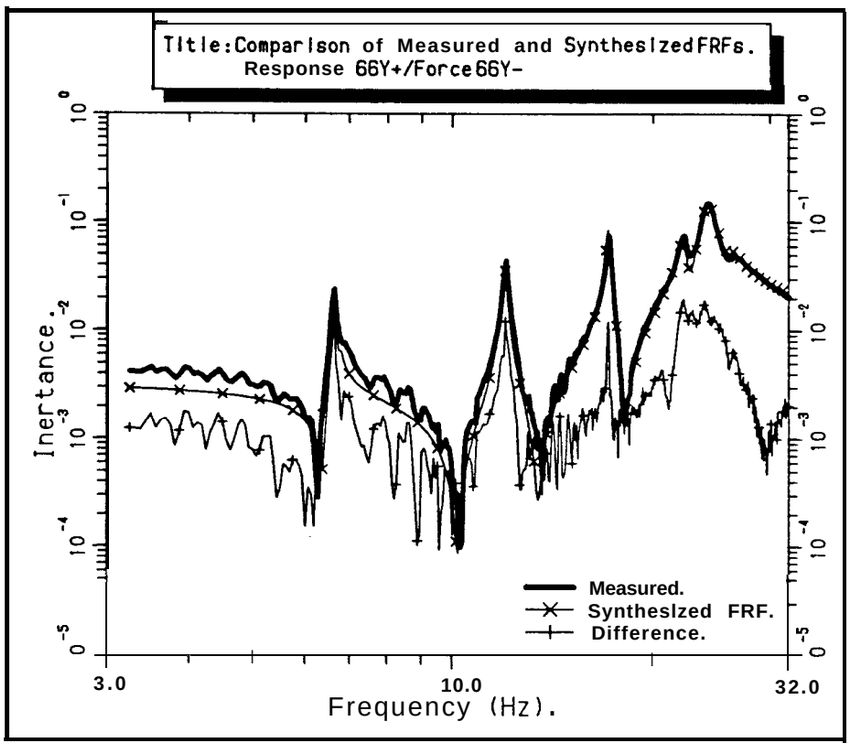

Comparison of Measured & Synthesised FRFs using the AFRF.

Figure 4.18

Note:

Throughout the complete assessment of measured and synthesised data, it should be remembered that the quantity and quality of the data are being assessed for their suitability for a particular purpose. The data may not have to be highly accurate in an absolute sense, just sufficiently accurate for the required purpose; a fact which can contribute to significant savings in cost and time.

4.5 Review of Chapter 4

Unless an analytical model or a F.E. model is available, the vibration properties of a structure must be derived from experimental measurements. The theoretical sensitivity analysis techniques and structural modification methods presume the availability of such data, from whichever source.

It is important to remember that the data obtained by different testing methods will not be identical because of practical differences in the way in which measurements are made. Many of the differences occur as a consequence of non-linearities in the structure which are excited to a greater or lesser extent with each different testing technique. Moreover, some testing methods allow variable frequency point spacing which enables data points to be concentrated in the areas of particular interest and greatest rates of change.

In a brief overview of a number of vibration testing techniques, the practical consequences of each method have been presented and discussed. It is possible to divide vibration testing techniques into two basic categories; sine testing (or more specifically, phase-resonance methods) and broadband testing (phase-separation methods). Both of these categories may be further sub-divided depending upon the number of excitation signals used, i.e. single-point testing and multi-point testing. Recent development of multi-point broadband testing has resulted in the INterleaved Spectral Excitation Technique (INSET), which seems to have great potential, provided that sufficient user control is available for multiple digital-to-analogue output channels in testing equipment.

An important point to remember when performing any vibration test is that, in almost all forms of testing, the equipment used to carry out the test will itself exert some influence on the structure under examination. There is interaction between moving parts of the shaker and the structure which can lead to excessive dynamic range in the measured force signal and, consequently, to poor quantification of the signal due to a limited dynamic range of the measuring equipment. The dynamic range of the force signal can be confined to manageable levels by appropriate matching of the shaker to the local structural characteristics.

Many of the potential problems with vibration testing only become apparent during the actual tests. Frequently, it is not possible to predict such problems beforehand either because there is no analytic model or because the model of the structure is unrepresentative. For this reason it is advocated strongly that a preliminary survey should be performed prior to the full measurement survey. In the preliminary measurement survey, which would consist of measuring at a small subset of the points for the complete survey, the measurement frequency range, necessary frequency resolution and the likely positions for structural modification can all be defined. The main advantage of the preliminary survey is that more effective use can be made of subsequent testing time and resources.

As part of the preliminary survey, and during the full survey, critical assessments of the quality of the measured data should be made. Preferably, these checks should be capable

of implementation at the earliest stage possible and they should be simple and easy to interpret. Reciprocity and repeatability are two methods for assessing the quality of measured data which have been used for many years. However, it has been found that much of the information that could be derived from these checks is lost because the respective FRFs are only compared by eye. Consequently, small differences between two large quantities are invariably overlooked despite the fact that the differences may be systematic and indicative of slight shifts in the structural resonance frequencies. To aid the assessment of data quality by these methods, the use of ‘difference functions’ alongside the actual FRFs has been found to be particularly beneficial.

Chapter 5

Incompleteness and Inaccuracy of Dynamic Models

5.1 Introduction

The theory for the impedance and modal coupling methods has been presented in chapter 2. Additionally, it has been shown that, providing each of the models used is a complete description of the component to which it refers, the results obtained from impedance or modal coupling methods are identical. In practice, however, the mathematical models used as descriptions of the dynamic characteristics of the components are incomplete and inaccurate.

In every experimental study there will always be a certain degree of inaccuracy and incompleteness. When a perfect and complete model is not available for reference, the degree of inaccuracy or incompleteness of an experimentally-derived model is very difficult to quantify. The quality of a model is often assessed by the ability to predict the effect of certain simple modifications, using the model as a description of the unmodified state. Measured and predicted characteristics of the modified structure are then compared and conclusions are formed as to the sufficiency of the base model used;[23] & [77]. In fact, this approach to assessing the adequacy of the model only indicates the suitability of the model for predicting the effect of the simple modification tested; the model may be highly unsatisfactory when used to predict the effects of another type of modification.

The terms ‘inaccuracy’ and ‘incompleteness’ are often used together in all-encompassing statements about why a particular modification prediction has been unsuccessful.

Although both definitions may apply, it is unfortunate that the terms are used in such close conjunction when the causes of inaccuracy and incompleteness in a model are very different.

5.2 Incompleteness

There are two quite distinct forms of incompleteness that can be present in a model;

(i) spatial incompleteness – where there are insufficient or inadequate measurement points on the structure; and,

(ii) **modal** incompleteness – where not all the modes of the system are included in the model.

5.2.1 Spatial Incompleteness

Spatial incompleteness has two main consequences – first, the mode shapes of a structure cannot be identified uniquely, and second, it may not be possible to incorporate certain joint configurations in predictions of the effects of modifications. While spatial incompleteness may not be a problem if all the relevant data are available for the degrees-of-freedom actively involved in a coupling, it becomes a very severe limitation if the incompleteness extends to some of the coupling degrees-of-freedom. The most frequently encountered example of this involves models lacking in rotational FRF properties at the coupling points. When such models are used to predict the effects of actual modifications that are coupled in both rotational degrees-of-freedom and translational degrees-of-freedom, the results are an underestimate of the actual effects because the modification attachment is less stiff in the prediction than in the actual case.

Rotational Degrees-of-Freedom and Spatial Incompleteness

For the majority of modal surveys, measurements are made of translational properties only; usually the translational acceleration at a point divided by the translational force input causing that response – the translational inertance FRF. Frequently, it is also the case that only one of the 3 translational responses is measured at any particular point. When one considers that all points have 6 degrees-of-freedom, it is evident that any model derived from measurement of a single degree-of-freedom must constitute a gross oversimplification for most structures. The rotational terms of the 6 degrees-of-freedom are neglected largely because of the difficulties involved in their measurement and the fact

that, progressing from, say, 3 translational measurements at a point, to all 6 degrees-of-freedom, represents a fourfold increase in the number of measurements to be made, stored and processed. There are, as yet, few proprietary rotational accelerometers or pure torque exciters and any rotational excitation or response terms in the complete FRF matrix have to be calculated from appropriate translational measurements.

Example of Spatial Incompleteness in the Coupling Degrees-of-Freedom

It has been mentioned earlier that a common source of spatial incompleteness is the omission of rotational degree-of-freedom properties, simply because they are difficult to measure accurately. In this example, the coupling of two free-free beams is considered,

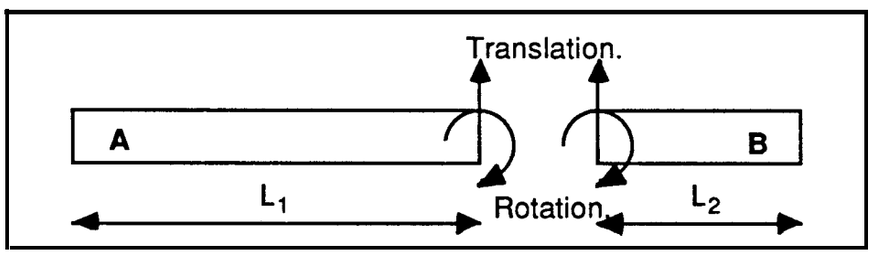

Coupling of Beam Elements.

Figure 5.1

(i) the beams are coupled together in the translational and rotational degrees-of-freedom in one plane. This represents a rigid joint between the beam elements, giving a coupled structure equivalent to a single beam of length L_1+L_2; and

(ii) the beams are coupled in a single transverse translational degree-of-freedom only. This represents a pin-joint between the beam elements – the transverse translational motions of the coupled ends of the beam are the same, but there is no constraint on the rotational motions of the coupled ends.

(i) When points of interest are confined to degrees-of-freedom involved in the coupling, the impedance coupling equation is in terms of 2x2 matrices, equation (2.34).

$$[\gamma] = [\alpha] - [\alpha]([\beta]+[\alpha])^{-1}[\alpha]$$

The point translational FRF for the interface of the coupled beams is plotted in Figure 5.2a.

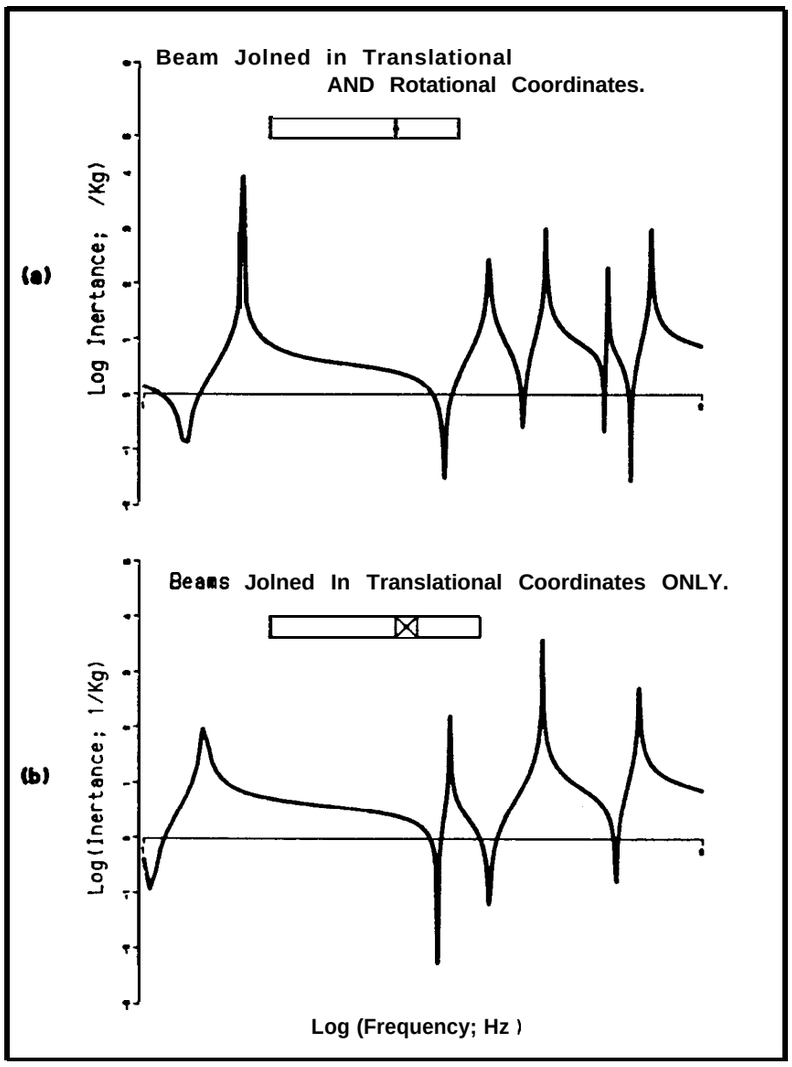

Beam FRFs for Various Joint Conditions.

Figure 5.2

(ii) For coupling of the transverse translational degree-of-freedom of the beams only, the impedance coupling equation reduces to equation (2.11) -

$$\frac{1}{\gamma} = \frac{1}{\alpha} + \frac{1}{\beta}$$

when interest is restricted to the transverse translational behaviour at the interface point and there are no passenger coordinates. The FRF for the beams, pin-jointed in this way, is also plotted in Figure 5.2b, below that for rigid coupling of the beams.

It can be seen that the two FRFs are markedly different. In the frequency range plotted, the rigidly joined beam (a) has 5 modes, whereas the pin-jointed beam (b) exhibits only

4 modes. As expected, the fundamental mode frequency is higher for the rigid beam, because the rigidly joined beam is stiffer than the pin-jointed beam.

For very stiff structures, measurement of the translational FRFs only for use in a coupling analysis is quite often satisfactory. Unfortunately, a large proportion of today's structures are insufficiently stiff for the implicit assumption that the rotational motion is negligible compared with the translational motion to be valid. In such situations, very careful consideration of the structures and inclusion of selected rotational terms in a coupling analysis becomes vital for valid predictions to be obtained.

Obviously, there are components and structures where symmetry indicates that there will be no response in a particular direction. However, although this may be the case for an individual component in isolation, it will not necessarily be the case when that component is attached as a modification to a larger, more complex, non-symmetric structure. It is then essential to have measured, or have available, all the FRFs of all the components.

Measurement of Rotational Degrees-of-Freedom

In vibration analysis, the rotational degrees-of-freedom are usually neglected when the FRFs are measured experimentally. The main reason for their exclusion is that they are difficult to measure and is not because they are unimportant. As shown above, the rotational degrees-of-freedom can be vital in certain circumstances.

'T-Block' Method for Measurement of Rotational Degrees-of-Freedom.

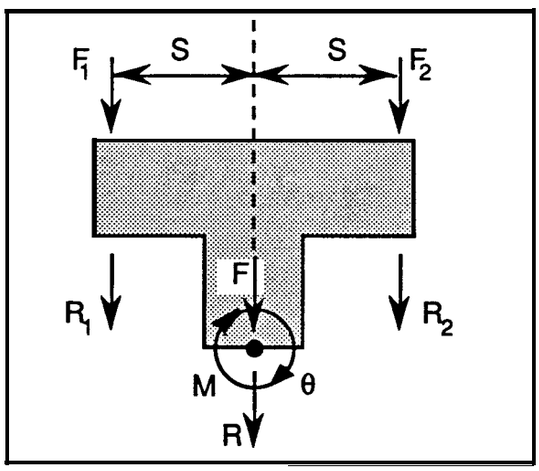

T-Block Transducer.

Figure 5.3

A T-block, shown schematically in Figure 5.3, is attached to the structure at the point of interest and translational FRF measurements are made on the block itself. By mathematical manipulation of the translational FRFs obtained, all the required FRFs, including those for the rotational degrees-of-freedom, may be calculated and, at the same time, the mass and inertia loading effects of the T-block on the base structure can be removed. The derivation of an equation for calculation of the rotational degree-of-freedom properties from T-block measurements is described fully in the work by Silva [9].

The transformation to produce the 'rotational' FRF data set for the attachment point from measurement of translational FRF data on the T-block is:-

$$[H] = [T_1].[H_m]\left[[T_2] - [M].[T_1].[H_m]\right]^{-1} \qquad \text{.....(5.1)}$$

where:-

$[H]$ = 'rotational' FRF data set for the attachment point.

$[T_1]$ = Transformation matrix containing information about the response positions on the T-Block.

$[H_m]$ = Matrix of measured 'translational' FRFs.

$[T_2]$ = Transformation matrix containing information about the forcing positions on the T- Block.

$[M]$ = 'Mass' matrix for the T-Block; used in the removal of the loading effects of the block on the structure.

Discussion of the Measurement of Rotational Degrees-of-Freedom

(i) T-Block Transducer

The main problem with this method is that of attaching the transducer to the structure with sufficient rigidity such that the behaviour of the structure is transmitted to the transducer faithfully, see Figure 5.4.

A further disadvantage of this method is the large physical size and mass of the T-block transducer. The whole transducer, consisting of at least two accelerometers, a force gauge and the T-block itself, can be prohibitively large and may have a significant mass-loading

effect at the measurement point. Although it is possible to 'subtract' this effect at a later stage, equation (5.1), the accuracy of the final results obtained depends to some extent on the mobility of the measurement point. If the point is not very mobile, the effect of the transducer will be comparatively small and the final results can be expected to be reasonably accurate. However, if the measurement point is highly mobile, the effect of the transducer may be so large that it dominates the structural response at that point, in which case the process of removing the effects of the transducer is likely to produce inaccurate results for the behaviour of the underlying structure. It is absolutely vital that accurate data are obtained for the sensitive points on the base structure if any meaningful predictions are to be made for the behaviour of a modified structure.

The only reason for using a T-block transducer is to enable calculation of the rotation/rotation FRF. The rotation/translation FRF can be derived by measuring the translation responses of two closely spaced points either side of the excitation position and, providing that the short length of structure between the two response points is rigid, calculation of the difference between the measured translational FRFs. By Maxwell's 'Rule of Reciprocity', the translation/rotation FRF is identical to the rotation/translation FRF. However, because it is difficult to apply a suitable pure torque excitation at the measurement point directly, the rotation/rotation FRF cannot be obtained quite so readily.

Methods for measuring rotational or angular response are not new. In fact, the design for just such an instrument,, based on a design similar to that of a moving mirror galvanometer, is reported in [82] from about 1960. Today, it should not be too difficult to adapt laser-based techniques for the (non-contact) measurement of translational response, to measurement of angular response. The design of a device to apply a pure torque excitation, of a reasonable amplitude, is more difficult to visualise.

(ii) Cross Axis Sensitivity of Transducers

Another problem that arises when trying to derive the rotational FRF set by the 'T-Block' method is that of the cross axis sensitivities of the accelerometers. The cross-axis sensitivities can be very important when differencing two FRF signals of similar size, particularly when the motion in one of the transverse directions is large. In such cases, the difference between the measured FRFs can be of the same order of magnitude as the cross axis sensitivity component. This is just the situation that may arise in calculations of the rotation/translation, translation/rotation and rotation/rotation FRFs, where the transformation from measured translational FRFs essentially involves differencing operations. A similar observation has also been made when calculating FRFs in the coordinate directions from angled forcing inputs (see chapter 6).

effect at the measurement point. Although it is possible to 'subtract' this effect at a later stage, equation (5.1), the accuracy of the final results obtained depends to some extent on the mobility of the measurement point. If the point is not very mobile, the effect of the transducer will be comparatively small and the final results can be expected to be reasonably accurate. However, if the measurement point is highly mobile, the effect of the transducer may be so large that it dominates the structural response at that point, in which case the process of removing the effects of the transducer is likely to produce inaccurate results for the behaviour of the underlying structure. It is absolutely vital that accurate data are obtained for the sensitive points on the base structure if any meaningful predictions are to be made for the behaviour of a modified structure.

The only reason for using a T-block transducer is to enable calculation of the rotation/rotation FRF. The rotation/translation FRF can be derived by measuring the translation responses of two closely spaced points either side of the excitation position and, providing that the short length of structure between the two response points is rigid, calculation of the difference between the measured translational FRFs. By Maxwell's 'Rule of Reciprocity', the translation/rotation FRF is identical to the rotation/translation FRF. However, because it is difficult to apply a suitable pure torque excitation at the measurement point directly, the rotation/rotation FRF cannot be obtained quite so readily.

Methods for measuring rotational or angular response are not new. In fact, the design for just such an instrument,, based on a design similar to that of a moving mirror galvanometer, is reported in [82] from about 1960. Today, it should not be too difficult to adapt laser-based techniques for the (non-contact) measurement of translational response, to measurement of angular response. The design of a device to apply a pure torque excitation, of a reasonable amplitude, is more difficult to visualise.

(ii) Cross Axis Sensitivity of Transducers

Another problem that arises when trying to derive the rotational FRF set by the 'T-Block' method is that of the cross axis sensitivities of the accelerometers. The cross-axis sensitivities can be very important when differencing two FRF signals of similar size, particularly when the motion in one of the transverse directions is large. In such cases, the difference between the measured FRFs can be of the same order of magnitude as the cross axis sensitivity component. This is just the situation that may arise in calculations of the rotation/translation, translation/rotation and rotation/rotation FRFs, where the transformation from measured translational FRFs essentially involves differencing operations. A similar observation has also been made when calculating FRFs in the coordinate directions from angled forcing inputs (see chapter 6).

To minimise the effects of cross-axis sensitivities, it is necessary to align the maximum cross-axis sensitivity direction of each accelerometer with the direction of minimum transverse motion at the attachment point, However, a polar plot of cross axis sensitivity is rarely available for each transducer and even if it were, exhaustive tests would be required to ascertain the direction of minimum transverse response at each location. Furthermore, it is not always possible to set a transducer at a particular angular orientation. For accelerometers with a threaded base which are attached to the structure by means of a stud, specific angular orientation can only be obtained by insertion of spacing shims, of the correct thickness, underneath the bases of the accelerometers: precise angular alignment is difficult to achieve (see section 5.3.1 for further discussion on cross-axis sensitivity effects).

(iii) Use of Synthesised FRFs

In the calculations to determine the rotational degree-of-freedom FRFs from 'T-Block' measurements, it is theoretically possible to use any form of FRF, e.g. the raw measured data, 'smoothed FRFs' or FRFs synthesised from a modal database. Although 'smoothed FRFs' or synthesised FRFs are noise-free, they may not contain all the important information inherent in the measured FRFs, e.g. exact residual information. If raw measured data, Figure 5.4, or smoothed data are used in the calculations, the inconsistent data gives rise to the phenomenon of 'breakthrough' [31]. The inconsistent resonance peaks of all the FRFs used in the calculations breakthrough into the derived results for the rotational degrees-of-freedom producing multiple peaks for each resonance.

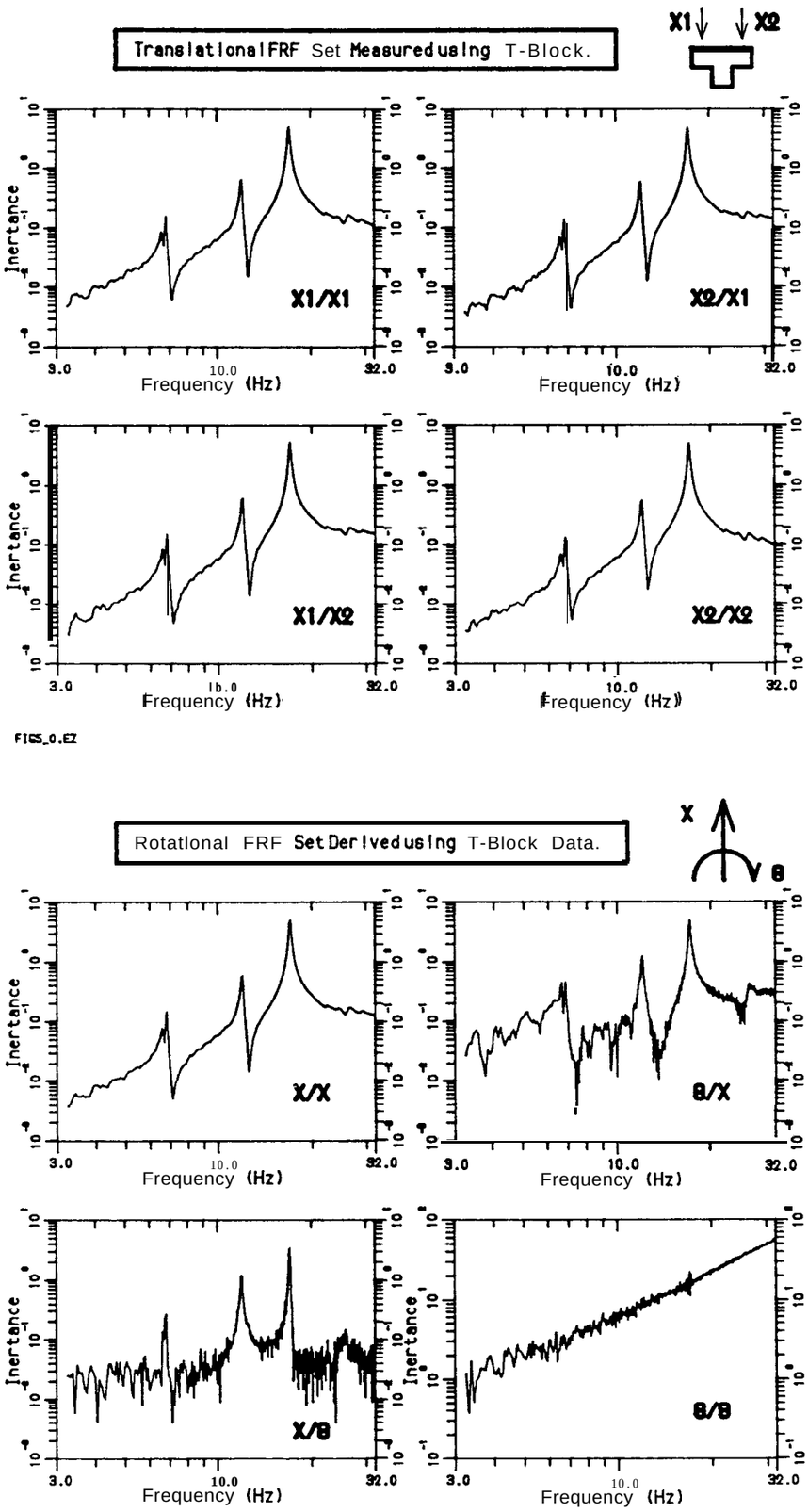

Comparison of Measured Translational & Derived Rotational FRFs.

Figure 5.4

Implications for the Use of Measured Rotational Properties in Coupling Procedures

The purpose of measuring rotational degree-of-freedom FRFs is so that they can be included in predictions of the effects of modifications. The inclusion of rotational degree-of-freedom properties allows more efficient use of modifying components through rotational as well as translational restraints at the interfaces. However, the underlying assumption in the modification prediction is that the interface joint between the component and the structure is rigid. If it is not rigid, then any predictions will be erroneous. In previous work, [36], and in the case study of chapter 6, it is shown that, the interface joint between the measurement-block and the structure is often **not** rigid. Because the joint cannot transmit the rotational motion adequately and since it may not be possible to alter the particular method of attachment, it may be better to consider the design of modifications which have pin-jointed end connections, the results of which can be predicted more accurately.

Consider the following procedures for prediction of the effect of a modification with particular reference to rotational properties.

(i)

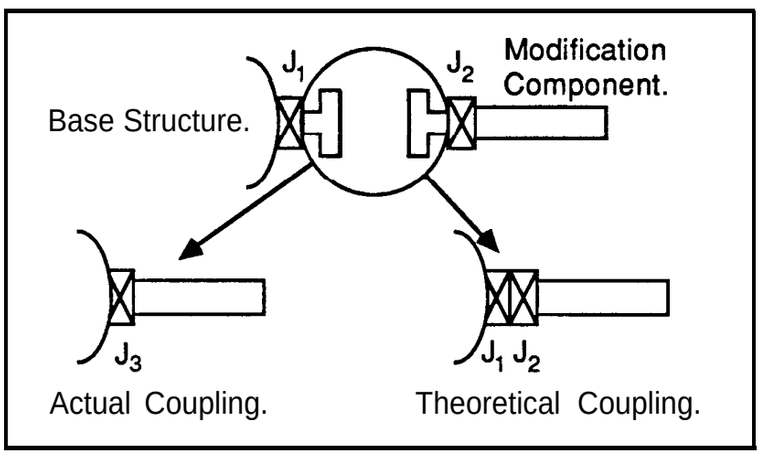

Schematic Representation of Coupling when FRFs for Both Components are Derived from Measurement.

Figure 5.5

FRFs for both the base structure and the modification component are derived from T-block measurements, as described earlier. The T-block is assumed to be rigid and its mass properties known. Therefore, it is possible to remove the effect of the T-block transducer from the base structure, leaving the FRFs for a point on the external side of a 'joint component', J_1, assumed to exist between the base structure and the T-block, Figure 5.5.

The same will apply for measurement of the modification component, except that this joint, J_2, may have different properties from those of J_1. When the actual modification is made, the base structure and modification component can be considered to be separated by yet another joint, J3. The theoretical prediction, using measured data, assumes a rigid connection between the external sides of J_1 and J_2, as shown in Figure 5.5, and only if $J_1+J_2=J_3$ will the theoretical prediction match the actual result. A special case of this condition is if all the joints are rigid, which is probably the only practical way of achieving good correlation between prediction and practice.

(ii)

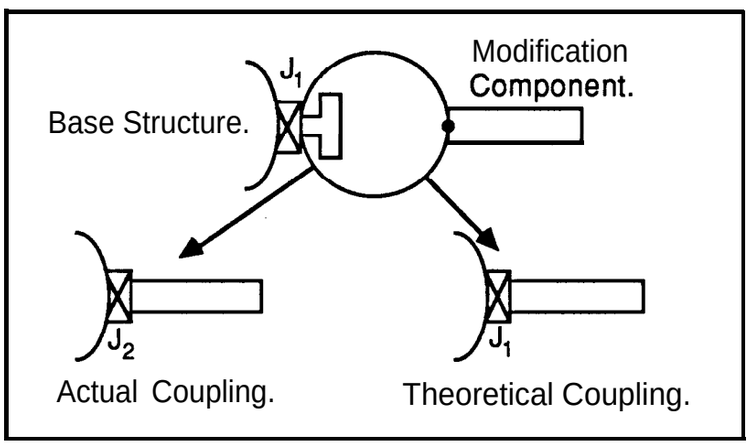

Schematic Representation of Coupling when FRFs for Components are Derived from Measurement and Theory.

Figure 5.6

FRFs for the base structure are derived from T-block measurements as for (i) above. Accurate theoretical FRFs are assumed to be available for the modification component. When the actual modification is made, the components are separated by the joint component J_2, Figure 5.6. In the theoretical prediction, though, J_1 separates the components. If $J_1=J_2$ the prediction and actual result will match. This condition is probably easier to achieve practically than that for (i) above.

5.2.2 Modal Incompleteness

If measured FRF data are used directly as the vibration model of a structure, then modal incompleteness does not arise because the contributions of all modes are automatically included in the measured data. If the FRFs are synthesised from a modal database, then, unless residual information is incorporated in the synthesis, only the contributions from a relatively small number of modes are included.

While this may be sufficient to describe the behaviour of the unmodified structure over the frequency range of interest, it may not be good enough when a modification is made.

Modal Incompleteness and the Use of Residual Correction Factors.

With an experimental measurement survey of a structure there are always practical limitations which prevent derivation of a complete model. Here, discussion is focussed on the problem of modal incompleteness and how some allowance can be made for the effects of out-of-range modes in the frequency range of interest.

Modal analysis theory is based on the assumption that the dynamic behaviour of a structure can be described completely by a summation of **all the** modal contributions. For a hysteretically damped model -

$$\alpha_{jk}(\omega) = \sum_{r=1}^{N} \left(\frac{{}_rA_{jk}}{\Omega_r^2 - \omega^2 + i\eta_r \Omega_r^2} \right) \qquad \ldots\ldots\ldots\ldots\ldots\ldots\ldots\ldots \quad (5.2)$$

Except for the very simplest lumped mass and spring systems the majority of practical structures have continuous distributions of mass, stiffness and damping and, consequently, have an infinite number of modes. The summation of equation (5.2) extends to infinity.

It is common for the measurements to span only the “frequency range of interest”, i.e. a frequency range covering modes of particular concern. Thus the measured frequency range covers only a small fraction of the total number of modes. Modes above or below the measured frequency range cannot be analysed and, therefore, they cannot be included in the modal database. Collectively, these modes are known as the out-of-range modes.

Following a modal analysis process, FRFs can be synthesised from information contained in the modal database. When the synthesised FRFs are compared with their measured counterparts, the influence of the out-of-range modes in the frequency range of interest becomes apparent. If the data are accurate and the modal analysis has been performed correctly, the synthesised resonance features will be defined clearly and correspond with the resonances on the measured FRFs.

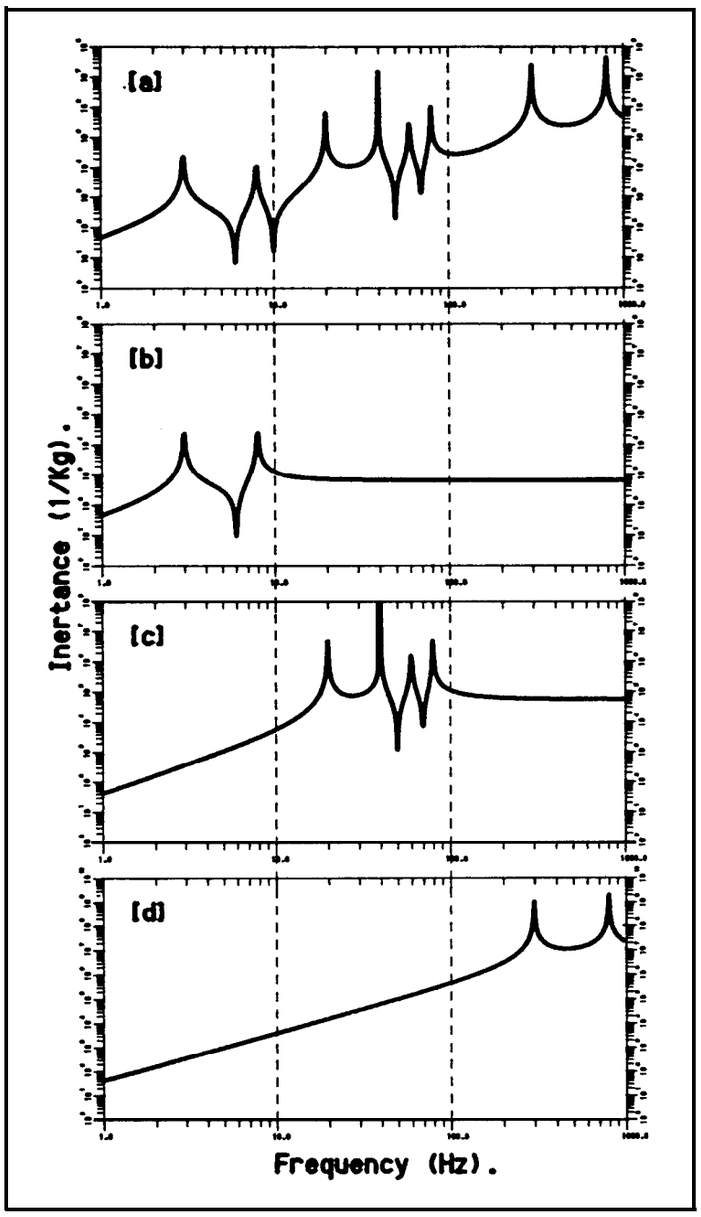

Representation of Residuals as Linear Functions.

Figure 5.7

In off-resonance regions, even though the data used in the synthesis are accurate, the correspondence between the measured and synthesised FRFs depends largely upon whether the out-of-range modes have any significant influence. If the actual out-of-range mode contributions are large, the synthesised FRF (which only contains information from the analysed modes) will differ from the measured FRF markedly. The most obvious differences are in the positioning of the anti-resonance features.

Equation (5.2) can be r-e-written in 3 sections to represent;

(a) the low-frequency out-of-range modes, (r=1 to L-l);

(b) the modes in the measured frequency range, (modes r=L to H); and,

(c) the high-frequency out-of-range modes, (r=H+1 to N).

$$\alpha_{jk}(\omega) = \sum_{r=1}^{L-1} \left(\frac{{}_rA_{jk}}{\Omega_r^2 - \omega^2 + i\eta_r \Omega_r^2} \right) + \sum_{r=L}^{H} \left(\frac{{}_rA_{jk}}{\Omega_r^2 - \omega^2 + i\eta_r \Omega_r^2} \right) + \sum_{r=H+1}^{N} \left(\frac{{}_rA_{jk}}{\Omega_r^2 - \omega^2 + i\eta_r \Omega_r^2} \right) \quad \ldots\ldots\ldots (5.3)$$

The term representing the low-frequency out-of-range modes is known as the **low-**frequency residual, and that representing the high-frequency out-of-range modes as the high-frequency residual, see Figure 5.7. It can be seen that the residual terms are dependent upon the force and response locations (j and k) and, hence, the residuals are **local** properties.

It is interesting to consider this equation for a narrow frequency band around a single mode. The centre term is the contribution of the singe mode of interest only. For well separated modes, where the effects of the high-frequency and low-frequency residual terms can be considered to be constant in the narrow frequency range of interest, equation (5.3) reduces to,

$$\alpha_{jk}(\omega) = \left(\frac{{}_rA_{jk}}{\Omega_r^2 - \omega^2 + i\eta_r \Omega_r^2} \right) + D \quad \ldots\ldots\ldots\ldots\ldots\ldots\ldots\ldots\ldots\ldots\ldots\ldots\ldots\ldots\ldots\ldots (5.4)$$

which is the basis of single-degree-of-freedom modal analysis methods.

In the circle-fitting technique of single-degree-of-freedom modal analysis, the displacement (D) of the circle (Figure 5.8) from the origin is a reflection of the residual effects. At resonance, the response is dominated by the contribution of that single mode, the constant residual effect can be insignificant in comparison.

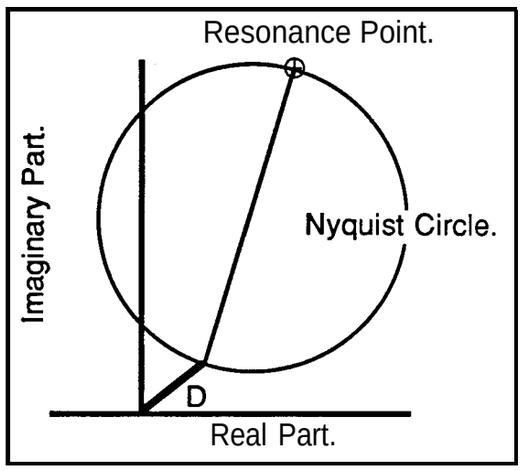

Figure 5.8

However, away from resonance, and particularly at anti-resonances, the response is formed from similar-sized contributions from a large number of modes. If the contributions from a series of modes are ignored, there will be a large error in the estimated response and the synthesised anti-resonances will be incorrectly positioned.

The relative importance of residual terms varies throughout the FRF matrix– for some FRFs the residuals are essential, while for others they may be insignificant. There are some general trends for the relative magnitudes of different residual terms but discussion of this aspect of residuals is left until later.

The assumption that residual effects are constant is only valid for narrow frequency bands around each resonance. Over a typical frequency range of interest containing several modes, residual effects will not be constant but, there are several ways in which they can be represented,

(1) as linear functions;

(2) as the effects of two fictitious modes, one above, and one below the measured frequency range; and

(3) by incorporation of sufficient modes from outside the frequency range of interest.

(1) Residuals as Linear Functions

By consideration of Figure 5.7, where the FRFs are displayed on a log-log plot, it can be seen that the low-frequency residual term could be approximated, in the frequency range

of interest, by a mass line (Figure 5.7b) and that the high-frequency residual term could be approximated by a stiffness line (Figure 5.7d).

For the low-frequency residual, where $\omega \gg \Omega_L$

$$\sum_{r=1}^{L} \left(\frac{{}_rA_{jk}}{\Omega_r^2 - \omega^2 + i\eta_r \Omega_r^2} \right) \approx \frac{-1}{\omega^2 . {}_rM_{jk}} \qquad \ldots\ldots\ldots\ldots\ldots\ldots\ldots\ldots (5.5)$$

where ${}_rM_{jk}$ = low-frequency 'mass-like' residual term.

and for the high-frequency residual, where $\omega \ll \Omega_H$

$$\sum_{r=H+1}^{N} \left(\frac{{}_rA_{jk}}{\Omega_r^2 - \omega^2 + i\eta_r \Omega_r^2} \right) \approx \frac{1}{{}_rK_{jk}} \qquad \ldots\ldots\ldots\ldots\ldots\ldots\ldots\ldots (5.6)$$

where ${}_rK_{jk}$ = high-frequency 'stiffness-like' residual term.

The accuracy of this approximation depends upon how well separated the out-of-range modes are from the frequency range of interest. The greater this separation, the closer the actual residual effects are to the asymptotic characteristics and the better are the approximations of linear functions for the residuals. As the out-of-range modes come closer to the frequency range of interest, the approximation of the residuals as linear functions becomes less and less valid.

Practical Implementation

Practical derivation of the residual terms involves the direct comparison of each pair of measured and synthesised FRF curves, [43]. The low- and high-frequency residual terms are then derived by fitting linear functions to the difference between the measured and synthesised FRFs on a log-log plot. By this method, it is only possible to derive residuals for terms that have a measured counterpart for direct comparison. This places a heavy burden on the measurement programme because it is necessary to have measured all terms in the upper or lower triangle of the FRF matrix if a complete set of residuals is to be generated.

A modal database can be generated from measurement of one row or column of the FRF matrix as an absolute minimum; for a system with N degrees-of-freedom, the minimum number of FRF measurements required is N. In contrast, a complete data set for the upper or lower triangle of the FRF matrix requires $\frac{N\,(N+1)}{2}$ measurements to enable calculation

of all the residuals. This represents a substantial increase in the size of the measurement survey and can lead to difficulties with -

- the number of degrees-of-freedom which may become prohibitively large, e.g. for a system with 12 degrees-of-freedom, the number of measurements is now 78 rather than the minimum of 12 required to form a modal database; and,

- restricted access to a number of locations may mean that it is not possible to excite the structure at these locations and hence there will be some pairs of degrees-of-freedom for which measured FRFs are unavailable.

For example, if it is not possible to excite at locations j or k, the FRF terms in the two shaded columns of Figure 5.9 cannot be measured directly. However, it is possible to measure terms in the 'j' and 'k' rows of the matrix – bar those marked with a cross – and hence, invoking the principle of reciprocity, all the FRF terms in the matrix can be determined except the 4 marked with crosses (the 'j' and 'k' point FRFs and the reciprocal 'j : k' transfer FRFs).

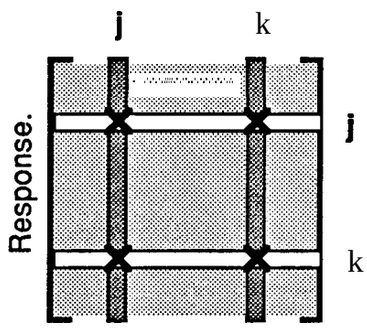

Figure 5.9

(2) Residuals as the Effects of Two Fictitious Modes, One Above, and One Below the Measured Frequency Range

The effects of out-of-range modes can be incorporated into the database by representing the residual effects by one fictitious mode above the frequency range of interest, and another fictitious mode below the frequency range of interest. There are two approaches to the derivation of the parameters for these fictitious modes -

(i) a local method in which a measured and synthesised FRF are compared with the aid of the AFRF. The tail of an undamped single-degree-of-freedom FRF can be fitted to the AFRF (rather like that shown in Figure 5.17) to produce parameter sets for low-frequency or high-frequency fictitious modes. These parameters will be valid for the single combination of force and response locations only, all other FRF terms must be analysed separately;

(ii) a global method in which parameters for the fictitious **single-degree-of-freedom** modes are derived in an iterative way. The estimation task can be performed with measured data from a single row or column of the **FRF** matrix to yield sets of modal parameters for the two fictitious modes– as for standard modal analysis – that can then be incorporated in the synthesis of all the FRF terms. One such method is reported by Cheung & Lee [72].

Practical implications for method (i) are the same as when using linear residual functions – a complete set of measured **FRFs** must be available for all the residuals to be calculated. For method (ii) a minimum of one row or column of measured **FRFs** is sufficient to enable calculation of all the residual effects.

(3) Extension of the Measured Frequency Range to Include Modes that have a Significant Influence **in the Frequency Range of Interest (Inclusion of 'Buffer Zones')**

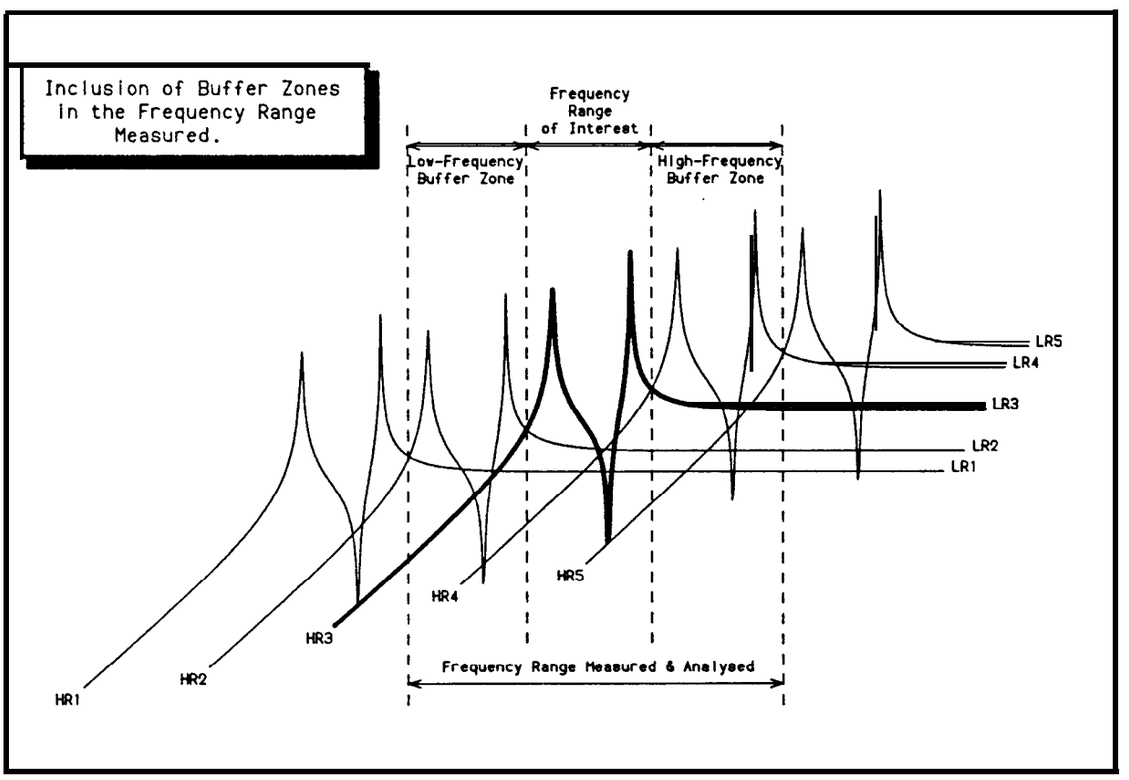

Inclusion of 'Buffer Zones' in the Measured Frequency Range

Figure 5.10

In simple systems it is easy to understand that if two modes are well separated their effect on each other is small. In contrast, if two modes are closely spaced, the effect of one mode on the other can be substantial.

By extending the measured frequency range beyond the "range of interest", two "buffer zones" are created, Figure 5.10, and the remaining unmeasured modes are moved further from the frequency range of interest. For the purposes of discussion we shall consider only the effects of modes below the frequency range of interest. The unmeasured low-frequency modes may have a substantial effect (LR_1) on the response in the low-frequency buffer zone, but their effect on the response in the frequency range of interest will be small. Therefore, over the frequency range of interest, it is acceptable to ignore the low-frequency residual due to the unmeasured modes. However, modes in the low-frequency buffer zone will affect the response in the frequency range of interest and this residual effect (LR_2) cannot be ignored. Analogous arguments apply for the effects of modes above the frequency range of interest.

The residual effects of buffer zone modes are incorporated in the frequency range of interest by extending the measurement and modal analysis task to include these modes, thus enlarging the modal database. In the buffer zones, the measured and synthesised FRFs may differ, but over the central frequency range of interest they should be well correlated.

Practical Implementation

This is probably the most straightforward method for improving the correlation of measured and synthesised FRFs over the frequency range of interest. The improvement is brought about by including more modes in the modal database. The correction is done in the modal domain rather than by addition of individual correction factors to each FRF in the frequency domain. Therefore, the measurement survey requirement returns to the measurement of a single row or column of the FRF matrix, but over an extended frequency range. The main difficulty with implementation of this technique is the selection of the new measurement frequency range – how many extra modes should be measured? Obviously this will depend on many factors such as the relative modal participation factors and the modal density. Usually though, the selection is done on a trial-and-error basis, whereby the number of modes is gradually increased until acceptable correlation of the measured and synthesised FRFs is achieved over the frequency range of interest.

Unfortunately, standard measurement and analysis methods do not allow for the rigid body modes of a structure to be incorporated in this way and they have to be included by

use of technique (1), in which the residuals are modelled as linear functions over the frequency range of interest.

Rigid Body Mode Residuals

At very low frequencies, unrestrained structures exhibit what is known as rigid body motion. There is no elastic deformation of the structure, it moves bodily in each of the six degrees-of-freedom at the centre of gravity. Mathematically, an unrestrained structure has six zero-frequency modes which correspond with the rigid body motions of the structure. As restraints are applied to the structure, the number of rigid body modes decreases, e.g. a single pin-joint coupling the structure to ground would restrain one translational degree-of-freedom and the number of rigid body modes is reduced to five accordingly. Although these rigid body modes are at zero frequency, their effects extend across the whole frequency range, in just the same way as do the effects of the elastic modes. Therefore, it may be necessary to include rigid body modes in the synthesis of FRFs. This is done, implicitly, when linear residual correction factors are calculated by comparison of measured and synthesised FRFs (see method (1) above). However, if it is known that the measured frequency range includes all the low-frequency elastic modes, the residual effects of the rigid body modes can be calculated directly from the static mass and inertia properties of the structure (if available) by application of basic rigid body mechanics equations. By definition, all the rigid body modes are **real** – all responses are either in-phase or 180° out-of-phase with the response at a reference point.

Depending upon the accuracy of the mass and inertia properties used for the structure [75], the theoretical rigid body residuals may be more accurate than those derived by comparison of measured and synthesised FRFs and, certainly, they will be more consistent.

Practical Example of the Need for, and the Incorporation of, Residuals

Figure 5.11 shows a measured FRF of a freely suspended aerospace structure together with that synthesised from a modal database. The measurement was made for a baseband frequency range up to 32 Hz and the transducers used had an operating frequency range down to about 3 Hz. Modal analysis of the measured FRF data yielded the modal parameters for 7 modes over the frequency range of interest from 3.2 Hz to 32 Hz. The synthesised function shown in Figure 5.11 was produced using modal data for the first 7 modes only.

As expected, there is reasonable agreement of the measured and synthesised FRFs in the regions close to the resonance peaks. However, away from the resonances, and particularly in the anti-resonance regions, the correlation of the two functions is poor due to the fact that the effects of out-of-range modes have not been included.

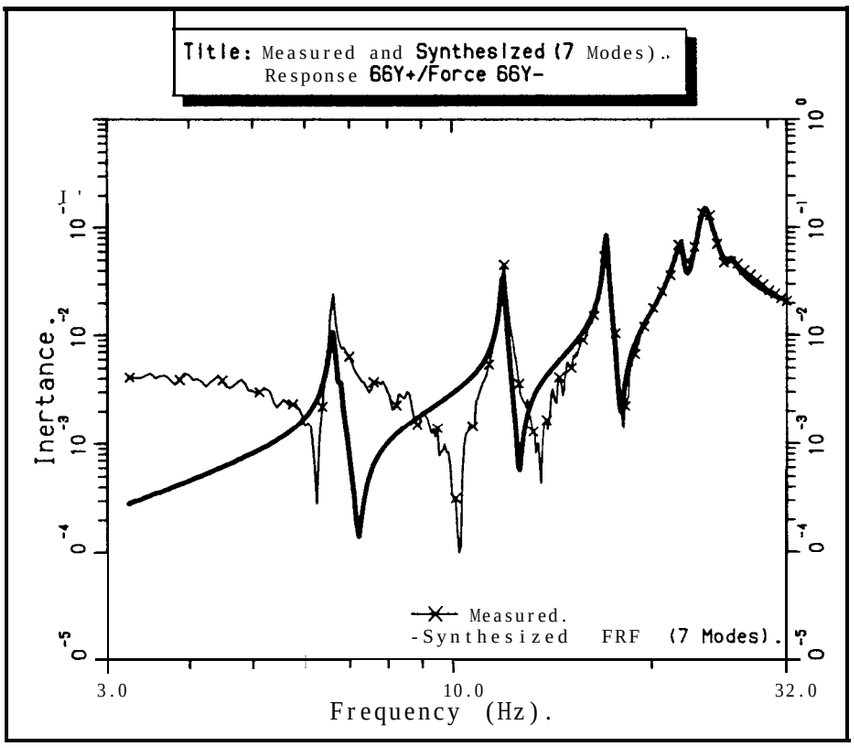

A Measured FRF Compared with a Synthesised FRF
(only 7 modes used in synthesis)

Figure 5.11

Two methods have been used for the inclusion of residual effects -

(i) the modal database has been extended to include higher frequency modes; and

(ii) theoretical low-frequency residuals have been calculated for the effects of the rigid body modes.

(i) The structure was re-measured up to a frequency of 64 Hz and the modal database extended accordingly. Four extra modes were found in the frequency range between 32 Hz and 64 Hz. The FRF was synthesised again (over the frequency range 3.2 to 32 Hz), but this time incorporating the contributions of all 11 modes up to 64 Hz. Over the frequency range of interest, the FRF synthesised using all 11 modes, Figure 5.12, appears virtually identical to that synthesised using only the first 7 modes. The difference

(AFRF) between these two synthesised FRFs is also calculated and plotted and it can be seen that it has the form of a tail to a single degree-of-freedom FRF. The significant discrepancies between the measured and synthesised FRFs shown in Figure 5.11, still remain. Therefore, it can be concluded that these differences must be due to the residual effects of the rigid body modes.

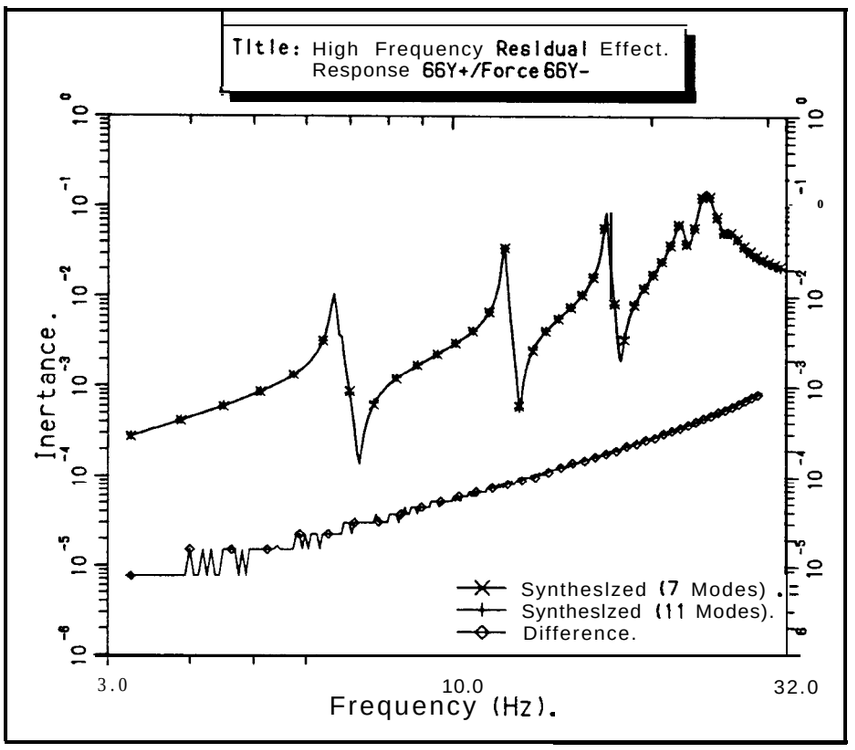

Comparison of FRFs Synthesised with 7 & 11 Modes.
The AFRF is used to Show the High-Frequency Residual Effect.

Figure 5.12

(ii) The mass and inertia properties of the structure were obtained from a F.E. model, [83], and basic rigid body mechanics was then employed to derive expressions for all the residual terms in the FRF matrix, i.e. $\left(\frac{\ddot{x}_{resp}}{F_{ref}}\right)$ for all the response and reference locations. These low-frequency residual terms were added to the FRFs synthesised using all 11 modes to produce the final set of FRFs; one of the point FRFs is shown in Figure 5.13.

The synthesised FRF including the low frequency residual terms now compares very well with the measured FRF, Figure 5.13; they overlay almost exactly. All the resonances, anti-resonances are correctly positioned and the only slight discrepancy is for the resonance magnitude of mode 1. The low frequency residual is large for this FRF term and, therefore, there is a large difference between the synthesised FRFs with and without

the residual. Use of the synthesised FRF without the residual term in any form of impedance coupling technique would give erroneous results for the characteristics of the modified structure.

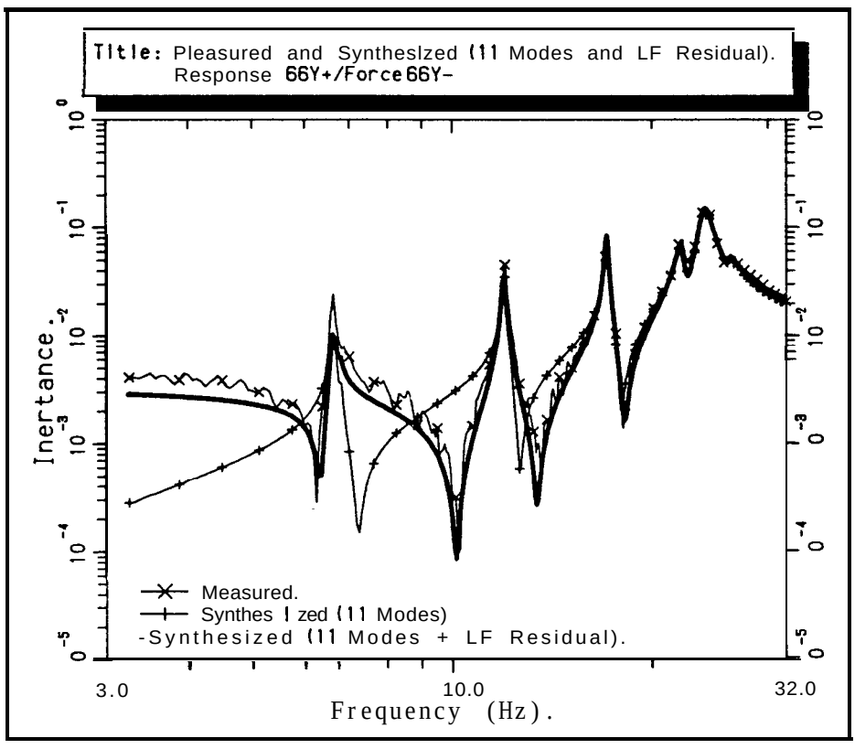

Comparison of Measured & Synthesised FRFs With and Without the Low-Frequency Residual

Figure 5.13

The Relative Sizes of Residuals in the FRF Matrix

There are certain trends in the sizes of the residuals over the FRF matrix. The residuals for point FRFs are generally larger than the residuals for transfer FRFs, with the differences becoming larger as the physical separation of the points on the structure increases. This can be explained simply by considering the signs of the modal constants in the summation equation for an FRF, equation (5.2) -

$$\alpha_{jk}(\omega) = \sum_{r=1}^{N} \left(\frac{{}_rA_{jk}}{\Omega_r^2 - \omega^2 + i\eta_r \Omega_r^2} \right)$$

For a point FRF, all the modal constants $({}_rA_{jk})$ have the same sign and hence a residual is the summation of a part of this series in which all the terms have the same sign. A characteristic of transfer functions is that the modal constants $({}_rA_{jk})$ VARY in sign. As

the physical separation of the points increases, there is a trend for the number of minima to increase (and the number of anti-resonances to decrease), giving rise to more sign changes in the series of modal constants. Summation of a part of this series results in a smaller value than if the modal constants had all been of the same sign. Consequently, the residuals for transfer functions tend to be smaller than the residuals for point FRFs.

This observation may be of use in reducing the number of FRF measurements necessary if the comparison methods of residual calculation are to be used. Where it is known the residuals will be small, it may not be necessary to measure the particular FRF for direct comparison.

Incorporation of Residual Effects in Modification Predictions using Impedance or Modal Coupling Methods

The theoretical basis of the impedance coupling and modal coupling methods has been presented in chapter 2. It was shown that, provided that **complete** models for the components were available, the predictions of the two coupling methods were identical. The impedance coupling method operates in the frequency domain and the modal coupling method operates in the modal domain.

Generally speaking, in an experimentally-based study, the models obtained will be inaccurate and incomplete. One form of incompleteness is modal deficiency and the preceding sections have examined some techniques by which the effects of out-of-range modes may be included in the frequency range of interest. It is important to be aware that the choice of residual correction technique can preclude the use of certain coupling methods in predictions of the effects of modifications and, likewise, prior selection of the coupling technique to be used has implications for the way in which residual effects are to be included (if any).

Residual correction methods can be categorised by the domain in which the correction is made;

(i) frequency domain methods – linear residual functions and/or the effects of ficticious modes calculated individually for each FRF element, and

(ii) modal domain methods – the effects of global ficticious modes and/or the extension of the modal database beyond the frequency range of interest.

Only recently has it been shown to be possible to incorporate frequency domain residual information directly into the modal coupling equations [88]. However, because FRFs can

be synthesised from a modal database, modal domain residual correction methods do not restrict the choice of coupling method – modal coupling and impedance coupling methods can be used equally well.

5.2.3 Illustrations of the Effects of Spatial and Modal Incompleteness

As an illustration of the implications and effects of using incomplete models for the prediction of the characteristics of a modified structure, we shall use the following undamped 3 degree-of-freedom mass and spring example.

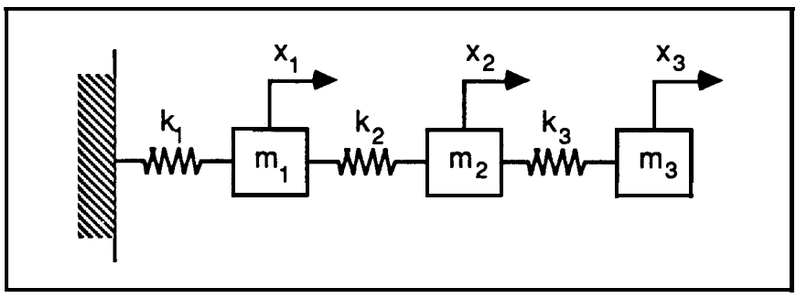

3 DoF Mass & Stiffness Example System

Figure 5.14

with, $m_1 = m_2 = m_3 = 1$ Kg.

$k_1 = k_2 = 1000$ N/m and $k_3 = 500$ N/m.

The matrix equation of motion for the system, shown in Figure 5.14, is :-

$$\begin{bmatrix} 1 & 0 & 0 \\ 0 & 1 & 0 \\ 0 & 0 & 1 \end{bmatrix} \begin{Bmatrix} \ddot{x}_1 \\ \ddot{x}_2 \\ \ddot{x}_3 \end{Bmatrix} + \begin{bmatrix} 2000 & -1000 & 0 \\ -1000 & 1500 & -500 \\ 0 & -500 & 500 \end{bmatrix} \begin{Bmatrix} x_1 \\ x_2 \\ x_3 \end{Bmatrix} = \begin{Bmatrix} 0 \\ 0 \\ 0 \end{Bmatrix} \quad \text{.....(5.7)}$$

Solution of this set of equations yields the following eigenvalues and eigenvectors which represent the modal database,

$$[\Omega_r^2] = \begin{bmatrix} 177 & 0 & 0 \\ 0 & 1000 & 0 \\ 0 & 0 & 2820 \end{bmatrix} \quad \text{and} \quad [\Phi] = \begin{bmatrix} -.285 & -.577 & .765 \\ -.520 & -.577 & -.630 \\ -.805 & .577 & .136 \end{bmatrix} \quad \text{.....(5.8)}$$

The natural frequencies are 2.12 Hz, 5.03 Hz and 8.45 Hz and the mode shapes are given by the eigenvector matrix which can be shown more clearly in pictorial form, Figure 5.15,

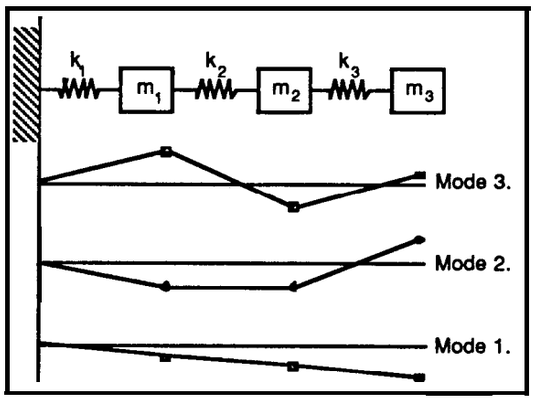

Mode Shapes for Unmodified System

Figure 5.15

FRFs for points on the system can be generated by substitution of the eigenvalues and eigenvectors in the following equation for an undamped system – modal synthesis.

$$\alpha_{jk}(\omega) = \sum_{r=1}^{N} \frac{({}_r\phi_j).({}_r\phi_k)}{\Omega_r^2 - \omega^2} \qquad \text{(5.9)}$$

where, $({}_r\phi_j)$ = j^{th} component of the r^{th} mode shape vector.

ω = frequency.

Ω_r = r^{th} resonance frequency

Modelling Spatial Incompleteness

Spatial incompleteness will be simulated by assuming that there is no information available for, say, location 2. In a practical situation, this is equivalent to omitting location 2 from the measurement survey.

For the system shown in Figure 5.14, the simulation of spatial incompleteness simply means that no FRF is available for location 2, and therefore the mode shapes are deficient for this location. At locations 1 and 3, the mode shape information is still correct. In terms of the modal database, spatial incompleteness affects the eigenvector matrix only – reducing the 1^{st} dimension. In this example, row 2 is eliminated from the eigenvector matrix, leaving -

$$[\Omega_r^2] = \begin{bmatrix} 177 & 0 & 0 \\ 0 & 1000 & 0 \\ 0 & 0 & 2820 \end{bmatrix} \quad \text{and,} \quad [\Phi_{Reduced}] = \begin{bmatrix} -.285 & -.577 & .765 \\ -.805 & .577 & .136 \end{bmatrix} \ldots . \text{(5.10)}$$

as the modal database simulating spatial incompleteness. The mode shapes of the spatially incomplete model would now be shown as Figure 5.16;

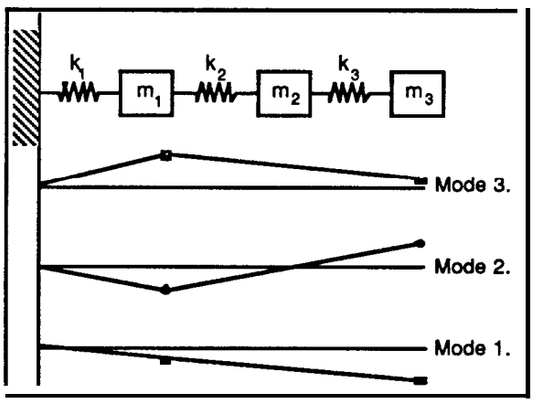

Spatially Deficient Mode Shapes for Unmodified System.

Figure 5.16

The reduced resolution of the mode shapes means that for mode 3 there appear to be no nodal points whereas there are, in fact, two.

It will be noted that it is still possible to synthesise exact FRFs using the data from equation (5.10) in equation (5.9) for combinations of force and response points that do not involve location 2, i.e. for $j \neq 2$ and $k \neq 2$ in equation (5.9).

Modelling Modal Incompleteness

Modal incompleteness will be simulated by assuming that there is no information available for the 3rd mode. This is equivalent to the practical situation where high frequency modes are omitted due to insufficient (a finite rather than an infinite) measurement frequency range.

Modal incompleteness means that certain modes have not been measured. Usually it is the very low frequency and/or rigid body modes, which are below the frequency range of interest, and the high frequency modes which are above the frequency range of interest that are missing. Both the eigenvalue and eigenvector matrices are affected. In this example, the order of the eigenvalue matrix is reduced by 1 and the 3rd column of the eigenvector matrix is eliminated, leaving the modal database simulating modal incompleteness as :-

$$[\Omega_r^2] = \begin{bmatrix} 177 & 0 \\ 0 & 1000 \end{bmatrix} \quad \text{and,} \quad [\Phi_{Reduced}] = \begin{bmatrix} -.285 & -.577 \\ -.805 & -.577 \end{bmatrix} \quad \ldots\ldots\ldots\ldots (5.11)$$

The mode shapes are exact for the 1st two modes, but it is no longer possible to synthesise FRFs that correctly represent the behaviour of the structure from this database even in the limited frequency range including modes 1 and 2. This is shown in Figure 5.17 for the point FRF at location 1. At frequencies away from the 1st two resonances, the FRFs for the complete model and the modally deficient model are different. The most obvious indication of the differences is in the location of the anti-resonances. If the two FRFs are subtracted to form the difference function (AFRF) previously described in chapter 4, the result is a single-degree-of-freedom FRF curve representing the contribution of the 3rd mode throughout the frequency range.

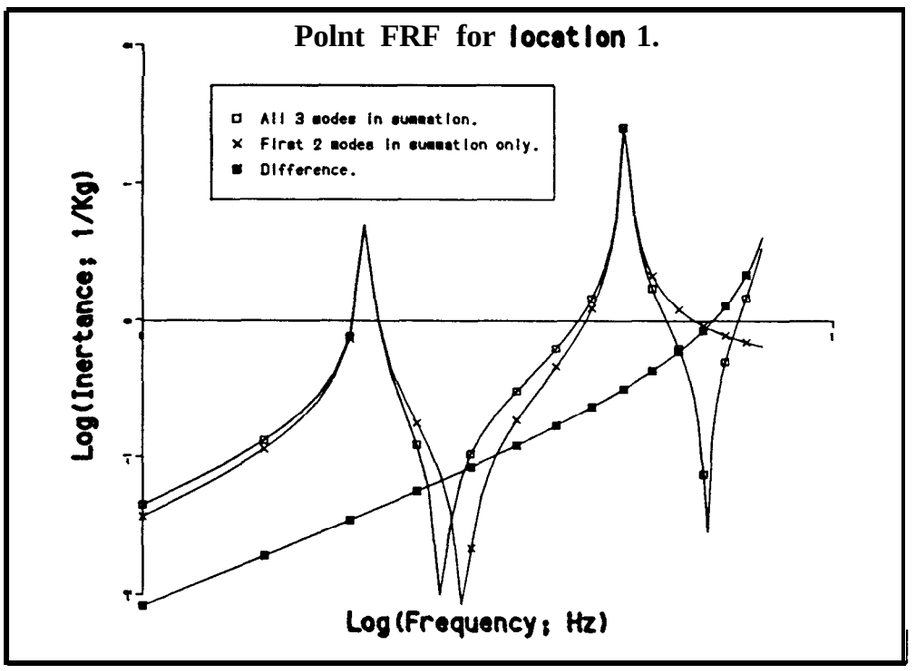

Illustration of Modal Deficiency in the Synthesis of a FRF

Figure 5.17

Effects of Modification to the System

Now, consider the effects of a very simple modification – a mass of 1 Kg (m_4) added at point 1; the mass m_1 is thus doubled from 1 Kg to 2 Kg.

Predictions Using the Complete Model

The exact solution can be found by direct solution of equation (5.7) with the modified value for m_1. Alternatively, the following equation may be used, derived from the modal coupling method in a similar manner to equation (2.63) -

$$\left[[\Omega_r^2] - \lambda^2\left([I] + [\Phi]^T \{t\}\ \{t\}^T [\Phi] m_4\right)\right]\{W\} = (0) \quad \ldots\ldots\ldots\ldots (5.12)$$

λ^2 is a new eigenvalue, and,

$\{W\}$ is a weighting vector defined such that -

$$\{\theta\} = [\Phi]\{W\} \quad \ldots\ldots\ldots\ldots (5.13)$$

and $\{\theta\}$ is an eigenvector of the modified system and $[\Phi]$ is the eigenvector matrix of the original system.

{t} is a tie vector representing the connection of the modification; in this case for a single-degree-of-freedom mass modification at location 1.

$$\{t\} = \begin{Bmatrix} 1 \\ 0 \\ 0 \end{Bmatrix}$$

Equation (5.12) can be written more concisely as -

$$[[A] - \lambda^2[B]]\{W\} = \{0\} \quad \ldots\ldots\ldots\ldots (5.14)$$

with, in this case,

$$[A] = \begin{bmatrix} 177 & 0 & 0 \\ 0 & 1000 & 0 \\ 0 & 0 & 2820 \end{bmatrix} \quad \text{and} \quad [B] = \begin{bmatrix} 1.081 & 0.164 & -.0218 \\ 0.164 & 1.333 & -.0441 \\ -.0218 & -.0441 & 1.585 \end{bmatrix} \ldots (5.15)$$

Solution of this system of equations yields the following eigenvalues for the modified structure.

$$[\lambda_r^2] = \begin{bmatrix} 162 & 0 & 0 \\ 0 & 731 & 0 \\ 0 & 0 & 2100 \end{bmatrix} \quad \ldots\ldots\ldots\ldots (5.16)$$

The new natural frequencies for the modified system are 2.03, 4.30, and 7.31 Hz, compared with the natural frequencies for the unmodified system of 2.12, 5.03, and 8.45 Hz, equation (5.8).

By use of equation (5.13), $\{\theta\} = [\Phi]\{W\}$

$$El\theta = \begin{bmatrix} -.285 & -.577 & .765 \\ -.520 & -.577 & -.630 \\ -.805 & .577 & ,136 \end{bmatrix} \begin{bmatrix} .999 & .999 & .231 & .123 \\ . & .035 & -.959 & .435 \\ & -.015 & .164 & .892 \end{bmatrix} \quad \ldots\ldots\ldots\ldots (5.17a)$$

and therefore, the new mode shape matrix is;

$$[\theta] = \begin{bmatrix} -.317 & .613 & .396 \\ -.531 & .329 & -.877 \\ -.786 & -.717 & .273 \end{bmatrix} \qquad (5.17b)$$

It is instructive to look at the weighting matrix [W] of equation (5.17a) to see the contributions of the unmodified system mode shapes in the mode shapes for the modified structure. The terms on the leading diagonal of the weighting matrix are close to unity, indicating that the predominant mode shape contributions are the respective unmodified mode shapes. However, it will be noted that, with increasing mode number, there is progressively more and more contribution of the other unmodified mode shapes in each new mode shape vector, i.e. the higher frequency mode shapes are affected to a greater extent than the lower frequency mode shapes for this particular modification.

Predictions using Incomplete Models

(1) Prediction using the Spatially Deficient Model

The spatially deficient model is represented by the modal database of equation (5.10). The eigenvalues are the same as those of the complete model, equation (5.8). In substituting the reduced matrices into equation (5.12), it will be seen that the resulting [A] and [B] matrices are identical to those for the full system matrices. Therefore, eigensolution gives the same eigenvalues and eigenvectors for the system of equations as found for the complete model. The natural frequencies for the modified system are still estimated correctly – a spatially deficient model produces correct results for the natural frequencies of the modified system, providing that the spatial deficiency does not extend to include the degrees-of-freedom actively involved in the coupling.

The effects of the reduced eigenvector matrix of the spatially deficient base model only become apparent when calculating the mode shape vectors for the physical system using equation (5.13). The new mode shape vectors are identical to those calculated using the complete system model except that, in this case, there is no information for location 2.

Using equation (5.9), FRFs for the modified system can be synthesised correctly for all combinations of force and response locations that do not involve location 2.

(2) Prediction using the Modally Deficient Model

The reduced modal database of equation (5.11) **is used** in equation (5.12). The whole system of equations is reduced from a 3x3 set to a 2x2 set, with -

$$[A] = \begin{bmatrix} 177 & 0 \\ 0 & 1000 \end{bmatrix} \quad \text{and} \quad [B] = \begin{bmatrix} 1.081 & 0.164 \\ 0.164 & 1.333 \end{bmatrix} \quad \text{.....(5.18)}$$

Eigensolution produces the following eigenvalues and new mode shape vectors for the modified system -

$$[\lambda_r^2] = \begin{bmatrix} 163 & 0 \\ 0 & 769 \end{bmatrix} \quad \text{and} \quad [\theta] = \begin{bmatrix} .277 & .518 \\ .539 & .468 \\ .785 & -.719 \end{bmatrix} \quad \text{.....(5.19)}$$

The base system was assumed to have only 2 modes and therefore, the modified system can have only 2 modes, each of which is a linear combination of the 2 unmodified mode shapes. There are differences between this prediction for the modified system and that using the complete model for both eigenvalues, equation (5.16), and the mode shapes, equation (5.17), although, in this example, the differences are not very large. The natural frequencies predicted for the **modified** system are now 2.03 and 4.41 Hz (compared with 2.03 and 4.30 Hz). The prediction of the first mode shape for the modified system differs from the exact answer at location 1 only, the modification site. For mode number 2, the errors in the mode shape prediction are larger and extend to location 2 as well.

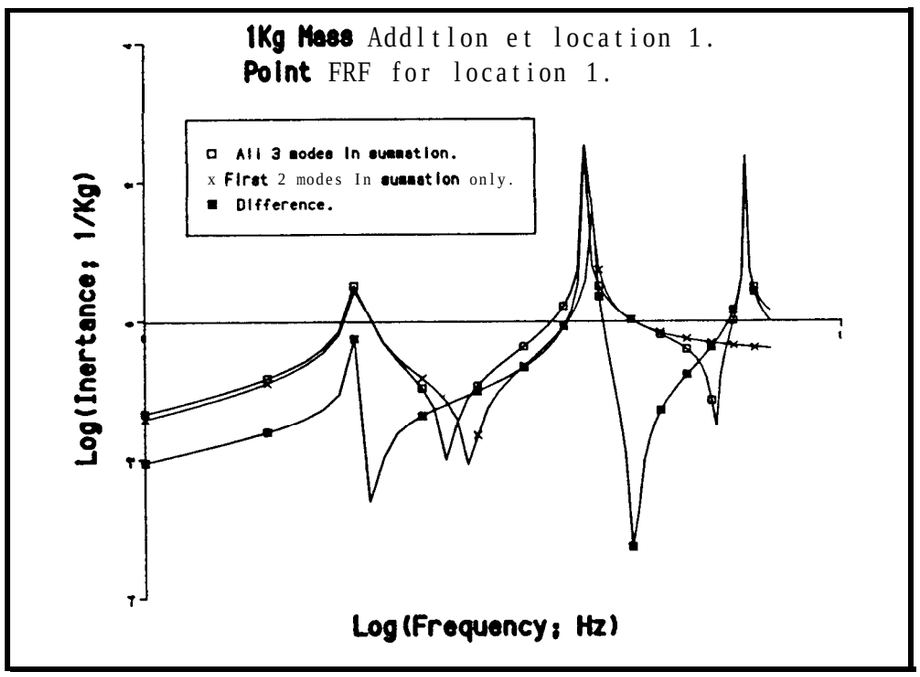

The Result of Modal Insufficiency on Prediction of the Effect of a Modification

Figure 5.18

If the parameters of equation (5.19) are used to synthesise FRFs of the modified system, significant differences can be seen when they are compared with the true FRFs. A comparison is presented in Figure 5.18 for the point FRF at location 1. The two FRF curves show different resonance frequencies as well as a different number of resonances. To aid the comparison, the difference between these two FRFs – the AFRF – has been calculated and plotted. It will be noted that it is no longer a simple single-degree-of-freedom FRF shape, as it was for the comparison of the complete and modally deficient FRFs of the unmodified system (Figure 5.17).

In this simple example, the effects of modal insufficiency have been compared with those of spatial insufficiency where the spatial insufficiency does not extend to the modification degrees-of-freedom. It has been shown that, under these circumstances, modal insufficiency is a greater problem than spatial insufficiency for the correct prediction of a modification. However, when the spatial incompleteness includes some of the degrees-of-freedom actively involved in the modification (e.g. rotational degrees-of-freedom) all results will be incorrect, illustrated by the example of joining two beams together, in section 52.1. The actual modification and that modelled theoretically are **not the** same. This can be a very much more serious problem than the spatial and modal insufficiencies discussed above. The importance of the deficient degree-of-freedom in the actual coupling is reflected by the sizes of the errors; if the deficient degree-of-freedom is very important in a modification coupling, the errors will be large.

In summary; spatial incompleteness is a severe problem only if it includes degrees-of-freedom actively involved in a modification. Spatial incompleteness is a **local** problem – modal incompleteness is a **global** problem. Spatial incompleteness is a factor which is independent of the type of model used, i.e. either raw measured FRF data or FRF data synthesised from a modal database. In theory, modal incompleteness is only present if modal analysis data are used as a description of the dynamic behaviour of the structure – raw measured FRF data contain the effects of **all** modes. Practically, though, there are several reasons why raw measured FRF data are rarely used directly in a modification prediction and therefore modal incompleteness is always present, to some degree, when the synthesised data are used instead.

5.3 Inaccuracy

Measurement inaccuracy is the inability to quantify the behaviour of the structure precisely. This inability can be subdivided into 2 types;

(i) the inability to transduce the motion of the structure without affecting its behaviour, and

(ii) the inability to quantify the transduced signals.

5.3.1 Transduction Inaccuracy

Selection of Transducers

The size and mass of the transducer has implications for its influence on the behaviour of the base structure. Careful selection of the accelerometer such that its mass is small when compared with the local mass of the test structure can help to avoid frequency shift problems. Almost all transducers have some effect on the structure and it is a matter of engineering judgement as to when the influence can be considered to be negligible, and hence, which transducer is appropriate.

It is very much better to use a signal directly from a transducer that has minimal effect on the structure than to try and compensate, at a later stage, for the effects of an inappropriate transducer. The greatest care and attention should be directed towards the acquisition of transducer signals giving a faithful representation of the actual behaviour of the structure in its base condition.

To some extent, the vibration frequency range influences the size of the transducer. For piezoelectric accelerometers, it is usually the case that the lower the frequencies to be measured the larger the transducer – because a large seismic mass is required to produce sufficient deformation of the crystal and thence a reasonable output charge signal. Alternatively, much smaller transducers based on miniature strain gauged cantilever beams are available, but these require careful handling and different drive and amplification equipment.

For FRF type measurements, there must be at least one force input transducer and one response transducer. The force transducer is often overlooked in transducer selection considerations because it is quite usual for there to be just a single force gauge, but a large number of response transducers. Since the force transducer signal is used in all the FRF calculations it is particularly important that the transducer responds to the true force input to the structure.

Instead of using a force gauge to measure the force input into the structure, the force can be calculated from measurements of the current fed to an electromagnetic shaker. From

basic electromagnetic principles it is known that a current-carrying conductor in a magnetic field experiences a force given by the expression-

$$F = B.I.L.N \quad \ldots\ldots\ldots\ldots\ldots\ldots\ldots\ldots\ldots\ldots\ldots\ldots\ldots\ldots\ldots\ldots\ldots\ldots\ldots\ldots\ldots\ldots (5.20)$$

where: F = force (N)
B = magnetic flux density (Webers/m^2)
I = current (amps)
L = length of conductor in flux field (m)
N = number of turns of length 1 in flux field

B, L and N remain fixed for a given shaker and hence the force applied to the structure is directly proportional to the current flowing in the coil of the shaker. When a constant current amplifier is used to drive the shaker, the force generated in the coil is constant and there is no need for any on-line measurement of current. The relationship between coil current and force applied to the coil can be derived from D.C. calibration measurements with subsidiary force measuring equipment.

Although this would seem to be an ideal solution to some of the force measurement problems, several important details must be borne in mind -

(i) a constant current amplifier with suitable capacity must be used. At resonance frequencies high powers may be required,

(ii) the constant current drive arrangement provides very little inherent damping;

(iii) the large amplitude range may cause problems with unwanted excitation of non-linearities; and

(iv) the moving components of the shaker and the pushrod are all considered as part of the structure. The force calculated is the force applied to the coil and not that actually transmitted through the pushrod-structure interface. If the mass of the moving components of the shaker is small compared with the structural mass (e.g. in ground vibration testing of aircraft structures) the errors caused by this assumption will be small. However, with lightweight structures the errors can be significant and here a force gauge is essential

Transducer Attachment Considerations

The purpose of a transducer is to convert one form of energy into another that can be quantified by remote instrumentation. In the case of an accelerometer, the energy of motion of component parts in the accelerometer is used to produce an electrical charge, or

to control an external electric current, which is then measured. The signal produced is a representation of the motion of the transducer. The implicit assumption is made that the motion of the transducer is identical to that of the structure. This will be the case providing that the transducer is rigidly attached to the structure. The attachment stiffness must be sufficiently high that, throughout the frequency range of interest, the motion of the transducer is identical to that of the attachment point on the structure. For low-frequency work, it is quite acceptable to attach the transducer with bees' wax or double-sided adhesive tape, but for high-frequency measurements, the transducer must be bolted to the structure firmly [25].

In a large measurement survey, a further consideration is whether all the transducers are to be fixed to the structure before the start of the test, or whether a small number of transducers are to be moved around the structure to all of the test points in turn. This is largely dictated by the size of the test, the number of transducers and the number of simultaneous data acquisition channels that are available. In a test where all the transducers remain fixed in place throughout the complete measurement phase, the structure does not change as different response points on the structure are measured. The structure will be slightly altered from the base condition, but the important point here is that no further changes occur throughout the measurement phase. When the measurements are made in a series of tests where a small set of transducers are moved around, the structure is altered differently for each test – a systematic error. The errors are most easily seen as different positions of the resonance peaks for each successive set of measured FRFs. Although the errors introduced in each test are potentially smaller than the overall error caused by attaching all the transducers at the start, the systematic errors make the task of analysis of the measured data significantly more complex.

Transducer Cross-Axis Sensitivity Influences

Transducers are designed to measure a particular quantity in a specific direction in relation to the construction of the transducer, e.g. acceleration in a direction perpendicular to the base of the transducer. Transducers are carefully designed and built such that motion of the transducer in directions other than the specified measuring direction has little effect on the output. Nevertheless, there is always some degree of cross-axis sensitivity which may influence the results adversely [13]. With care, this can be minimised by suitable alignment of the transducer, but it is necessary to have a polar plot of the transducer cross-axis sensitivity which identifies the cross-axis sensitivity of the transducer as a function of the direction of cross-axis excitation, Figure 5.19.

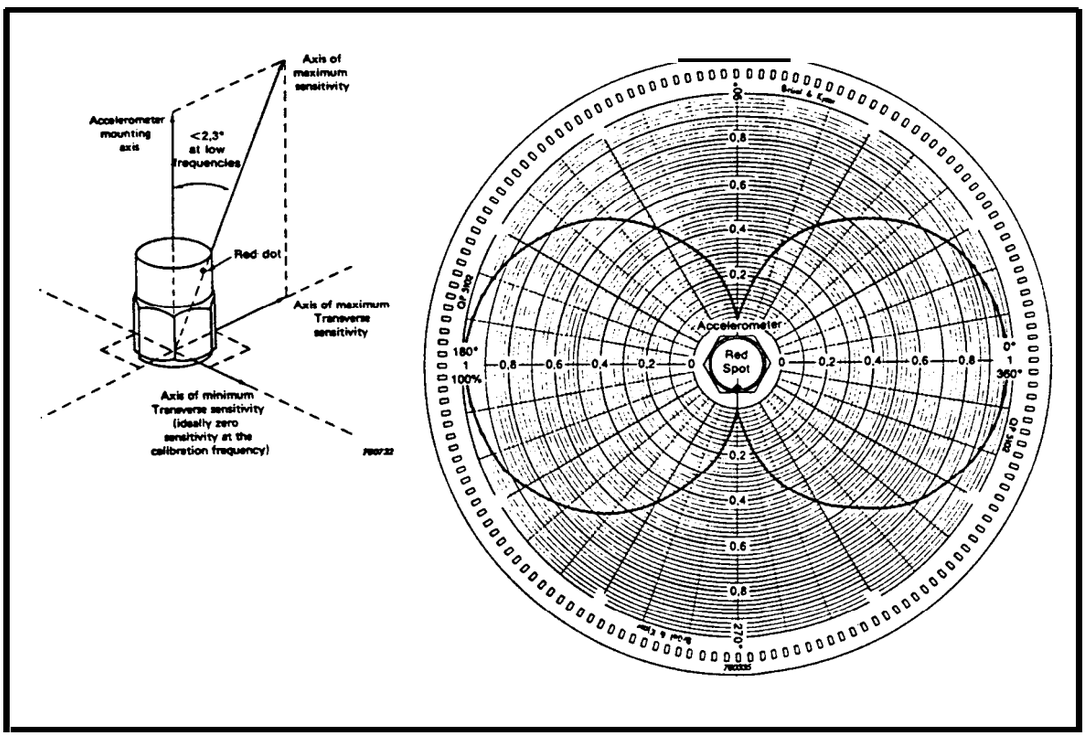

Vectorial Representation and Polar Plot of Cross-Axis Sensitivity.
(Figures courtesy of Brüel and Kjær)

Figure 5.19

For minimum cross-axis effect, the direction of minimum cross-axis sensitivity should be aligned with the direction of the maximum cross-axis response of the structure. There are several difficulties with implementation of such a procedure;

(i) a polar plot of cross-axis sensitivity is seldom supplied with each transducer;

(ii) a preliminary measurement survey is necessary to deduce the directions of maximum cross-axis motion at the measurement points;

(iii) the directions of maximum cross-axis motion will alter with the excitation frequency as different modes become more prominent; and

(iv) it can be quite difficult to set a particular angular orientation of the transducer because of the fixing methods used.

In the light of these difficulties, it is unusual for much consideration to be given to cross-axis sensitivity influences.

Cross-axis sensitivity effects can be of particular importance when trying to calculate rotational degree-of-freedom properties from two sets of closely spaced translational

degree-of-freedom FRF measurements. The calculation of the rotation/translation, translation/rotation, and rotation/rotation FRFs from the translation/translation data essentially involves differencing operations. When the motion in one of the transverse directions is large, the difference between the measured FRFs can be of the same order of magnitude as the cross-axis sensitivity component, so that the calculated rotational degree-of-freedom properties will contain significant errors.

5.3.2 The Use of Dummy Transducers

The systematic error incurred as a result of moving the transducers around on the structure during the course of the test can be turned into a single error by the use of dummy transducers. Instead of instrumenting the whole structure with transducers at the outset of the test program, dummy transducers are used. The dummy transducers are designed to have similar mass properties to the real transducers. The dummies are systematically replaced (temporarily) by the real transducers for the measurements, until all of the measurement locations have been covered. The results from this type of test should be the same as if a complete set of real transducers had been attached to the structure at the outset. The use of dummy transducers for response measurements is an established practice; what is rarely considered is the use of dummy force transducers at the excitation locations. These may be just as applicable as dummy response transducers when a series of single point tests are performed to measure several columns of the FRF matrix. It is suspected that the use of dummy force transducers is generally overlooked because of the very much smaller number of forcing locations compared with the number of response locations in the majority of vibration tests. Additionally, the conception of exactly what a dummy force transducer has to represent is somewhat obscure – unlike the response transducer counterpart. To understand this problem, some background details of the construction of force and response transducers is appropriate. The diagrams of Figures 5.20 and 5.21 show typical cross-sections of a piezoelectric accelerometer and a piezoelectric force gauge.

A Piezoelectric Accelerometer

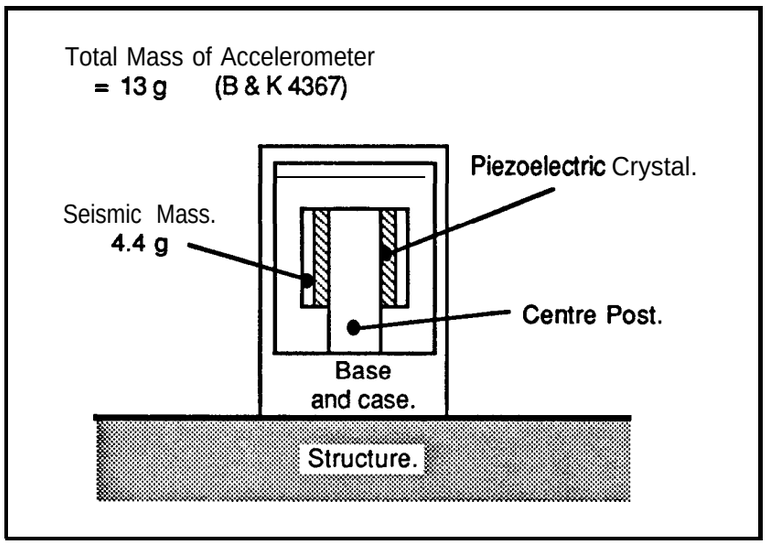

Cross-Section of a Piezoelectric Accelerometer

Figure 5.20

The cross-section of a typical piezoelectric accelerometer is shown in the above diagram, Figure 5.20. There are four basic components; a base/case, a centre post, an annular section of piezoelectric ceramic and an annular seismic mass element. The piezoelectric ceramic and seismic mass are arranged concentrically around the centre post. The base of the accelerometer moves with the motion of the structure to which it is attached, and to cause equivalent motion of the seismic mass, a force must be applied – Newton's 1st Law. This force is transmitted through the piezoelectric crystal which deforms as a consequence. The deformation produces a charge in the piezoelectric crystal which is proportional to the deformation and hence, ultimately, to the acceleration of the seismic mass and the structure.

The important point to note here is that the apparent mass of the accelerometer, as seen by the structure, is the same in the axial and lateral directions and equal to the total mass of the transducer.

A Piezoelectric Force Transducer

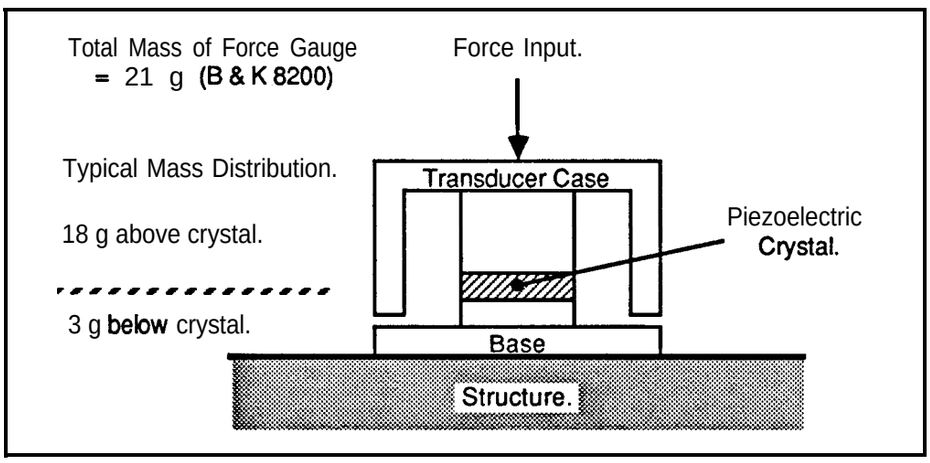

Cross-Section of a Force Transducer

Figure 5.21

The force transducer, Figure 5.21, works on the same principle as the accelerometer, but more directly – the deformation of a piezoelectric crystal produces a charge output proportional to the force transmitted. The shaker applies a force through the case of the force gauge to the top of the piezoelectric crystal. The lower end of the crystal is fixed to the base of the transducer which is, in turn, attached to the structure. In the axial direction, the force applied to the structure is that transmitted through the piezoelectric crystal (measured) minus the force that is required to accelerate the base of the force gauge. For this reason, the mass of the base of the force gauge is kept as small as possible to minimise the effect on the structure. The mass of the transducer case is irrelevant in the axial direction. Lateral motion of the structure causes lateral motion of the whole force gauge and since no forces are measured in the lateral directions, the total mass of the force gauge has an effect on the structure.

The ratio of the apparent mass of a force gauge in the axial and lateral directions, as seen by the structure, is small; $\frac{3}{21}$ g for the B&K 8200 Type of force gauge, Figure 5.22.

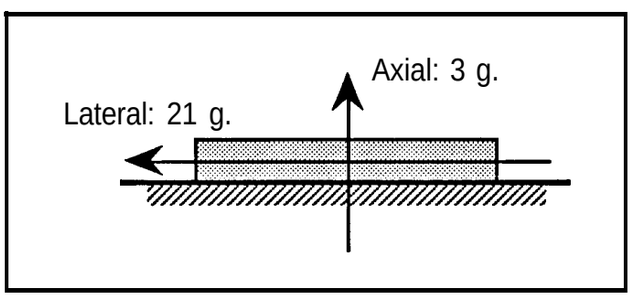

Figure 5.22

The problem with the use of dummy force gauges arises because the structure "sees" the mass of the force gauge differently in the axial and transverse directions. Axially, only the base mass of the force transducer is seen by the structure; in the transverse directions, the full mass of the force transducer is seen by the structure. An inert dummy force gauge cannot represent these different effects.

If the force gauge were to be mounted upside-down (incorrectly), with the larger mass attached to the structure, then there would not be such different apparent loading influences on the structure in the axial and transverse directions. The ratio of axial and lateral apparent masses is now $\frac{18}{21}$ g, Figure 5.23.

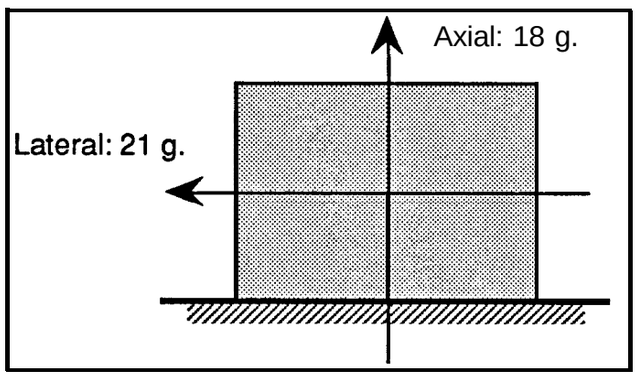

Figure 5.23

With this arrangement, it is possible to use dummy force gauges, in the same way as dummy accelerometers, to obtain consistent measurements of the structure as the force and response locations are moved around. However, to deduce the true FRF characteristics of the underlying structure, it will be necessary to subtract the effects of all the point mass additions at the force and response locations once a model of the measured structure has been produced.

As the amount of transverse motion increases, the lateral motion of the force transducer has a greater effect on the response. Normally, when the predominant motion is in the axial direction of the force transducer, the cross-axis **motion** of the force transducer has only a small influence on the measured **FRFs.** However, when two sets of closely spaced translational FRF measurements are made, with the intention of using them in calculations to derive rotational degree-of-freedom FRF properties, the cross-axis motion of the force transducer can have a large effect on the final derived results, despite the fact that there is only a relatively small influence on each of the measured translational **FRFs** (see section 5.2.1). This is especially evident if there is a high degree of rotational motion.

5.3.3 Errors in Quantification of Transduced Signals

Once the transducer and conditioning equipment has converted the force or response quantities into electrical signals, the signals have to be quantified. Nowadays, the measurement instrumentation is primarily digital in nature and a large proportion of the errors in quantification of these signals are associated with details of digital signal processing. There is a large quantity of published literature relating to digital signal processing techniques and it is not proposed to enter into any lengthy discussion of these topics here.

Calibration errors are also a common source of inaccuracies in measured data.

Dynamic Range of the Measuring Equipment

The force and response signals returning to the analyser from the transducers are analogue signals. The analysers work with digital representations of these analogue signals. The interface process is called Analogue to Digital conversion. The signals are sampled at regular intervals and the instantaneous value of the analogue signal is compared with fixed, discrete, digital levels in the analogue-to-digital converter (ADC). The digital level which most closely approximates the instantaneous value of the analogue signal is selected. ADCs have a fixed number of discrete levels – usually expressed in terms of the number of binary bits used to describe the levels. A 12 bit ADC is typical of the type found in many analysers today. The dynamic range of the ADC is expressed as the ratio of the maximum to the minimum signal level that can be resolved, in db. For a 12 bit ADC there are $(2^{12} - 1) = 4095$ possible levels, i.e. anything smaller than $\frac{1}{4095}^{th}$ of the input range cannot be resolved. The dynamic range of a 12 bit ADC is 72.25 db.

Before the start of a measurement, the input range for each signal is scaled to make the best possible use of the dynamic range available. The ranges are set using the peaks of the input signals. Providing that the dynamic range of the analogue input signal is less than 72 db, the digital representation will be quite adequate. However, if the analogue signal has a dynamic range greater than 72 db, very small levels in the signal cannot be resolved and they are all represented as zero.

Lightly damped structures can produce analogue response signals with a dynamic range greater than 72 db, in which case, the range is truncated upon conversion to a digital signal. The errors become evident at small response levels, i.e. at the anti-resonance frequencies. Where the response levels are high, at resonance frequencies, the

quantisation of the analogue response signals is quite adequate. The same analogue-to-digital conversion is applied to the force signals, only, in this case, the conversion errors are more apparent at low force levels, i.e. at the resonance frequencies. Therefore, in the absence of noise, the definition of the resonance and anti-resonance features will be equally poor if the analogue force and response signals have similar, excessive, dynamic ranges. If the response signal has an excessive dynamic range while the range of the force signal is much less, errors will occur at anti-resonances and not at resonances. Alternatively, if the force signal has a large dynamic range, the errors occur at the resonances and not at the anti-resonances. For more detailed discussion on how the dynamic range of the force signal can be influenced by the interaction of the shaker with the structure under test, see section 4.3.

5.4 Review of Chapter 5

All vibration models – analytic, F.E. or experimentally-derived – are incomplete and inaccurate representations of the dynamic behaviour of real structures. The analytic or F.E. model can describe completely and accurately the behaviour of the idealised 'paper model' of the structure. The overall insufficiencies of the model are a direct result of the paper description of the structure. Joint conditions may be incorrectly modelled and the distribution of damping is often ignored or crudely approximated. With an experimentally-derived model the incompleteness is caused by insufficient measurement points – structural responses are only measured at a few discrete points – and by analysis of only a small subset of the structural modes.

In this chapter, attention has been focussed on the causes of incompleteness and inaccuracy in experimentally derived models, how these deficiencies can be minimised and the consequences of using incomplete models in predictions of the effects of structural modifications. The terms spatial and modal incompleteness have been defined to describe the two forms of incompleteness commonly found with experimentally derived models. Spatial incompleteness is discussed with particular reference to the measurement and use of rotational FRF properties which are notoriously troublesome to measure and, for this reason, they are frequently overlooked in measurement surveys. However, this absence of rotational degrees-of-freedom in a coupling analysis can provide a convenient explanation of the subsequent inability to predict accurately the effects of a modification! The procedure for calculating rotational degree-of-freedom properties from translational measurements made on a T-block transducer is examined carefully and some probable causes of errors have been identified. It has been stated that the only reason for using a T-block is to facilitate the collection of sufficient data for calculation of the rotation/rotation

FRF. If the structure is locally stiff, the angular response can be derived equally well from closely spaced transducers placed directly on the structure. With this arrangement and a linear excitation position mid-way between the response transducers, it is possible to derive the translation/translation, the rotation/translation and, by reciprocity, the translation/rotation FRFs at the measurement point. The rotation/rotation FRF cannot be derived with this arrangement and it is for this reason alone that the T-block appendage is used. As yet, there are no simple and direct methods for applying a pure torque excitation which are unaffected by any translational motion of the structure that may occur. A fundamental problem which has emerged is related to the attachment of the T-block transducer to the structure and, indeed, the subsequent attachment of any modification. Usually it is assumed that these joints are absolutely rigid In practice, however, the joints will not be rigid and the results for the rotational degree-of-freedom properties will contain some influence of the joint. Only if the joint conditions for the T-block transducer are identical to those of a subsequent modification -which is a rather unlikely event – will the model used in a prediction of the effects of the modification be an accurate representation. It would be possible, theoretically, to include separate 'joint components' between the structure and the T-block or the modification, but the practical difficulties and uncertainties involved in the determination of the dynamic properties of these joint components are likely to be prohibitive.

Modal incompleteness arises from the use of modal analysis data where insufficient modes have been measured, analysed and included in the modal model. Various methods have been described which allow for compensation of the effects of the out-of-range modes. The main purpose of residual correction methods is to provide a better basic model of the dynamic characteristics of the structure that can be used in predictions of the effects of modifications. A practical example is used to show how the need for residual corrections can be identified and the improvement in the FRF model that is possible by inclusion of residual terms.

Further examples have been presented which illustrate the effects of modal and spatial incompleteness on the results of a simple coupling analysis. It is shown that the most serious effects occur when the spatial incompleteness of the model extends to include some of the degrees-of-freedom that are actively involved in a modification coupling. Modal incompleteness has, potentially, the next most serious effect, followed by spatial incompleteness where the incompleteness is confined to passenger coordinates only. In this last case of spatial incompleteness the results that are obtained will be correct, it is just that they are insufficiently extensive to describe the behaviour of the modified structure completely in a spatial sense.

The question of inaccuracy has been divided into two distinct areas; transduction inaccuracy; and quantification inaccuracy. These forms of inaccuracy arise at opposite ends of the measurement chain. The transduction inaccuracy is the inability to obtain some form of signal that describes accurately the force input or the response output of the base structure. Several factors may contribute to this inaccuracy – loading of the structure by the measuring equipment, inappropriate attachment of the transducers to the structure and the influence of cross-axis motion on the outputs from the transducers. Once the signals have been produced, environmental interference can corrupt the data before it reaches the measuring apparatus. The data acquisition equipment can introduce inaccuracies in the data as a consequence of digitisation processes. It has been shown that this can be a particular problem with lightly damped structures that have large dynamic ranges in the force and response signals.

Chapter 6

Case Study; A Helicopter Structure

6.1 Introduction

The vibration environment of a helicopter is probably ‘one of the most severe of any aircraft. The excitations are primarily due to the periodic change in the velocity and incidence of the airstream seen by the rotor blades when the helicopter is in forward flight. Additionally, there are excitations due to the interaction of each blade with the wash of preceding blades and the tail rotor. Yet further sources of excitation arise from the gearbox and transmission between the engines and rotors. All of these excitation sources are largely avoided in fixed wing aircraft. Overall, the excitation frequencies tend to be relatively low, but the forcing levels are very high.

A helicopter airframe has been used in detailed investigations of many aspects of vibration measurement, modal analysis and sensitivity analysis, leading on to the prediction of the effects of various modifications.

A preliminary survey of the structure was performed in which more stringent methods than normal were used to check the repeatability and reciprocity of measurements. This was followed by a full measurement survey where attempts were made to derive FRF properties for rotational degrees of freedom. Modal analysis of a full set of translational degree-of-freedom FRF data was performed and the final resulting synthesised FRFs, including residual terms, are compared with the original measured FRFs.

One of the difficulties encountered in the present exercise was an inability to measure certain FRFs directly due to inaccessibility of points for excitation – a problem frequently encountered with experimental measurements. The idea of forcing at an angle and then calculating the desired FRF using other additional FRF information was explored. It is shown that this technique can yield acceptable results for those FRFs that cannot be measured directly but that the method has many problems in common with those found with the measurement of rotational degree-of-freedom properties.

Measurement of rotational degree-of-freedom FRF properties using the T-block method was also investigated, and the results highlighted the importance of a 'rigid' joint between the T-block and the structure in order to obtain a full set of high quality rotational FRF data. Application and measurement of a pure torque excitation for derivation of FRFs relating rotational response due to rotational excitation is still the main obstacle in the measurement of a complete set of rotational FRF data at the present time since the measurement of rotational response is comparatively easy.

The sensitivity analysis method (chapter 3) has been used to indicate the sensitive degrees-of-freedom and hence the places where modifications could be made most efficiently. The predictions of sensitivity for Single Degree-of-Freedom (SDoF) modifications have been verified experimentally. Additionally, more practical modifications – adding a mass (3 coupled translational degrees-of-freedom) and adding a spring between two points – have been made and the measured and predicted FRFs for the modified structure are compared.

Some simplified predictions of the new resonance frequencies of the modified structure, based on the sensitivity analysis results, have been found to compare well with the measured results for the modified structure.

The helicopter structure used for all the work reported here is currently located in the Dynamics Laboratory at the Royal Aerospace Establishment (R.A.E.) in Farnborough.

6.1.1 Details of the Helicopter Test Structure

Photograph of the Helicopter.

Figure 6.1

The test structure is based on a standard helicopter which has had all the internal electronic equipment, cabin seating and doors removed. The main and tail rotor blades have also been removed. To prevent rattles of the transmission system, the tail rotor hub and links are attached to a wooden clamping fixture, and the four main rotor blade attachments are bolted to the arms of a cruciform structure made of steel beam sections. The whole helicopter is freely suspended by a steel hawser between the cruciform and a purpose-built gantry frame, Figure 6.1.

To allow comparison of the results of this work with previous experimental measurement and F.E. analysis surveys, [83] & [84], and current F.E. analysis work at R.A.E., the coordinate axes and location of points have been defined in the same way. Only two points – 49 and 66 – have been used for this work, but multiple degrees of freedom have been included. Point 49 is mid-way along the leading edge of the tailplane and point 66 is located on the intermediate gearbox at the base of the tail fin, see Figure 6.2.

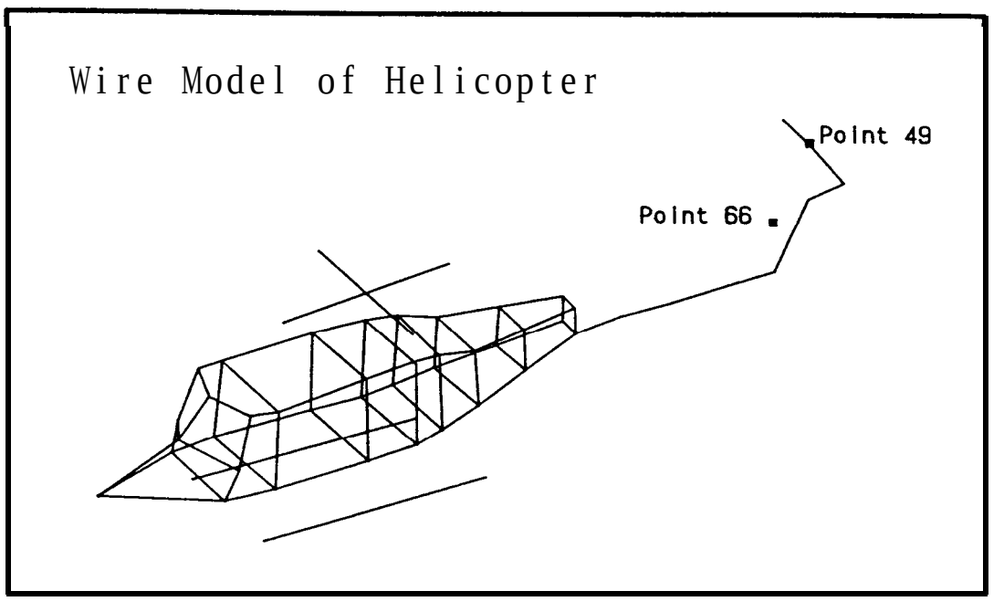

Wire Model of the Helicopter Structure.

Figure 6.2

A further reason for choosing the points used previously was that the excitation fixtures (steel blocks) and triaxial accelerometer blocks (aluminium) were already in position on the helicopter.

6.2 Experimental Set-Up

6.2.1 Details of Measurement Equipment

The measuring equipment is centred around a Gen-Rad 2515 Computer Aided Test System. The excitation signal is generated in the Gen-Rad 2515, from where it is fed through a Kemo bandpass filter unit to an H.H. Electronics power amplifier, and then on to a Ling Dynamics shaker. It has been found necessary to install a filter unit in this signal path to smooth out the excitation signal generated within the Gen-Rad 25 15. If this is not done, a large amount of high frequency energy associated with step changes in the digital signal is fed to the structure unnecessarily, leading to noise on the measured force and response signals. Furthermore, filtering out the low frequency components of the excitation signal (less than 3 Hz) reduced the extent to which the shaker bounced around on its suspension throughout the excitation sweep. Because the helicopter is a massive structure compared with the Type V409 shaker used, the shaker was bolted to a reaction mass of approximately 50 Kg to achieve reasonable force levels at the low frequencies. To

keep the rocking excitation to a minimum, efforts were made to try and keep the centre of gravity (C.G) of the whole arrangement in line with the forcing axis of the shaker.

A wire pushrod was used between the shaker and the force gauge (PCB Type 208B) attached to the helicopter. The pushrod decouples the structure and the shaker system in all degrees-of-freedom except the primary translational excitation degree-of-freedom. For the majority of the tests, a pushrod 100 mm in length and made of 1 mm diameter 'piano wire' was used.

The vibration response of the helicopter was measured using Entran type EGA 125-F accelerometers. These are very small and light, and are based on miniature strain gauged cantilever beams with seismic masses at their tips. Each accelerometer has a mass of just 1 g, and hence the loading effect of all 6 accelerometers on the helicopter is negligible. The accelerometers are connected to Vishay strain gauge amplifiers (Type 2120) which amplify the strain gauge bridge signal to a suitable level for input to the Gen-Rad 2515.

The Gen-Rad has 12 bit Analogue to Digital Converters (ADCs) on the inputs, which limit the dynamic range of the equipment to 72 db. Resonances are captured well because the auto-ranging facility enables the ADCs to be used to their full extent. However, the anti-resonances, which are frequently 3 or 4 orders of magnitude (60 or 80 db) smaller than the resonance peaks, are sometimes lost due to insufficient resolution in the ADCs.

A schematic diagram of the measuring equipment set-up is shown in Figure 6.3.

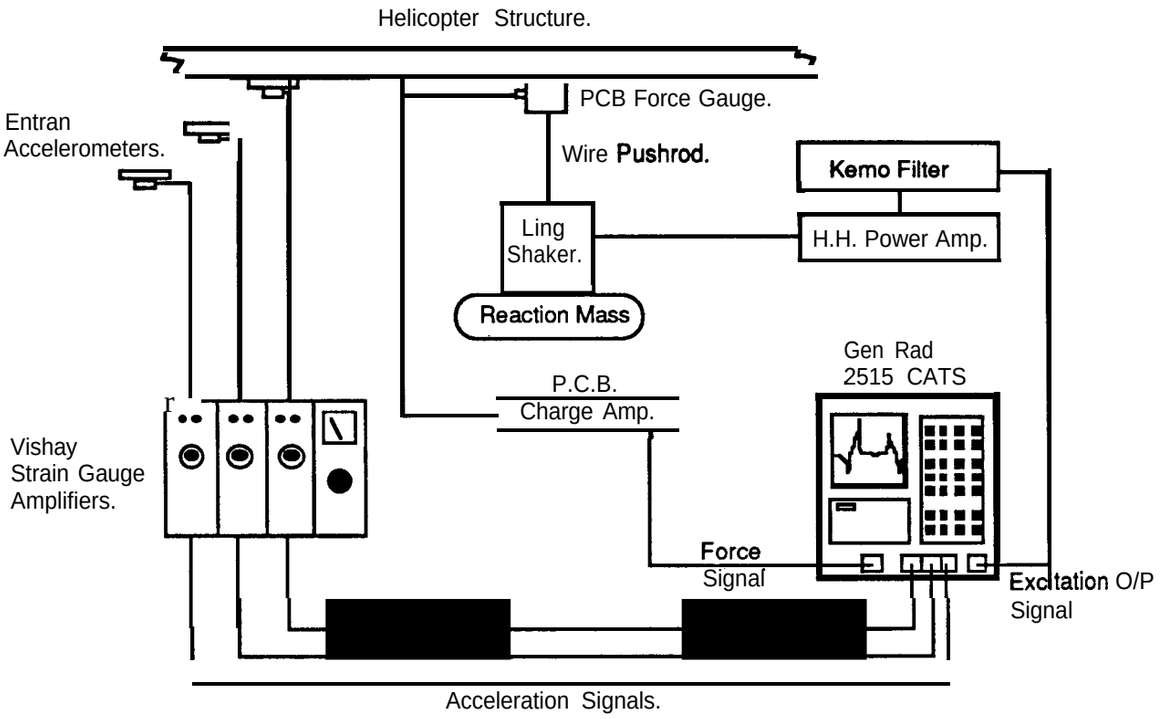

Schematic Diagram of the Measuring Equipment.

Figure 6.3

6.2.2 Calibration of Measurement Channels

Before any measurements were made on the helicopter, channels were calibrated using a ratio calibration technique. All the accelerometers were fixed to a freely suspended mass which was then excited by a shaker driving through a force gauge in just the same way as measurements are performed on the helicopter itself. The strain gauge amplifier gains were adjusted until the measured inertances all had values equal to (l/calibration mass) across the whole frequency range. There are several advantages to this type of calibration over alternative methods such as absolute calibration:-

- it is a relatively simple method,
- **the complete** measurement chain is checked out and calibrated; and
- the possibility of error is small.

6.3 Measurement of Translational FRF Properties

A single-point random testing method was selected for these measurements to make the best possible use of the response channels and to allow use of the 'repeated random' excitation signal available as part of the Gen-Rad RTA (Real Time Acquisition) data acquisition program. For the modal analysis stage an SDRC program, MODAL PLUS, was used.

The helicopter is situated in a fairly quiet environment and all the possible sources of rattles inside the structure have been removed and, with the use of repeated random excitation, good quality FRFs were achieved with only four averages. For most of the measurements, the FRFs hardly changed at all throughout the averaging process. It must be noted, however, that any transient behaviour associated with starting the excitation, had had sufficient time to decay while the input levels were being adjusted (either manually or by auto-ranging).

6.3.1 Preliminary Phase

(i) Excitation Source Level Effects

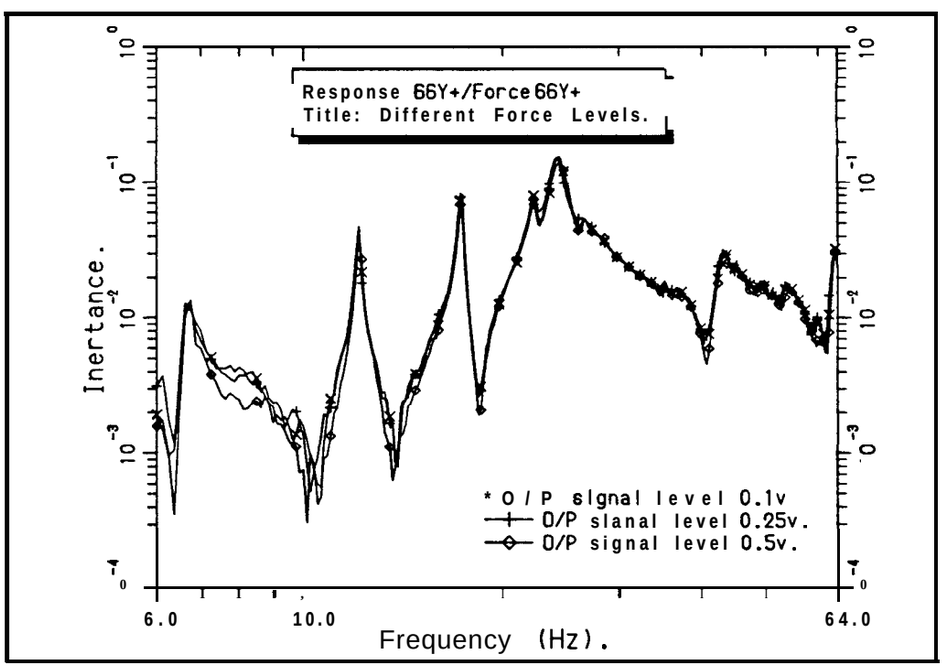

FRF Measurements for Different RMS Forcing Levels

Figure 6.4

In the preliminary measurement phase, the effect of using different excitation levels was investigated together with the repeatability of measurements. The purpose of this was to try and discover whether there were any major non-linearities and whether the structure was stable over time.

A baseband frequency range of 64 Hz was used for all these measurements which were made exciting at point 66 in the Y-coordinate direction with a 100 mm long pushrod, for excitation source levels of 0.25 v, 0.5 v, 0.1 v and then a repeat measurement at 0.25 v. The point FRFs measured are superimposed in Figure 6.4. for comparison. With reference to previous experimental work [84] and the F.E. analysis [83], the following natural frequencies (Table 6.1) can be identified;

Mode	Natural Frequency (Hz)	Description
1	6.54	Fuselage 1st lateral bending.
2	6.64	Fuselage 1 st vertical bending.
3	12.00	Tailplane 1 st vertical bending.
4	14.04	Fuselage 2nd vertical bending.
5	17.17	Tailplane 1 st F/A bending.
6	22.34	Cruciform.
7	23.93	Torsion of tailcone assembly.
8	26.21	Fuselage 3rd vertical bending.

Table 6.1

Several observations can be made from the FRFs shown in Figure 6.4;

(a) the frequency resolution (0.125 Hz) is insufficient at low frequencies, i.e. below 20 Hz;

(b) there appears to be little difference between the FRFs measured at different excitation levels; but

(c) the minimum and maximum excitation level FRFs bound all the FRFs; and

(d) there does not seem to be any shifting of the resonance frequencies with differing excitation levels.

As observations (b) to (d) are concerned with the **differences** between FRFs, it is instructive to calculate and plot the ΔFRFs. The FRF made at an excitation source level of 0.25 v is used as the reference FRF; Figure 6.5 shows the difference for 0.5 v excitation.

It should be noted that the scales for the FRF and the difference function are the same on the plot and that the difference is the magnitude of the **vector difference** between the FRFs, calculated at each frequency point. From Figure **6.5** it can be seen that the average difference across the whole frequency range is about 10% of the maximum inertance of the FRF. However, in the regions close to the resonances at 11 and 17 Hz the difference function shows sharp increases (rising to about 50% of the resonance peaks) which are indicative of slight shifts in the resonance frequencies since the magnitudes of the FRFs in the resonance regions appear to be unchanged

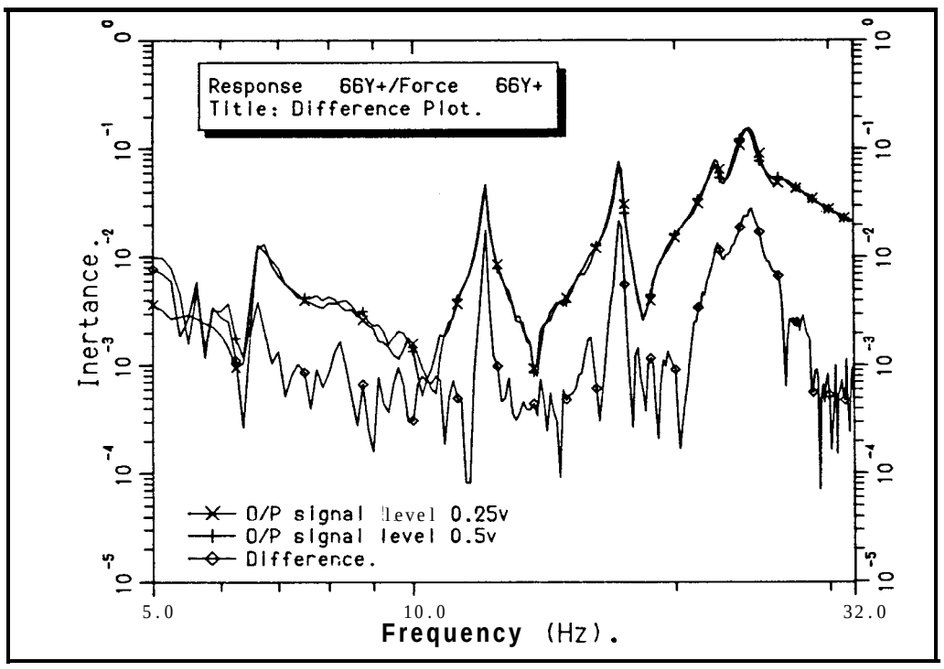

AFRF Plot for Measurements at Different Forcing Levels

Figure 6.5

The broad peak in the AFRF at around 24 Hz indicates that the difference is not only caused by a shift in resonance frequency, but that there are also differences in the magnitudes of the FRFs in this region. This **can be** seen by careful inspection of the original FRFs.

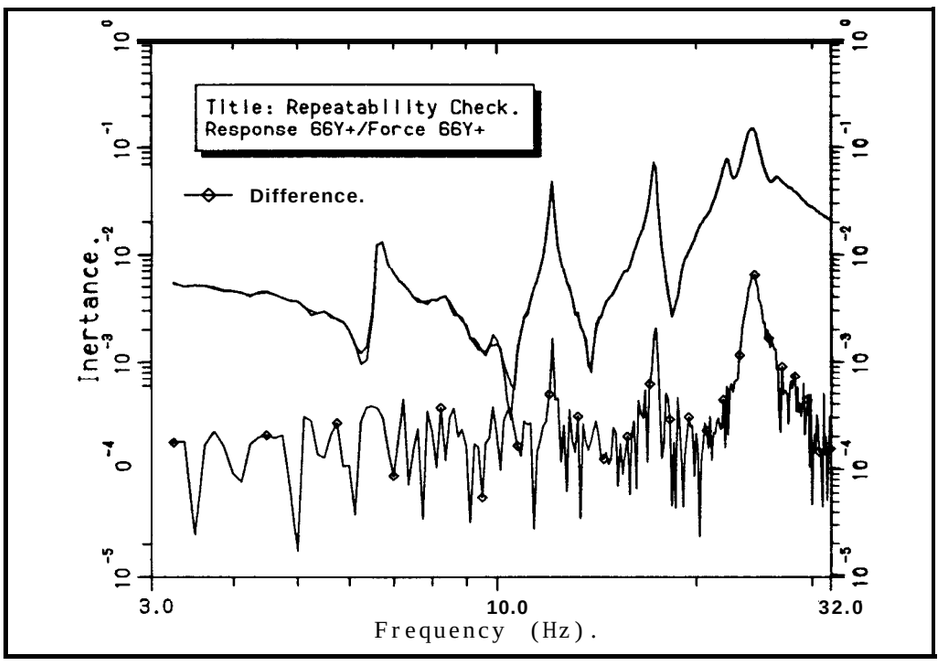

Repeatability Check with the AFRF

Figure 6.6

In Figure 6.6 the FRFs measured using nominally the same excitation source levels are compared. As would be expected, the differences are smaller than those measured with different excitation levels but there are still identifiable peaks in the difference function corresponding with the resonances. Nothing has been changed on the structure between the two measurements. The differences are caused by variation of the structure with time. There is little that can be done to improve this aspect of testing.

(ii) Reciprocity Checks

One of the reciprocity checks is shown in Figure 6.7, comparing FRFs R49Z+/F66Y- and R66Y+/F49Z-: measurements between different points and in different coordinate directions. Once again, the measurements suffer from insufficient frequency resolution at the the low frequency region and this could have some bearing on the poor results around 6.5 Hz. The reciprocity looks good for the mode at about 11 Hz, but there is obviously a frequency shift of the 17 Hz mode which is clearly indicated by the difference function. The FRFs themselves do not show that there is also a frequency shift for the 11 Hz mode, but this is shown by the difference function.

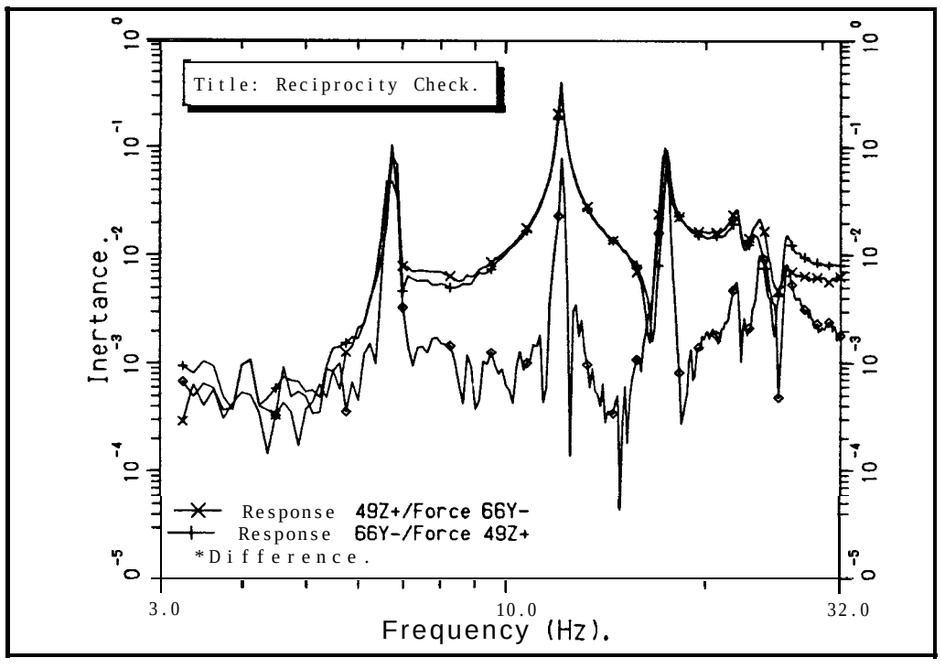

Reciprocity Check with the AFRF

Figure 6.7

It will be seen later that the poor reciprocity between coordinates 49Z and 66Y in the region of the 11 and 17 Hz modes is a result of shaker loading effects on the structure at point 49. The inconsistent loading was brought about as a consequence of space limitations which necessitated the use of a 20 mm pushrod for excitation in the Z-direction at point 49, rather than the 100 mm pushrod used elsewhere.

(iii) Definition of Frequency Range and Frequency Resolution

It has already been mentioned (in (i)) that the baseband measurements up to 64 Hz (using 512 lines; resolution 0.125 Hz) had insufficient frequency resolution for definition of the low frequency modes. It was decided that doubling the resolution, to 0.0625 Hz (a 32 Hz baseband measurement), would be adequate to define all the FRF terms for analysis of the high frequency modes and for the purposes of estimating high frequency residual terms. Baseband measurements to 16 Hz and 8 Hz with frequency spacings of 0.03125 Hz and 0.015625 Hz respectively, will be used to define specific FRFs in sufficient detail for modal analysis of the low frequency modes.

6.3.2 Full Measurement Survey for Translational Degrees-of-Freedom

It was intended that the complete FRF matrix shown in Figure 6.8 should be measured in the full survey, despite the fact that modal analysis only requires a minimum of one row or column to identify fully the modes tested. However, it is usual to measure more FRFs than the minimum set required to ensure that none of the modes has been missed by poor choice of excitation location. Measurement of the complete matrix, or even just the upper triangle, is excessive from the modal analysis point of view, but it is vital if a full set of residual terms are to be calculated from comparison of synthesised and measured data. Residual terms cannot be calculated for the whole matrix through knowledge of only one row or column.

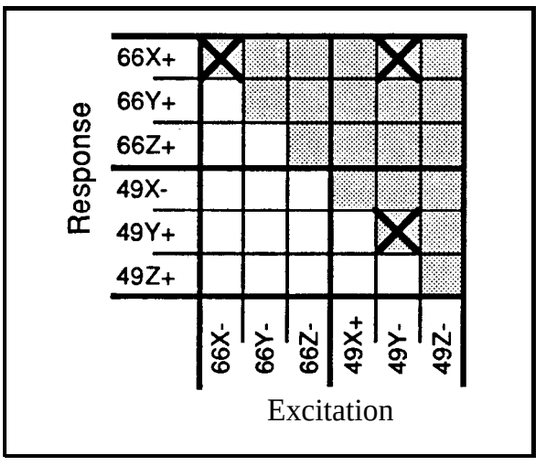

FRF Matrix Representation for the Helicopter Case Study

Figure 6.8

At the start of the full survey, six accelerometers were bolted to triaxial mounting blocks already attached to the structure and none of the accelerometers was moved throughout the tests. A single force gauge was moved to each excitation coordinate in turn. For the majority of measurements a pushrod 100 mm in length was used, except for excitation at point 49 in the Z direction where, because of space limitations, it was necessary to use a pushrod only 20 mm long.

Several difficulties with the excitation arrangements soon became apparent;

(i) point 66 is located on the side of the intermediate gearbox which is usually concealed beneath fuselage fairings. This made excitation at point 66 in the X-direction (66X) very awkward and, additionally, excitation in the Z-direction could only be achieved by using a short extension tube added on to the pushrod; and,

(ii) point 49 is located on the leading edge of the tail-plane at mid-span. Excitation in the Y direction (along the leading edge of the tailplane) was only possible with the aid of a **pushrod** extension of about 1 m length. There was a resonance of this extended **pushrod** arrangement within the 32 Hz measurement band and the resulting **FRFs** were all rather poor, with generally low coherence levels.

As a result, measurements involving excitation at either 66X or 49Y were abandoned for the initial phases of this study. As a consequence of this, it was not possible to obtain measured **FRFs** for the 3 elements marked with an 'X' in the upper triangle of the matrix shown in Figure 6.8 and, hence, residual terms for these elements of the matrix could not be derived by comparison of **measured** and synthesised functions.

Excitation in the Y-direction at point 66 produced a set of **FRFs** in which all the modes were reasonably well defined and hence 66Y was chosen as the reference **degree-of-freedom** for the set of **FRFs** to be used in the modal analysis procedures. The shaker was returned to coordinate **66Y,** and measurements for all of the 6 response positions were performed four times using baseband measurements to **8, 16, 32** and 64 Hz. Point **FRFs** for coordinate **66Y,** for all the four frequency ranges, can be seen in Figures 6.9 to 6.12.

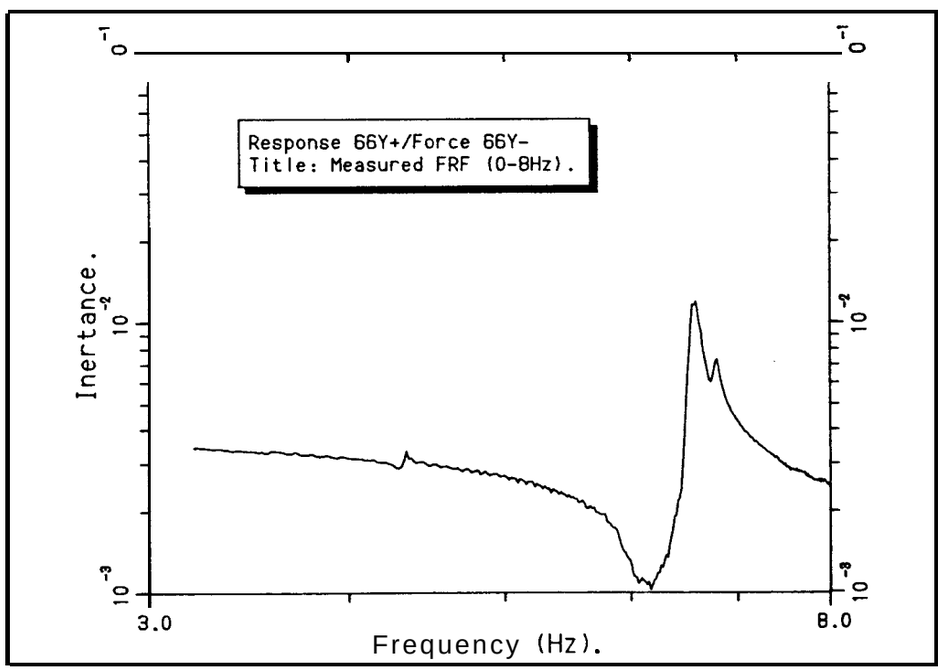

Figure 6.9

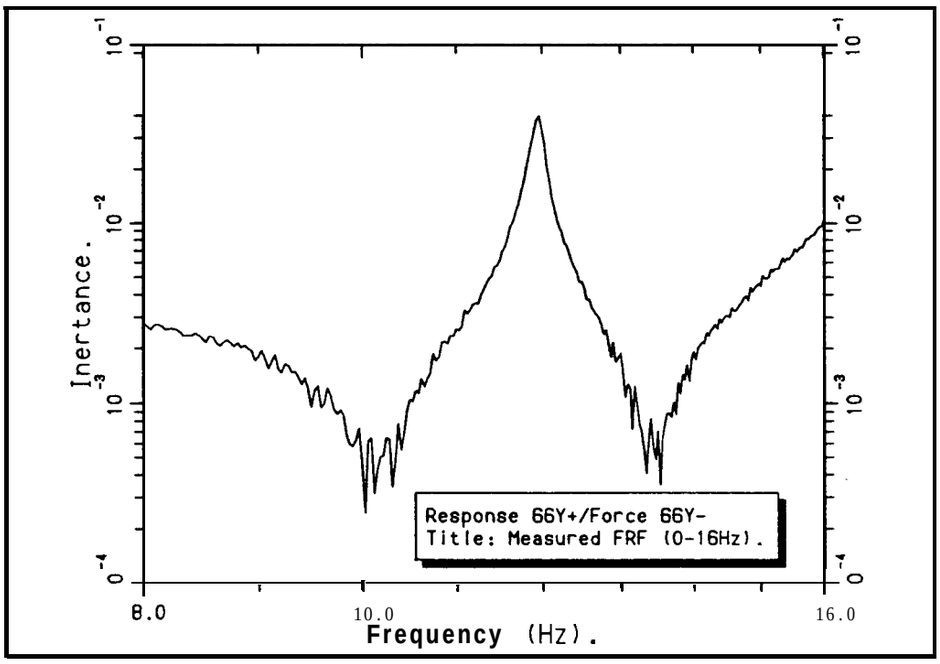

Figure 6.10

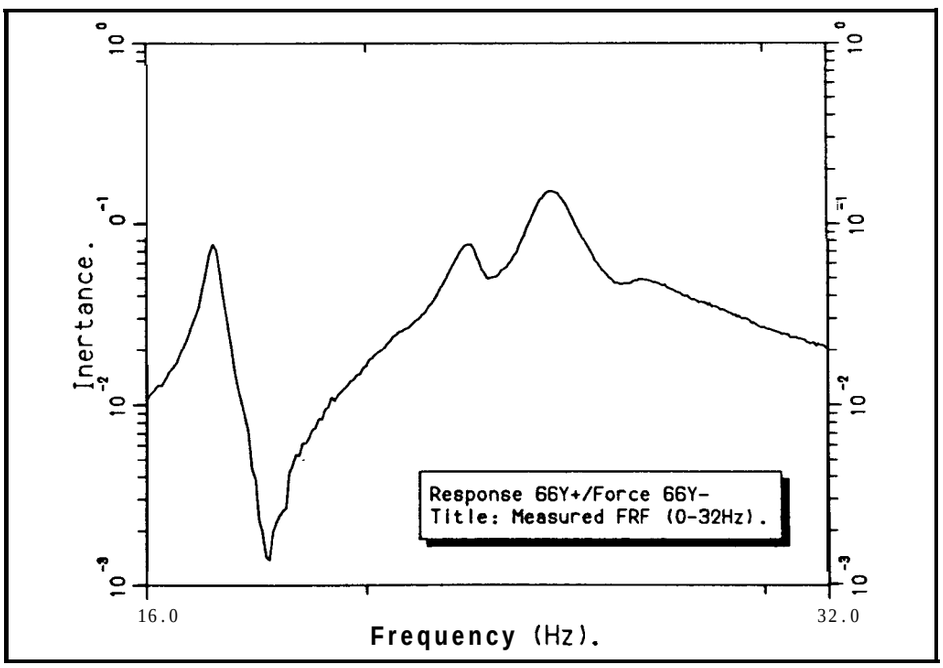

Figure 6.11

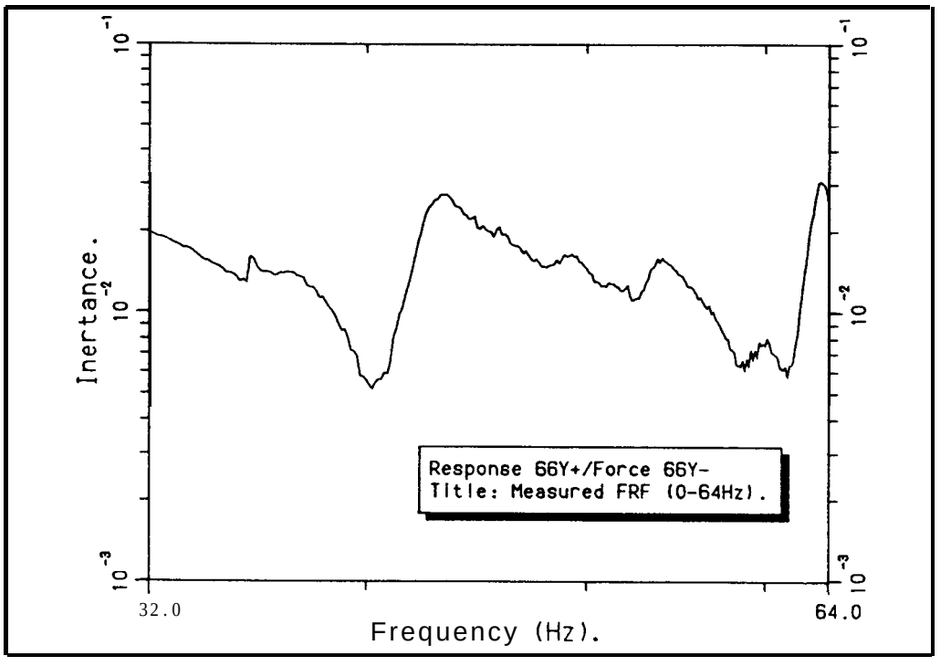

Figure 6.12

6.3.3 Excitation at an Angle to the Coordinate Axes

Although the point FRFs for excitation at 49Y and 66X could not be measured easily by direct means, it was thought that it might be possible to derive them from additional measured data made with the excitation direction inclined to the coordinate axes. The following simple example shows how this can be done; the full analysis to produce FRFs in the coordinate axes from such measurements is given in Appendix C. Satisfactory results proved to be difficult to obtain when experimentally measured input data were used.

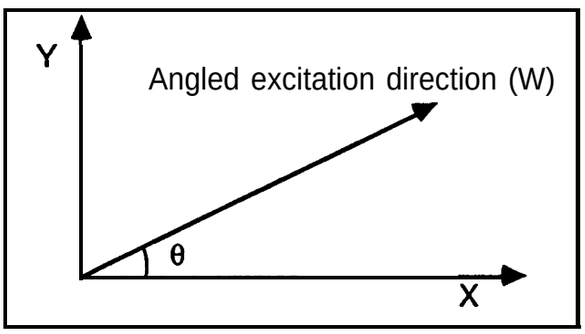

Definition of Axes for Angled Excitation.

Figure 6.13

For example, referring to Figure 6.13, assume that it is not possible to excite in the X-direction and that normal FRFs have already been obtained for excitation in the Y-direction. For angled excitation tests, the force is measured in the direction W and the responses are measured in the X- and Y- coordinate directions. FRFs produced from these measurements are Y/W and X/W. Now, combining these angled excitation FRFs together with the normal X/Y FRF it is possible to derive Y/Y and X./X FRFs (Appendix C). The Y/Y FRF, which, it is assumed, has already been measured in the normal way is available for comparison with the derived Y/Y FRF.

(i) Excitation at Point 66

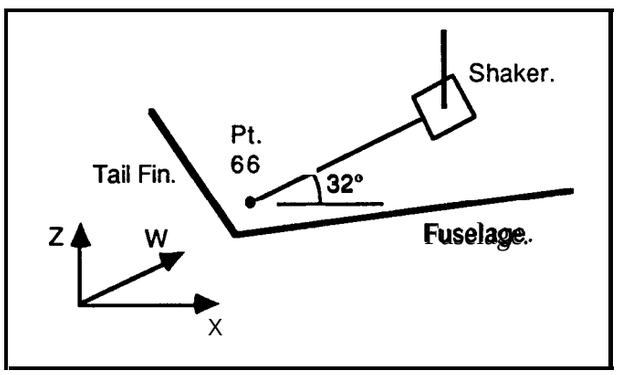

Schematic View of Angled Excitation at Point 66.

Figure 6.14

The shaker was set up as shown in Figure 6.14, with the forcing direction at an angle of 32° to the X-axis. Even with the shaker in this position, it was necessary to use a 200 mm pushrod extension tube with a 20 mm pushrod to gain access and to avoid resonances of the pushrod arrangement in the measurement frequency band. The excitation force was measured in the direction of the excitation (W) and the responses were measured in the X, Y and Z coordinate directions, as before.

Movement of the shaker during these tests was found to be more of a problem than it had been before. The reason for this was that since the shaker had been rotated in its gimbals, the centre of gravity of the shaker and reaction mass arrangement was now no longer in line with the excitation axis. This resulted in quite severe rocking of the shaker on its suspension, particularly at low frequencies.

Results for Point 66

Point FRF results for coordinate 662 are presented in Figure 6.15. There are 3 functions superimposed on this plot; the point FRF measured directly, the point FRF derived from angled forcing and the vector difference between these two FRFs. Over the range 3.2 to 11 Hz, the derived FRF compares favourably with the FRF measured directly, although there are differences in the location of the first anti-resonance. Above 11 Hz, the derived result is not particularly good compared with the FRF measured directly; the difference function often being of the same magnitude as the FRF itself. Assuming this poor correlation also extends to the derived point FRF for 66X (Figure 6.16), for which there is no measured FRF for direct comparison, the derived FRF will be of little use in any modal analysis procedure.

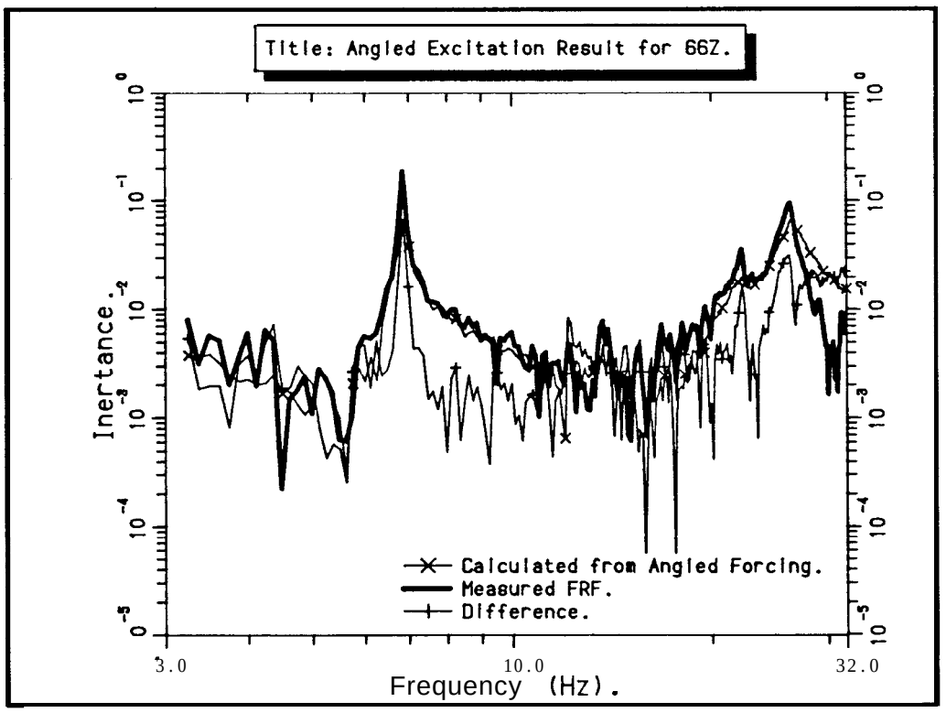

Angled Excitation Result for Coordinate 662

Figure 6.15

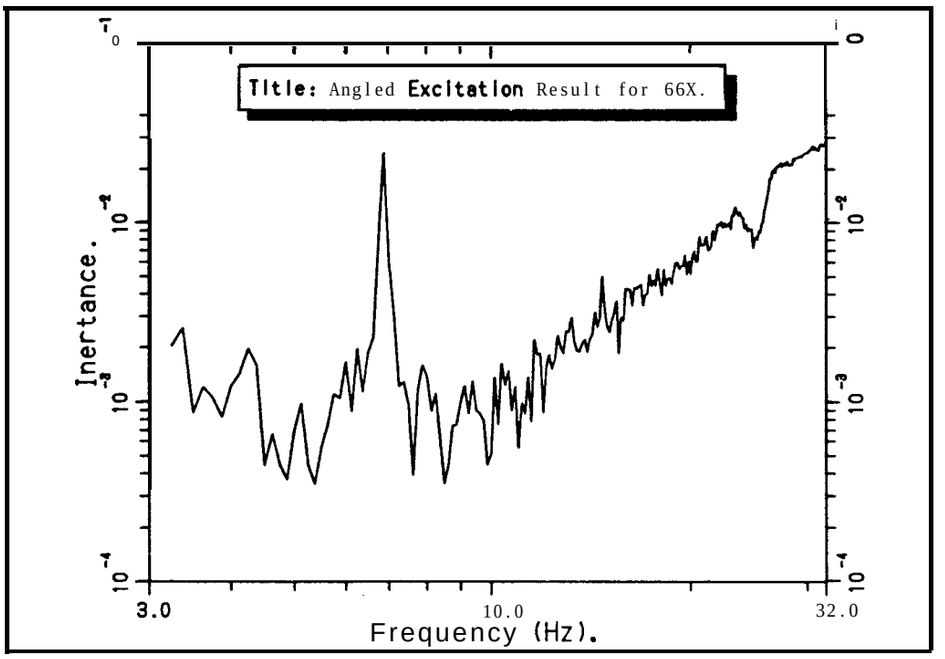

Angled Excitation Result for Coordinate 66X

Figure 6.16

(ii) Excitation at Point 49

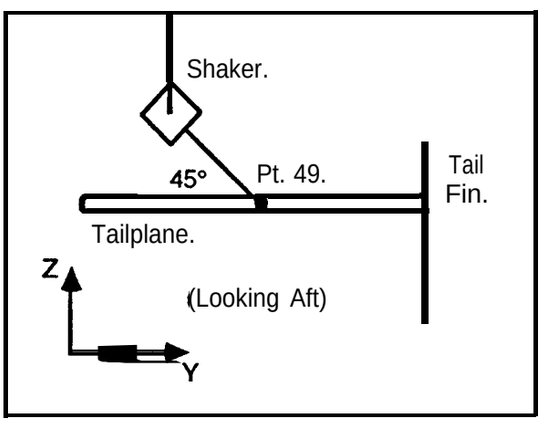

Schematic View of Angled Excitation at Point 49.

Figure 6.17

Similar measurements were made at point 49, except that here the excitation angle was 45° (Figure 6.17) and it was only necessary to use a pushrod extension tube of 90 mm on the 20 mm pushrod to gain access.

Results for Point 49

(a) 49Z

The results for coordinate 49Z are presented in Figure 6.18 in the same format as used previously for 66Z. This time, however, the level of agreement between the measured and derived FRFs is generally much better, exhibiting a similar level of agreement to that found for the reciprocity. In comparing the measured and derived FRFs, the positioning of the anti-resonances between modes 2 and 3 is the most obvious discrepancy. Furthermore, the difference function shows that there are large discrepancies at the resonance frequencies. It would not seem unreasonable to expect the derived point FRF for 49Y (Figure 6.19) to be equally as good as that for coordinate 492, in which case it could be used quite successfully in a modal analysis procedure.

The peaks in the difference function at the resonances are, once again, indicative of resonance frequency shifts caused by the shaker system loading the structure differently for each of the measurements involved. It has already been noted that point 49 is particularly sensitive to shaker loading in the X and Z directions.

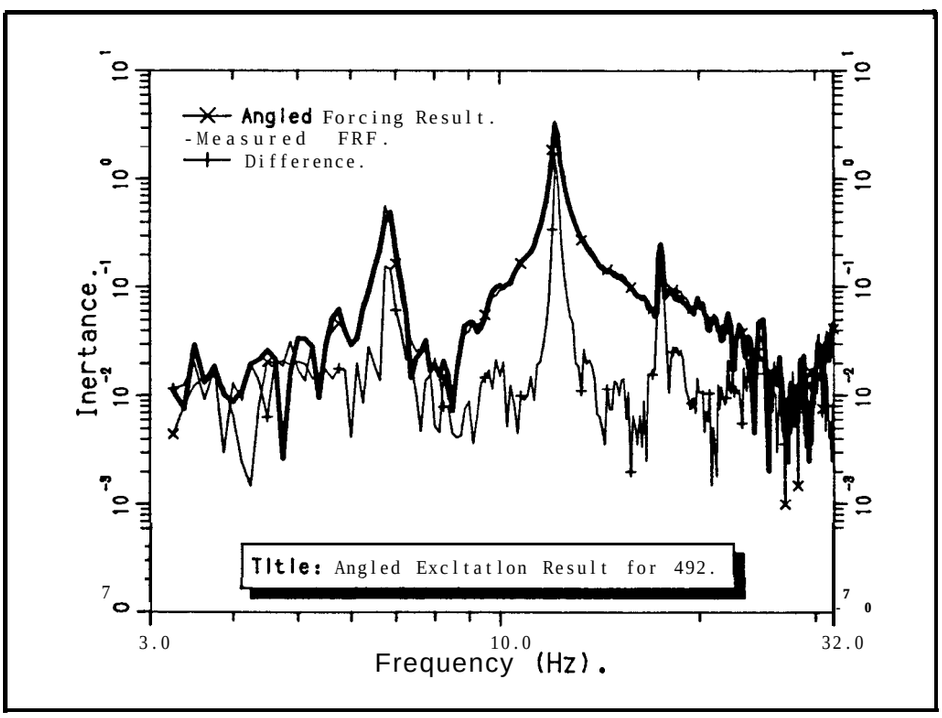

Figure 6.18

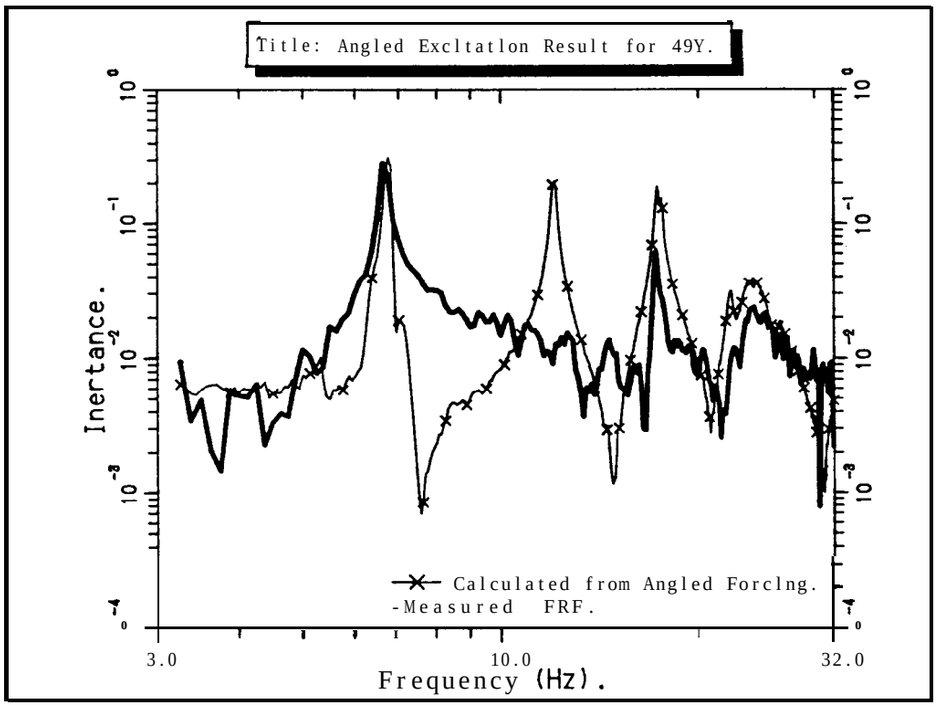

Figure 6.19

(b) 49Y

The derived point FRF for 49Y has been plotted, Figure 6.19, together with the original point FRF for 49Y measured using a 1 m pushrod extension tube. Here, the quality of the measured FRF is inferior to that of the derived FRF. The resonance at about 11 Hz is not shown on the measured FRF, whereas it can be seen clearly on the derived FRF. The use of the derived FRF could prove to be beneficial in this case.

6.3.4 Comments on the Use of the Angled Excitation Technique

These examples of the angled excitation technique show considerable variability in the results. The probable cause of the poor quality results for point 66 is that the FRF for response in the X-direction (along the fore-aft axis of the helicopter) due to excitation in the Z-direction (vertical axis) is used in the calculation. The responses measured along the fore-aft axis of the helicopter at point 66 have all been very small and difficult to measure accurately. This is probably due to the fact that the X-direction axis passes through both the helicopter centre of gravity and point 66 and that the axial stiffness of the fuselage is significantly larger than its flexural or torsional stiffness.

The angled excitation results for point 49 are very much better than those for point 66. Point 49 is located on a more mobile part of the helicopter and the measured FRFs used in the angled excitation calculations are of a higher quality than those for point 66.

In general, by use of the angled excitation technique it is possible to derive FRFs which cannot be measured directly due to difficulties of access for excitation. The technique appears to work best for points on a mobile part of the structure where the FRF has pronounced modal characteristics. The FRFs are derived using raw measured data which include all the effects of out-of-range modes. Therefore, in theory, the derived FRFs should also contain all the relevant information about out-of-range modes and this is the primary reason for using this form of the data since comparison of a synthesised FRF with its derived counterpart enables calculation of residual correction factors for the synthesised FRF. This is of particular importance for point FRFs because these FRFs usually require the largest residual corrections (see chapter 5).

6.4 Measurement of Rotational Degrees-of-Freedom

The need for measurement of rotational degree-of-freedom FRF properties has been discussed in chapter 5, where the possible consequences of their omission from a coupling analysis are illustrated. One objective of this case study is a demonstration of the ability to predict accurately the effects of a modification. Therefore, to have the best possible chance of success in the prediction, it is necessary to measure the rotational degree-of-freedom FRF properties. Once they have been measured in a preliminary survey, the sensitivity analysis study will reveal whether or not they are of particular importance and warrant more extensive investigation in the full measurement survey.

Attempts have been made to measure these rotational degree-of-freedom FRF properties using the T-block method described in chapter 5 and in references [9] and [81]. The dimensions of the T-block and its mass properties are given in Appendix D. Initially, the measurements were made to enable calculation of θ_X and θ_Z at point 66 but, subsequently, the procedure was repeated for θ_Y at point 49 also.

6.4.1 Measurements at Point 66

The results for θ_X and θ_Z at point 66 are very similar and, therefore, only those for θ_X will be described in detail in this section.

The translational FRF data measured on the T-block were assessed for quality in the same way as the standard translational FRF data have been; by repeatability and reciprocity checks. A typical repeatability check is shown in Figure 6.20. The two FRF measurements were made on different days and the T-block was removed and the transducers stripped off between measurements. The AFRF has been calculated and is plotted together with the FRF curves. On the whole, the repeatability is good with an average difference of about 10% across the complete frequency range. Once again there are slight frequency shifts of the 11 and 17 Hz modes which give rise to the sharp peaks in the difference function at these frequencies.

A typical reciprocity check for the translational FRF measurements on the T-block is shown in Figure 6.21. The reciprocity is very good: there are the sharp peaks in the difference function at the resonance frequencies, but elsewhere the differences are approaching the noise floor for the measurements.

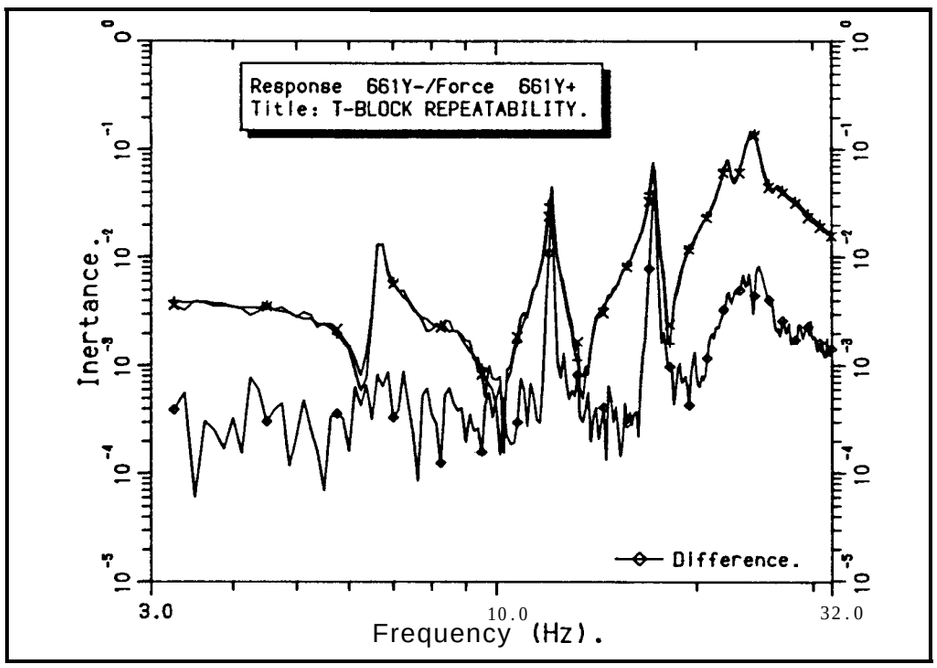

Repeatability Measurements on the T-Block

Figure 6.20

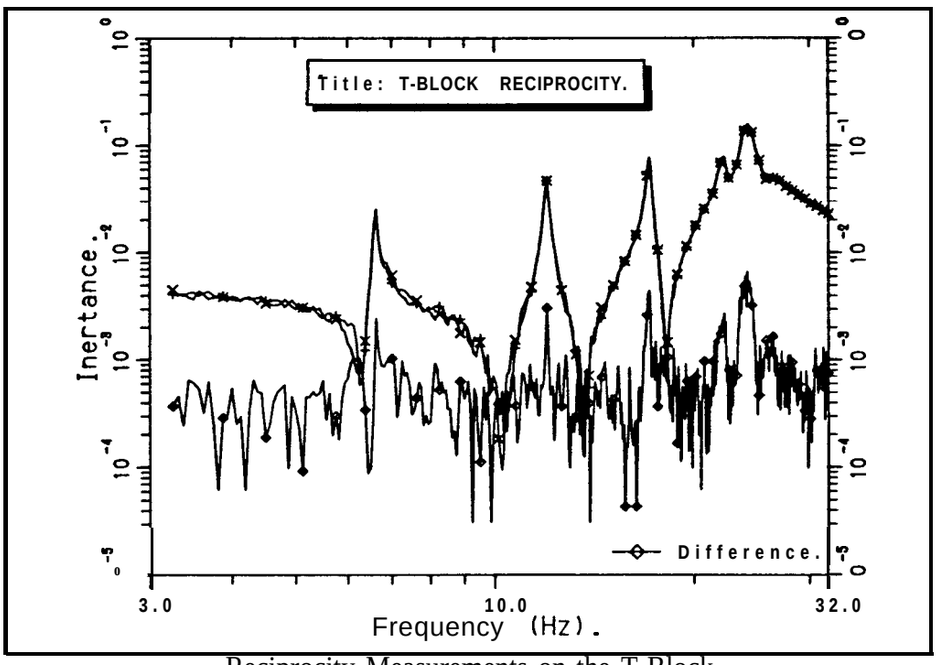

Reciprocity Measurements on the T-Block

Figure 6.21

Results for Point 66

Transformation of the measured T-block translational FRF data set, as described in chapter 5 (section **5.2.1),** produces the following rotational FRF data set for the point of attachment of the T-block to the structure:-

(i) **Translation/Translation** FRF Results

The translation/translation FRF from the transformation can be seen in Figure 6.22, along with the same FRF that was measured directly. There is good agreement between the two **FRFs,** especially considering that they were measured on different days and by different methods. However, the transformation to obtain this FRF is essentially an averaging of the **FRFs** measured on the T-block,

$$\frac{1}{a}\left(\frac{R_1}{F_1}+\frac{R_2}{F_1}+\frac{R_1}{F_2}+\frac{R_2}{F_2}\right)$$

Any slight discrepancies, such as those found in the reciprocity and repeatability checks, are averaged out.

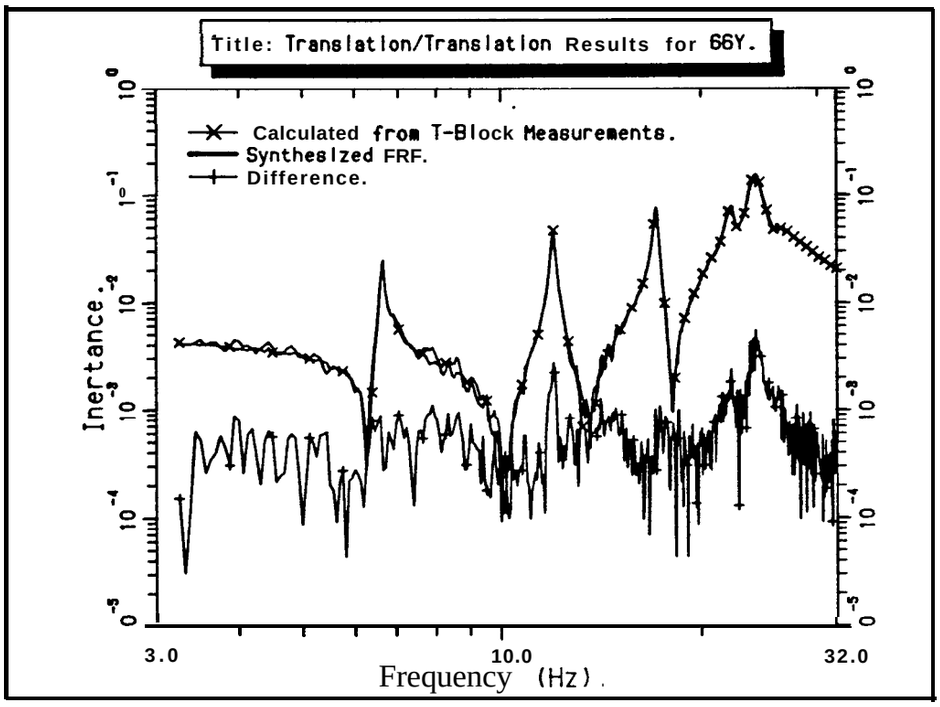

Translation/Translation Results for Coordinate 66Y

Figure 6.22

(ii) Translation/Rotation and (iii) Rotation/Translation FRF Results

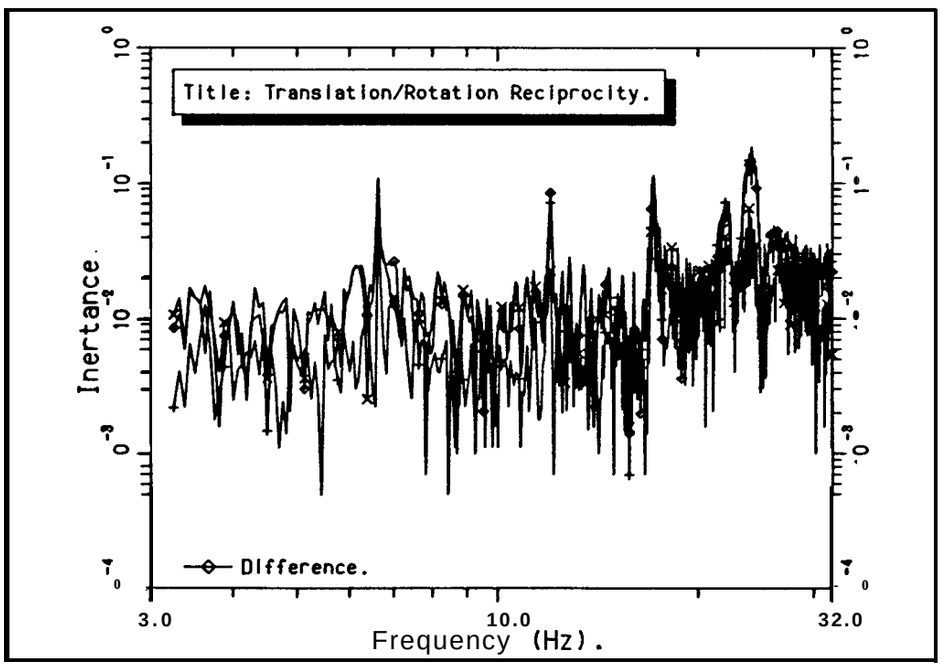

Reciprocity of Translation:Rotation FRFs

Figure 6.23

These two, supposedly, reciprocal translation:rotation FRFs are shown in Figure 6.23. The difference function is also plotted, but it is difficult to distinguish. The results are very poor; they are so noisy that the resonance peaks are almost lost; there are no clear anti-resonance features. Overall, the reciprocity is very bad – the magnitude of the difference is almost the same as the magnitudes of the FRFs themselves throughout the whole frequency range.

For these FRFs, the calculation formula is:-

$$\frac{1}{4S}\left[\left(\frac{R_1}{F_1} - \frac{R_2}{F_2}\right) + \left(\frac{R_1}{F_2} - \frac{R_2}{F_1}\right)\right]$$

where, S = separation of points on the block.

$\frac{R_1}{F_2}$ and $\frac{R_2}{F_1}$ are reciprocal terms whose reciprocity has been checked (Figure 6.21). The difference function in Figure 6.21 plot essentially gives the value of $\left(\frac{R_1}{F_2} - \frac{R_2}{F_1}\right)$.

$\frac{R_1}{F_1}$ and $\frac{R_2}{F_2}$ are the point FRFs on the T-block and they are shown with their difference in Figure 6.24 below.

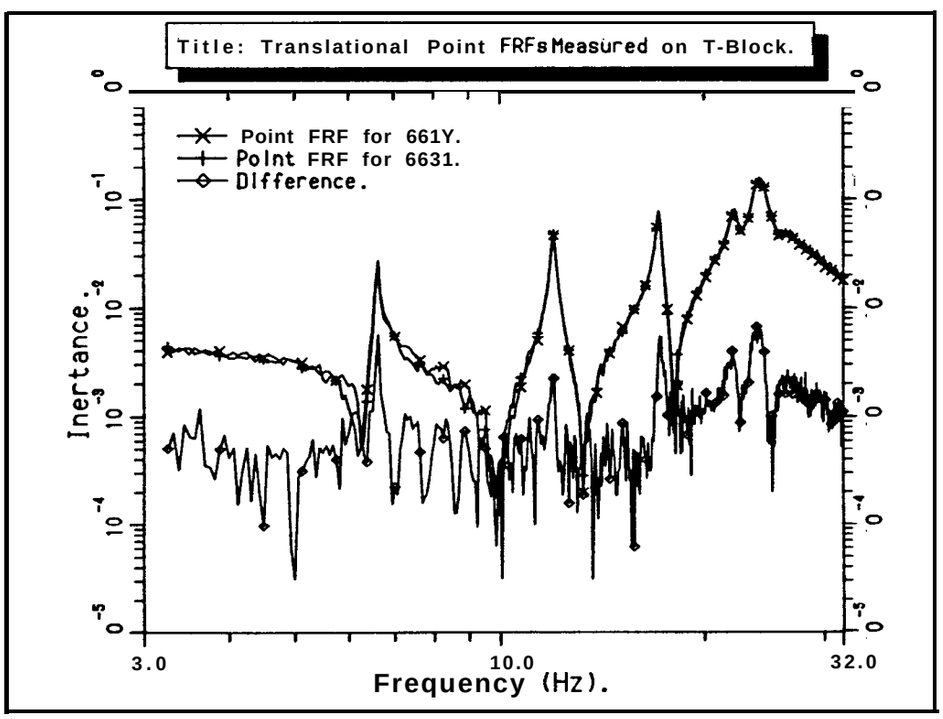

Translational Point FRFs Measured on T-Block

Figure 6.24

It will be noted that the difference functions of Figures 6.21 and 6.24 are largely noise, each with a similar mean value. The translation/rotation FRF of Figure 6.23 is given by a scaled average of these two difference functions (Figures 6.21 and 6.24), and it is now not too difficult to see why the translation/rotation FRF is so poor. The primary cause is calculation of the small difference between two large numbers which have come directly from measurements. The calculation is essentially the average of two differences.

(iv) Rotation/Rotation FRF Results

The formula for calculation of the rotation/rotation FRF can be expressed simply as:-

$$\frac{1}{4S^2}\left[\left(\frac{R_1}{F_1}+\frac{R_2}{F_2}\right)-\left(\frac{R_1}{F_2}+\frac{R_2}{F_1}\right)\right]$$

In this formula the inner terms are the sum of the point FRFs and the sum of the reciprocal FRFs respectively; shown in Figure 6.25. Each of these terms is smoother than its constituent parts. The rotation/rotation FRF is essentially the scaled difference of these two sums.

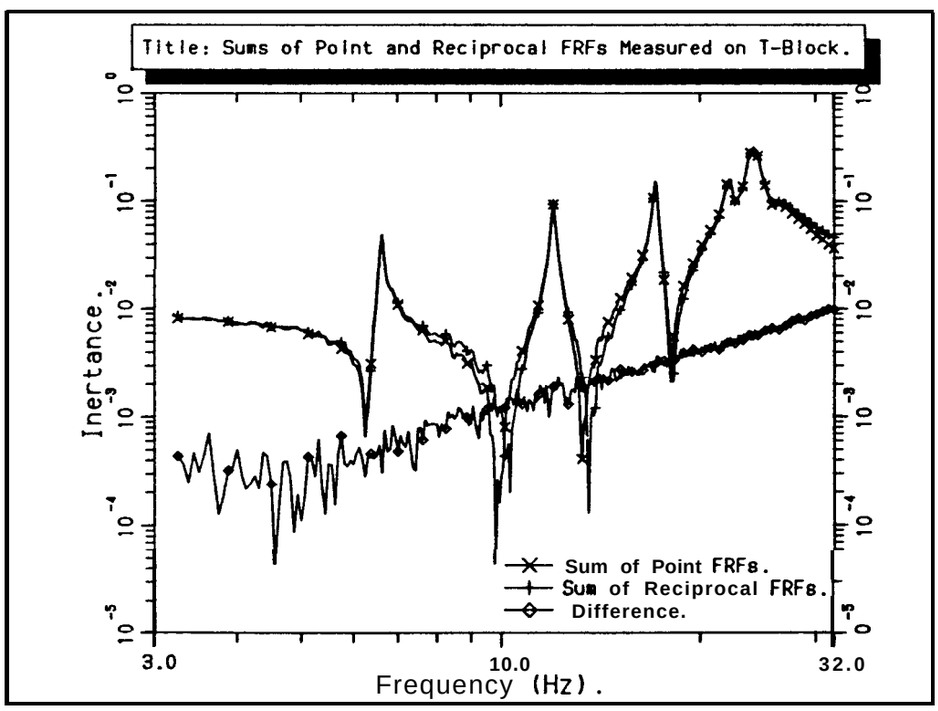

Sums of Point & Reciprocal FRFs Measured on the T-Block

Figure 6.25

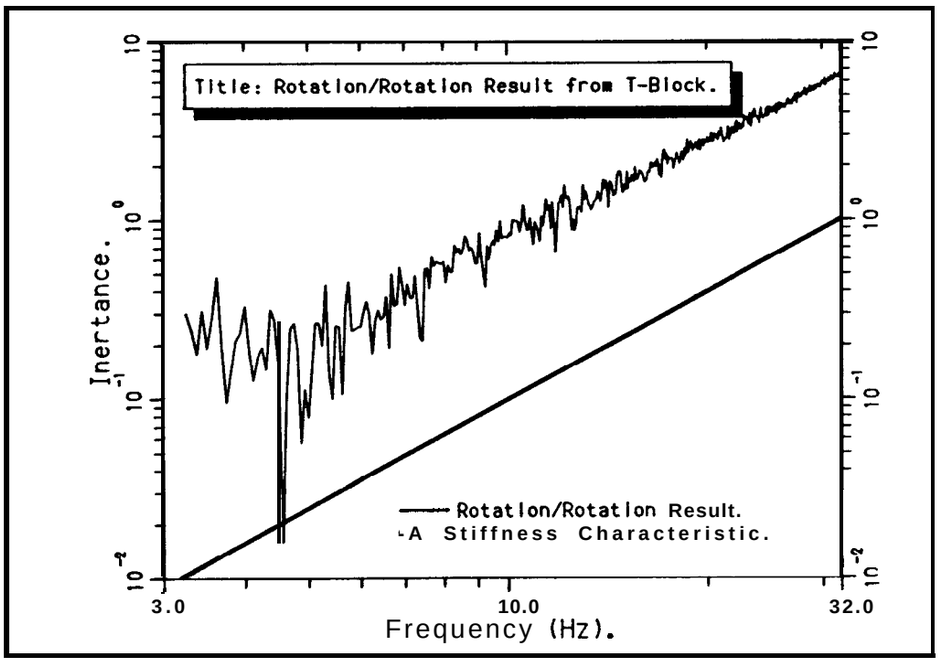

Rotation/Rotation FRF Derived from T-Block Measurements

Figure 6.26

The θ_X rotation/rotation FRF shown in Figure 6.26 has a surprising characteristic – that of a straight line. There is very little 'noise' and there are no resonance or anti-resonance features. The line has a slope of +2 on a log-log plot of inertance, which means that it is a stiffness line – indicating a pure torsion spring. There is no detectable modal behaviour. By using the information from a point on this line, the torsional stiffness represented by this FRF was calculated as 6.18E3 Nm/rad.

When the translational FRF measurements for θ_Z were transformed to the rotational set, the results were found to be similar to those for θ_X above but, the rotation/rotation results were **identical** to those for θ_X, another perfect straight line of slope +2; a torsional stiffness of 6.18E3 Nm/rad, again.

These results indicated that the rotation/rotation properties derived using the T-block at point 66 on the helicopter had **no** modal characteristics and were independent of the orientation of the T-block (θ_X or θ_Z). Because such characteristics are highly unlikely for the helicopter, it was strongly suspected that what had been measured was the attachment stiffness of the T-block to the helicopter. In comparison with the local stiffness of the helicopter, the attachment stiffness was small and would have to have been increased very substantially before the true rotational behaviour could be measured accurately. Similar measurements were made at point 49, for the θ_Y rotational properties, in the hope that the local stiffness at this point would be low enough for the T-block attachment stiffness to be

adequate for transmission of the structural motion. Unfortunately the T-block attachment stiffness was again insufficient and poor results were obtained.

At this stage it was decided that, to avoid the need for rotational FRF data and to save a considerable amount of time and effort, any subsequent modifications to be made to the helicopter would have to be pin-jointed. This simplification is often made implicitly when measurement of the rotational FRF properties is not even considered, or just overlooked. Furthermore, the discussion presented in section 5.2.1 has exposed some fundamental discrepancies between the assumptions made in the theory and in the practice of coupling rotational degrees-of-freedom.

6.4.2 Bedplate Measurement

To confirm the suspicion that the T-block attachment stiffness had been measured, the T-block was moved to a large bed-plate and bolted down in a similar way to that used to fix it to the helicopter. Translational measurements were made on the T-block and then transformed to form the rotational set. The rotation/rotation FRF again had a perfect stiffness line characteristic, but this time it had a value of 7.18E3 Nm/rad, slightly higher than that measured on the helicopter. A smaller attachment stiffness on the helicopter can be explained by the fact that the T-block is bolted to an excitation block which is stuck to the helicopter with 'Plastic Padding' whereas the T-block is bolted to the bedplate directly. The Plastic Padding interface is the source of the extra flexibility measured.

Further confirmation that the rotational stiffness measured was, in fact, the attachment stiffness of the T-block was provided by some theoretical calculations of this stiffness; Appendix E. Although the theoretical rotational stiffness does not agree exactly with that measured, it is of the right order and the discrepancies can be accounted for by some of the assumptions made regarding key dimensions and material properties used in the analysis.

6.4.3 Discussion of the Measurement of Rotational Degrees-of-Freedom

(i) T-Block Transducer

The results obtained here demonstrate clearly the difficulties associated with measurement of rotational degree-of-freedom FRFs using the T-block transducer method. The main

problem was attaching the transducer to the structure with sufficient rigidity that the behaviour of the structure could be correctly detected by the transducer.

(ii) Cross-Axis Sensitivity of Transducers

The influence of accelerometer cross-axis sensitivities on the rotational FRF results derived from T-block measurements has already been discussed in chapter 5. It was suggested that the cross-axis effects could be minimised by careful angular orientation of the accelerometers, but this is not always possible. In this instance, the triaxial accelerometer blocks and the T-block were all pre-drilled to accept the accelerometers aligned with the coordinate directions. With accelerometers having a threaded base and attached to the structure with a stud, specific angular orientation can only be obtained by insertion of spacing shims of the correct thickness underneath the bases of the accelerometers: precise angular alignment is difficult to achieve.

(iii) Use of Synthesised FRFs

All the calculations made here to determine the rotational degree-of-freedom FRFs have used the raw measured translational FRFs. It has been suggested [25] that 'smoothed FRFs' or FRFs synthesised from a modal database would be better. This would necessitate a modal analysis of the measured data first and, although the synthesised FRFs are noise-free, they may not contain all the important information inherent in the measured FRFs, e.g. exact residual information. It is important to remember that the synthesised FRFs can only represent, at best, what has been measured by the transducers; any attachment flexibility effects will be included in the synthesised FRFs, just as they are included in the measured FRFs. There is no way of differentiating between the component of the response caused by the base structure and that caused by the attachment flexibility. Therefore, the use of synthesised FRFs in these calculations may have resulted in smooth well-defined rotational degree-of-freedom FRFs, but it is doubtful whether the underlying characteristics would have changed significantly.

6.5 Modal Analysis of the Translational FRF Data Set

A SDRC program – Modal Plus, implemented on the Gen-Rad 2515 – was used for Modal Analysis of the measured translational FRF data set.

6.5.1 Polyreference Analysis

Four different force input locations have been used, one at a time, for the 32 Hz and 64 Hz baseband measurements; i.e. a series of single-point tests have been performed rather than one multi-point test. The use of multiple single point tests has led to some inconsistencies in the measured data due to different loading effects of the excitation system on the helicopter at each of the forcing locations. For 8 Hz and 16 Hz baseband measurements, F'RF data are available for only one forcing location, 66Y.

The Polyreference analysis method has been used over the 8 and 16 Hz baseband frequency ranges with a single reference location – equivalent to a Complex Exponential analysis. For the 32 and 64 Hz baseband data, two out of the four reference locations have been chosen for the analysis; 66Y and 492. The reference locations are at different points on the helicopter and in different coordinate directions.

In this analysis a total of 11 modes were extracted from the 64 Hz baseband frequency measurements. There are two close modes at around 6.5 Hz which proved to be quite difficult to separate, requiring the highest frequency resolution data to achieve reasonable results. Another problem which compounds the situation is that the second of the two close modes has a damping value of about 0.3%, less than half that of the first mode (-0.7%). Above 32 Hz the modes are generally more highly damped, less well defined and consequently more troublesome to analyse than those in the frequency range of interest (3.2 to 32 Hz). Since the modes above 32 Hz are only used to account for high frequency residual terms in the frequency range of interest, the exact values of the parameters are not of prime importance as long as the overall residual effects are correct. The parameter and mode shape data are presented in Tables 6.2 and 6.3.

Throughout the modal analysis process, analytical FRFs were generated and compared with measured FRFs in the resonance regions. The quality of the analysis was assessed by the level of agreement between the analytical and the measured FRFs. This was judged by eye. In the off-resonance regions, there can be large discrepancies because, at this stage, no account has been made for the effects of out-of-range modes. The reliability of the results was checked by performing the complex exponential analysis for several slightly different narrow frequency bands around each of the resonance peaks, with different numbers of roots in each of the analyses. If the answers for the non-computational roots (frequencies) were within 1 or 2% for each analysis and the damping, mode coefficient [78] and phase compared favourably, then the results were taken as acceptable estimates.

Label	Frequency	Damping	Amplitude	Phase	Ref.	Res.
1	6.57	.009	3.12E-3	1.571	66Y-	66Z+
2	6.74	.003	2.58E-3	-1.571	66Y-	66Z+
3	11.92	.006	9.06E-3	1.571	66Y-	66Z+
4	17.06	.006	1.16E-2	1.571	66Y-	66Z+
5	22.17	.017	1.49E-2	-1.571	66Y-	66Z+
6	24.08	.021	1.01E-2	1.571	66Y-	66Z+
7	26.24	.015	9.70E-2	-1.571	66Y-	66Z+
8	42.47	.025	1.62E-2	-1.571	66Y-	66X+
9	51.14	.045	2.19E-2	-1.571	66Y-	66X+
10	52.26	.018	4.72E-2	1.571	66Y-	66X+
11	53.58	.035	0.11	-1.571	66Y-	66X+

Mode Parameter Table. Table 6.2

Mode	Location	X Coeff.	Y Coeff.	Z Coeff.
1	49	2.214E-2	-5.431 E-2	5.308E-2
	66	7.557E-4	-1.055E-2	8.355E-3
2	49	1.690E-2	-7.201 E-3	-3.495E-2
	66	2.783E-3	-1.453E-3	-1.834E-2
3	49	1.440E-1	-1.200E-2	-3.752E-1
	66	3.492E-3	-3.706E-2	2.101E-2
4	49	-6.714E-1	-8.483E-2	-9.969E-2
	66	9.016E-4	-8.416E-2	1.908E-2
5	49	3.862E-2	2.264E-2	5.890E-3
	66	3.043E-3	-4.862E-2	-6.448E-3
6	49	7.172E-2	5.139E-2	1.353E-2
	66	1.568E-2	-1.468E-1	3.199E-3
7	49	-2.657E-2	-2.649E-3	1.212E-2
	66	-3.042E-3	-1.412E-2	-3.766E-2
8	49	2.435E-2	3.660E-2	-4.833E-2
	66	-2.417E-3	-1.838E-2	-8.348E-4
9	49	2.260E-3	2.029E-3	2.385E-2
	66	-1.526E-3	-2.738E-3	-1.164E-3
10	49	-5.023E-3	-1.281 E-2	-4.158E-2
	66	8.094E-3	4.200E-3	-2.601 E-3
11	49	4.066E-3	1.263E-2	4.541 E-2
	66	-9.594E-3	6.541 E-4	4.148E-3

Mode Shape Table. Table 6.3

6.5.2 Synthesis of FRFs from the Modal Database

The modal database generated by the method described above was used to synthesise all the FRFs in the upper triangle of the FRF matrix (Figure 6.8), over the 32 Hz baseband frequency range. The primary purpose of this was validation of the modal database by comparison of synthesised and measured FRFs for excitation locations other than 66Y. When this was done two trends immediately became apparent;

(i) the off-resonant characteristics of the measured and synthesised FRFs were often significantly different; and,

(ii) for several sets of response and excitation coordinates there were differences between measured and synthesised FRF resonance frequencies for modes 3 and 4.

Differences between measured and synthesised FRFs in the off-resonant regions are almost certainly due to the effects of out-of-range modes which have not yet been incorporated in the synthesised FRFs.

Errors in the 3rd and 4th mode resonance frequencies between the measured and synthesised FRFs are a confirmation of the behaviour noted earlier: that, with excitation at point 49, the transverse loading effect of the shaker system on the helicopter causes shifts in some of the resonance frequencies. By definition, all the synthesised FRFs have the same resonance frequencies – those contained in the parameter table (Table 6.2) – and it is the measured resonances which contain the changes.

Calculation of Residuals by Comparison of Measured and Synthesised FRFs

Within Modal Plus there is a facility for calculating residual terms for a synthesised FRF if the measured counterpart is available for comparison. Here, calculation of low-frequency residual inertance terms was required to account for the rigid body modes of the helicopter. Rigid body inertances are all real – (l/mass) – but the program produces complex residual terms by default. There was no direct way of calculating real-valued residual terms and so it was necessary to calculate the complex residual inertances and then truncate to the real part only (N.B. For all of the residuals calculated, the imaginary parts were at least an order of magnitude smaller than the real parts). There were only 4 elements in the full 6x6 FRF matrix for which residual terms could not be calculated because of unavailability of certain measured FRFs – 66X/66X; 49Y/66X; 66X/49Y and 49Y/49Y, see Figure 6.8.

The low frequency residual inertances can be seen in Table 6.4, where they are shown in the matrix grid pattern.

	Excitation.					
Resp.	66X+	66Y+	66Z+	49X-	49Y+	49Z+
66X-	N/A	-.1 OE-3	.59E-4	.45E-4	N/A	-.64E-3
66Y-		.34E-2	-.17E-3	-.47E-3	.31 E-2	.66E-3
66Z-			.18E-2	.00	-.31 E-4	.43E-2
49x+				.00	.13E-5	.00
49Y-					N/A	.00
49Z-						.00

N/A ≡ Not Available

Low Frequency Residual Terms from Comparison of Measured and Synthesised FRFs.

Table 6.4

It must be noted that the analyses to determine these low-frequency residual terms were not very satisfactory. In many cases, significantly different results were obtained when the measured and synthesised FRFs were compared over different frequency ranges. The low-frequency residual results presented in Table 6.4 are those that gave the closest agreement between the measured and synthesised FRFs. The positioning of the anti-resonances in the synthesised FRFs was particularly useful in this assessment.

Theoretical Calculation of Residual Terms

In the above section the low-frequency residual terms have been found by comparing the synthesised FRFs with their measured counterparts. There were 3 functions in the upper triangle of the FRF matrix for which the measured FRFs were not available, hence low-frequency residuals could not be calculated for these functions. It was felt that an incomplete database of residual terms of questionable accuracy was not a good starting point for predictions of the effects of modifications; recall the discussions in chapter 5 on the effects of using incomplete and inaccurate models in modification predictions. Fortunately in this case, the low frequency residual terms only represent the rigid body modes of the helicopter – the lowest frequency flexural modes have been measured – and it is possible to derive the low frequency residual terms from the rigid body properties of the structure. In this case, the mass and inertia properties of the helicopter were obtained from a F.E. model of the helicopter at the R.A.E. Famborough, and basic rigid body mechanics was then employed to derive expressions for all the low-frequency residual

terms in the FRF matrix, i.e. $\left(\frac{\ddot{x}_{resp}}{F_{ref}}\right)$ for all the response and reference locations. They are all purely real valued and are shown in Table 6.5.

	Excitation.					
Resp.	66X+	66Y+	66Z+	49x+	49Y+	49Z+
66X+	.36E-3	.22E-5	-.26E-4	.36E-3	.27E-5	-.31E-4
66Y+		.31E-2	-.13E-6	-.41E-3	.37E-2	-.24E-4
66Z+			.28E-2	-.31E-3	.16E-5	.34E-2
49x+				.46E-3	-.49E-3	-.38E-3
49Y+					.47E-2	.29E-3
49Z+						.43E-2

Theoretical Low Frequency Residual Terms.

Table 6.5

For 66X/66X the residual term is very close to (l/total mass of test structure). This is because coordinate 66X passes through the centre of gravity of the helicopter.

An initial comparison of the low-frequency residual results presented in Tables 6.4 and 6.5 reveals large discrepancies:-

(i) the signs of a number of the residual terms are different; and,

(ii) the residual values are frequently very different.

In mitigation though, the residual terms for each FRFfrom the two estimation methods should be compared together with a measure of the overall inertance level for the FRF term under consideration. For example, consider an FRF with a high overall inertance which requires a comparatively small residual correction of, say, $0.1x10^{-3}$ Kg^{-1}. Now, assume that another residual estimation indicates a residual correction of $0.1x10^{-6}$ Kg-r. On initial comparison of these residual terms in isolation, the difference between $0.1x10^{-3}$ Kg^{-1} and $0.1x10^{-6}$ Kg^{-1} looks to be very significant but, in fact, compared with the size of the FRF itself, **both** estimates of the residual are negligible.

6.5.3 Comparison of Measured and Synthesised FRFs

In Figures 6.27 and 6.28, a selection of measured FRFs are plotted alongside the synthesised versions, with and without low frequency residual terms added. As a general rule, correlation of measured and synthesised FRFs in anti-resonance regions provides a much better check on the whole analysis than correlation in the resonance regions where

the response is dominated by a single mode and good results may be achieved by using a single degree-of-freedom approximation (this is the basis of **SDoF** modal analysis methods). In anti-resonance regions, the contributions from **all the** modes combine and cancel out. Even if only one of the modal contributions is estimated incorrectly, the position of the anti-resonance will be altered.

(i) Response **66Y+/Force 66Y-,** (Figure 6.27)

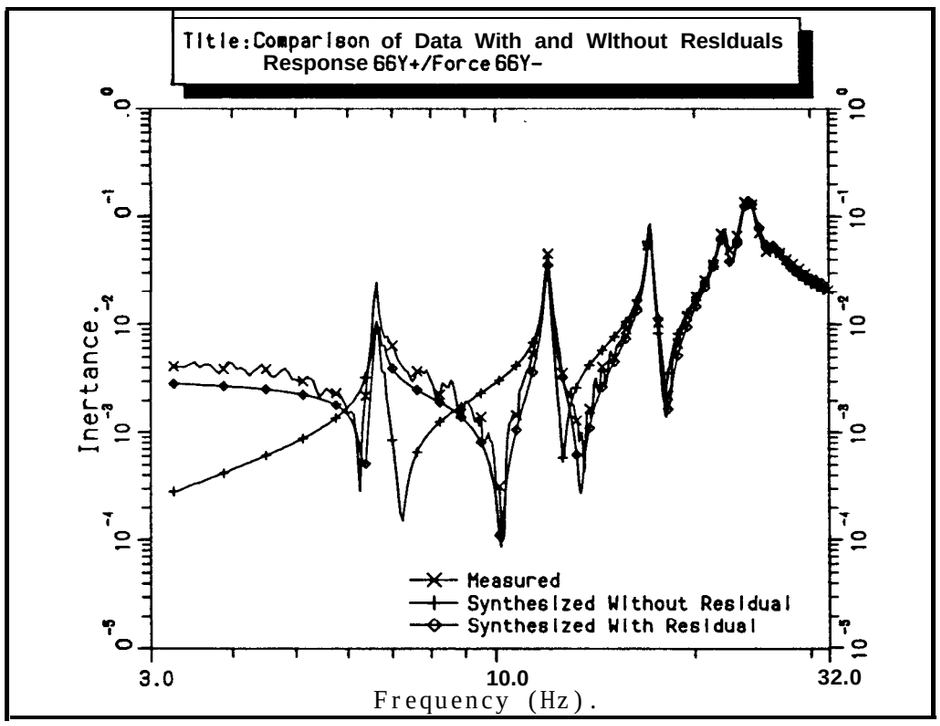

Comparison of **FRFs** With & Without Residuals **(66Y+/66Y-)**

Figure 6.27

The low-frequency residual correction term is most important for this FRF, as shown by the marked effect it has on the FRF characteristics in the low-frequency part of the range. The most obvious effects of the residual addition are the appearance of an anti-resonance at a frequency just below the **first** resonance and the shift of the anti-resonance between modes 3 and 4 from about 7 Hz to about 10 Hz. The residual correction has virtually no effect in resonance regions. With the residual correction applied, all the synthesised **anti-**resonance features are positioned correctly and the synthesised FRF agrees very well with the measured FRF right across the frequency range.

(ii) Response 66Y+/Force 49X+, (Figure 6.28)

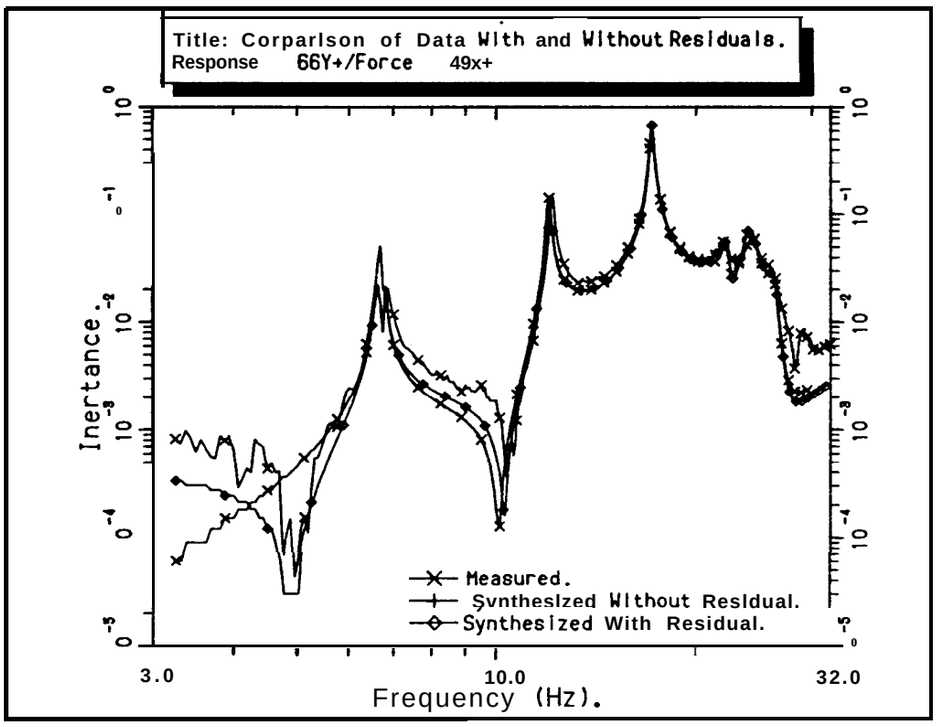

Comparison of FRFs With & Without Residuals (66Y+/49X+)

Figure 6.28

For these FRFs the agreement between the measured and the synthesised FRF with the low frequency residual term is seen to be generally good. The level of agreement tends to become better with increasing frequency. The amplitude estimates for modes 1 and 2 are slightly incorrect and this is probably the cause of the poor correlation of the measured and synthesised anti-resonance between modes 2 and 3. At the low frequency end of the range, the residual has a large effect on the synthesised FRF, but as the frequency increases, the magnitude of the FRF increases generally and the residual has proportionally less effect.

There is a small difference between the resonance frequencies for mode number 3 of the measured and synthesised FRFs. This is a problem with the measured FRF, not the analysis or synthesis; there was some loading of the helicopter by the excitation system at point 49 which has cause the small increase in the frequency for mode number 3 in the measured FRF.

6.6 Sensitivity Analysis

The sensitivity analysis procedure developed in chapter 3 has been applied to data collected from the modal survey of the helicopter. Where synthesised data are required, those derived from polyreference analysis together with theoretical residual terms have been used.

6.6.1 Extraction of Input Data for Sensitivity Analysis

All the necessary information can be extracted from the point FRFs; the resonance frequencies, the anti-resonance frequencies and a data point on each of the FRFs to fix the curves in the Y-axis. The resonances are obvious features which are not too difficult to determine reasonably accurately, even by simple cursoring. The anti-resonances can be troublesome to locate however, if raw FRF data are used. The first anti-resonance for many of the FRFs would have been particularly difficult, or impossible, to locate using raw data for the helicopter. There are no reliable data available for frequencies less than about 3 Hz since frequencies below this were filtered out from the excitation signal. Additionally, the piezoelectric force gauge was at the limit of its operating range at 3 Hz. The poor quality of the FRF data in the anti-resonance regions is closely linked with the input magnitude resolution of the measuring instruments used, see chapter 5.

In this analysis the problem was overcome by the use of FRFs synthesised from the modal database where the anti-resonances are defined just as clearly as the resonances. Nevertheless, great care had to be taken to ensure that the synthesised anti-resonance frequencies matched those measured. The anti-resonance frequencies were found from these synthesised FRF curves using a ‘valley picking’ routine available within Modal Plus and the resonance frequencies were taken from the modal analysis parameter table, although use of data obtained with a ‘peak picking’ routine would have been equally valid. The resonance and anti-resonance frequencies for all the point FRFs are listed in Table 6.6, together with several coordinates on each of the curves, to be used as reference points. The information was then entered into the sensitivity analysis program to produce all the mode sensitivities for each of the location points and directions.

Anti-resonance Frequency (Hz)	Resonance Frequency (Hz)	Reference Points
Location 66X		
6.50	6.74	
11.81	11.92	1) $0.235 \cdot 10^{-3}$ Kg-' @ 6.31 Hz
23.38	24.08	2) $0.212 \cdot 10^{-2}$ Kg-' @ 6.81 Hz
25.75	26.24	3) $0.707 * 10^{-3}$ Kg-' @ 8.31 Hz
Location 66Y		
6.25	6.57	
10.13	11.92	1) $0.195 * 10^{-2}$ Kg-' @ 8.13 Hz
13.38	17.08	
18.19	22.17	2) $0.567 \cdot 10^{-2}$ Kg-' @ 11.50 Hz
22.69	24.08	
26.00	26.24	3) $0.551 \cdot 10^{-2}$ Kg-' @ 15.31 Hz
Location 66Z		
5.31	6.74	
11.69	11.92	1) $0.545 * 10^{-2}$ Kg-' @ 6.13 Hz
16.88	17.06	2) $0.719 \cdot 10^{-2}$ Kg^{-1} @ 8.31 Hz
20.69	26.24	3) $0.618 * 10^{-2}$ Kg-' @ 12.38 Hz
Location 49X		
1.50	6.57	
6.63	6.74	1) $0.298 \cdot 10^{-1}$ Kg-' @ 9.19 Hz
7.19	11.92	
12.50	17.06	2) $0.892 \cdot 10^{-1}$ Kg-' @ 13.81 Hz
21.88	22.17	
23.69	24.08	3) $0.855 \cdot 10^{-1}$ Kg-' @ 16.50 Hz
25.81	26.24	
Location 49Y		
4.50	6.57	
11.81	11.92	1) $0.531 * 10^{-2}$ Kg-' @ 5.31 Hz
16.38	17.06	2) $0.755 \cdot 10^{-1}$ Kg-' @ 6.38 Hz
21.27	22.17	3) $0.139 * 10^{-1}$ Kg-' @ 9.81 Hz
23.38	24.08	
Location 49Z		
2.81	6.57	
6.63	6.74	1) $0.148 \cdot 10^{-1}$ Kg-' @ 4.88 Hz
8.19	11.92	2) $0.292 * 10^{-1}$ Kg-' @ 7.50 Hz
16.94	17.06	3) $0.368 \cdot 10^{-1}$ Kg-' @ 11.30 Hz

Input Data for Sensitivity Analysis Table 6.6

6.6.2 Sensitivity Analysis Results

(i) Low Frequency Asymptotes

In addition to the mode sensitivities for each point, the analysis produces a theoretical value of the low frequency asymptote for the FRF curve – either mass or stiffness, depending upon whether the structure is free or grounded. The value of this asymptote is calculated from the same input data as are used in the calculation of the sensitivities; resonance and anti-resonance frequencies and a reference point. The theoretical asymptotic value can then be used as a check on how well the assumed model approximates the actual data. If the theoretical and measured values have a close correlation then the assumed model is reasonable and the sensitivities produced can be expected to be reliable. If they do not agree, then some explanation must be sought. The low frequency asymptotic values for different reference points were calculated and compared with each other and with the values derived from the measured FRF curves.

Point	Theoretical Value	Sensitivity Analysis Results. 1	2	3
66X	.36E-3	.51E-3	.47E-3	.60E-3
66Y	.31E-2	.30E-2	.31E-2	.31E-2
66Z	.28E-2	.30E-2	.29E-2	.27E-2
49x	.46E-3	.73E-3	.73E-3	.74E-3
49Y	.47E-2	.48E-2	.45E-2	.51E-2
49Z	.43E-2	.44E-2	.46E-2	.49E-2

Static Accelerance Results (Units: Kg^{-1})

Table 6.7

Theoretical values for the low frequency residual properties of the helicopter were calculated as part of the modal analysis. These residuals are the low frequency asymptotes of the FRFs – the Static Accelerances and they have been used for comparison with the static accelerance results from the sensitivity analysis. The calculations have been repeated three times, with different reference points, for all the point FRFs. The results can be seen in Table 6.7. There is generally close agreement of the sensitivity analysis estimates of the static accelerances for each of the point FRFs. The largest variation is for the 66X degree-of-freedom and this is a reflection of the difficulties with measurement and analysis of the data from this coordinate, which is comparatively immobile. On the whole, the sensitivity analysis static accelerances agree quite closely with the theoretical residual values. There are two exceptions; coordinate 66X and coordinate 49X. In both these instances the theoretical residual value is lower than that calculated in the sensitivity analysis. It will be

noticed from the listings of Table 6.6 for the anti-resonance frequencies that the first anti-resonance in the point FRF for degree-of-freedom 49X is at 1.5 Hz – very much lower than the first anti-resonance frequency in any of the other point FRFs. The calculations are sensitive to the positioning of this first anti-resonance and this affects the results calculated.

It has also been found that the choice of reference point (which is used in the calculation of the static accelerance) can influence the results from the sensitivity analysis. It is believed to be better to choose reference points where the measured and synthesised FRFs have close agreement; i.e. close to, but not at, resonance frequencies and away from anti-resonance regions of the FRF curve.

(ii) Resonance Frequency Sensitivities

The resonance frequency sensitivities for each coordinate are shown in Table 6.8. Only the mass sensitivities are given. The stiffness sensitivities follow directly from these mass sensitivities (see chapter 3) and the ranking of coordinates for single degree-of-freedom mass or stiffness modifications is identical. The different reference points (Table 6.6) gave rise to small variations in the sensitivity values, but this was not considered to be too important since the sensitivity analysis is only intended for use as a means of ranking the degrees-of-freedom in their order of importance for modification. Provided that variations in the sensitivities are not sufficient to alter the ranking order, the analysis is satisfactory. Prediction of the effect of a mass or stiffness modification with the sensitivity analysis data is considered to be of secondary importance and always liable to some degree of error because of the definition of sensitivity as the **initial** rate of change of the resonance frequency with point single degree-of-freedom mass or stiffness alterations.

		SDoF Mass Sensitivity (%/Kg)					
Mode	Natural Frequency	66X	66Y	66Z	49x	49Y	49Z
1	6.57		-.011		-.044	-.260	-.168
2	6.74	-.002		-.087	-.069		-.333
3	11.92	-.000	-.021	-.009	-.313	-.009	-1.91
4	17.06		-.047	-.003	-2.92	-.040	-.067
5	22.17		-.091		-.172	-.038	
6	24.08	-.001	-.247		-.227	-.061	
7	26.04	-.002	-.046	-.167	-.269		

Resonance Frequency Sensitivities for the Helicopter.

Table 6.8

The extent of variation found in the sensitivity values tended to increase with increasing frequency. This is to be expected because the theory presented in chapter 3 is based on the use of an expression involving the product of terms for **all** modes which is truncated to include only the measured modes. The effects of the high frequency modes, which have been excluded, are felt most strongly by those modes at the upper end of the frequency range of interest and, therefore, it is these mode sensitivities that are determined least accurately.

From the sensitivity results, Table 6.8, it is immediately obvious that point 66 is insensitive to any form of single degree-of-freedom modification, whereas modification at point 49, in the X and **Z** directions, will produce comparatively large shifts in the resonance frequencies for modes 4 and 3 respectively. Modification at point 49 in the Y direction (along the axis of the tailplane) is ineffective for all but the first mode – lateral bending of the fuselage.

6.6.3 Comparison of Theory with Experiment for a SDoF Mass Modification

The sensitivity analysis technique has been developed as a means for ranking the coordinates in their order of importance for single degree-of-freedom modification. As a method for predicting the actual shifts in resonance frequencies from given modifications the technique can only be expected to yield accurate answers if the modification is small or if the variations in resonance frequencies are linear for the particular modification (see Figures 3.12 and 3.24). Single degree-of-freedom mass modifications were made experimentally and the actual resonance frequencies for the modified structure were compared with those predicted from the sensitivity analysis results to establish the size of errors associated with these predictions.

(i) SDoF Mass Modification at Point 49Z

The sensitivity of mode number 3 (11.916 Hz) to mass modification at point 49Z is -1.9%/Kg. Therefore, to achieve a reasonable shift in the resonance frequency – say 1 Hz – the single degree-of-freedom mass change required is 4.42 Kg. Using laboratory weights bolted together, a modification with a mass of 4.62 Kg was constructed. This mass modification was attached at point 49 (in the Z-direction) by means of a standard excitation pushrod 18 mm long by 1 mm in diameter. This ensured that the mass had little effect in any coordinate other than 49Z and would act as a single degree-of-freedom modification. Re-calculation shows that the actual mass modification of 4.62 Kg should

produce a downwards shift of 1.05 Hz for mode number 3, resulting in a resonance frequency of 10.87 Hz for the modified structure. The next largest frequency shift predicted is -0.104 Hz (1.5%) for mode number 2.

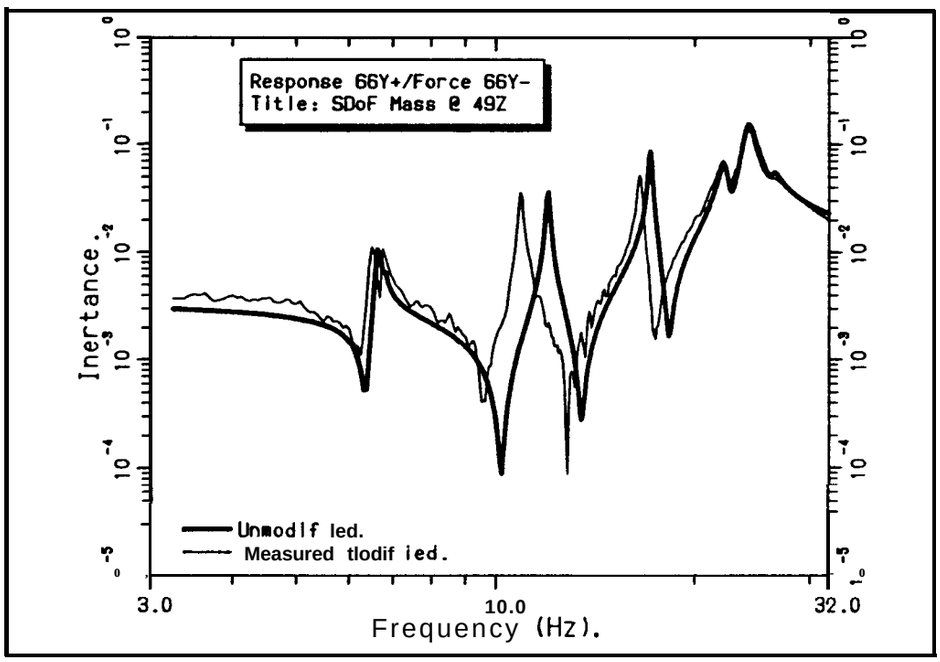

Effects on the Point FRF for 66Y of SDoF Mass Modification at 492

Figure 6.29

The modified helicopter structure was excited in the Y-direction at point 66 and translational response measurements were made in the X, Y and Z coordinate directions at points 66 and 49. The point FRF curves for coordinate 66Y of the modified and unmodified structure are shown in Figure 6.29, from which it can be seen that there was indeed a marked shift (1.1 Hz) in the resonance frequency for mode number 3, but little change in all the other resonances, except that modes 1 and 2 now appear as a single peak on the FRF plot. The resonance frequency of mode number 3 for the modified structure has been measured as 10.8 Hz, which compares well with the 10.87 Hz predicted.

It should be noted that, for the FRFs measured with excitation at 66Y and single degree-of-freedom modification at 492, there are shifts in all the anti-resonance frequencies. Another series of FRF measurements were taken with the excitation applied in the Z-direction at point 49; the same degree-of-freedom as the modification. The point FRF from this series of measurements is shown in Figure 6.30 together with that for the unmodified structure. The major anti-resonance frequencies for this degree-of-freedom are **not** changed as a result of the modification and this confirms that the modification made was indeed a single degree-of-freedom modification, effective only in the Z-direction at

point 49 (see chapter 3). If the modification had had significant effects in any degree-of-freedom other than 49Z, then the anti-resonance frequencies of the point FRF at 49Z would have shown changes also.

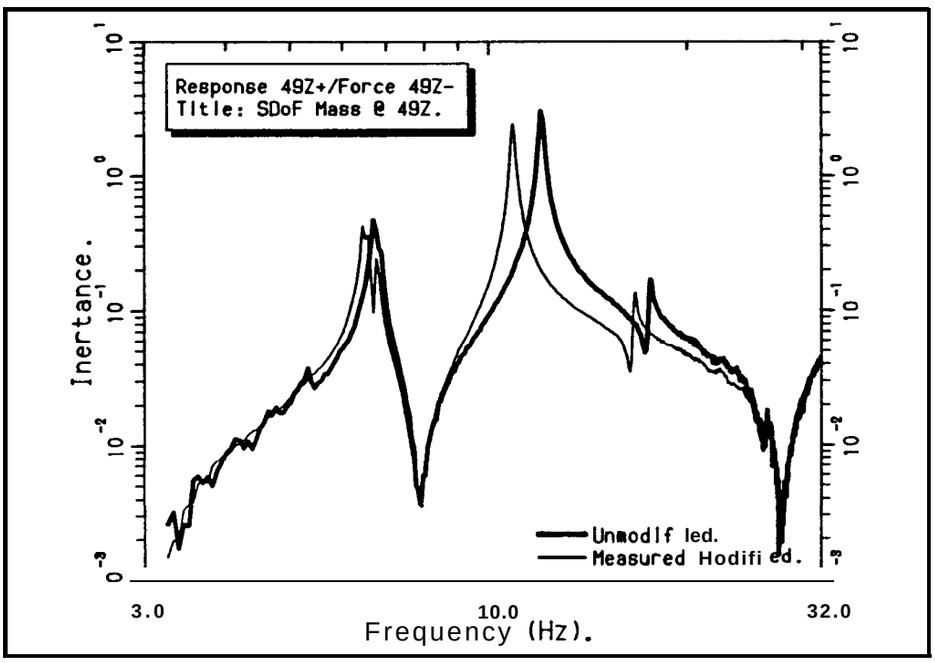

Effects on the Point FRF for 49Z of SDoF Mass Modification at 49Z

Figure 6.30

Inspection of the point FRFs for 492, Figure 6.30, shows that there is a discrepancy between the resonance and anti-resonance frequencies in the region of 17 Hz. The sensitivity of mode number 4 to single degree-of-freedom modification in the Z-direction does not account for the shift observed. The problem is a result of the different pushrods used for the two measurements. For the original measurement of the unmodified structure, a pushrod of length 20 mm was used because of space limitations, but, when the single degree-of-freedom mass modification was made at 49Z the whole helicopter pitched tail down sufficiently to allow use of the 100 mm pushrod. It was the lateral restraint of the helicopter by the short pushrod used in the original measurement, that caused the 4th mode frequency to be raised slightly. The preceding anti-resonance frequency is also raised by a similar amount.

point 49 (see chapter 3). If the modification had had significant effects in any degree-of-freedom other than 49Z, then the anti-resonance frequencies of the point FRF at 49Z would have shown changes also.

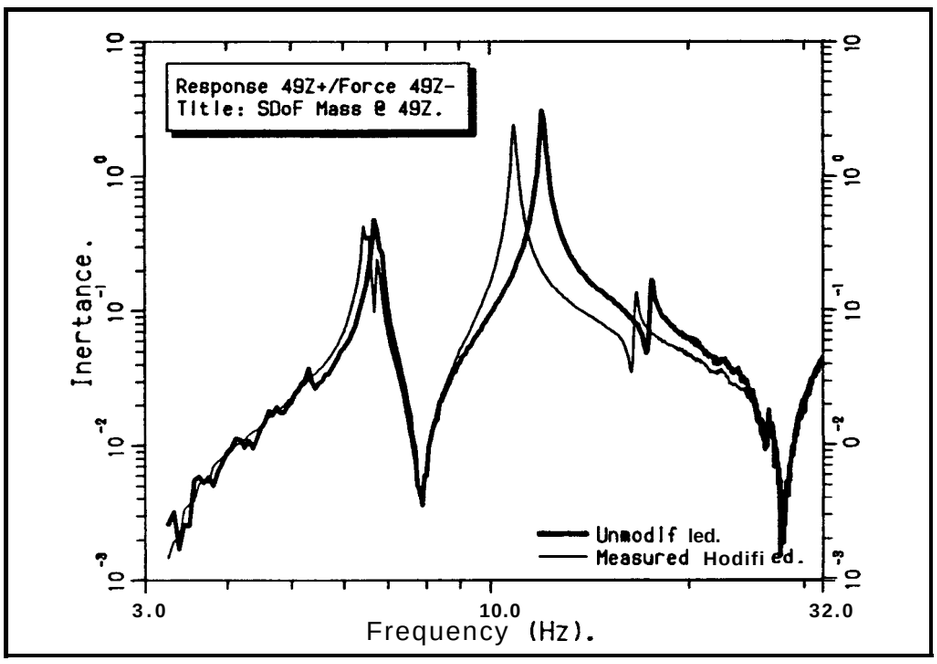

Effects on the Point FRF for 49Z of SDoF Mass Modification at 49Z

Figure 6.30

Inspection of the point FRFs for 492, Figure 6.30, shows that there is a discrepancy between the resonance and anti-resonance frequencies in the region of 17 Hz. The sensitivity of mode number 4 to single degree-of-freedom modification in the Z-direction does not account for the shift observed. The problem is a result of the different pushrods used for the two measurements. For the original measurement of the unmodified structure, a pushrod of length 20 mm was used because of space limitations, but, when the single degree-of-freedom mass modification was made at49Z the whole helicopter pitched tail down sufficiently to allow use of the 100 mm pushrod. It was the lateral restraint of the helicopter by the short pushrod used in the original measurement, that caused the 4th mode frequency to be raised slightly. The preceding anti-resonance frequency is also raised by a similar amount.

(ii) SDoF Mass Modification at Point 49X

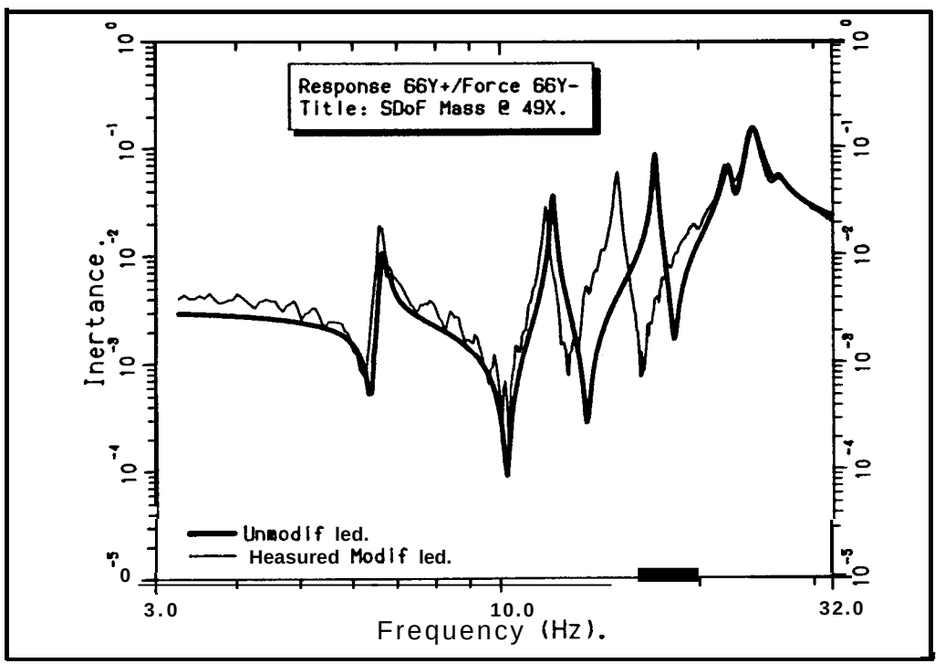

Effects on the Point FRF for 66Y of SDoF Mass Modification at 49X

Figure 6.31

The same 4.62 Kg mass modification was attached to point 49 by a pushrod in the X-direction in the horizontal plane. In this situation however, the mass was freely supported from an independent structure. FRFs were measured using excitation at 66Y and it can be seen (Figure 6.31) that there is a large downwards shift of mode number 4 to 14.93 Hz (-12.5%). The shift in the resonance frequency of mode number 4 (17.061 Hz) predicted from the sensitivity analysis is -2.302 Hz (-13.5%), giving a resonance of 14.759 Hz for the modified structure, which compares well with the measured results. There is little change in all the other mode frequencies, as expected.

6.7 Prediction of Effects of Actual Modifications

Once a sensitivity analysis has been completed successfully, the next stage in the solution of a structural vibration problem is the design and selection of a modification that most effectively exploits the sensitive locations on the structure to bring about a desired alteration in the dynamic characteristics. Once a modification has been designed, its effect on the structure can be assessed mathematically (see chapter 2). By this means it is possible to ascertain whether the modification will have the desired effect and whether or

not it will be adequate. If the modification is not satisfactory, it can be redesigned and the mathematical coupling process repeated.

In the typical sequence of events described above, there is one major assumption that is often overlooked; that the mathematical prediction of the dynamic characteristics of the modified structure is a correct and true representation of the behaviour of the modified structure. The underlying theory for predicting the effects of structural modification is fairly simple but this only serves to mask the difficulties that may be encountered when it is used in a practical situation.

The following examples illustrate some of the problems found when using measured FRFs for the base structure and theoretical FRFs for the modification component. The effects of two different types of modification to the helicopter have been studied,

(i) a mass modification at point 49; and,

(ii) a stiffness between points 49 and 66.

The predictions of changes to the structure's properties have been accomplished using the impedance coupling technique which is discussed fully in chapter 2.

6.7.1 Mass Modification

Actual Coupling in 6 Degrees-of-Freedom;
Theoretical Coupling in 3 Degrees-of-Freedom

The effects of single degree-of-freedom mass modifications at point 49 have been investigated (section 6.6.3) and the agreement between measured and predicted resonance frequencies for the modified structure was quite reasonable. However, a single degree-of-freedom mass modification is not a very practical case and would rarely be contemplated in practice. The most likely implementation of a mass modification is to bolt the mass in position – a coupling involving all 6 degrees-of-freedom (see chapter 5). Such a modification has been attempted at point 49 where the mass was attached as shown in the diagram of Figure 6.32. Measurements of the modified helicopter's dynamic characteristics were made and it was found that the modification had a greater effect than when attached as a SDoF modification in either of the X- or Y- directions alone.

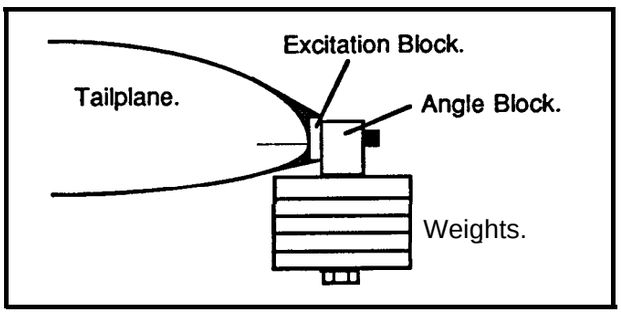

6 Degree-of-Freedom Point Mass Modification.

Figure 6.32

A computer program was written to perform the theoretical coupling analysis in 3 degrees-of-freedom. The mass was considered to be acting equally in all three translational degrees-of-freedom at point 49. FRFs for the unmodified and modified helicopter are presented in Figure **6.33,** where it can be seen that the modification has major effects on modes 3 and 4 – the sensitive modes – and relatively little effect on any of the other modes.

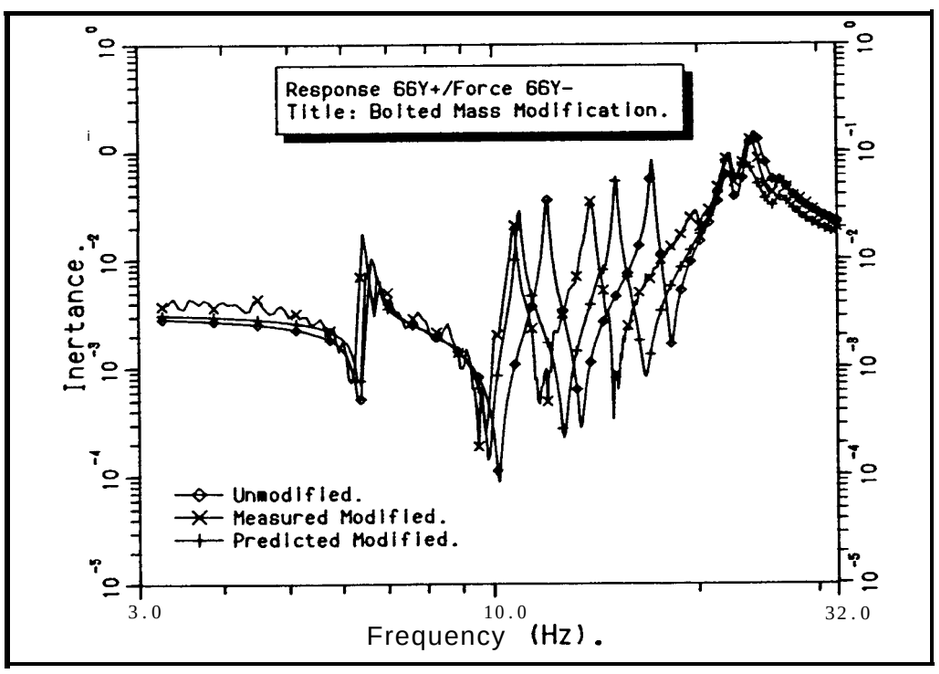

Comparison of Point FRFs for 66Y for the Bolted Mass Modification

Figure 6.33

For mode number 3 the actual modification causes a greater downwards frequency shift than that predicted theoretically by the coupling procedure; a predicted resonance

frequency of 10.86 Hz compared with a measured resonance frequency of 10.65 Hz. The unmodified resonance frequency is 11.92 Hz

There is a much larger discrepancy between the predicted and measured resonance frequencies for mode number 4. Once again, the measured resonance frequency for the modified helicopter (13.84 Hz) is considerably lower than that predicted (15.04 Hz). The unmodified resonance frequency is 17.06 Hz.

However, it was known that there was a major deficiency with the theoretical prediction; no FRF data for the rotational degrees-of-freedom were available because they could not be measured and, therefore, by default all the rotational degrees-of-freedom were assumed to be free. It is common for such sweeping assumptions to be made in practice without further consideration of the real implications.

Discrepancies such as these are probably unacceptable for real-life applications. The predicted FRFs do not properly match the behaviour of the modified helicopter and could be dangerously misleading.

When examining the FRF curves of Figure 6.33 it is important to compare the FRFs as a whole, rather than just looking at the correspondence of predicted and measured resonance frequencies for the modified condition. In Figure 6.33 the measured FRF for the modified helicopter has an anti-resonance at about 16 Hz while the predicted FRF has a resonance at the same frequency. There is a difference in the FRF magnitudes near this frequency of approximately 100 times. Although this is the worst situation, there are many other areas where the differences in the magnitudes of the predicted and measured FRFs are of the order of 10 times.

This mass modification used has quite a high rotational inertia about the X- and Y- axes. It is suggested that it is the coupling of this rotational inertia by bolting the mass to the tailplane that is the cause of the discrepancies. In the theoretical predictions using the impedance coupling method, no rotational inertia effects are included and this is believed to explain why the actual modification has a greater effect than that assumed in the prediction.

Actual Coupling in 3 Degrees-of-Freedom;
Theoretical Coupling in 3 Degrees-of-Freedom

(i) Short Mass

Since it was not feasible to include rotational degrees-of-freedom in the coupling procedure the actual modification was altered to mimic the theoretical model, to find out whether a better level of agreement could be achieved between the measured and predicted results. This time, the mass was attached at point 49 via a very short (≈2 mm) turned down section of bar, which acted like a pin-joint; see the diagram of Figure 6.34. The full effect of the mass (4.62 Kg) was felt by the helicopter in the Z-direction, while in the X- and Y-directions the effective mass modification was much less (0.47 Kg). This was calculated by assuming the mass modification to be a uniform beam pin-jointed at one end. The rotational effects are decoupled, but so too is much of the mass in the X- and Y-directions.

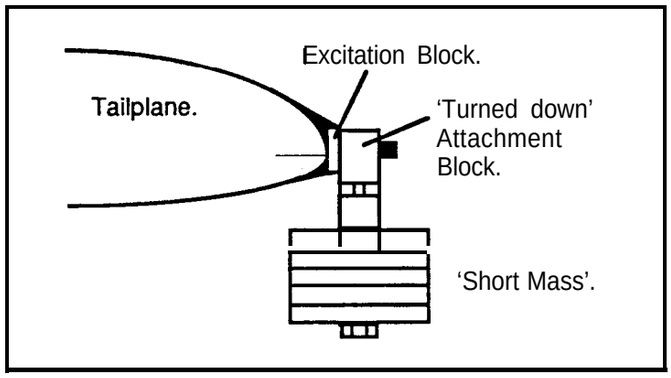

Short Mass: 3DoF Point Mass Modification.

Figure 6.34

FRF measurements were made for this modification. Throughout the tests, the mass could be seen moving in relation to the helicopter, proving that the link was indeed flexible. Slight alterations were made to the computer program to allow different mass effects to be added in each of the coordinate directions. The results from this new theoretical prediction for the point FRF at 66Y may be seen in Figure 6.35. Comparison of the theoretical results with those measured for the actual modification indicates a much higher level of agreement than beforehand. All the new resonances and anti-resonances are estimated fairly accurately. However, when the results for the modified structure are compared with those for the unmodified structure, it will be seen that there is only an appreciable alteration for mode number 3; all the other modes remain largely unaffected. The results for this modification are very similar to those for a single degree-of-freedom modification

in the Z direction, because most of the effect in the X- and Y-directions is removed by the pin-joint connection.

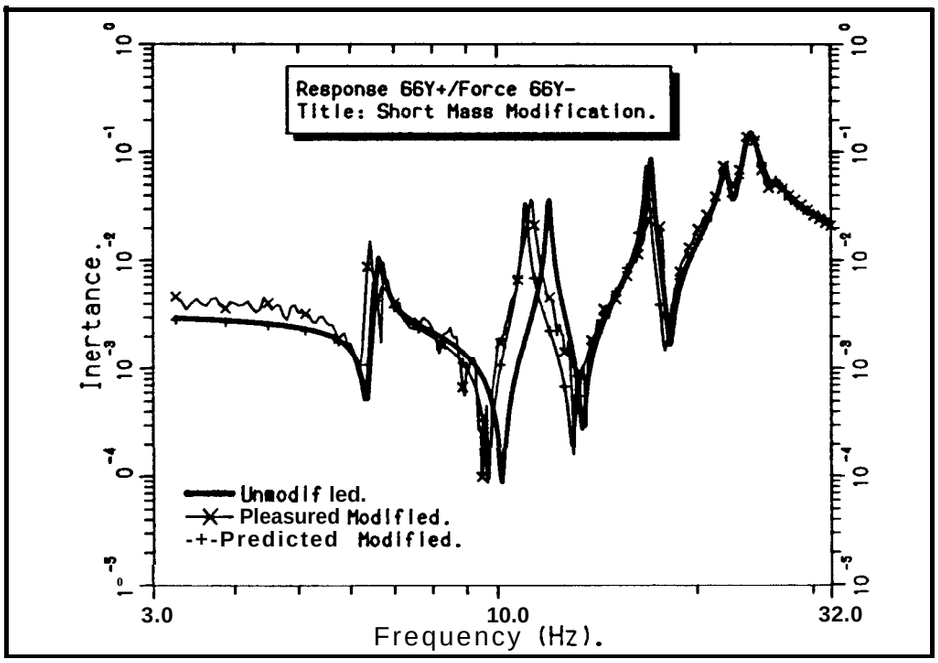

Comparison of Point FRFs for 66Y for the 'Short Mass' Modification

Figure 6.35

(ii) Extended Mass

The reason why, for the previous modification, the apparent mass in the X- and Y-directions is so small is that the mass is too concentrated and too far away from the attachment point. It was not possible to raise the mass any closer to the attachment point, so another modification had to be designed. The criterion was that the modification should have a high moment of inertia in the X- and Y-directions about its centre of gravity. This was achieved easily, as shown in Figure 6.36. The total mass of this modification was 4.87 Kg and the effective mass in the X- and Y-directions was calculated to be 2.1 Kg. To check this result a point FRF measurement was made at the attachment point on the extended mass. The resulting FRF should have been a horizontal line, but the measurements showed a characteristic rolling off indicative of an anti-resonance just above 32 Hz (the measurement frequency range). Over the frequency range 5 to 20 Hz, the apparent mass was calculated as between 1.667 and 2.222 Kg. In preference to using the theoretical effective mass, an average measured value of 1.9 Kg has been taken as the effective mass in the X- and Y-directions for the coupling prediction.

It is interesting to compare the measured resonance frequencies for the modified structure with those predicted using the full impedance coupling method, and those predicted using the results from the sensitivity analysis. Predictions using the sensitivity analysis are set out in Table 6.9. Sensitivities less than 0.1%/Kg have been ignored.

		49x Mass =1.9Kg		49Y Mass = 1.9Kg		492 Mass = 4.87Kg		Predictions		Measured	
Mode (Hz)	Unmod. Freq (%/Kg)	Sens. (Hz)	Shift (%/Kg)	Sens. (Hz)	Shift (%/Kg)	Sens. (Hz)	Shift (Hz)	Sens. Freq. (Hz)	Coupling Freq. (Hz)	Modified Freq. (Hz)	Unmod. Freq.
1	6.57			-.26	-.03	-.17	-.05	6.48	6.44	6.44	6.57
2	6.74					-.33	-.11	6.63	6.69	6.61	6.74
3	11.92	-.31	-.07			-.19	-1.11	10.74	10.91	10.76	11.92
4	17.06	-.29	-.09					16.11	16.09	15.94	17.06
5	22.17	-.17	-.07					22.09	22.14	22.16	22.17
6	24.08	-.23	-.10					23.97	24.03	24.07	24.08
7	26.24	-.27	-.14					26.10	26.19	26.21	26.24

Frequency Predictions for the Extended Mass Modification.

Table 6.9

The effects of modification in each of the coordinate directions have been assumed to be completely independent of the modifications in the other directions. It can be seen that there is good agreement between the sensitivity predictions, the impedance coupling predictions and the actual measurements for all the modes apart from mode number 4, where the sensitivity analysis prediction gives a significant overestimate of the frequency shifts. This is not unexpected because the sensitivity analysis only gives the initial change in frequency with single degree-of-freedom mass modification. Nevertheless, the sensitivity-based prediction is a simple method that can be used for preliminary determination of the resonance frequencies for a modified structure. These results show that quite accurate results are indeed possible. In practice, though, it would be prudent to treat all of the predictions based on the sensitivity analysis results with caution.

6.7.2 Stiffness Modification

The second type of modification to the helicopter selected for investigation was a stiffness modification between the tailplane and the fuselage. In this case, the stiffness modification was achieved by stretching a single strand of thin stainless steel wire between points 49 (on the tailplane) and point 66 (on the intermediate gearbox). A tensioned wire has several practical advantages for this investigation; it can be considered to be pin-jointed at the ends – no rotational FRF properties are required – and it has a negligible mass compared with

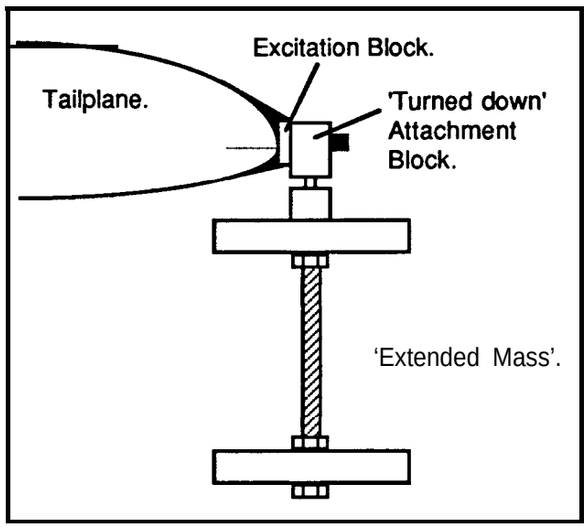

Extended Mass: 3 Degree-of-Freedom Point Mass Modification.
Figure 6.36

Measurements of the actual modified structure were made as before and the 66Y point FRF result is shown in Figure 6.37a together with the theoretical prediction and the unmodified condition. In Figure3.37b the AFRF is plotted alongside the measured and predicted FRFs for the modified structure. It can be seen that the predicted and measured results for the modified helicopter show better than those for the short mass described in (i) above. The resonances and anti-resonances are predicted more accurately, and there is now an appreciable shift in the resonance frequency for mode number 4 as well as that for mode number 3. Away from resonance the AFRF has a magnitude of about 20% of the FRFs themselves and much of the variation in the AFRF is due to the irregularities in the measured FRF. When viewed with Figure 6.5 (a AFRF plot for different forcing levels) the two ΔFRFs are seen to be quite similar. Therefore, it can be concluded that the mathematical models of both the helicopter and the modification are adequate in this case, producing a very satisfactory result for the properties of the modified structure – especially when it is noted that this modification produces frequency shifts of almost 10% for mode numbers 3 and 4, and these frequency shifts are predicted accurately.

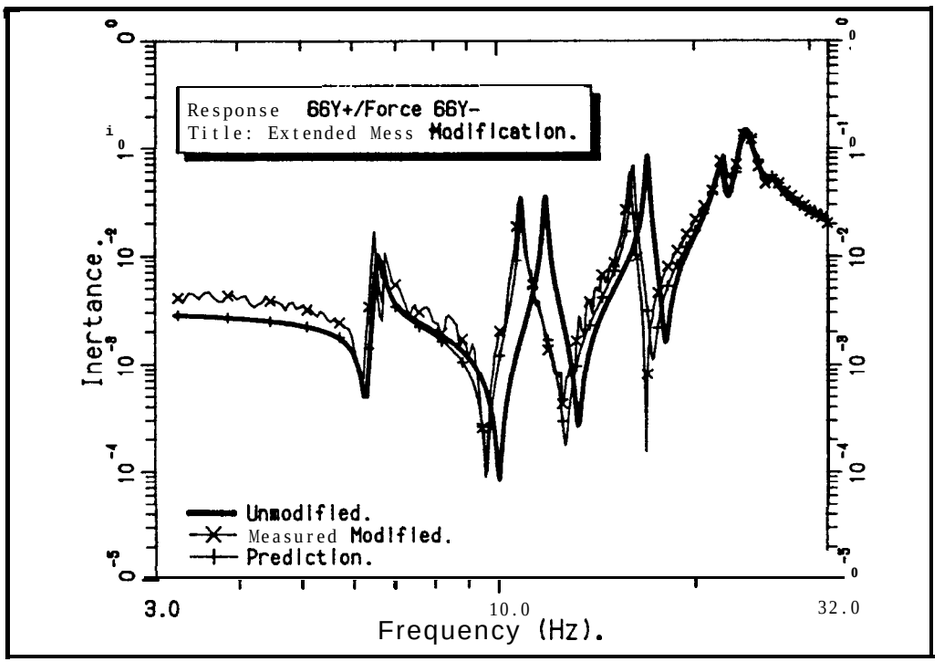

Comparison of Point FEW for 66Y for the 'Extended Mass' Modification

Figure 6.37a

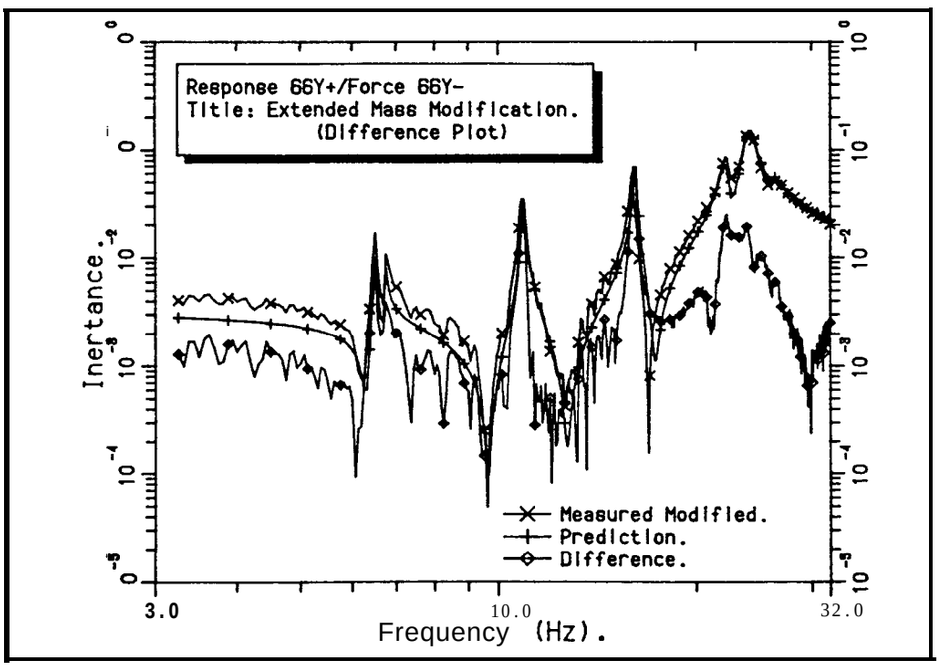

Difference Plot

Figure 6.37b

modification will be described first, followed by a discussion of the practical implementation of the modification and measurement of the modified helicopter.

Measurement of the Axial Stiffness of the Wire Modification

Experience with the mass modification has shown that it is much better to measure the properties of the modification component rather than make assumptions to obtain theoretical values. For the tensioned wire modification, it was necessary to measure its axial stiffness, including that of the loops formed in the ends of the wire for the purposes of attachment.

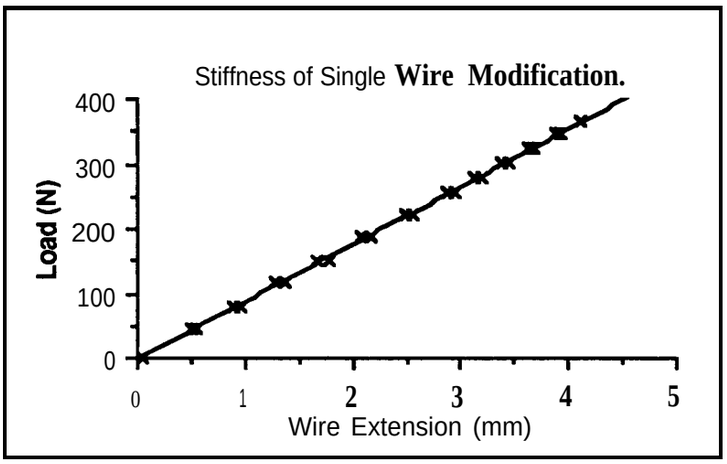

Experimental Results for the Stiffness of the Single Wire Modification

Figure 6.38

The wire was suspended from a support frame and loaded with laboratory weights. Extension of the wire was measured with a dial gauge positioned between the frame and the weight carrier. After pre-conditioning, where the wire was left fully loaded overnight, the load-extension graph of Figure 6.38 was measured (measurements include both loading and unloading of the wire). The stiffness of the wire is the slope of the load-extension graph line, i.e. 89.1 kN/m

Theoretical Coupling

The tensioned wire was assumed to act exactly like a pin-ended spring. There are a total of 6 translational degrees-of-freedom involved in the coupling, 3 at each end of the spring. However, before the impedance coupling technique could be applied it was necessary to transform the synthesised FRFs for the helicopter and the spring into a consistent global coordinate system. The global coordinate system chosen was that of the helicopter.

An inertance or receptance matrix for a free spring element does not exist, but an impedance matrix can be defined directly. The impedance matrix for the spring modification component was defined initially 'in a coordinate system in which the X-direction lay along the spring axis. From knowledge of the coordinates of points 49 and 66, a transformation matrix was formed from the direction cosines of the local X-, Y- and Z- axes in the global coordinate system, Appendix F. This transformation, equation (6.1), was then used to produce an impedance matrix for the spring in the global coordinate system

$$[Z_g] = [\lambda]^T [Z_l] [\lambda] \quad \text{...} (6.1)$$

where, [Z] = Impedance matrix for spring.
(subscripts g and 1 refer to global and local coords.)
$[\lambda]$ = Transformation matrix.

Adding the impedance matrices for the helicopter and the spring modification produced an impedance matrix for the coupled structure which was then inverted and the resulting FRFs for the modified helicopter were then transformed back into the coordinate system used for the original measurements.

The order in which the transformation and inversion processes are carried out should not make any difference to the final results. Three slightly different coupling procedures were tried and the results compared as a means for checking that the modification prediction methods had been applied correctly.

(a) Coupling in Helicopter Coordinate System (method described above)
- (i) form stiffness matrix for spring in local coords;
- (ii) transform to datum coords;
- (iii) read inertance matrix for helicopter in datum coords;
- (iv) invert inertance matrix for helicopter in datum coords;
- (v) add impedance matrices for helicopter and spring in datum coords; and,
- (vi) invert to form inertance matrix for modified helicopter in datum coords.

(b) Coupling in Spring Coordinate System.
- (i) form stiffness matrix for spring in local coords;
- (ii) read inertance matrix for helicopter in datum coords;
- (iii) transform inertance matrix for helicopter to local coords;
- (iv) invert inertance matrix for helicopter in local coords;
- (v) add impedance matrices for helicopter and spring in local coords;
- (vi) invert to form inertance matrix for modified helicopter in local coords; and,
- (vii) transform back to datum coords.

(c) Coupling in Spring Coordinate System.

Reverse the transformation and inversion processes (iii) & (iv) and (vi) & (vii) in method (b) above.

The results were all identical.

Practical Implementation of the Taut-Wire Modification

The modification is a 1 mm diameter single strand stainless steel wire 1.55 m in length, with loops formed at the ends. Additional components were necessary to attach the wire to the helicopter at each end, and to tension the wire once it was **fixed** in place. At point 49, on the tailplane, a shaped pad was stuck to the leading edge with Plastic Padding. The wire was attached to this pad by a removable pin passing through the loop in the wire. The other end of the wire was connected to a small turnbuckle attached to the intermediate gearbox (point 66) through an angle bracket. The turnbuckle was used to tension the wire, thus preventing it becoming slack at any time throughout the excitation sweep. Measurements of the point FRF at point 66 in the Y-direction, for varying tensions in the wire, demonstrated that the required tension was not very great and that once the modification effect had been established, the behaviour did not alter as the tension was increased quite substantially, Figure 6.39. The wire tension was set at about half the maximum tried, and a full set of FRF measurements were made for the modified helicopter, using excitation in the Y-direction at point 66.

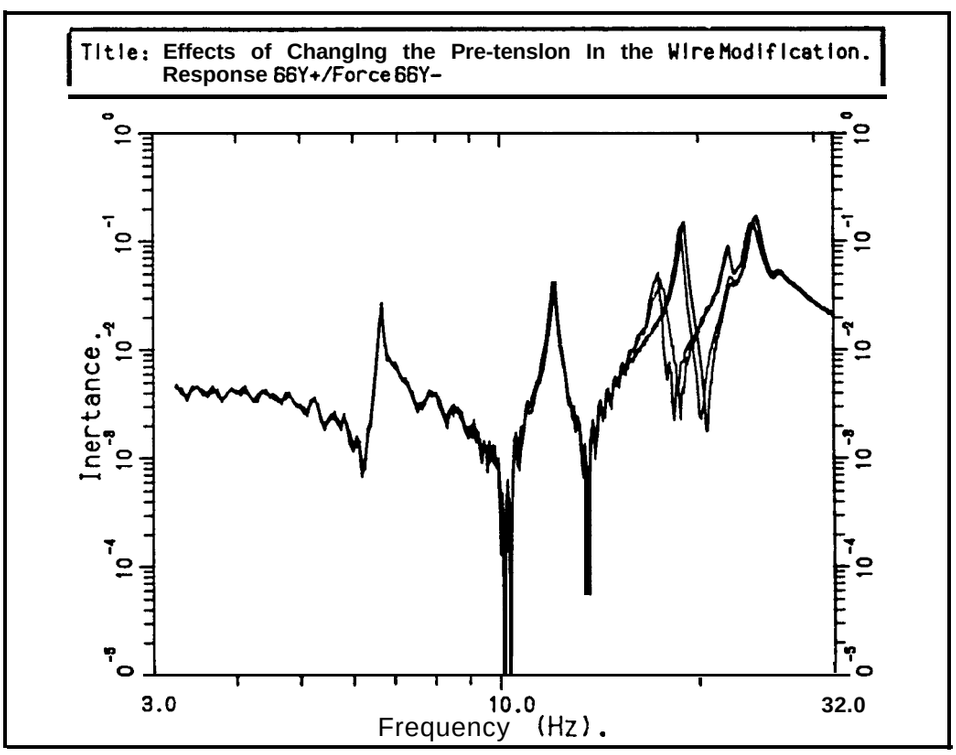

Effects of Changing the Pm-tension in the Wire Modification

Figure 6.39

Comparison of Measured and Predicted FRFs for the Single Taut-Wire Modification

FRF measurements for the modified helicopter have been made for only one excitation (coordinate 66Y) and, therefore, comparison of measured and predicted results is limited to FRFs for this reference location. A comparison of point FRFs for coordinate 66Y before and after modification is presented in Figure 6.40 where it can be seen that the stiffness modification has a large effect on mode number 4 and virtually no influence on any of the other modes. Qualitatively, this is correctly predicted, but the frequency shift for mode number 4 is overestimated; for the unmodified helicopter mode 4 has a natural frequency of 17.06 Hz; the measured frequency for the modified structure is 18.93 Hz (+10.9%) while the predicted frequency is 19.7 Hz (+15.5%). In turn, this overestimation affects the positioning of neighbouring anti-resonance features. Nevertheless, the results are encouraging in that none of the other modes shows any frequency shift in either the measured or predicted FRFs.

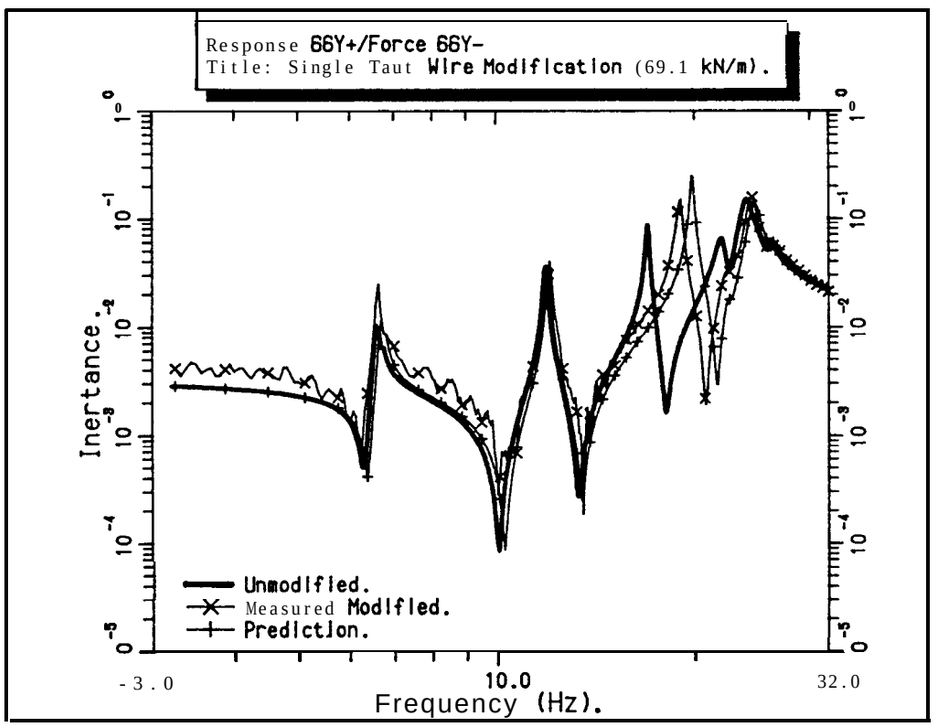

Comparison of Point FRFs for 66Y for the 'Single Taut-Wire' Modification (89.1 kN/m)

Figure 6.40

The prediction overestimates the effect of the modification: the actual modification is not as stiff as that assumed in the coupling procedure. The sensitivity analysis results were used to estimate a value of spring stiffness that would produce the same effect as as the actual modification. After two iterations, a spring stiffness of 60 kN/m was found to

produce predicted results that matched the measured modified results very closely. Since the measured static stiffness of the modification was 89.1 KN/m, the modification appears to be only 67% effective when it is in place. The new predicted point FRF for 66Y with the 60 kN/m stiffness is shown in Figure 6.41 for comparison with the measured result; the level of agreement is at least as good as that for the measured and synthesised FRFs for the unmodified helicopter.

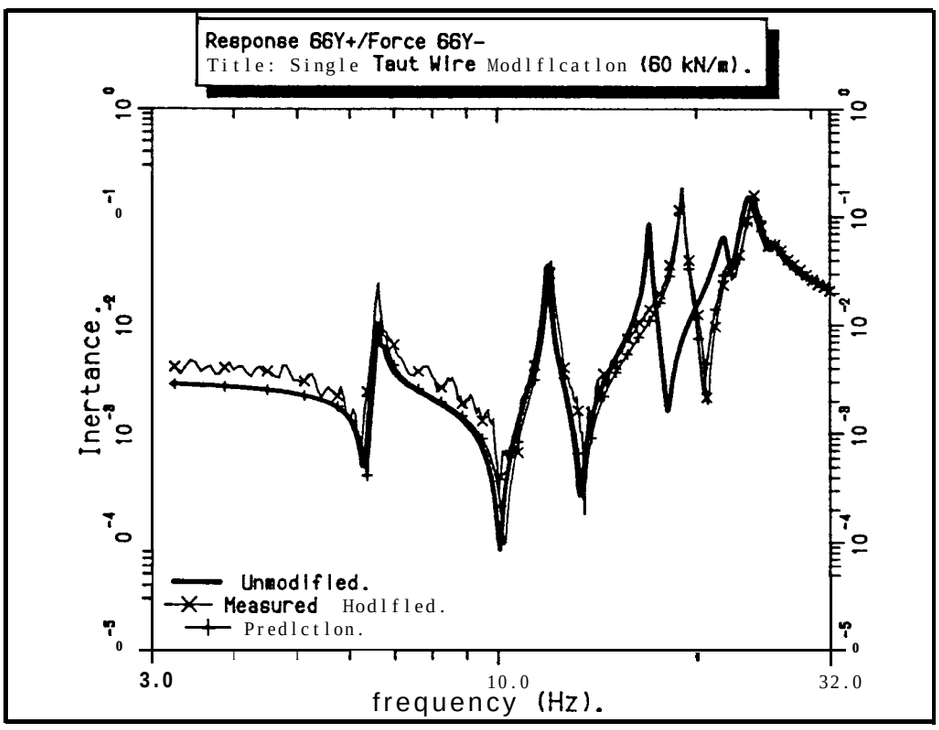

Comparison of Point FRFs for 66Y for the 'Single Taut-Wire* Modification (60 kN/m)

Figure 6.41

Comparison of Measured and Predicted FRFs for a Double Taut-Wire Modification

Two strands of the same wire were used to produce a modification having twice the stiffness of the previous case. The above procedures were repeated using a theoretical stiffness value of 178.2 kN/m, and it was again found that the prediction gave an overestimate of the measured resonance frequency for mode number 4; measured at 20.2 Hz (+18.4%) and predicted to be 21.1 Hz (+23.7%). Sensitivity analysis results were employed to give an adjusted stiffness value of 102 kN/m (57%) for which the prediction of the effects of modification agreed well with those measured, Figure 6.42.

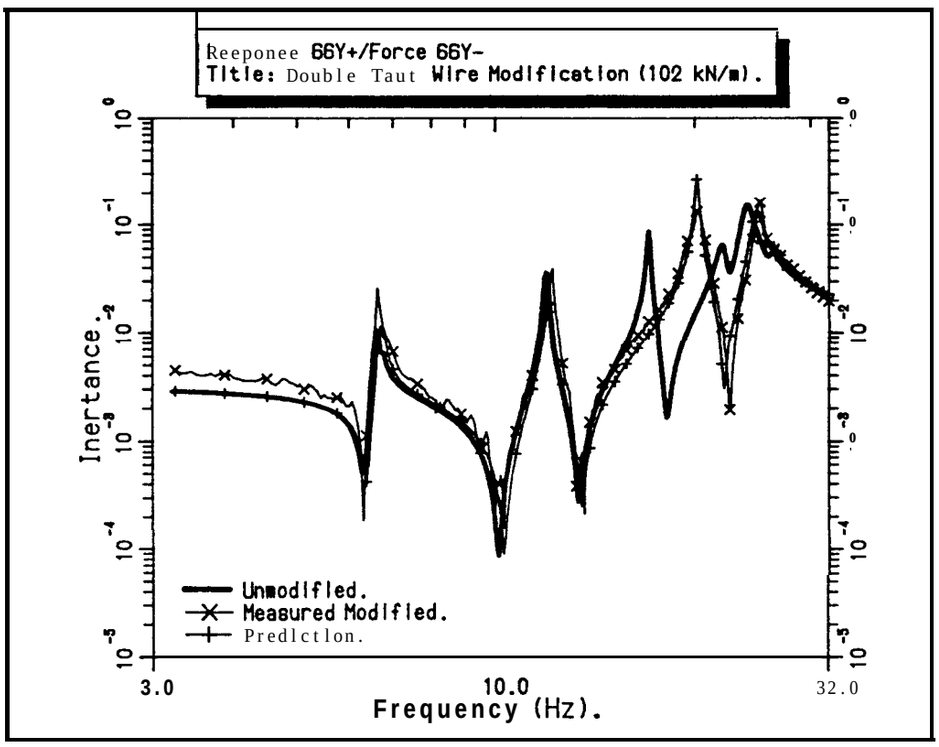

Comparison of Point FRFs for 66Y for the 'Double Taut-Wire' Modification (102 kN/m)

Figure 6.42

6.7.3 Discussion of Results for the Wire Modification

The discrepancies between the predicted and measured results were thought at first to be due to incorrect theoretical values for the stiffness element. When the stiffness of the modification was adjusted, very good prediction results could be obtained. Two possibilities that could account for the lower actual stiffness of the wire modification have been investigated and these are discussed below.

(i) Insufficient Tension in the Wire.

If the wire becomes slack at any time during the vibration, the modification constitutes a non-linearity – a one-sided spring – and this could account for the discrepancies observed. The operating tension level in the wire must always be positive.

The preliminary tests where the wire pre-tension was varied over a wide range (Figure 6.39.) have demonstrated that this is not the cause of the problem. The characteristics of the structure did not change when the wire remained in tension throughout the complete test.

(ii) Incorrect Wire Stiffness Assumed in the Prediction.

Care was taken to measure the stiffness of the actual wire modification for use in the theoretical prediction. The static stiffness was measured several times and the results were repeatable. Nevertheless, it was thought that with the tumbuckle as part of the modification, the dynamic stiffness may be different. The following method was used to measure the dynamic stiffness of the total wire modification.

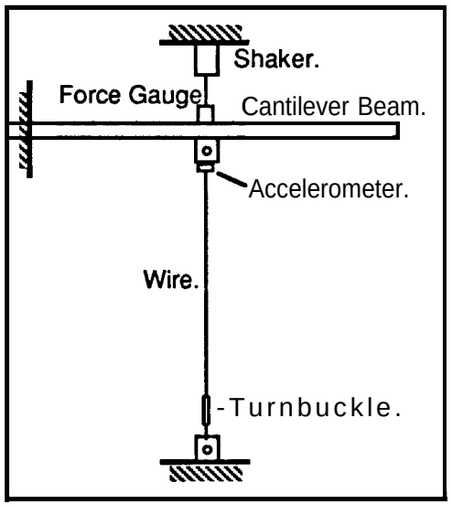

Experimental Arrangement for Measurement of the 'Dynamic Stiffness' of the Single Wire Modification

Figure 6.43

A simple cantilever beam arrangement was set-up, as shown in Figure 6.43. A point FRF measurement was made at a point about half-way along the beam. The wire modification was then attached at the measurement point and tensioned with the turnbuckle. Another measurement was made for the point FRF of the modified structure. The point FRFs before and after modification of the beam can be seen in Figure 6.44 and there are several points that it is worth noting:-

(i) the resonances are clearly defined,

(ii) there are significant shifts in the resonance frequencies when the modification is made (e.g. 13.5 Hz to 26 Hz);

(iii) the anti-resonances are defined clearly, but limitations of the analogue-to digital conversion process are evident;

(iv) the anti-resonance frequency does not change when the modification is made. This indicates that the modification is in a single degree-of-freedom and that it is made at the measurement point (chapter 3);

(v) only a light pre-tension of the wire was necessary; and,

(vi) all the measurements were repeatable.

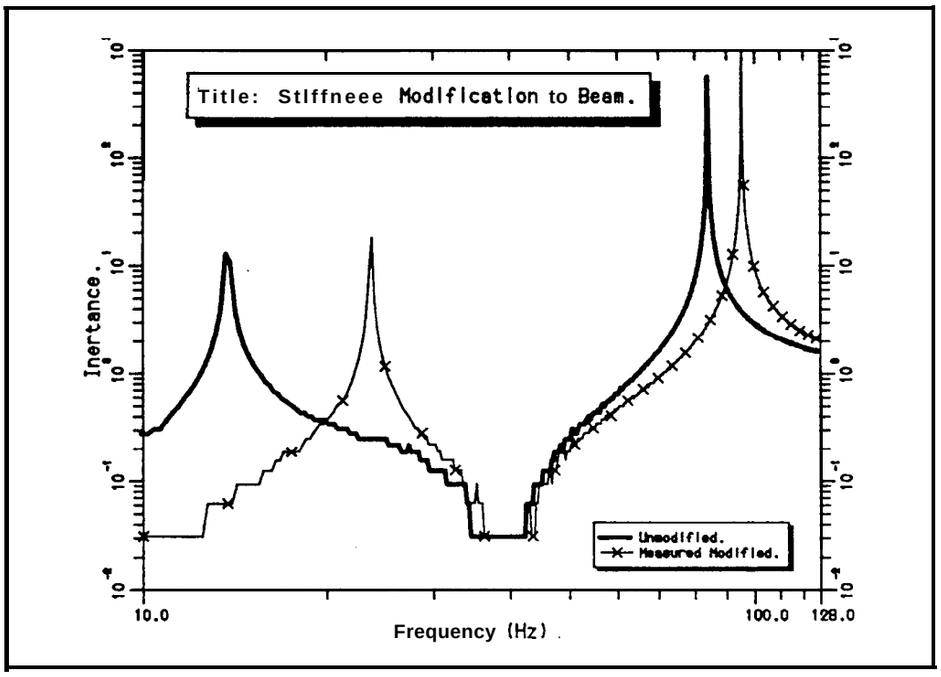

FRFs Before and After Modification to the Beam

Figure 6.44

With the assumption that the modification is a single degree-of-freedom modification at the measurement point, it is a simple process to work back from the point FRFs for the unmodified and modified structure, using equation (2.11), to find the FRF characteristics of the modification itself;

$$\frac{1}{\alpha} = \frac{1}{\alpha_a} + \frac{1}{\alpha_b}$$

where, α = inertance

and subscripts, a = unmodified beam

b = wire modification

c = modified beam.

α_a and α_c have been measured, so

$$\alpha_b = \frac{\alpha_a \alpha_c}{\alpha_a - \alpha_c} \qquad \text{.....(6.2)}$$

This calculation has been performed with the raw measured data shown in Figure 6.44 and the result is presented in Figure 6.45: a straight line of slope +2 on an inertance plot –

a stiffness line, as would be expected for the properties of the wire modification. In the frequency range around the anti-resonances of the unmodified and modified beam, the results for the properties of the modification are very poor. This is a direct consequence of the data acquisition digitisation errors that occur for the very small responses measured at these frequencies. The approximate value of the stiffness was calculated as 87.8kN/m; once again very close to the static stiffness measured and used in the theoretical predictions.

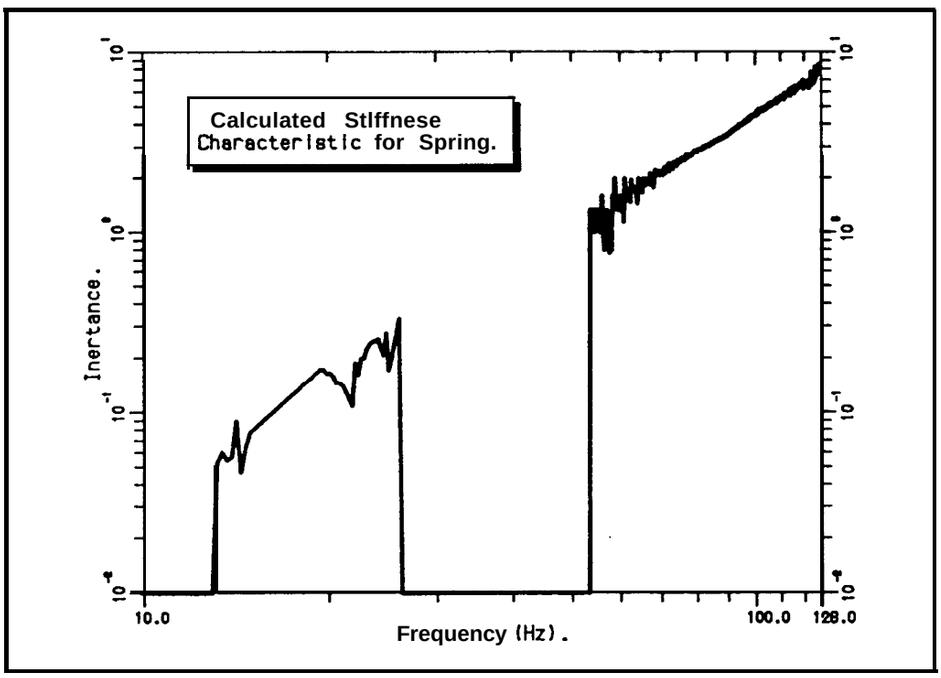

Calculated Stiffness Characteristic for the Single Wire Modification

Figure 6.45

Neither of these possibilities can account for the 30% reduction in apparent stiffness of the modification when it was applied to the helicopter.

More Detailed Study of the Dynamic Behaviour of the Tailplane

The search for an explanation of the discrepancies observed between the measured and predicted results for the wire modifications led to a closer examination of the interface between the tailplane and the fin of the helicopter. The tailplane is attached to the fin at a single point, approximately a tenth of the base chord back from the leading edge. The joint itself is some form of elastomeric bush arrangement and this fact has introduced the possibility of non-linear behaviour as the cause of the discrepancies observed

To investigate the possibility of non-linear behaviour of the tailplane joint for the 4th mode of vibration (17 Hz; tailplane fore/aft bending), a series of sine sweep measurements, at different levels of excitation input, were carried out using a Solartron 1172 Frequency Response Analyser (FRA). The equipment was set-up with the excitation applied in the Y-direction at point 66 and the response was measured at point 49 in the X-direction.

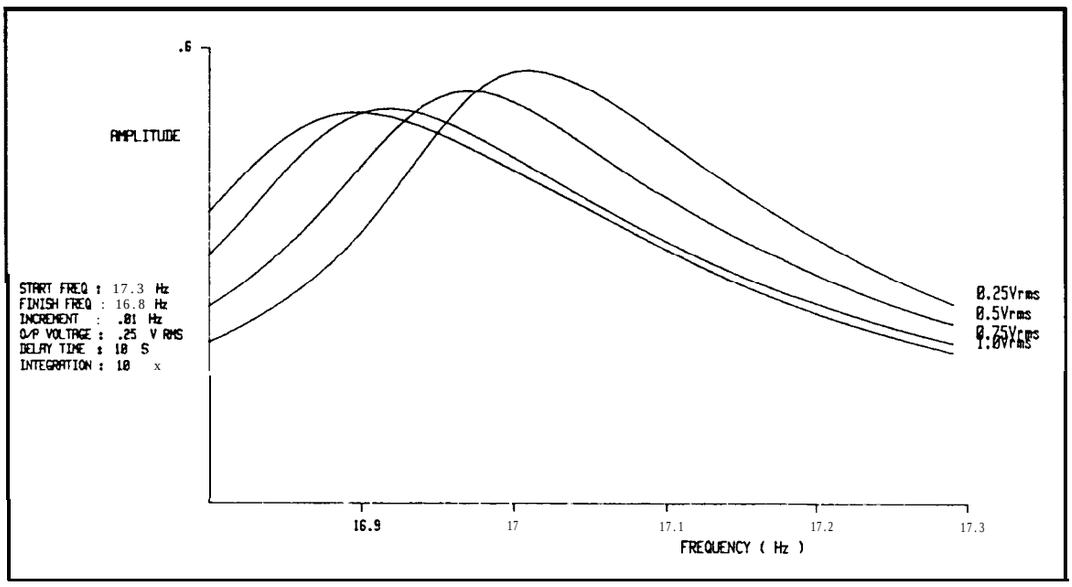

Sine Test FRFs for Mode 4, Measured with Different Excitation Levels

Figure 6.46

Measurements were made sweeping up and sweeping down over the frequency range 16.8 to 17.3 Hz and the results from the measurements were compared to ensure that a sufficiently low sweep rate was used. The power amplifier was set to constant current configuration and four measurement sweeps were taken for excitation signal levels of 0.25v, 0.5v, 0.75v and 1.0v from the FRA. The results are shown in Figure 6.46, from which it can be seen that;

(i) the resonance frequency drops as the forcing level increases;

(ii) the maximum inertance amplitude reduces with increasing force level;

(iii) the incremental reductions in resonance frequency and maximum amplitude become progressively smaller as the force increases – it would appear that, above a certain force, there will be no further changes in resonance frequency and maximum amplitude (however, this aspect could not be investigated any further due to the already large levels of response for the tailplane); and,

(iv) the FRFs measured with force levels of 0.25v and 0.5v are not symmetric about their resonance frequency points.

These observations lead to the conclusion that the tailplane joint is, indeed, non-linear and has the characteristic of a softening spring; as force is increased, the stiffness (slope of the line) reduces.

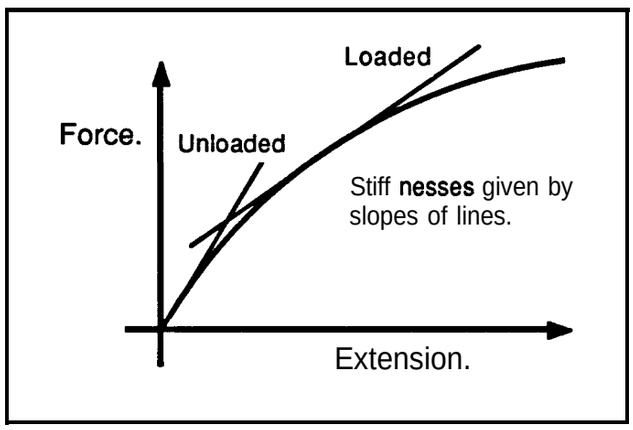

A Softening Spring Characteristic.

Figure 6.47

A softening spring characteristic like that shown in Figure 6.47 helps to explain the differences observed between the measured and predicted results for the helicopter with the wire modification. Consider the following hypothesis in which it is assumed that the wire modification acts in two stages; (i) the effect of the wire pm-load on the structure, and (ii) the stiffness effect of the wire itself:

> The wire modification acts across the tailplane joint and the effect of the wire pre-load on the joint is to cause the stiffness of the joint to reduce (a softening spring). The natural frequency of the tailplane fore/aft bending mode drops as a consequence of the reduced joint stiffness. The base condition of the helicopter is altered by the effect of the pre-load alone. Now, when the stiffness of the wire modification is included, the effect is added to the new base condition created by the pre-load, raising the natural frequency of the 4^{th} mode again. The final predicted result for the frequency of the 4^{th} mode is not as high as when the pre-load effect is ignored in the prediction.

In order to try and test the mechanism proposed in this hypothetical argument, some further measurements were necessary. The object was to investigate whether application of a pre-load to the tailplane would cause the natural frequency of mode number 4 to drop sufficiently to account for the differences between the measured and predicted results for

the wire modification. It was difficult to apply a pre-load force to the tailplane without introducing any other modification effects. As a compromise, a long **length** of thin bungee cord was tensioned and attached, at one end, to the tailplane. The bungee cord had a low stiffness which, together with a length of approximately 8 **m,** meant **that** the force applied to the tailplane was nearly constant throughout the vibration test. Furthermore, the thin bungee had a mass of only 74 g and so the mass loading effect was negligible. A tension of about 60 N was the maximum that could be achieved with this thin bungee cord and this was considerably less than the estimated pre-load of 600 N in the wire. The results of some sine sweep tests of the helicopter with and without the bungee in position are shown in Figure 6.48.

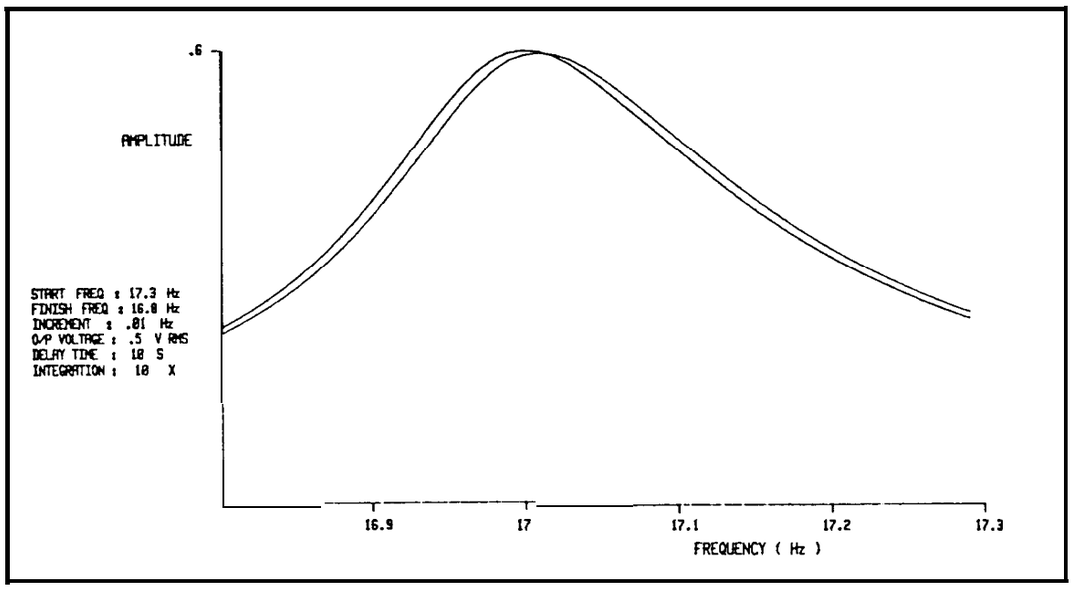

Sine **Sweep** Test **FRFs** of the Helicopter With and Without the Bungee

Figure 6.48

Analysis of these two curves has yielded the following results;

Without Bungee		**With Bungee**	
Resonance:	17.010 Hz	Resonance:	17.000 Hz
Phase:	180.78’	Phase:	180.79’
Damping Loss Factor: (variance 0.1%)	0.0115	Damping Loss Factor: (variance 0.1%)	0.012
Modal constant	7.69x10-3 Kg-’	Modalconstant	**6.97x10^{-3}** Kg’

The differences between the natural frequencies for mode number 4, with and without the bungee, are very small. The tension in the bungee was considerably less than the

estimated pre-tension in the wire and this could explain why there is only a small difference between the measured natural frequencies with and without the bungee modification. It was not possible to increase the tension in the thin bungee and, so, a larger size of bungee cord was used. Unfortunately, although the larger bungee could be tensioned to approximately 170 N, the mass loading effect of the bungee on the tailplane was much larger than before (493 g), and it was difficult to assess what caused the downwards shift in the natural frequency, the mass loading effect or the tension.

A further question to be addressed is why was this non-linearity effect was not picked-up during the preliminary tests with the wire, when the pre-load was varied over a wide range? This could be explained if the joint non-linearity was similar to a bi-linear softening spring, e.g. Figure 6.49, rather than a progressively softening spring, as shown in Figure 6.47. For a bilinear softening spring a small initial pre-load would move the mean operating point from the high- to the low-stiffness regime. A further increase in the pre-load would not produce any further change in the stiffness. The initial prediction of the effect of the wire modification is based on the, incorrect, assumption that the joint stiffness is linear and of the high stiffness value, because the measurements of the unmodified structure only exercise the structure in the high stiffness regime. In fact, the pre-load changes the base condition to a state which is not incorporated in the modal database produced from the initial measurements. If it were possible to identify accurately the new base condition of the helicopter, then it is probable that a prediction using the true value of the wire stiffness (89.1 kN/m) would produce better results.

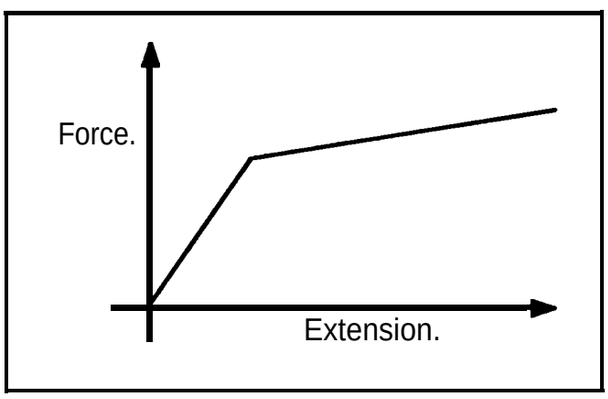

Bi-linear Softening Spring Characteristic.

Figure 6.49

In the preliminary survey of the helicopter, measurements were made at different forcing levels (section 6.3.1) to try and ascertain whether there were any non-linearities that could cause problems. No indications of the non-linearity in the tail joint were found at that stage. In hindsight, it is obvious why not. The initial checks using different forcing levels

were made using a broadband random testing technique– any form of random testing on a non-linear structure tends to linearise the results. Furthermore, the original random excitation did not allow the structural response levels to build-up to such an extent as with the sine testing method and, therefore, the non-linear&es, which are amplitude dependent, were not exercised to the same degree.

6.7.4 Modification Prediction Using Raw Experimental FRF Data

Impedance coupling methods for the prediction of the effects of modifications use FRF data (chapter 2). The FRF data can be obtained from test, modal analysis, or F.E. modelling and analysis. Modal analysis and F.E. analysis FRF data are subject to assumptions made about the structure whereas test data contain all the information and no assumptions are made about the nature of the structure. It is sometimes suggested that it may be better to use raw measured FRF data in the impedance coupling procedures. However, there are several major drawbacks to the use of such data:-

(i) it can be difficult and/or expensive to obtain a consistent data set.

(ii) it can be difficult to measure all the FRFs required (spatial incompleteness – chapter 5).

(iii) limitations of the equipment used in random testing for FFT analysis can lead to poor quality FRFs in the vicinity of anti-resonances.

Despite these drawbacks, a predominantly measured FRF data set for the helicopter has been used in a prediction of the effects of the extended mass modification. Wherever an FRF matrix term has been measured, it has been used, however, there were still 4 terms for which measured FRFs were unavailable (R66X/F66X, R66X/F49Y, R49Y/F66X, and R49Y/F49Y, identified in Figure 6.8). Since the modal analysis had already been performed, appropriate synthesised FRFs were available and these have been used instead. There are a total of 36 terms in the FRF matrix for the helicopter, the measured FRFs account for 89% of the matrix and the remainder are synthesised from the modal database.

For the extended mass modification component, the same theoretical FRF data were used as for the prediction described in section 5.1.2 (ii). The 66Y point FRF for the modified structure calculated using:- (i) the raw data set, and (ii) the synthesised data set for the helicopter are presented in Figure 6.50 together with the FRF for the unmodified state. It

can be seen that the result using raw data agrees well with that using synthesised data for the new resonances and anti-resonances of the 3rd and 4th modes. It is also apparent that there are still major resonance-like peaks at the unmodified resonance frequencies in the prediction using raw data. This phenomenon was observed by Henderson [14] and is termed 'breakthrough'. It is caused because the raw data does not come from a consistent data set – each resonance has a very slightly different natural frequency for each measured curve. In this instance, it is the result of different interaction of the shaker with the helicopter at different points and variation of the helicopter's properties with time. Simultaneous multi-point excitation tests may improve the consistency, but it is still very unlikely that the whole FRF matrix could be measured at one time and so there will always be some variation.

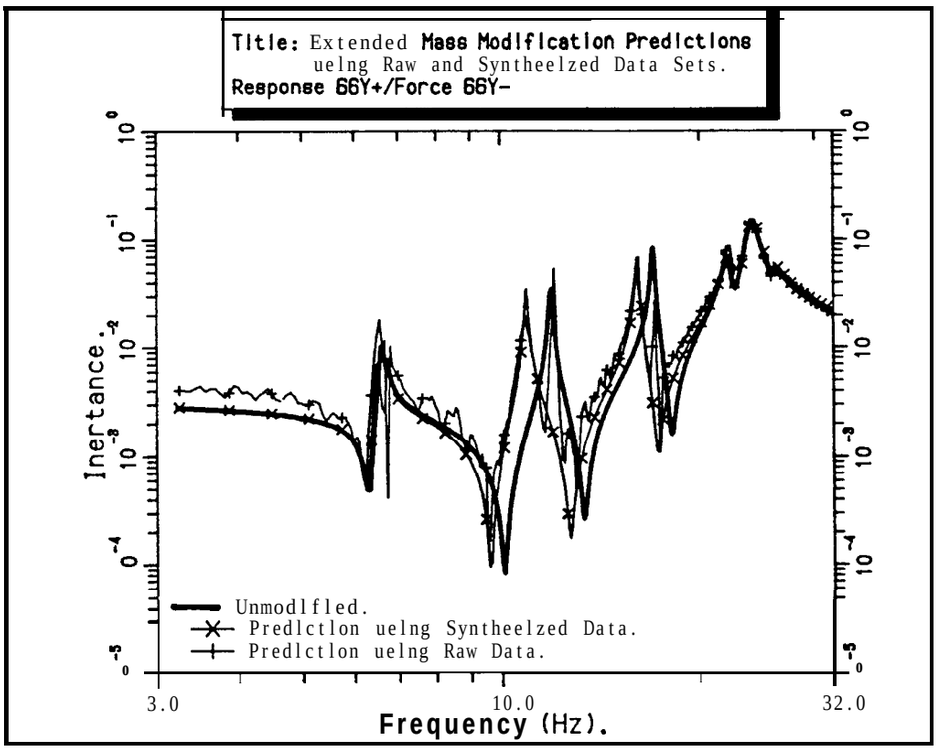

Comparison of Results Using Raw & Synthesised Data in Predictions of the Effects of the Extended Mass Modification

Figure 6.50

Definition of the anti-resonances in the prediction using raw data is of a similar quality to those measured for the unmodified condition. The prediction using synthesised data has clear, sharply defined anti-resonances in the same way as the synthesised data for the unmodified structure.

Using the raw data in this way provides confirmation that the modal analysis model of the helicopter, from which the synthesised FRF data were created, is adequate for this particular modification and that sufficient modes and residual terms have been included in the synthesised FRF data set.

6.7.5 Presentation of Data

Composite Response Spectra

The ultimate aim of a structural modification process, such as that described here, is the overall improvement in the vibration characteristics of the structure under its normal operating conditions. Reduction of the vibration level at one point may be accompanied by a severe increase elsewhere. Furthermore, the actual responses will be dependent upon the magnitudes and location of multiple force inputs. While multiple forcing does not influence the resonance frequencies, it does affect the off-resonance behaviour. For this reason it is important to examine a weighted composite response spectrum to assess the overall behaviour of a structure. An estimate of the magnitude of each force input is required so that response spectra for each location may be generated. An indication of the overall performance of the structure is obtained by forming a weighted sum of these spectra. The weighting to apply to each response spectrum would reflect the importance attached to the motion at each particular location, e.g. a location on the pilot's seat in a helicopter would have a much higher weighting than a location on, say, part of the undercarriage. Integration of the composite response spectrum over a small, key, frequency range yields a number which can be used as a performance indicator. Different modifications will give different performance indicators and the best modification can then be selected.

To investigate the use of composite response spectra, various FRF data for the helicopter have been summed together:-

(i) raw measured data for the unmodified helicopter;
(ii) synthesised data for the unmodified helicopter;
(iii) raw measured data for the helicopter modified with the extended mass; and,
(iv) data predicted for the helicopter modified with the extended mass.

For each example, the magnitudes of the 6 FRFs for coordinate 66Y excitation are added together to form the composite response spectrum, i.e. all the FRFs are given equal weighting and no phase information is used. Comparisons of these composite spectra are presented in Figures 6.54 and 6.55.

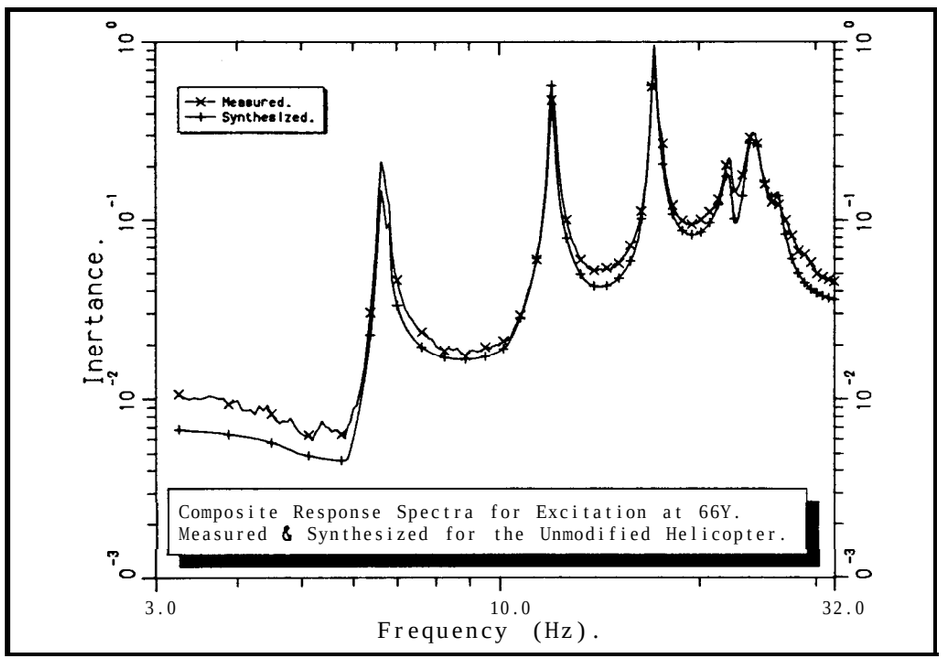

Composite Response Spectra for Excitation at 66Y
Measured & Synthesised Data for the Unmodified Helicopter

Figure 6.51

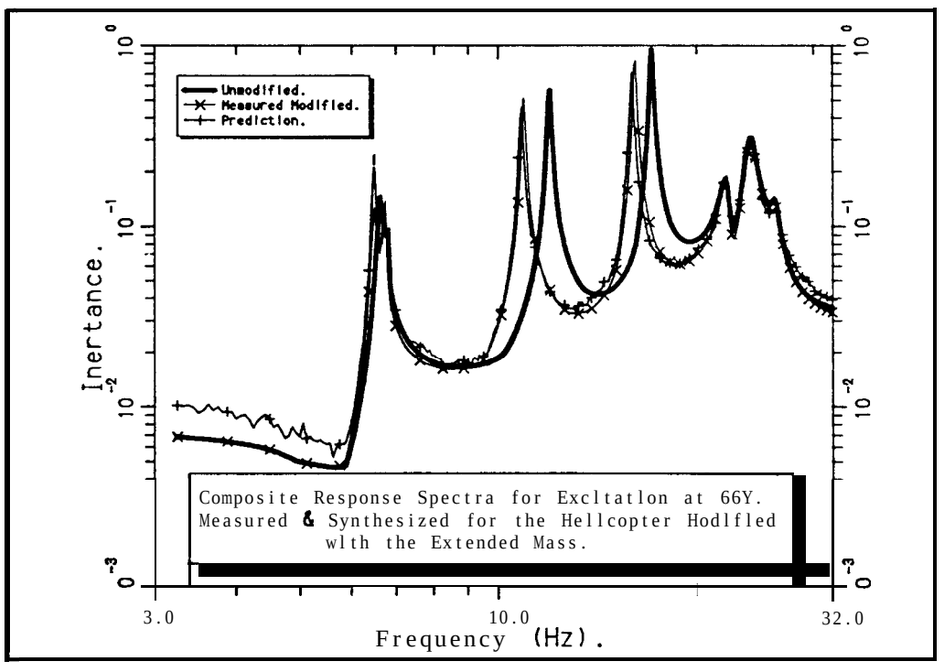

Composite Response Spectra for Excitation at 66Y
Measured & Synthesised Data for the Helicopter Modified with the Extended Mass

Figure 6.52

It will be seen that these composite response spectra have typical resonance characteristics of an FRF, but no anti-resonance features. This is simply due to the fundamental difference between resonances and anti-resonances. Resonances are global properties – they have the same frequencies regardless of where they are measured on the structure but, not all FRFs have anti-resonances at identical frequencies. When the FRFs are added the anti-resonance features disappear, while the resonance features are reinforced,

It will be seen from Figure 6.51, showing the measured and synthesised FRFs of the unmodified helicopter, that there are now only small discrepancies in the off-resonance regions for the composite spectra. The summation process has smoothed out the irregularities in the individual raw data FRFs. The agreement between the composite response spectra for the raw and synthesised data close to resonances is generally good.

The composite response spectra, shown in Figure 6.52, for the helicopter with the extended mass modification are superimposed on the composite spectrum for the unmodified state to indicate the substantial effects of this simple modification. There are slight differences in the predicted and measured resonance frequencies for modes 3 and 4, but these differences are small in comparison with the changes from the unmodified state. The prediction has underestimated the actual effect by a small amount.

Correlation Plots

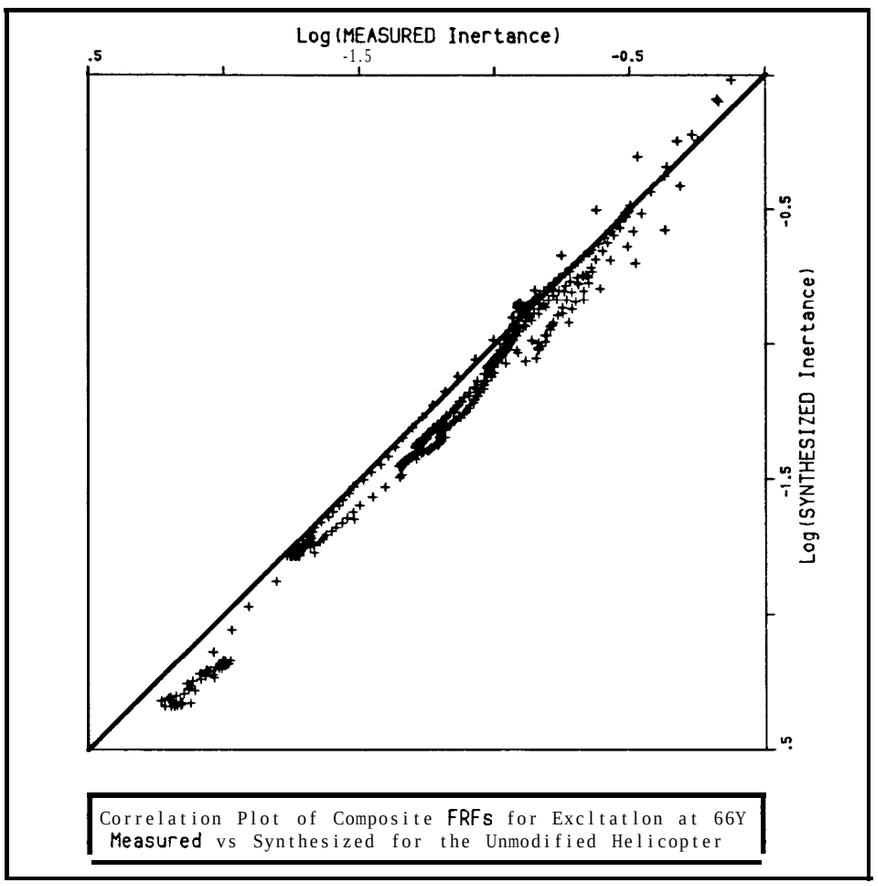

Figure 6.53

Another alternative method of presentation has been used for comparison of this data-&relation Plots, Figures 6.53 and 6.54. When there is perfect correlation of the two data sets, the points lie on a straight line of slope **+1,** passing through the origin. Deviation from this line indicates correlation errors. It can be seen from Figure 6.53 that there is generally good correlation between the measured and synthesised data for excitation in the Y-direction at point 66. There are no obvious loop characteristics at high inertance values which tend to indicate incorrect estimation of the natural frequencies.

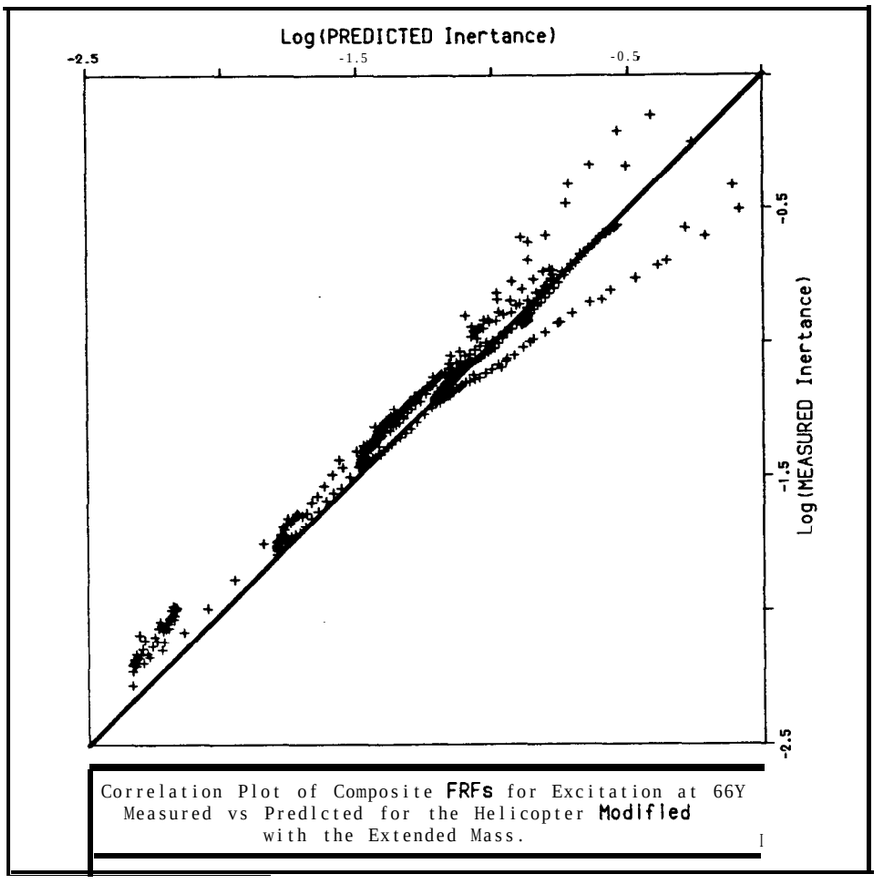

Figure 6.54

In the correlation plot of the measured and predicted data for the extended mass modification (Figure 6.54) there are discrepancies around the natural frequencies which show up as loops in the plots towards the top right-hand end of the correlation line, i.e. the large inertance values at resonances indicating erroneous prediction of the resonance frequencies for the modified structure. Similar 'loop characteristics' in this type of plot were noted by Kirsenboim [90] for FRFs measured with sine excitation at different force levels. In [90], estimation of the loop area is taken as a measure of the degree of non-linearity exhibited by the test structure. The main disadvantage of this type of plot is that there is no indication of frequency, so it is not easy to see which mode is incorrectly predicted from this plot alone.

6.8 Review of Chapter 6

There were two main objectives of the case study on the helicopter:

(i) evaluation of the data assessment and sensitivity analysis techniques with a set of experimentally-derived data; and,

(ii) demonstration of the present ability to predict the effects of a modification.

From initial measurements of the helicopter it was found that the resonance frequencies were approximately equal to those measured in previous tests, and comparable with the frequencies predicted from F.E. models. The AFRF was used successfully in assessment of measured data for repeatability and reciprocity. Small differences between response functions were shown clearly by peaks in the AFRF. Visual comparisons of FRFs for repeatability and reciprocity checks are a highly subjective method of assessment and would not have yielded the same quality or quantity of information.

Restricted access to several points on the helicopter prevented measurement of the complete FRF matrix. Such measurement restrictions are not uncommon and, in fact, it is rarely possible to measure the complete FRF matrix. Fortunately this is not usually too much of a problem because, by modal analysis and synthesis techniques, a full set of FRFs can be generated from measurement and analysis of a single row or column of the FRF matrix. Attempts were made to derive specific FRFs from FRF measurements made at an angle to the coordinate axes. Where the point under consideration was situated on a reasonably mobile part of the structure, derivation of FRFs in the Cartesian axis coordinate directions from angled excitation measurements proved to be a viable proposition. However, for a point on a comparatively immobile part of the structure, the transformations to form the desired FRFs involved small differences of large numbers and, together with the added problem of rather 'noisy' measured FRFs, the results were of a rather poor quality and certainly not good enough for incorporation in any modal analysis procedure.

It should be noted that although it is theoretically possible to use measured FRFs directly in an impedance coupling procedure this is not often feasible because, as mentioned above, the complete FRF matrix is rarely measured.

Difficulties were also encountered with measurement of rotational degree-of-freedom FRF properties by the T-block method. Despite careful checks of reciprocity and repeatability of translational FRFs measured on the T-block, transformation of these FRFs to a 'rotational set' yielded poor results for all terms involving at least one rotational coordinate

although the point translational FRFs derived from measured T-block data matched closely those measured in the traditional way. Some rotational FRFs were ill-defined – due to use of measured data directly in the transformations – but, more seriously, the rotation/rotation FRFs had no modal features, just the characteristics of a simple spring element. Eventually the cause of this behaviour was traced to the flexibility of the joint between the T-block and the helicopter. The interface joint was much less stiff than the surrounding structure and motion of the T-block relative to the helicopter tended to dominate the measured response. Unless the attachment can be made with sufficient rigidity to ensure that motion of the structure is transmitted to the accelerometers faithfully over the frequency range of interest, the measured FRFs will contain an unknown contribution from the joint flexibility. In structural modification predictions it is sometimes assumed that a rotational transducer block is joined to the structure in the same way as a subsequent modification would be, and hence, that the unknown effects of the joint will be the same in each case. Although successful modification predictions based on this assumption have been reported, [9], there is little direct evidence to support this assumption for general application. For this investigation, modifications were confined largely to those in which rotational degree-of-freedom properties were not actively involved in the coupling, i.e. pin-jointed modifications.

After a full measurement survey of the translational degree-of-freedom FRFs of the helicopter, the Polyreference technique was used successfully for modal analysis of the data. Two methods were then employed for evaluation of the low-frequency residual terms associated with rigid body motion of the helicopter (there was no requirement for high-frequency residuals because the measured frequency range extended sufficiently above the frequency range of interest),

(i) by comparison of synthesised and measured FRFs; and,

(ii) by rigid body mechanics calculations with mass and inertia properties supplied from a F.E. model of the helicopter.

It was not possible to generate residual corrections for all the FRF elements by the comparison technique because not all FRFs had been measured and, also, it was found that residual terms generated by rigid body mechanics calculations were more consistent than those calculated by comparison of measured and synthesised FRFs. The low-frequency residual corrections were added to the synthesised FRFs which then compared very well with their measured counterparts with the exception of FRFs for excitation at coordinate 66X – along the fuselage axis.

The measurements for this case study of the helicopter confirm that it is quite feasible to measure sufficient, consistent and accurate data for modal analysis and subsequent structural dynamic modification prediction for a large and complex structure, by means of successive single-point excitation tests.

The new sensitivity analysis method (developed in chapter 3) was applied to the point FRFs and the results correctly identified that mode 3 was particularly sensitive to modification at coordinate 49Z and that mode 4 was sensitive to changes at 49X. Input data for the sensitivity analysis – resonance and anti-resonance frequencies – were easily obtained by use of peak- and valley-picking routines on the synthesised FRFs. Checks on the static accelerance of each plot showed, repeatable and consistent results for all point FRFs except those for coordinates 66X and 49X.

Two types of modification have been used in demonstrations of the ability (or failure) to predict the effects of structural modifications on the dynamic characteristics of the helicopter:

(i) several mass modifications; and,

(ii) a stiffness modification between two points on the helicopter.

Predictions of the effects of a single degree-of-freedom modification are trivial in comparison to other, more extensive, modifications. However, a single degree-of-freedom mass modification was used to demonstrate that anti-resonance frequencies remain unchanged for all FRFs that have at least one coordinate in common with the single degree-of-freedom modification.

When a mass modification was bolted to the helicopter – a coupling involving all 6 degrees-of-freedom – prediction of the effects based on models deficient in rotational information was found to give incorrect results. The size of errors between the predicted and measured FRFs for the modified structure gave an indication of the importance of the rotational degrees-of-freedom in the coupling. However, when a modification which did not involve any rotational degrees-of-freedom was made– the extended mass modification – the predicted and measured FRFs showed a high level of agreement. For this modification the actual major resonance frequency shifts were predicted reasonably accurately from the sensitivity analysis results, but the theoretical analysis of chapter 3 indicated that all such predictions should be treated with the utmost caution.

A tensioned single-strand steel wire was used as a stiffness modification between the tailplane and the intermediate gearbox on the helicopter. The actual modification

approximated a pin-jointed stiffener between the two points, but, despite careful measurements for the dynamic properties of the modification, it was still not possible to predict its effects on the dynamic characteristics of the helicopter accurately. The single mode frequency that would move significantly was correctly identified, together with the fact that all other mode frequencies would remain virtually unchanged, however, the magnitude of the single frequency shift was significantly over-estimated. Initially the problem was thought to be with the dynamic characteristics of the wire modification or the attachment fixtures but, subsequently, it was found to be a non-linearity in the tail-plane joint which was only exercised sufficiently when the wire was connected and tensioned. Motion of the tail-plane joint during testing of the unmodified helicopter was too small to show-up the non-linear effects.

These coupling exercises have demonstrated that, although theoretical techniques for prediction of the effects of a modification are well developed, practical implementation of the methods is not simple and straightforward. The most serious problem is usually incomplete, rather than inaccurate, dynamic models of the component parts. Nevertheless, with care and attention to detail during the early planning and data acquisition stages, many of the problems can be overcome or, at least, their effects minimised. The success of the ‘extended mass‘ modification predictions are an indication of what can be achieved.

Chapter 7

Conclusions

7.1 Conclusions

7.1.1 Collection and Assessment of Experimental Data

At the outset of any structural modification exercise based on the use of experimentally-derived data, it is important that the general type and possible location of any modifications are pre-defined and clearly stated. It is rare for there to be a completely free choice of the type and location of modifications and the earlier that these practical restrictions are recognised the better. Furthermore, careful consideration should be given to the way in which the final modifications will be attached. If bolted, riveted or welded joints will be used (involving considerable rotational restraint at the joint) then it is vital that dynamic data for rotational degrees-of-freedom are also measured for incorporation in modification predictions.

The use of experimentally-derived data as a basis for prediction of the effects of structural modification has several advantages. The most important advantage is that measured data are a record of exactly how a structure behaved during a particular test, whereas theoretically-derived data constitute an idealised representation of the dynamic behaviour of a structure based on a series of assumptions about structural detail and deformation characteristics. It is important to remember that the dynamic model of a structure can only be as accurate as the data from which it is derived (measured or theoretical). For this reason a means for assessing the quality of measured data is desirable. In this work, the

'difference frequency response function' (AFRF) has been used extensively in the assessment of reciprocity, repeatability and synthesised data. The AFRF is a very simple and versatile function that has the same characteristics as a standard FRF. It can be formed from measured data directly and, consequently, any adjustments to the measurement technique that may be necessary can be accomplished at the earliest possible stage. The AFRF highlights differences between FRFs that may be overlooked normally. If a AFRF peak coincides with a resonance frequency of the FRFs, a slight difference in the resonance frequencies of the two FRFs is probably the cause. When a AFRF peak occurs elsewhere in the frequency range it is unlikely to be as sharp as that found at a resonance frequency nor to have such a large magnitude and it is probably the result of magnitude differences between the FRFs.

The new sensitivity analysis technique is based on the use of resonance and anti-resonance frequencies derived from measured point FRFs. Resonance frequency information of sufficient accuracy can be obtained from measured FRFs with the aid of a peak-picking routine. Anti-resonance frequencies can be more troublesome to locate precisely than resonance frequencies and this is particularly true with broadband measurements where amplitude resolution in anti-resonance regions is often poor and the true anti-resonances may not be obvious. The definition of an anti-resonance can be improved if the broadband test is conducted over a narrow frequency range or if a zoom measurement technique is used – thus increasing the frequency resolution and possibly reducing the overall dynamic range of the FRF in the measured frequency band. A more efficient measurement technique is that of sine testing whereby measurements are made at discrete frequencies. Sine testing has several distinct advantages,

- quantification of the response at each discrete excitation frequency is completely independent of that at any other frequency: all frequency points are defined to the same percentage accuracy;
- the structure only responds to a single frequency input and hence the signal to noise ratio is very much higher than for broadband measurements; and,
- the measurement method does not restrict the distribution of points throughout the frequency range. Data points may be concentrated in resonance and anti-resonance regions, where the rates of change with frequency are high. Where the FRF varies more slowly data points can be spread out.

It is always important to remember the fundamental difference between a resonance and an anti-resonance; a resonance is a global property and an anti-resonance is a local property. Anti-resonance frequencies are dependent upon the choice of excitation and response coordinates whereas natural frequencies are not. As a consequence, anti-resonance frequencies of derived functions – such as **ΔFRFs,** rotational **FRFs** and **FRFs** in different coordinate systems – will **not** have the same anti-resonance frequencies as the measured **FRFs** used in their generation. Data points cannot be grouped in the frequency range as necessary without some prior knowledge of where the anti-resonances of the derived functions will be located.

The importance of a thorough and carefully planned preliminary survey of the dynamic characteristics of **all** the components involved in a structural modification must be emphasised. Results from the preliminary surveys enable identification of the sensitive degrees-of-freedom, 'tuning' of modifications to exploit these most sensitive **degrees-of-**freedom and optimisation of the full test program such that the most important data are measured with the greatest accuracy.

The use of shaker excitation techniques in a preliminary survey can be time consuming because the shaker has to be re-positioned and realigned for each separate measurement. Usually, high quality data are obtained but, in proportion to the time taken for a complete measurement survey, such a lengthy preliminary survey may not be justifiable. An alternative method of testing is to use impact excitation but this also has disadvantages; e.g. the low total energy input, poor repeatability and poor results when non-linearities are present. However, further investigation is required, on a real structure, to ascertain whether the results obtained from impact testing are acceptable for the purpose of ranking the coordinates in a sensitivity analysis.

7.1.2 Refinements of the Impedance Coupling Method

With the growing complexity of structures in recent years, there has been a trend for the size of dynamic models to increase. This has brought with it a penalty in terms of computation time when the dynamic models are used in impedance coupling predictions. A development of the impedance coupling technique has been found that decreases the computation time very significantly by reducing both the size and the number of matrix inversions necessary. Further development of this method has now extended it for use with simple spring type modifications which do not have inertance matrix representations. In addition to marked increases in computational speed, these new formulations are

potentially more accurate than the original methods because there is less opportunity for the build-up of errors with numerical inversion of large matrices. The size of the matrix for inversion is limited to the number of interface coordinates and, consequently, improvements in speed will be greatest for systems which have a low ratio of interface coordinates to the total number of coordinates.

7.1.3 Development of a New Sensitivity Analysis Technique – A Guide to Structural Modification

Sensitivity analysis techniques are frequently used in theoretical (F.E.) studies to locate the most suitable type and site for a modification to bring about a desired change in the dynamic behaviour of a structure. In this study a relatively simple sensitivity analysis technique has been developed that can be used with measured data from a preliminary survey of the structure. This new sensitivity analysis technique enables the differential sensitivity $\left.\frac{d\Omega_p}{dm}\right|_{m=0}$ of any particular resonance frequency to be calculated for single degree-of-freedom mass (or stiffness) modifications. The value of this differential sensitivity for infinitesimal single degree-of-freedom mass or stiffness modifications is the criterion upon which coordinates are ranked in their order of importance for influence on the resonance frequency of a particular mode. For many applications, particularly aerospace structures, the smaller the modification that has the desired effect, the better – unnecessary mass represents wasteful loss of revenue-earning payload. The coordinate ranking information can be valuable in several different ways,

- identification of the coordinates at which modification is most appropriate;
- provision of guidelines for the design of a real modification to exploit all of the most sensitive coordinates;
- identification of the coordinates at which the loading effects of the measurement apparatus (transducers, shaker, etc.) on the structure are most likely to affect the FRF results; and,
- help in production of a test schedule for the full measurement phase in which limited time and resources can be used efficiently to collect only the most important data.

This new technique is intended, initially, as a ‘guide to structural modification’ only.

Resonance frequency sensitivity equations have been derived for both grounded and free types of structure for single degree-of-freedom mass or stiffness modifications. Additionally, it has been shown that the stiffness sensitivity equation can also be used with difference FRFs between two coordinates for the sensitivities of modes to internal stiffness modifications between two points. This is especially useful since an internal stiffness modification is a much more practical type of modification than a single degree-of-freedom spring modification in which one end of the spring is connected to ground. In just the same way that resonances may be shifted away from an excitation frequency to reduce a vibration problem, so it may also be possible to move a particular structural anti-resonance to coincide with an excitation frequency. A similar analysis has been performed for the anti-resonance frequency sensitivity at one point due to single degree-of-freedom mass modification at a remote point (Note; for FRFs which have at least one coordinate in common with the single degree-of-freedom modification, none of the anti-resonance frequencies change). In addition to point FRF measurements required for the resonance frequency sensitivity, transfer measurements are necessary for evaluation of the anti-resonance frequency sensitivity. It should be noted that, in general, repositioning anti-resonances may not be as efficient as repositioning resonances for the control of structural vibration because anti-resonances are local, and not global, properties of a structure.

All of the sensitivity equations developed in this work (for resonances and anti-resonances) are based on a rational fraction form of representation for an FRF. The exact rational fraction representation of an FRF involves products of an infinite number of resonance and anti-resonance frequencies. In practice, the number of terms in the products is limited to the number of modes measured. Provided that the ratio $\left(\frac{\omega^2}{\Omega_N^2}\right) \ll 1$, the FRF synthesised from this rational fraction formulation is an accurate representation of the actual FRF. The measured frequency range should extend to include several modes beyond those in the frequency range of interest to ensure that this criterion is met.

All FRFs can be represented in rational fraction form. For point FRFs all resonances and anti-resonances have real frequency values, but for transfer FRFs, some of the 'anti-resonance' frequencies may be imaginary. An imaginary anti-resonance frequency corresponds with a minimum between two resonance peaks instead of the zero of a real anti-resonance.

It has been shown (section 6.7.1) that the new sensitivity analysis technique can be used successfully to predict the most effective coordinates for modification but that, except under certain circumstances (such as for small modifications), use of the 1st and 2nd order

sensitivity values in a Maclaurin's series expansion should not be relied upon to give good estimates of the new resonance frequencies for a modified structure, particularly when predicting the effects of 'large' modifications. (It should be noted that similar restrictions will also apply to the use of **any** sensitivity parameters howsoever derived). Theoretically it is possible to continue the differentiation process to obtain higher order sensitivity parameters but this is not really a practical proposition. For ranking of coordinates in an order of importance it is not necessary to measure the resonance and anti-resonance frequencies to a high degree of accuracy, provided that the overall ranking is not altered by slight variations in the frequencies. The reliability of a ranking can be checked by recalculations with small, but representative perturbations of the resonance and anti-resonance frequencies supplied.

An important physical concept used during the development of the sensitivity analysis technique is that none of the anti-resonance frequencies moves for FRFs with at least one coordinate in common with the single degree-of-freedom modification made. This phenomenon can be used as a very simple practical test of whether an intended single degree-of-freedom modification is indeed active in only one degree-of-freedom.

7.1.4 Inaccuracy and Incompleteness of Experimentally-Derived Dynamic Models

Any experimentally-derived mathematical model of the dynamic characteristics of a structure will be incomplete and inaccurate; it is the degrees of incompleteness and inaccuracy that are important. Some factors which affect the accuracy of measured vibration data are as follows,

- selection of the most appropriate transducers for the application (measurement capacities vs transducer size);
- attachment of transducers to the structure;
- cross-axis sensitivities of transducers;
- loading of the structure by the measurement equipment (transducers and shaker system, etc.). It has been shown that, in some circumstances, mounting the force gauge upside-down may make the loading effects of the force gauge more consistent – particularly when there is large cross-axis motion – and hence more amenable to subsequent loading corrections; and,

- accuracy of equipment used to quantify the transduced signals (e.g. limited dynamic range and digitization errors).

Incompleteness in a dynamic survey can take two forms,

i) Modal incompleteness – where insufficient modes are included either by poor choice of excitation point or frequency range; and,

ii) Spatial incompleteness – where measurements are made at insufficient coordinates on the structure.

Modal incompleteness restricts the frequency range over which any synthesised FRFs are valid. Spatial incompleteness in a set of measured FRFs means that structural mode shapes cannot be defined uniquely. If the spatially incomplete data set is used in a modification prediction, the quality of the results depends on whether the spatial incompleteness extends to some of the interface coordinates, i.e. whether FRFs for all the degrees-of-freedom actively involved in the coupling are included. If all the data for the interface coordinates are included in the coupling, predictions for the characteristics of the modified structure will be accurate in a global sense (modified resonance frequencies and damping values) but still incomplete in the spatial sense (non-unique definition of mode shapes). However, if the spatial incompleteness extends to the interface degrees-of-freedom in a coupling prediction, the results will be incorrect in both the global and the local senses. The degree of error will be largely a reflection of the relative importance of the degrees-of-freedom omitted from the mathematical coupling procedure. The most frequent cause of spatial incompleteness in measured data is the absence of rotational information. Rotational type measurements are often 'overlooked' in measurement surveys because there are relatively few transducers for direct measurement of rotations. Furthermore, accurate derivation of rotational data from suitable translational measurements can be difficult to achieve. Some work is being done on the development of transducers for the measurement of rotational response data but, this alone, will not facilitate direct measurement of the complete FRF matrix – methods for application and measurement of a pure torque excitation are also necessary.

The lack of success with accurate measurement of rotational FRF properties of a test structure has led to doubts about the incorporation of rotational degree-of-freedom data in modification predictions. The traditional, implicit, assumption is that the interface joint between the rotational transducer and the test component is either rigid or identical to the condition that will pertain when the component and structure are joined. There is little

evidence to support such assumptions in the majority of cases. Measured rotational degree-of-freedom FRF properties will, therefore, always contain an unknown contribution from the joint flexibility which will propagate into any modification predictions. Until an accurate reliable and easy-to-use method for the measurement of all rotational degree-of-freedom FRF properties becomes available, the use of modification components including rotational restraints should be questioned seriously. Pin-jointed modification components have no rotational constraint and hence there is no need for rotational degree-of-freedom properties. Pin-joints do, however, severely reduce the potential effectiveness of certain modifications, e.g. a pin-jointed beam modification is substantially less stiff than a bolted beam (encastré). Nevertheless, in the interest of being able to predict the behaviour of a modified structure accurately and reliably, the reduced effectiveness of such modifications may be an acceptable penalty in order to avoid unforseen problems caused by inaccurate assumptions about joint characteristics.

7.1.5 The Helicopter Case Study

The inability to measure acceptable rotational degree-of-freedom FRF properties of the helicopter restricted the case study to the use of simple pin-jointed modifications – mass additions and wire stiffness modifications.

The case study of a helicopter structure has allowed a very limited trial of the data assessment and sensitivity analysis techniques on real measured data. The modal database for translational degrees-of-freedom, created from the measured data, was judged to be of a good quality based on a comparison of measured and synthesised functions using the AFRF. Very successful prediction results were obtained for the helicopter modified with a mass, but the results for the taut wire modification were not quite so good. The prediction correctly identified the mode with the greatest shift in frequency, but the extent of the frequency shift was over-estimated. In subsequent investigations to ascertain the cause of this over-estimation of the wire's modification effect, it was found that the tailplane joint condition altered as a result of the modification – the base structure became different to that used in the mathematical prediction. Pre-tension in the wire caused the joint to operate in a different stiffness regime. Measurements of the structure's FRFs at low amplitudes of vibration did not show up the non-linear characteristics of the joint which only appeared with very large displacements. Furthermore, it is doubtful whether any non-linearities would have been detected had it been possible to test the helicopter with the joint pre-stressed. Once again, measurements at different dynamic force levels and relatively small amplitudes, would have shown the structure to be linear, albeit with a different stiffness.

7.2 Summary of Topics Investigated

In a fmal review of the work presented in this thesis it is considered that contributions to the understanding of 'Structural Modification from Experimental Data' have been made in the following areas;

- reformulation and refinement of the impedance coupling method to give very much improved computational efficiency and the ability to cope with all forms of modification component;
- the value of a preliminary survey;
- the use of a AFRF in the assessment of repeatability and reciprocity and for comparison of measured and theoretical data;
- the development of a simple sensitivity analysis technique based on experimentally-derived resonance and anti-resonance data for ranking possible structural modification sites in their order of importance for influencing each particular mode;
- the use of preliminary survey sensitivity analysis results in definition of a full measurement test programme;
- illustration of the possible errors that can be incurred when 1^{st} and 2^{nd} order sensitivities are used in prediction of the effects of 'large' modifications;
- the key importance that rotational degrees-of-freedom can play in the outcome of a coupling analysis has been demonstrated once again. The present practical ability for prediction of the effects of modifications involving rotational restraint at the attachment points has been reviewed;
- demonstration of some problems with prediction of the effects of modifications that can be caused by the presence of non-linearities – an illustration of just how far removed experimental practice is from theory;
- discussion of the causes of incompleteness and inaccuracy in an experimentally-based dynamic survey and the consequences for prediction of the effects of modifications are discussed at length;

7.3 Recommendations for Future Study

As a consequence of this study various aspects of vibration testing and theory have been identified for future study to improve the understanding and application of the techniques developed. Some general topics that should be considered in any further studies are outlined below (N.B. some tasks in the following list are much more substantial than others),

- investigation of impact testing as a quick and efficient method for collection of preliminary survey data;
- development of techniques and equipment for accurate and reliable measurement of rotational degree-of-freedom FRF properties – particularly the design and development of a practical torque exciter,
- detailed investigation of actual joint conditions between; (a) transducer and component, and (b) between two components;
- development of a simple assessment method to show when a given joint can be considered to be ‘rigid’;
- research into alternative measurement or analysis techniques for the accurate identification of anti-resonance frequencies – particularly with reference to broadband type measurements (anti-resonance frequencies can be identified accurately at present if a discrete sine dwell test method is adopted);
- development of ‘on-line’ methods for evaluation of the quality of measured data in addition to the use of the AFRF with repeatability and reciprocity data;
- investigation into whether suitable approximations can be found for the sensitivity analysis equations that give acceptable results but use less of the resonance and anti-resonance frequencies – noting the apparently simple shape of the curve showing the relationship of resonance frequency to mass added, Figure 3.23;
- the relationship of this new sensitivity analysis method to that known as Vincent’s Circle;

- extension of sensitivity analyses for use with modifications other than single degree-of-freedom masses or springs (or ‘internal stiffness’ modifications);

- use of the sensitivity analysis techniques in tailoring a modification and its dynamic properties to produce desired shifts in several resonance frequencies of the base structure simultaneously;

- incorporation of sensitivity analysis techniques into some form of ‘optimisation’ program for consideration of the best place to make a modification to achieve alterations in several mode frequencies;

- what is the physical explanation, if any, of an imaginary anti-resonance frequency? and,

- can any simplified approximation to the sensitivity analysis equations be used to predict the resonance frequencies of a modified structure more accurately than a Maclaurin’s series expansion with 1st and 2nd order differential coefficients only (chapter 3 and Figure 3.25)?

REFERENCES

References

1. **Ewins. D.J. and Griffin. J.**
"A State-of-the-Art Assessment of Mobility Measurement Techniques - Results for the Mid-Range Structures"
Journal of Sound and Vibration, (1981) **78(2),** 197-222

2. **Ewins. D.J.**
"Uses *and Abuses of Modal Testing".*
IMAC **3, 1985.**

3. **Stroud. R.C.**
"Excitation, Measurement and Analysis Methods for Modal Testing".
Joint ASME/ASCE publication.
Combined Experimental/Analytical Modeling of Dynamic Structural Systems; Substructure Synthesis Methods.
June, 1985.

4. **Stroud. R.C.**
"The Modal Survey of the Galileo Spacecraft".
Sound and Vibration, Vol. 18, No. 4, pp 28-34
April, 1984.

5. **Ewins. D.J. and Sainsbury. M.G.**
"Mobility Measurements for the Vibration Analysis of Connected Structures".
The Shock and Vibration Bulletin, (1972) **42(1),** 105-121

6. **Damms. S.M.**
"Mobility Measurements on a Beam and a Dynamic Absorber".
RAE Technical Memorandum Aero 1842.
May, 1980.

7. **Elliott. K.B, and Mitchell. L.D.**
'The Effect of Modal Truncation on Modal Modification".
IMAC ***5,*** 1987, pp 72-78.

8. **Silva. J.M.M.**
"On the Influence of the Pushrod in Mechanical Impedance Testing".
Dynamics Section Report, Imperial College, University of London.
October, 1975.

9. **Silva. J.M.M.**
"Measurements and Applications of Structural Mobility Data for the Vibration Analysis of Complex Structures".
PhD. Thesis, Imperial College, University of London.
March, 1978.

10. **Mitchell. L.D.**
'A Method for Designing Stingers for use in Mobility Testing".
IMAC **2, 1984.**

11. **Heiber. G.M.**
"Non-Toxic Stingers".
IMAC 6, 1988, pp 1371-1379.

12. **Gleeson. P.T.**
"Errors in Mobility Measurement Caused by Base Strain Effects in Accelerometers".
Dynamics Section Report, Imperial College, University of London.
January, 1977.

13. **Gleeson. P.T.**
"Limitations of Accelerometers in the Measurement of Rotational Mobilities".
Dynamics Section Report, Imperial College, University of London.
February, 1973.

14. **Ewins. D.J.**
"Measurement and Application of Mechanical Impedance Data" (3 Parts).
JSEE Vol 14.3, 15.1, 15.2 1975-1976.

15. **Skingle. G. W.**
"First-Time Experiences of Practical Modal Testing and Analysis".
Dynamics Section Report No. 8606, Imperial College, University of London.
June, 1986.

16. **Hopton. G.W.**
"Relationships between Analysis Errors and Complex Mode Shapes".
IMAC 5, pp 381-388.

17. **Olsen. N.**
"Excitation Functions for Structural Frequency Response Measurements".
IMAC ***2, 1984.***

18. **Lang. G.F.**
Editorial.
Sound and Vibration, October 1985.

19. **Williams. R. and Vold. H.**
"The Multiphase-Step-Sine Method for Experimental Modal Analysis".

20. **Skingle. G. W.**
"A Review of the Procedure for Structural Modification Using Frequency Response Functions".
Dynamics Section Report No. 87 10, Imperial College, University of London.
May, 1987.

21. **Skingle. G. W.**
"ΔFRFs and Dimensionless ΔFRFs in the Study of Structural Modification".
Dynamics Section Report No. 8706, Imperial College, University of London.
March, 1987.

22. **Deel. J.C. and Luk. Y.W.**
"Modal Testing Considerations for Structural Modification Applications".
IMAC 3, 1985, pp 46-52.

23. **Black. I. et al.**
"Modal Survey of the Intelsat VI Cradle and Carrier Structure for a Shuttle Launched Spacecraft".
IMAC ***5,*** pp 478-487.

24. **Brown. D.L, Allemang. R.J, Zimmerman. R, and Mergeay. M.**
"Parameter Estimation Techniques for Modal Analysis".
SAE Congress and Exposition, Detroit.
1979.

25. **Ewins. D.J.**
"Modal Testing; Theory and Practice".
Research Studies Press, 1985.

26. **Stroud. R.C.**
"Excitation, Measurement and Analysis Methods for Modal Testing".
Joint ASME/ASCE publication.
Combined Experimental/Analytical Modeling of Dynamic Structural Systems; Substructure Synthesis Methods, June 1985.

27. **Füllerkrug. U.**
"Survey of Parameter Estimation Methods in Experimental Modal Analysis".
IMAC 5, 1987, pp 460-467.

28. **Salter. J.P.**
"Steady State Vibration".
Kenneth Mason Press, 1969.

29. **Goyder. H.G.D.**
"Methods and Application of Structural Modeling from Measured Structural Frequency Response Data".
Journal of Sound and Vibration, (1980), 68(2), pp 209-230.

30. **Wei. M.L.**
'Modal Scaling Considerations for Structural Modification Application".
IMAC 5, 1987, pp 1531-1537

31. **Henderson. F.N.**
The Influence of Rotational Coordinates in a Dynamic Coupling Analysis",
MSc Thesis, Imperial College, University of London.
October, 1984.

32. **Crowley. S.M, Javidinejad. M. and Brown. D.L.**
"An Investigation of Structural Modification Using an H-Frame Structure".
IMAC 4, 1986, pp 1268-1277.

33. **Smiley. R.G.**
"Rotational Degrees of Freedom in Structural Modification".
IMAC 2, 1984.

34. **O'Callahan. J.C.**
"Study of a Structural Modification Procedure with Three-Dimensional Beam Elements using a Local Eigenvalue Modification Procedure".
IMAC 2, 1984.

35. **Ewins. D.J. and Gleeson. P.T.**
"Experimental Determination of Multi-directional Mobility Data for Beams".
Journal of Sound and Vibration Bulletin, (1975) 45(5), pp 153-173.

36. **Mead. S.M. and Heron. K.H.**
"A Technique to Measure the Full Mobility Matrix for One or More Points of a Structure at Acoustic Frequencies".
RAE Technical Report No. 83072, September, 1983.

37. **Licht. T.R.**
"Angular Vibration Measurement Transducers and their Configuration".
IMAC 3,1985.

38. **O'Callahan. J.C.**
"Determination of Rotational Degrees of Freedom for Moment Transfers in Structural Modifications" .
IMAC 3, 1985.

39. **Haisty. B.S. and Springer. W.T.**
"A Simplified Methodfor Extracting Rotational Degree-of-Free&m Information from Modal Test Data".
International Journal of Analytical and Experimental Modal Analysis, Vol 1(3), July, 1986, pp 35-39.

40. **Avitable. P.**
"Expansion of Rotational DoF for Structural Dynamic Modification" .
IMAC 5, 1987, pp 950-955

41. **Bishop. R.E.D. and Johnson. D.C.**
"The Mechanics of Vibration".
Cambridge University Press, 1960.

42. **Ewins. D.J.**
'Modal Test Requirements for Coupled Structure Analysis using Experimentally Derived Component Models".
Joint ASME/ASCE publication.
Combined Experimental/Analytical Modeling of Dynamic Structural Systems; Substructure Synthesis Methods, June 1985.

43. **Lamonita. M.A.**
"On the Determination and Use of Residual Flexibilities, Inertia Restraints and Rigid Body Modes".
IMAC 1, 1982, pp 153-159.

44. **Snyder. V.W.**
"Modal Synthesis using Eigenvalue Modification".
IMAC 1, 1982, pp 1134-1137.

45. **Lang. G.F.**
"Modal Testing Principles".
Solartron Instruments Technical Report No. 023/87.

46. **Luk. Y.W. and Mitchell. L.D.**
'Analytical and Geometric Substructuring via Dual Modal Space Structural Modification".
IMAC 2, 1984, pp 50-57.

47. **Luk. Y.W. and Mitchell. L.D.**
"Implementation of the Dual Modal Space Structural Modification Method".
IMAC 2, 1984, pp 930-936.

48. **Craig. R.R. Jr**
"A Review of Time-Domain and Frequency-Domain Component Mode Synthesis Methods" .
Journal of Modal Analysis, April 1987, pp 59-72.

49. **Jones. R. and Iberle. K.**
Structural Modification: A Comparison of Techniques".
IMAC 4, 1986, pp 59-65

50. **Jetmundsen. B, Bielawa. R.L, and Flannelly. W.G.**
"Generalized Frequency Domain Substructure Synthesis".
Journal of the American Helicopter Society, January 1988, pp 55-64.

51. **Jones. R.P.N.**
"The Effect Of Small Changes in Mass and Stiffness on the Natural Frequencies and Modes of Vibrating Systems".
Int. J. Mech. Sci. Vol. 1, 1960, pp 350-355.

52. **Skingle. G.W.**
"Order of Importance Ranking for Degrees of Freedom in a Coupling Analysis".
Dynamics Section Report No. 87019, Imperial College, University of London. October, 1987.

53. **Wang. J, Heylen. W, and Sas. P.**
"Accuracy of Structural Modification Techniques".
IMAC ***5, 1987,*** pp 65-71.

54. **Patrick. G.B, and Wei. Y.S.**
"Practical Sensitivity Analysis".
IMAC ***5, 1987,*** pp 21-25.

55. **Fox. R.L. and Kapoor. M.P.**
"Rates of Change of Eigenvalues and Eigenvectors" .
AIAA Journal, Vol. 6, No. 12.
December, 1968.

56. **Vanhonacker. P.**
The Use of Modal Parameters of Mechanical Structures in Sensitivity Analysis-, System Synthesis- and System Identification Methods".
Ph.D. Dissertation, Katholieke Universiteit Leuven.
1980.

57. **Vanhonacker. P.**
"Sensitivity Analysis of Mechanical Structures, Based on Experimentally Determined Modal Parameters".
IMAC 2, 1984, pp 534-541

58. **Chou. Y.F and Chen. J.S.**
"Structural Dynamics Modification via Sensitivity Analysis".
IMAC ***3, 1985,*** pp 483-489.

59. **Vincent. A.H.**
"A Note on the Properties of the Variation of Structural Response with respect to a Single Structural Parameter, when Plotted in the Complex Plane".
Westland Helicopters Limited Report, GEN/DYN/RES/010R.
1973.

60. **Done. G.T.S. and Hughes. A.D.**
"The Response of a Vibrating Structure as a Function of Structural Parameters".
Journal of Sound and Vibration, (1975) 38(2), 255-266.

61. **Done. G.T.S, Hughes. A.D. and Webby. J.**
"The Response of a Vibrating Structure as a Function of Structural Parameters - Application and Experiment".
Journal of Sound and Vibration, (1976) 49(2), 149 -159.

62. **Gaukroger. D.R.**
"Applications of Vincent's Circle Analysis to Undamped Structures".
RAE Technical Report No. 82025.
March, 1982.

63. **Sobey. A.J.**
"Helicopter Vibration Reduction through Structural Manipulation".
Sixth European Rotorcraft and Powered Lift Aircraft Forum, Bristol, England.
September, 1980.

64. **Sobey. A.J.**
"Improved Helicopter Airframe Response Through Structural Change".
Ninth European Rotorcraft Forum, Stresa, Italy.
September, 1983.

65. **Hanson. H.W. and Calapodas. N.J.**
"Evaluation of the Practical Aspects of Vibration Reduction Using Structural Optimization Techniques".
Journal of the American Helicopter Society, 25(3), pp 37-45.
July, 1980.

66. **Skingle. G. W.**
"Resonance and Anti-Resonance Sensitivities for SDoF Mass and Stiffness Modifications".
Dynamics Section Report No. 8802, Imperial College, University of London.
January, 1988.

67. **Frazer. R.A, Duncan. W.J, and Collar. A.R.**
"Elementary Matrices".
Cambridge University Press, 1946.

68. **Tse. F.S, Morse. I.E, and Hinkle. R.T.**
"Mechanical Vibrations: Theory and Applications".
Allyn and Bacon, Inc, 1963.

69. **Wallack. P, Skoog. P, and Richardson. M.**
"Simultaneous Structural Dynamics Modification (S^2DM)".
IMAC *6,* 1988, pp 1033-1038.

70. **Zipling. Z, Tian. H, and Hamilton. J.**
"An Effective Aproach to Determine Natural Frequencies and Mode Shapes of Constrained Beams Using Lagrange Multipliers".
IMAC *6,* 1988, pp 1509-1512.

71. **White. R.G, and Pinnington.R.J.**
"Practical Application of the Rapid Frequency Sweep Technique for Structural Frequency Response Measurement".
Aeronautical Journal, May 1982.

72. **Chung. K.R, and Lee. C.W.**
"An Efficient Methodfor Compensating Truncated Higher Modes in Structural Dynamics Modification".
Proc. Instn. Mech. Engrs, Vol 200, No. Cl.
1986.

73. **Flannelly, W.G.**
"Natural Anti-Resonances in Structural Dynamics".
Kaman Aerospace Corporation.
September, 1971.

62. **Gaukroger. D.R.**
"Applications of Vincent's Circle Analysis to Undamped Structures".
RAE Technical Report No. 82025.
March, 1982.

63. **Sobey. A.J.**
"Helicopter Vibration Reduction through Structural Manipulation".
Sixth European Rotorcraft and Powered Lift Aircraft Forum, Bristol, England.
September, 1980.

64. **Sobey. A.J.**
"Improved Helicopter Airframe Response Through Structural Change".
Ninth European Rotorcraft Forum, Stresa, Italy.
September, 1983.

65. **Hanson. H.W. and Calapodas. N.J.**
"Evaluation of the Practical Aspects of Vibration Reduction Using Structural Optimization Techniques".
Journal of the American Helicopter Society, 25(3), pp 37-45.
July, 1980.

66. **Skingle. G. W.**
"Resonance and Anti-Resonance Sensitivities for SDoF Mass and Stiffness Modifications".
Dynamics Section Report No. 8802, Imperial College, University of London.
January, 1988.

67. **Frazer. R.A, Duncan. W.J, and Collar. A.R.**
"Elementary Matrices".
Cambridge University Press, 1946.

68. **Tse. F.S, Morse. I.E, and Hinkle. R.T.**
'Mechanical Vibrations: Theory and Applications".
Allyn and Bacon, Inc, 1963.

69. **Wallack. P, Skoog. P, and Richardson. M.**
"Simultaneous Structural Dynamics Modification (S^2DM)".
IMAC 6, 1988, pp 1033-1038.

70. **Zipling. Z, Tian. H, and Hamilton. J.**
"An Effective Aproach to Determine Natural Frequencies and Mode Shapes of Constrained Beams Using Lagrange Multipliers".
IMAC 6, 1988, pp 1509-1512.

71. **White. R.G, and Pinnington.R.J.**
"Practical Application of the Rapid Frequency Sweep Technique for Structural Frequency Response Measurement".
Aeronautical Journal, May 1982.

72. **Chung. K.R, and Lee. C.W.**
"An Efficient Methodfor Compensating Truncated Higher Modes in Structural Dynamics Modification".
Proc. Instn. Mech. Engrs, Vol 200, No. Cl.
1986.

73. **Flannelly, W.G.**
"Natural Anti-Resonances in Structural Dynamics".
Kaman Aerospace Corporation.
September, 1971.

74. **Duncan, W.J.**
"Mechanical Admittances and their Applications to Oscillation Problems".
H.M.S.O., London.
1947.

75. **Ewins, D.J, and Imregun, M.**
"State-of-the-Art Assessment of Structural Dynamic Response Analysis Methods (DYNAS)".
Shock and Vibration Bulletin, Vol. 56, Part 1
August, 1986.

76. **Van Belle, H.**
"Higher Order Sensitivities in Structural Systems."
AIAA Journal, Vol. 20, pp *286-288*
1982.

77. **Wang. B.P,**
"Structural Dynamic Modification using Modal Analysis Data".
IMAC *3,* pp *42-45*

78. **SDRC**
"User Manual for Modal Plus Modal Analysis, Version 9".

79. **Skingle. C.W.**
"New Developments in Ground Vibration Testing: Experimental Aspects".
Paper Presented at The Royal Aeronautical Society Conference on
Ground Vibration Testing Of Aerospace Structures.
November, 1986.

80. **Brüel and Kjær.**
"Digital Signal Analysis using Digital Filters and FFT Techniques".
Selected Reprints from Technical Review.
January, 1985.

81. **Skingle. G. W.**
"Study of a Simple Point Modification to the Nastran Tower".
Dynamics Section Report No. 8701, Imperial College, University of London.
January, 1987.

82. **AGARD**
"Manual on Aeroelasticity"
Volume (iv), Chapter 1; pp 23-26
1960.

83. *"Dynamic Analysis of the Westland Lynx XX907 Helicopter Airframe: Final Report on the Construction of the Finite Element Model and the Preliminary Correlation with Test Data".*
SDRC Report No. 83052

84. **Matthews. J.T.**
"Report on the 3rd Phase Experimental Investigation of the Lynx XX907 Helicopter".
SDRC Report No. 85132A

85. **Flannelly, W.G.**
'Static *Acceleration Coefficient".*
Kaman Aerospace Corporation, Report No. WP 73 - 3
January, 1973.

86. **Przemieniecki, J. S.**
"Theory **of** *Matrix Structural Analysis".*
McGraw Hill, 1968.

87. **Rocklin, G.T., Crowley, J. and Vold, H.**
"A Comparison of H_1, H_2 and H_v Frequency Response Functions".
IMAC 3, 1985.

88. **Urgueria, A.P.V.**
"A Refined Modal Coupling Technique for Including ResidualEffects of Out-of-Range Modes."
IMAC 7, 1989, pp 299 - *303.*

89. **To, W.M.**
"Structural Modification Analysis Using Rayleigh Quotient Iteration."
Dynamics Section Report No. 89001, Imperial College, University of London.
January, 1989.

90. **Kirshenboim, J.**
'Theory *and Practice of Modal Identification Applied to Helicopter Structures."*
PhD. Thesis, Imperial College, University of London.
September, 198 1.

APPENDICES

Appendix A

Algebraic Manipulations for the Reformulation of the Impedance Coupling Method (see chapter 2)

Note: Equation numbers follow on from those in chapter 2.

The inertance of a coupled structure can be expressed as follows,

$$[C] = [B_A]([B_A] + [A_A] - [A_A].[I_A].[B_A])^{-1}[A_A] \quad \ldots\ldots\ldots (2.17)$$

where,

$$[A_A] = \begin{bmatrix} A_{11} & A_{12} & 0 \\ A_{21} & A_{22} & 0 \\ 0 & 0 & I \end{bmatrix} \quad [B_A] = \begin{bmatrix} I & 0 & 0 \\ 0 & B_{22} & B_{23} \\ 0 & B_{32} & B_{33} \end{bmatrix} \quad \text{and} \quad [I\&=[\ \begin{matrix} I & 0 & 0 \\ 0 & 0 & 0 \\ 0 & 0 & I \end{matrix} \quad \ldots\ldots\ldots (2.18)$$

Then,

$$[A_A].[I_A].[B_A] = \begin{bmatrix} A_{11} & A_{12} & 0 \\ A_{21} & A_{22} & 0 \\ 0 & 0 & I \end{bmatrix}.\begin{bmatrix} I & 0 & 0 \\ 0 & 0 & 0 \\ 0 & 0 & I \end{bmatrix}.\begin{bmatrix} I & 0 & 0 \\ 0 & B_{22} & B_{23} \\ 0 & B_{32} & B_{33} \end{bmatrix} = \begin{bmatrix} A_{11} & 0 & 0 \\ A_{21} & 0 & 0 \\ 0 & B_{32} & B_{33} \end{bmatrix} \quad \ldots\ldots\ldots\ldots (2.19)$$

and, $[B_A] + [A_A] - [A_A].[I_A].[B_A] =$

$$\begin{bmatrix} I & 0 & 0 \\ 0 & B_{22} & B_{23} \\ 0 & B_{32} & B_{33} \end{bmatrix} + \begin{bmatrix} A_{11} & A_{12} & 0 \\ A_{21} & A_{22} & 0 \\ 0 & 0 & I \end{bmatrix} - \begin{bmatrix} A_{11} & 0 & 0 \\ A_{21} & 0 & 0 \\ 0 & B_{32} & B_{33} \end{bmatrix} = \begin{bmatrix} I & A_{12} & 0 \\ 0 & A_{22}+B_{22} & B_{23} \\ 0 & 0 & I \end{bmatrix} \quad \ldots\ldots\ldots\ldots (2.20)$$

Now, it can be shown that:

$$\begin{bmatrix} I & A_{12} & 0 \\ 0 & A_{22}+B_{22} & B_{23} \\ 0 & 0 & I \end{bmatrix}^{-1} = \begin{bmatrix} I & -A_{12}.[A_{22}+B_{22}]^{-1} & A_{12}.[A_{22}+B_{22}]^{-1}.B_{23} \\ 0 & [A_{22}+B_{22}]^{-1} & -[A_{22}+B_{22}]^{-1}.B_{23} \\ 0 & 0 & I \end{bmatrix} \quad \ldots\ldots\ldots (2.21)$$

which, on substitution into equation (2.17), gives;

$$[C] = \begin{bmatrix} I & 0 & 0 \\ 0 & B_{22} & B_{23} \\ 0 & B_{32} & B_{33} \end{bmatrix} . \begin{bmatrix} I & -A_{12}.[A_{22}+B_{22}]^{-1} & A_{12}.[A_{22}+B_{22}]^{-1}.B_{23} \\ 0 & [A_{22}+B_{22}]^{-1} & -[A_{22}+B_{22}]^{-1}.B_{23} \\ 0 & 0 & I \end{bmatrix} . \begin{bmatrix} A_{11} & A_{12} & 0 \\ A_{21} & A_{22} & 0 \\ 0 & 0 & 1 \end{bmatrix} \quad \ldots\ldots (2.22)$$

and therefore;

$$[C] = \begin{bmatrix} A_{11}-A_{12}.[A_{22}+B_{22}]^{-1}.A_{21} & A_{12}-A_{12}.[A_{22}+B_{22}]^{-1}.A_{22} & A_{12}.[A_{22}+B_{22}]^{-1}.B_{23} \\ B_{22}.[A_{22}+B_{22}]^{-1}.A_{21} & B_{22}.[A_{22}+B_{22}]^{-1}.A_{22} & -B_{22}.[A_{22}+B_{22}]^{-1}.B_{23}+B_{23} \\ B_{32}.[A_{22}+B_{22}]^{-1}.A_{21} & B_{32}.[A_{22}+B_{22}]^{-1}.A_{22} & -B_{32}.[A_{22}+B_{22}]^{-1}.B_{23}+B_{33} \end{bmatrix} I \quad \ldots\ldots (2.23)$$

Now, this matrix may be split up into two matrices, the first of which contains inertance properties of the unmodified components alone:

$$\begin{bmatrix} A_{11} & A_{12} & 0 \\ A_{21} & A_{22} & 0 \\ 0 & 0 & B_{33} \end{bmatrix} - \begin{bmatrix} A_{12}.[A_{22}+B_{22}]^{-1}.A_{21} & A_{12}.[A_{22}+B_{22}]^{-1}.A_{22} & -A_{12}.[A_{22}+B_{22}]^{-1}.B_{23} \\ A_{21}-B_{22}.[A_{22}+B_{22}]^{-1}.A_{21} & A_{22}-B_{22}.[A_{22}+B_{22}]^{-1}.A_{22} & B_{22}.[A_{22}+B_{22}]^{-1}.B_{23}-B_{23} \\ -B_{32}.[A_{22}+B_{22}]^{-1}.A_{21} & -B_{32}.[A_{22}+B_{22}]^{-1}.A_{22} & B_{32}.[A_{22}+B_{22}]^{-1}.B_{23} \end{bmatrix} I \quad \ldots\ldots (2.24)$$

and, by consideration of the terms in the middle row of the second matrix;

$$\begin{aligned} A_{21} - B_{22}.[A_{22}+B_{22}]^{-1}.A_{21} &= \left(I - B_{22}.[A_{22}+B_{22}]^{-1}\right).A_{21} \\ &= ([A_{22}+B_{22}] - B_{22}).[A_{22}+B_{22}]^{-1}.A_{21} \\ &= A_{22}.[A_{22}+B_{22}]^{-1}.A_{21} \quad \ldots\ldots (2.25) \end{aligned}$$

Similarly,

$$A_{22} - B_{22}.[A_{22}+B_{22}]^{-1}.A_{22} = A_{22}.[A_{22}+B_{22}]^{-1}.A_{22} \quad \ldots\ldots (2.26)$$

and

$$B_{22}.[A_{22}+B_{22}]^{-1}.B_{23} - B_{23} = -A_{22}.[A_{22}+B_{22}]^{-1}.B_{23} \quad \ldots\ldots (2.27)$$

Equation (2.24) becomes:

$$[C] = \begin{bmatrix} A_{11} & A_{12} & 0 \\ A_{21} & A_{22} & 0 \\ 0 & 0 & B_{33} \end{bmatrix} - \begin{bmatrix} A_{12}.[A_{22}+B_{22}]^{-1}.A_{21} & A_{12}.[A_{22}+B_{22}]^{-1}.A_{22} & -A_{12}.[A_{22}+B_{22}]^{-1}.B_{23} \\ A_{22}.[A_{22}+B_{22}]^{-1}.A_{21} & A_{22}\,[A_{22}+B_{22}]^{-1}.A_{22} & -A_{22}.[A_{22}+B_{22}]^{-1}.B_{23} \\ -B_{32}.[A_{22}+B_{22}]^{-1}.A_{21} & -B_{32}.[A_{22}+B_{22}]^{-1}.A_{22} & B_{32}.[A_{22}+B_{22}]^{-1}.B_{23} \end{bmatrix} \quad \text{(2.28)}$$

or, more concisely as:

$$[C] = \begin{bmatrix} A_{11} & A_{12} & 0 \\ A_{21} & A_{22} & 0 \\ 0 & 0 & B_{33} \end{bmatrix} - \begin{Bmatrix} A_{12} \\ A_{22} \\ -B_{32} \end{Bmatrix} . [A_{22}+B_{22}]^{-1} . \{ A_{21} \quad A_{22} \quad -B_{23} \} \qquad \ldots\ldots (2.29)$$

Notes:

- only one matrix inversion is necessary;
- the matrix for inversion only contains information relating to the interface coordinates of each component;
- the first matrix of equation (2.28) is a representation of the unmodified characteristics of the components, with 'A' as the reference component;
- the second matrix of equation (2.28) is a matrix of the differences between the unmodified and the modified representations of the components.

Appendix B

Intermediate Steps in the Derivation of the 1st and 2nd Order Mass Sensitivity Equations for a Grounded Structure (see chapter 3)

Note: Equation numbers without the 'B' prefix refer to those in chapter 3.

The resonance frequencies for a grounded structure modified with a single degree-of-freedom mass (m) are given by solution of the following polynomial equation in Ω_R.

$$m\,\Omega_R^2\,C_{jj}\prod_{i=1}^{N-1}\left(1-\frac{\Omega_R^2}{j\omega_i^2}\right)-\prod_{r=1}^{N}\left(1-\frac{\Omega_R^2}{\Omega_r^2}\right)=0 \qquad \text{.....(B1) or (3.26)}$$

The sensitivity of resonance frequencies to single degree-of-freedom mass modifications is given by differentiation of equation (B 1) with respect to mass,

$$C_{jj}\,m\left[\Omega_R^2\frac{d}{dm}\left\{\prod_{i=1}^{N-1}\left(1-\frac{\Omega_R^2}{j\omega_i^2}\right)\right\}+2\Omega_R\frac{d\Omega_R}{dm}\prod_{i=1}^{N-1}\left(1-\frac{\Omega_R^2}{j\omega_i^2}\right)\right]$$
$$+\,C_{jj}\,\Omega_R^2\prod_{i=1}^{N-1}\left(1-\frac{\Omega_R^2}{j\omega_i^2}\right)-\frac{d}{dm}\left\{\prod_{r=1}^{N}\left(1-\frac{\Omega_R^2}{\Omega_r^2}\right)\right\}=0 \qquad \text{.....(B2)}$$

Now,

$$\frac{d}{dm}\left\{\prod_{i=1}^{N-1}\left(1-\frac{\Omega_R^2}{j\omega_i^2}\right)\right\}=2\Omega_R\frac{d\Omega_R}{dm}\prod_{i=1}^{N-1}\left(1-\frac{\Omega_R^2}{j\omega_i^2}\right)\sum_{i=1}^{N-1}\left(\frac{1}{\Omega_R^2-j\omega_i^2}\right) \qquad \text{.....(B3)}$$

and, similarly,

$$\frac{d}{dm}\left\{\prod_{r=1}^{N}\left(1-\frac{\Omega_R^2}{\Omega_r^2}\right)\right\}=2\Omega_R\frac{d\Omega_R}{dm}\prod_{r=1}^{N}\left(1-\frac{\Omega_R^2}{\Omega_r^2}\right)\sum_{r=1}^{N}\left(\frac{1}{\Omega_R^2-\Omega_r^2}\right) \qquad \text{.....(B4)}$$

Therefore, by substitution of equations (B3) and (B4) into equation (B2) and after rearrangement, we obtain,

$$\frac{d\Omega_R}{dm} = \frac{\Omega_R \; C_{jj} \prod_{i=1}^{N-1}\left(1 - \frac{\Omega_R^2}{jj\omega_i^2}\right)}{2 \prod_{r=1}^{N}\left(1 - \frac{\Omega_R^2}{\Omega_r^2}\right)\left[\sum_{r=1}^{N}\left(\frac{1}{\Omega_R^2 - \Omega_r^2}\right) - \sum_{i=1}^{N-1}\left(\frac{1}{\Omega_R^2 - jj\omega_i^2}\right) - \frac{1}{\Omega_R^2}\right]} \quad \ldots\ldots (B5)$$

As the mass modification tends to zero, equation (B5) can lead to some computational problems due to the form of the denominator. Expansion and further rearrangement of the denominator eventually yields the following equation which is well behaved for all values of mass addition,

$$\frac{d\Omega_R}{dm} = \frac{\Omega_R \; C_{jj} \prod_{r=1}^{N-1}(\Omega_r^2) \prod_{i=1}^{N-1}\left(1 - \frac{\Omega_R^2}{jj\omega_i^2}\right)}{2\left[\frac{\Omega_N^2 - \Omega_R^2}{\Omega_N^2} \cdot \sum_{i=1}^{N-1}\left(\frac{\Omega_i^2 - jj\omega_i^2}{jj\omega_i^2 - \Omega_R^2} \prod_{r\neq i}^{N-1}(\Omega_r^2 - \Omega_R^2)\right) - \frac{1}{\Omega_R^2}\prod_{r=1}^{N-1}(\Omega_r^2 - \Omega_R^2)\right]} \quad \ldots\ldots (B6)$$

and in the limit as the mass addition tends to zero, Ω_R tends to Ω_p leaving,

$$\left.\frac{d\Omega_P}{dm}\right|_{m=0} = \frac{-C_{jj}.\Omega_p.\prod_{r=1}^{N}(\Omega_r^2).\prod_{i=1}^{N-1}(jj\omega_i^2 - \Omega_p^2)}{2.\prod_{i=1}^{N-1}(jj\omega_i^2).\prod_{r\neq p}^{N}(\Omega_r^2 - \Omega_p^2)} \quad \ldots\ldots\ldots\ldots (B7) \text{ or } (3.29)$$

For the 2nd order sensitivity, equation (B6) must be differentiated with respect to mass once more. To simplify the procedure, we shall write equation (B6) as follows,

$$\frac{d\Omega_R}{dm} = \frac{C_{jj}}{2} \cdot \prod_{r=1}^{N-1}(\Omega_r^2) \cdot \Omega_R \cdot \prod_{i=1}^{N-1}\left(1 - \frac{\Omega_R^2}{jj\omega_i^2}\right) \cdot (D)^{-1} \quad \ldots\ldots\ldots\ldots (B8)$$

where,

$$(D) = \left(\frac{\Omega_N^2 - \Omega_R^2}{\Omega_N^2}\right) \cdot \sum_{i=1}^{N-1}\left(\frac{\Omega_i^2 - jj\omega_i^2}{jj\omega_i^2 - \Omega_R^2} \prod_{r\neq i}^{N-1}(\Omega_r^2 - \Omega_R^2)\right) - \frac{1}{\Omega_R^2}\prod_{r=1}^{N-1}(\Omega_r^2 - \Omega_R^2)$$

$$\ldots\ldots (B9)$$

Then,

$$\frac{d^2\Omega_R}{dm^2} = \frac{C_{ii}}{2} \cdot \prod_{r=1}^{N-1}(\Omega_r^2)\left[\Omega_R \prod_{i=1}^{N-1}\left(1 - \frac{\Omega_R^2}{jj\omega_i^2}\right) \cdot \frac{d}{dm}\{(D)^{-1}\} + (D)^{-1}\frac{d}{dm}\left\{\Omega_R \prod_{i=1}^{N-1}\left(1 - \frac{\Omega_R^2}{jj\omega_i^2}\right)\right\}\right] \quad \text{.....(B10)}$$

Now, $$\frac{d}{dm}\{(D)^{-1}\} = -1(D)^{-*}\&\{(D)\} \quad \text{.....(B11)}$$

and,

$$\frac{d}{dm}\{(D)\} =$$

$$\frac{d}{dm}\left\{-\Omega_R^2 \cdot \prod_{r=1}^{N-1}(\Omega_r^2 - \Omega_R^2)\right\} + \frac{d}{dm}\left\{\left(\frac{\Omega_N^2 - \Omega_R^2}{\Omega_N^2}\right) \cdot \sum_{i=1}^{N-1}\left(\frac{\Omega_i^2 - jj\omega_i^2}{jj\omega_i^2 - \Omega_R^2}\prod_{r\neq i}^{N-1}(\Omega_r^2 - \Omega_R^2)\right)\right\} \quad \text{..... (B12)}$$

or, $$\frac{d}{dm}\{(D)\} = \frac{d}{dm}\{(D1)\} + \frac{d}{dm}\{(D2)\} \quad \text{..... (B13)}$$

Now,

$$\frac{d}{dm}\{(D1)\} = \frac{2}{\Omega_R} \cdot \frac{d\Omega_R}{dm} \cdot \left[\frac{1}{\Omega_R^2}\prod_{r=1}^{N-1}(\Omega_r^2 - \Omega_R^2) + \sum_{r=i}^{N-1}\prod_{\substack{sfr \\ s\neq i}}^{N-1}(\Omega_s^2 - \Omega_R^2)\right] \quad \text{.....(B14)}$$

and,

$$\frac{d}{dm}\{(D2)\} =$$

$$2\,\Omega_R \frac{d\Omega_R}{dm} \cdot \left\{\left(1 - \frac{\Omega_R^2}{\Omega_N^2}\right)\left[\sum_{i=1}^{N-1}\left(\frac{\Omega_i^2 - jj\omega_i^2}{jj\omega_i^2 - \Omega_R^2}\,\frac{\prod_{r\neq i}^{N-1}(\Omega_r^2 - \Omega_R^2)}{jj\omega_i^2 - \Omega_R^2} - \sum_{r\neq i}^{N-1}\prod_{\substack{s\neq r \\ sfi}}^{N-1}(\Omega_s^2 - \Omega_R^2)\right)\right]\right.$$

$$\left. - \frac{1}{\Omega_N^2}\sum_{i=1}^{N-1}\left(\frac{\Omega_i^2 - jj\omega_i^2}{jj\omega_i^2 - \Omega_R^2}\prod_{r\neq i}^{N-1}(\Omega_r^2 - \Omega_R^2)\right)\right\} \quad \text{.....(B15)}$$

Therefore, collect terms to obtain,

$$\frac{d}{dm}\left\{(D)^{-1}\right\} = -2\frac{d\Omega_R}{dm}(D)^{-2}\left\{\frac{1}{\Omega_R}\left(\frac{1}{\Omega_R{}^2}\prod_{r\neq 1}^{N-1}(\Omega_r{}^2-\Omega_R{}^2)+\sum_{r=1}^{N-1}\prod_{s\neq r}^{N-1}(\Omega_s{}^2-\Omega_R{}^2)\right)\right.$$

$$+\Omega_R\left(1-\frac{\Omega_R{}^2}{\Omega_N{}^2}\right)\sum_{i=1}^{N-1}\left(\left(\frac{\Omega_i{}^2-jj\omega_i{}^2}{jj\omega_i{}^2-\Omega_R{}^2}\right)\left[\frac{1}{jj\omega_i{}^2-\Omega_R{}^2}\prod_{r\neq i}^{N-1}(\Omega_r{}^2-\Omega_R{}^2)-\sum_{r=i}^{N-1}\prod_{\substack{s\neq r\\ s\neq i}}^{N-1}(\Omega_s{}^2-\Omega_R{}^2)\right]\right)$$

$$\left.-\frac{\Omega_R}{\Omega_N{}^2}\sum_{i=1}^{N-1}\left(\frac{\Omega_i{}^2-jj\omega_i{}^2}{jj\omega_i{}^2-\Omega_R{}^2}\right)\prod_{r\neq i}^{N-1}(\Omega_r{}^2-\Omega_R{}^2)\right\} \quad \text{.....(B16)}$$

or,
$$\frac{d}{dm}\left\{(D)^{-1}\right\} = -2\frac{d\Omega_R}{dm}(D)^{-2}.(*) \quad \text{.....(B17)}$$

with,

$$(*)=\left\{\frac{1}{\Omega_R}\left(\frac{1}{\Omega_R{}^2}\prod_{r\neq 1}^{N-1}(\Omega_r{}^2-\Omega_R{}^2)+\sum_{r=1}^{N-1}\prod_{s\neq r}^{N-1}(\Omega_s{}^2-\Omega_R{}^2)\right.\right.$$

$$+\Omega_R\left(1-\frac{\Omega_R{}^2}{\Omega_N{}^2}\right)\sum_{i=1}^{N-1}\left(\left(\frac{\Omega_i{}^2-jj\omega_i{}^2}{jj\omega_i{}^2-\Omega_R{}^2}\right)\left[\frac{1}{jj\omega_i{}^2-\Omega_R{}^2}\prod_{r\neq i}^{N-1}(\Omega_r{}^2-\Omega_R{}^2)-\sum_{r=i}^{N-1}\prod_{\substack{s\neq r\\ s\neq i}}^{N-1}(\Omega_s{}^2-\Omega_R{}^2)\right]\right)$$

$$\left.-\frac{\Omega_R}{\Omega_N{}^2}\sum_{i=1}^{N-1}\left(\frac{\Omega_i{}^2-jj\omega_i{}^2}{jj\omega_i{}^2-\Omega_R{}^2}\right)\prod_{r\neq i}^{N-1}(\Omega_r{}^2-\Omega_R{}^2)\right\} \quad \text{.....(B18)}$$

Also,

$$\frac{d}{dm}\left\{\Omega_R.\prod_{i=1}^{N-1}\left(1-\frac{\Omega_R{}^2}{jj\omega_i{}^2}\right)\right\} = \Omega_R.\frac{d\Omega_R}{dm}.\left[2\Omega_R.\sum_{i=1}^{N-1}\left(\frac{1}{\Omega_R{}^2-jj\omega_i{}^2}\right)+\frac{1}{\Omega_R}\right].\prod_{i=1}^{N-1}\left(1-\frac{\Omega_R{}^2}{jj\omega_i{}^2}\right)$$

..... (B19)

Now, bring together equations **(B6),** (B **10),** (B **17), (B** 18) and **(B** 19) to give,

$$\frac{d^2\Omega_R}{dm^2}=\frac{d\Omega_R}{dm}\left(-2\frac{d\Omega_R}{dm}(D)^{-1}(*)\right)+\left(\frac{d\Omega_R}{dm}\right)^2\left[2\Omega_R.\sum_{i=1}^{N-1}\left(\frac{1}{\Omega_R{}^2-jj\omega_i{}^2}\right)+\frac{1}{\Omega_R}\right]$$

..... (B20)

and, eventually,

$$\frac{d^2\Omega_R}{dm^2} = \left(\frac{d\Omega_R}{dm}\right)^2\left[\frac{-4}{C_{jj}.\Omega_R}.\frac{d\Omega_R}{dm}.(*).\prod_{i=1}^{N-1}\left(\frac{jj\omega_i^2}{\Omega_i^2(jj\omega_i^2 - \Omega_R^2)}\right) + 2\Omega_R\sum_{i=1}^{N-1}\left(\frac{1}{\Omega_R^2 - jj\omega_i^2}\right) + \frac{1}{\Omega_R}\right]$$

..... (B21) or (3.46a)

Note:

- the analysis for a free structure is very similar but slightly more straightforward!

Appendix C

Derivation of FRFs in Coordinate Directions from Measurements with Excitation at an Angle to the Axes

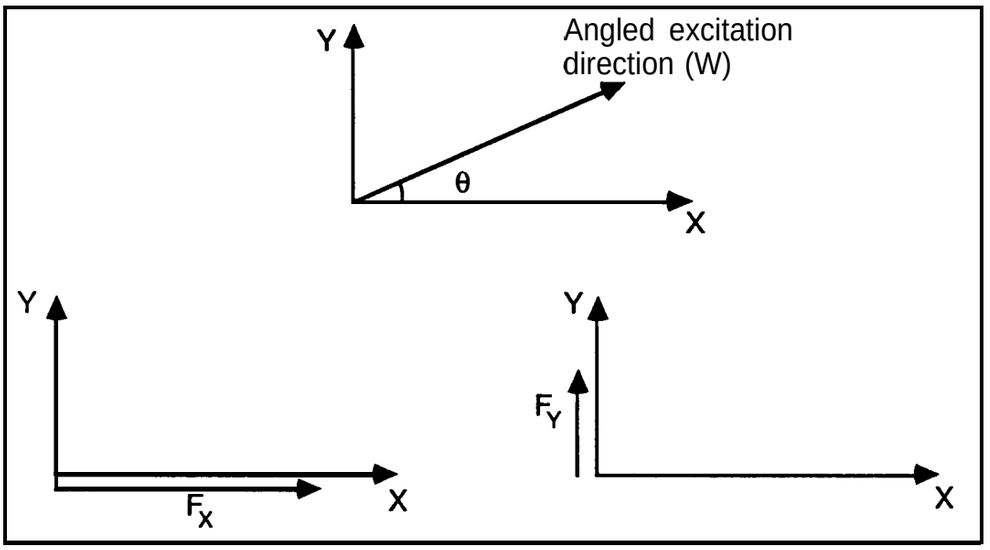

$$R_x = \alpha_{xx} F_x = \alpha_{xx} F_w \cos(\theta) \qquad R_x = \alpha_{xy} F_y = \alpha_{xy} F_w \sin(\theta)$$

$$R_x = \alpha_{xy} F_x = \alpha_{xy} F_w \cos(0) \qquad R_x = \alpha_{yy} F_y = \alpha_{yy} F_w \sin(\theta)$$

Therefore, **total** responses in the X- and Y- axes are :-

$$R_x = \alpha_{xx} F_w \cos(\theta) + a_{,,} F_w \sin@) = (\alpha_{xx}.\cos(\theta) + \alpha_{xy}.\sin(\theta)) F_w$$

and,

$$R_y = \alpha_{xy} F_w \cos(\theta) + \alpha_{yy} F_w \sin(\theta) = (\alpha_{xy}.\cos(\theta) + \alpha_{yy}.\sin(\theta)) F_w$$

Hence,

$$\frac{R_x}{F_w} = (\alpha_{xx}.\cos(\theta) + \alpha_{xy}.\sin(\theta))$$

and,

$$\frac{R_y}{F_w} = (\alpha_{xy}.\cos(0) + \alpha_{yy}.\sin(\theta))$$

Providing either a_{xx} , α_{xy} or α_{yy} is known, then the other terms may be calculated from knowledge of $\frac{R_x}{F_w}$, $\frac{R_y}{F_w}$ and the angle of excitation θ.

Appendix D

T-Block Transducer Mass Properties, and Transformations to Derive RotationalFRF Properties

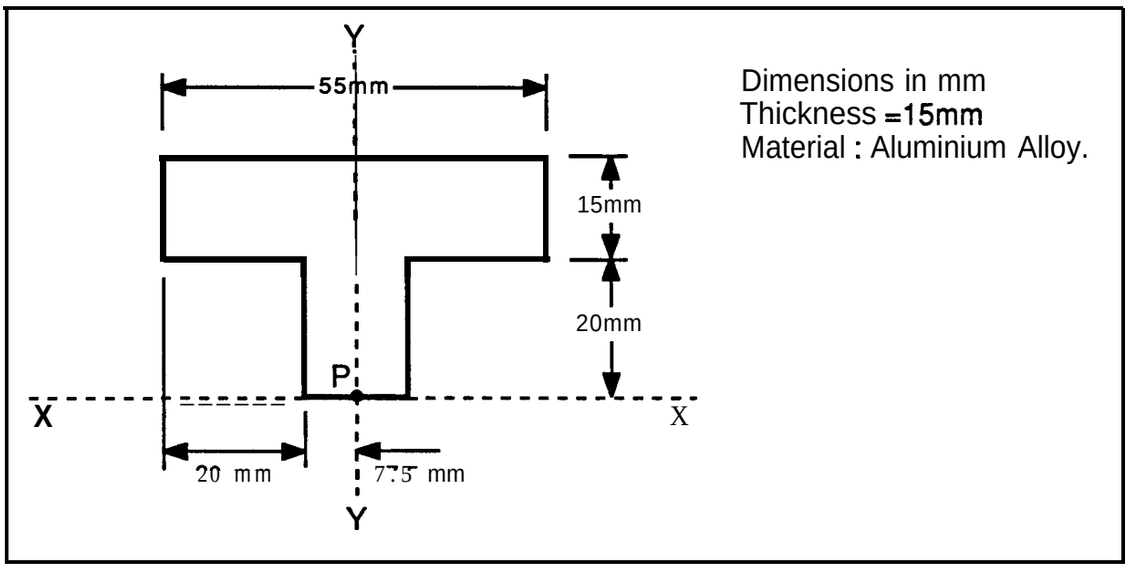

T-Block Transducer.

I_{xx} = 27.7 * 10^{-6} KgM2 & I_{yy} = 8.7 * 10^{-6} KgM2

Therefore, since Ip = I_{xx} + I_{yy} Ip = 36.4 * 10^{-6} KgM^2

Inclusion of Accelerometer and Pushrod Adapter Mass in the Inertia Calculation.

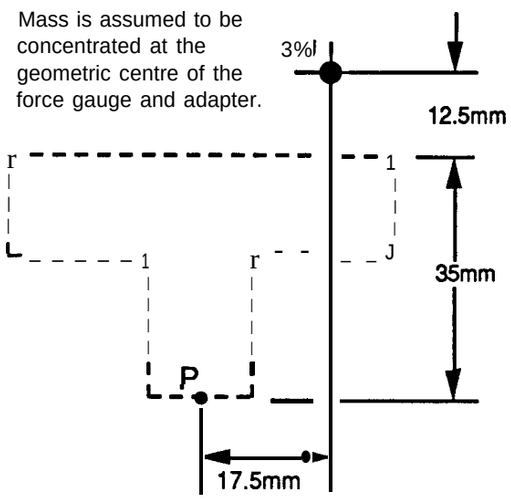

Ip for force gauge = 89.7 * 10^{-6} KgM^2

Therefore, total Ip = 126.1 * 10^{-6} KgM^2

For this investigation, only a small amount of 'rotational' information was required, and so the matrices were all (2x2), and the [T,] ,[T_2], and [M] matrices were defined as follows:-

$$[M] = \begin{bmatrix} m & 0 \\ 0 & I_P \end{bmatrix}$$

m = 47.2 * 10^{-3} Kg.
Ip = 126.1 * 10^{-6} KgM2

$$[T_1] \quad \begin{bmatrix} \frac{1}{2} & 1 \\ 1 & \\ \frac{}{2S_1} & \frac{1}{2S_1} \end{bmatrix}$$

S_1 = 21.5 * 10^{-3} M

$$[T_2] = \begin{bmatrix} 1 & 1 \\ S_2 & -S_2 \end{bmatrix}$$

S_2 = 17.5 * 10^{-3} M

Appendix E

Theoretical Calculation of T-Block Attachment Stiffness

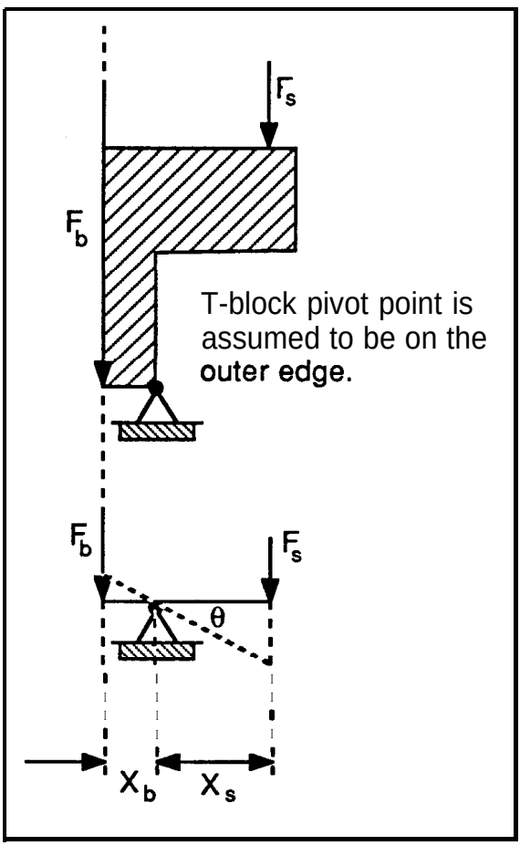

The applied torque is F_sX_s, and for equilibrium, $F_bX_b = F_sX_s$ ..... (E1)

Now, rotational stiffness $= \frac{\text{Torque}}{\text{Angle}} = \frac{F_sX_s}{\theta} = \frac{F_b.X_b}{\theta}$ ..... (E2)

The bolt stiffness = $K_b = \frac{F_b}{e_b}$

where e_b = extension of bolt.

but, $e_b = X_b\theta$ in rads for small angles, and therefore,

$K_b = \frac{F_b}{X_b\,\theta}$, giving $F_b = K_b X_b \theta$ ..... (E3)

and, substituting for F_b in (E2),

the attachment stiffness $= \frac{X_b}{\theta} K_b X_b \theta = K_b X_b^2$ ..... (E4)

Now, consider the bolt alone,

Young's Modulus $E = \frac{\text{Stress}}{\text{Strain}} = \frac{FL}{Ae} = \frac{FL}{eA}$ ..... (E5)

and,

Stiffness $K = \frac{F}{e}$ therefore $E = K \cdot \frac{L}{A}$ ..... (E6)

and hence, $K_b = \frac{E.A_b}{L_b}$ ..... (E7)

where, E = Young's Modulus of bolt material
L_b = original length of bolt.

Substituting (E7) into (E4),

Attachment rotational stiffness $= X_b^2 . \frac{E.A_b}{L_b}$ ..... (E8)

Assuming the following:-

& = 7.5 mm
E = 207 * 10^9 Nm^{-2} (for mild steel)
bolt core diameter = 3.5 mm
Therefore, A_b = 9.62 * 10^{-6} m^2
L_b = 30 mm

and hence, the attachment rotational stiffness = $3.73 * 10^3$ Nm/rad.

This value for the attachment rotational stiffness is of the same order of magnitude as that found experimentally, and it provides yet further confirmation that the experimental results were just measurements of the attachment stiffness.

Appendix F

Coordinate Transformation Matrices for the Stiffness Modifications to the Helicopter

Reference [86]: Theory of Matrix Structural Analysis
J. S. Przemieniecki
McGraw Hill.
1968.

The matrix equation relating displacements in the local coordinate system, $[U_L]$, to those in the datum system, $[U_D]$, is:-

$$[U_L] = \left[\begin{array}{ccc} \lambda_{ox} & | & \\ \lambda_{oy} & | & 0 \\ \lambda_{oz} & | & \\ \text{----} & \text{----} & \text{----} \\ & | & \lambda_{ox} \\ 0 & | & \lambda_{oy} \\ & | & \lambda_{oz} \end{array}\right] [U_D]$$

where, $\lambda_{ox} = [\, l_{ox} \; m_{ox} \; n_{ox} \,]$
$\lambda_{oy} = [\, l_{oy} \; m_{oy} \; n_{oy} \,]$
$\lambda_{oz} = [\, l_{oz} \; m_{oz} \; n_{oz} \,]$

represents matrices of direction cosines for the OX, OY and OZ directions respectively, measured in the datum system. $[U_D]$ represents element displacements in the datum system.

The direction cosines for the X- axis in the local coordinate system have been calculated from the coordinates of points 49 and 66:-

$l_{ox} = 0.78216$ $m_{ox} = 0.45614$ $n_{ox} = 0.42445$

We now require direction cosines of Y- and Z- axes in the local coordinate system. The orientation of the perpendicular Y- and Z- axes in the Y - Z plane is arbitrary.

To find the direction cosines for a Z- axis in the local coordinate system, choose an arbitrary point, P=lj, and assume this point lies in the local coordinate X - Y plane. Then, the vector product: $\hat{x} \wedge P = z$ is a vector along the new Z- axis (N.B. The order of this product retains a right-hand axis sense). The direction cosines of the local coordinate Z-axis are found by normalizing this Z vector: $\frac{z}{|z|} = \hat{z}$, which leads to:-

$l_{oz} = -0.47696 \qquad m_{oz} = 0.0 \qquad n_{oz} = 0.87892$

The direction cosines of the Y- axis in the local coordinate system are found simply from the following vector product : $\hat{y} = \hat{z} \wedge \hat{x}$

$l_{oy} = -0.40091 \qquad m_{oy} = 0.88990 \qquad n_{oy} = -0.21756$

The complete transformation matrix is shown below.

$$[\lambda] = \begin{bmatrix} 0.782 & 0.456 & 0.424 & 0.000 & 0.000 & 0.000 \\ -0.401 & 0.889 & -0.218 & 0.000 & 0.000 & 0.000 \\ -0.477 & 0.000 & 0.879 & 0.000 & 0.000 & 0.000 \\ 0.000 & 0.000 & 0.000 & 0.782 & 0.456 & 0.424 \\ 0.000 & 0.000 & 0.000 & -0.401 & 0.889 & -0.218 \\ 0.000 & 0.000 & 0.000 & -0.477 & 0.000 & 0.879 \end{bmatrix}$$

Now, from the definition of the FRF matrix in the local coordinate system -

$$[U_L] = [H_L] \,.\, [F_L]$$

which can be expressed in terms of the datum coordinate system properties as -

$$[\lambda] \,.\, [U_D] = [H_L] \,.\, [\lambda] \,.\, [F_D]$$

therefore, $[U_D] = [\lambda]^{-1} \,.\, [H_L] \,.\, [\lambda] \,.\, [F_D]$

but, $[U_D] = [H_D] \,.\, [F_D]$

and hence, $[H_D] = [\lambda]^{-1} \,.\, [H_L] \,.\, [\lambda]$

The FRF matrix in the datum coordinate system $[H_D]$ can be calculated from that in the local coordinate system $[H_L]$ providing the transformation matrix $[\lambda]$ is known. Furthermore, it should be noted that the transformation matrix $[\lambda]$ will be orthogonal and hence $[\lambda]^{-1} = [\lambda]^T$

Therefore, $[H_D] = [\lambda]^T \,.\, [H_L] \,.\, [\lambda]$